AN INVESTIGATION OF SOME PROBLEMS IN DRYING OF TASMANIAN EUCALYPT TIMBERS

by

WU QINGLIN B.E.

Submitted in fulfilment of the requirements

for the degree of

MASTER OF ENGINEERING SCIENCE

in the

Faculty of Engineering

University of Tasmania

AUSTRALIA

July 1989

I hereby declare that, except as stated herein, this thesis contains no material which has been accepted for the award of any other degree or diploma in any university and that, to the best of my knowledge or belief, this thesis contains no copy of paraphrase of material previously published or written by any other person, except where due reference is made in the text of the thesis.

Wu Qinglin

CONTENTS

Abstract		4
Additional Publications		6
Acknowledgements		7
Chapter 1.	Introduction	1
Chapter 2.	Preliminary Studies of the Problems of Drying Timber	8
Chapter 3.	Air Flow through a Timber Stack	38
Chapter 4.	Development of the Heat and Mass Transfer Model for Drying of Tasmanian Eucalypt	93
Chapter 5.	The Drying of the Tasmanian Eucalypt	145
Chapter 6.	The Mechano–sorptive Effect in the Direction Perpendicular to Grain	163
Chapter 7.	Conclusion	187
References		192
Appendix A.	Nomenclature	198
Appendix B.	Derivation of the Equation (2.3)	204
Appendix C.	A Technique for Interpolating moisture Concentrations at the Edges of Slices	208
Appendix D.	Results from Chapter 5	213
Appendix E.	Computer Programs	
	A: Program HMBALA in Fortran 77	218
	B: Program HMMODEL in Turbo Pascal	222

ABSTRACT

A detailed investigation of the air flow through a timber stack with the flow both along and across the board is described. Measurements of velocity profile and turbulence level at various distances from the leading edge are presented to show the structure and development of the boundary layer flow under various free stream velocities. Existing theories on the laminar separation at entrance and the transition process from laminar to turbulent flow in the separated shear layer and the development of the boundary layer flow are examined and compared with experiments. Surface shear stress and friction factor are estimated from the measurement of the static head drop and boundary layer properties along the flow passage. These are used to predict heat and mass transfer coefficients with the Reynolds analogy between heat, mass and momentum transfers.

A simplified model based on the concept of "free water" and "bound water" sharply separated by a fibre saturation point (FSP) is proved to be a useful concept for conveying preliminary idea but not sufficiently accurate for a detailed understanding of the drying of Tasmanian eucalypt timbers. Experimental evidence of surface temperature changes during drying and the formation of dry patches has led to an approach based on detailed measurements of the boundary layer flow and a coupled heat and mass transfer model within the boundary layer.

In the model, the transfer of moisture within the wood is assumed to be a diffusion process in which the diffusion coefficient is independent of the moisture content and the driving force is the moisture concentration as in true molecular diffusion. The transfer of heat is modelled by considering the convective heat transfer over the board surface and the conduction heat transfer inside the board. The governing transport equations are solved numerically based on analytical solutions. The model has been validated by measuring moisture contents of slices of boards during drying.

Successful drying of Tasmanian eucalypt timber from green to EMC with the test procedure outlined in the process of research is made for the quarter–sawn boards. The effect of edge drying on the overall drying behaviour of the whole board is shown and the analytic solution of the two dimensional diffusion equation is quoted.

A literature survey on the mechano–sorptive effect is made as entry to the subject. Tests with the Tasmanian peppermint eucalypt timber are conducted under bending conditions and the stresses are applied in the direction across the grain. It is shown that nearly linear relationships could be fitted between the average moisture content and mechano–sorptive effect of the wood over the whole moisture content range, but the slope of the line changes at about FSP. The slope of the line also appears to be dependent upon the initial moisture content and temperature of the wood. It is also shown that change of the loading direction from along grain to across grain results in a large increase in the mechano–sorptive effect.

ADDITIONAL PUBLICATIONS

The following papers were presented at the Fourth Australasian Conference on Heat and Mass Transfer, New Zealand, May (1989):

1. Air Flow Through a Timber Stack:

   By Qinglin Wu, A.R. Oliver* and P.E. Doe**

2. A Heat and Mass Transfer Model for Drying
   Tasmanian Eucalypt Timber

   by Qinglin Wu, A.R. Oliver and P.E. Doe

* Emeritus Professor of Civil and Mechanical Engineering,
University of Tasmania

** Senior Lecturer in Mechanical Engineering
University of Tasmania.

ACKNOWLEDGEMENTS

The author is grateful to a large number of people and would like to take this opportunity of expressing his sincere thanks to all who were of assistance in the course of this project. In particular he is most grateful to Dr. P.E. Doe, his supervisor, and Prof. A.R. Oliver for their help, suggestions and many discussions concerning this work. The fruits that are gathered herein are blossoms of the seeds sown and natured by both of them. He also wishes to thank the staff of the Tasmanian Timber Promotion Board, namely Mr. K. Ralph , R. Mills and S. Goodwin for their kindly lending of their available materials and their assistance in the maintenance of equipment.

The author also wishes to express his gratitude to the Australian Timber Research Institute for the financial support provided in the process of research.

The author likewise wishes to thank Dr. P.E. Jolly of the University of Queensland for the help in his first year in Australia.

CHAPTER 1

INTRODUCTION

The successful use of timber in its various applications depends on its satisfactory drying from a newly felled condition to its specified working moisture content. Although undried timber is used successfully in many applications, drying to the equilibrium moisture content is necessary from the point of view of serviceability. In order to achieve such low moisture content, the use of kiln–drying is often required. At present, the drying schedules used in these kilns have been developed by trial and error over many years of operation. This situation results in unnecessary degrade of the dried timber and decreases its market value.

During the development of new schedules, the internal stresses that arise in the wood are major factors to consider because they cause problems such as surface checks, honeycombing, and residual stresses. These stresses are caused by inherent differences in the shrinkage properties of clear wood and wood containing defects, and also as a result of the moisture gradients in the drying wood. As the former are usually small when samples are carefully selected off the saw, the drying stresses resulting from moisture gradients have usually been of most concern. The main constraint, therefore, that controls the speed and efficiency of a drying schedule is the risk of damaging the timber. Thus, in order to improve existing schedules and develop new ones, a greater understanding of drying stress development is required.

A general concept of how the stresses develop inside of wood as it dries was well documented in the forest products literature[1,2,3,4] and can be described as follows. Under the normal drying conditions, the surfaces of sawn boards tend to come to the equilibrium moisture content of the prevailing conditions and the outer zones of the wood dry below the fibre saturation point. Thus, the fibres at the surface tend to shrink, but are restrained by the fibres at the inner zones which are in a relatively green condition and have not begun to shrink significantly. Because of this restraint, the outer zones are stressed in tension, and as a reaction, the interior zones are stressed in compression. When the tensile stress exceeds the proportional limit, tension set takes place in the outer zones. The tensile stress in outer zones and the compressive stress in the center zones gradually proceed to their maximum values, then decrease. As drying goes on, succeeding inner zones tend to shrink and thus change from compression to tension. The maximum tensile stresses develop in those zones, which are not as big as the maximum stresses developed in the outer slices. When the tensile stresses in the surface zones reduce to zero, there is nearly always some tension set left in these zones. As drying still continues, the centre and outer zones shrink further. Due to the tension set left in the outer zones, the centre zones change from compression to tension. As a reaction to this, the outer zones change from tension to compression (stress reversal). After stress reversal, the outside zones gradually proceed to a maximum compressive stress and the centre zones to a maximum tensile stress.

A detailed analysis of this problem obviously requires knowledge both on the moisture transport and the stress–strain development. These two stages are coupled as the buildup of stresses is strongly influenced by the

changing moisture content and the rheological properties of the wood. The movement of moisture is, however, dependent only on the heat and mass transfer processes within the air over the wood surface and inside the wood and appears to be much less dependent on the stress field.

It is well known, qualitatively, that the velocity, dry bulb temperature and humidity of the incoming air are controlling factors and that these interact with the diffusion of water within the wood to set up moisture gradients within the timber. However, very few detailed investigations of the boundary layer flow through a timber stack and its influence on the board surface conditions have been reported, although a large number of researches were conducted to account for the moisture transfer processes from inside the wood and from the board surface. Skaar[5] in analysis of methods for determining the moisture diffusion coefficient in wood separated moisture sorption into external (surface) and internal (through the wood) resistances that were mass transport dependent. The boundary condition was based on the fact that the rate at which moisture was emitted from the surface of a drying material at any particular time was equal to the rate at which the moisture diffused to the surface from the interior. Hart[6] discussed the effective surface moisture content of wood during sorption. He presented a psychrometric approach to the surface conditions which depends on simultaneous heat and mass transport. Schaffner[7] used an empirical relationship to express the surface moisture concentration as a function of time in solving the diffusion equations for drying of Tasmanian Eucalypt timber. This relationship was obtained by fitting the experimental data measured under specified drying conditions. Nadler et al[8] in modelling the

moisture diffusion used a mass transfer approach to account for the surface boundary condition. He expressed this by equating the moisture flux toward the board surface by internal diffusion to the moisture flux away from the board surface by convection into the bulk air stream. The scarcity of experimental data on the surface heat and mass transfer coefficients which are functions of the fluid flow, the thermal properties of the fluid medium, and the geometry of the system, has undoubtedly hampered the development of more realistic heat and mass transfer models to describe the process of drying. This thesis presents a study of these effects because it is the tendency towards differential shrinkage that sets up the stresses which can cause surface checking or degrade.

The stress dependence of the rheological properties of wood is complicated by such properties of the wood as elastic, linear, nonlinear, mechano–sorptive, viscoelastic reactions occurring in the drying process. Schniewind[9] reviewed the characteristics of the most significant models, that had been proposed to explain creep in wood, during the exceptionally active research period of 10 years prior to that date. Most of those theoretical models were intended to represent mechanical (visco–elastic) creep effects, and they involved claims that responses could be represented by linear relationships. However, Schniewind noted that, although some data appeared to show linear associations in some conditions and over very restricted ranges of stress and strain effects, the linear assumption was invalid generally. In any case, those theories were completely inadequate in respect of mechano–sorptive effects. Grossman[10] noted additional theories, particularly to represent the mechano–sorptive effect. However, he

commented that the data showed that those hypotheses were unsatisfactory. Grossman outlined the various features of mechano–sorptive behaviour which had been recorded. He thus suggested that for wood and wood products, an acceptable model should : (a) indicate reasons for the typical mechano–sorptive reactions; (b) be closely related to the basic structure of wood; and (c) be compatible with all the data, including those exhibiting responses to previous stress history of the specimens. Recent researches are those of Ashworth[11], Kawai et al[3], Schaffner[7], Morgan et al[12], Lessard et al[13], Oliver[4], Rice and Youngs[14]. It must be pointed that except Oliver, who considered linear as well as nonlinear components of instantaneous strain and both mechano–sorptive and viscoelastic creep in his model, other models have partially or totally ignored the nonlinear, mechano–sorptive and viscoelastic responses of the wood.

The reason for most of the models ignoring nonlinear and creep behaviour of wood appears to be partially due to unawareness of the creep phenomena, and partially due to shortage of data and complexity when putting them into a model. The first paper on the mechano–sorptive effect did not appear until 1962, and thereafter there was still no extensive data reported in the forest product literature. This situation has led to people like Kawai simply lumping the mechano–sorptive effect with the mechanical creep in late 1979, and people like Lessard still ignoring the creep effect as late as 1982. Oliver's results clearly indicate that once these phenomena are taken into account, more realistic numerical values of the stress prediction can certainly be reached. However, lack of data such as the effect of temperature on the mechano–sorptive effect and the initial distribution of

moisture and growth stresses, and less understanding of recoverable and irrecoverable creep flow phenomena and the effect of collapse and the reconditioning process prevent those researchers properly including those different phenomena in their models.

Therefore, development of a mathematical model to predict the internal drying stress rests heavily upon the further understanding of heat and mass transfer process involved in wood drying and some rheological properties of the wood. The investigation presented in this study forms part of the larger project on the mathematical modelling of the drying behaviour of Tasmanian eucalypt timber. This study deals in greater depth with the heat and mass transfer process involved in the drying of that material. Particular attention is paid to provide an experimental basis for the air flow through a timber stack. A detailed one–dimensional model describing the heat and mass transfer process is presented and verified experimentally. Also, tests on the mechano–sorptive behaviour are conducted.

Chapter 2 describes the first preliminary attempt to relate the experimental measurement to the existing computer program DRYWOOD and discusses some of the sources of difference.

Chapter 3 presents measurements of the air flow through a timber stack. The details of the flow development, turbulence generation, and surface friction for the flow both along and across the board are discussed.

Chapter 4 describes the details of the development of a heat and mass transfer model for drying of Tasmanian eucalypt timber and the experiments which are conducted to verify the proposed model.

Successful drying of Tasmanian eucalypt timber from green to EMC with the application of the general test procedure outlined in the process of the research is presented in Chapter 5. The effect of edge drying to the overall drying behaviour of the whole board through a complete drying process is also discussed.

Chapter 6 describes a literature review on the mechano–sorptive effect and some tests on the Tasmanian peppermint eucalypt timber.

Chapter 7 provides the conclusion to the thesis.

CHAPTER 2

PRELIMINARY STUDIES OF THE PROBLEMS OF DRYING TIMBER

Wood drying involves a coupled process of moisture transport and changing values of temperatures and drying stresses inside the timber. This process is controlled by both external drying conditions (temperature, relative humidity, and air velocity) and wood variables (specimen size, relative dimension in the three different structural directions, and various physical properties). Because of the complex interrelationship of those variables, wood drying schedules have been mainly developed on an empirical basis. Recently, however, computer simulation studies on moisture transport and stress development inside the timber have laid the groundwork for a more fundamental understanding of the drying process. These studies seem to offer useful guidance in the directions of the better control, increased rates of drying in the later stages, and ultimately automatic kiln control.

One of the models proposed to predict moisture change and the drying stress development was contributed by Oliver[4]. This model takes account of the effects of timber's nonlinear properties, mechanical creep and mechano–sorptive effect. Numerical results from the released computer simulation program——DRYWOOD[15] have been proved credible by extensive field and laboratory testing.

The experiments described in this chapter were designed to further the understanding of the behaviour of timber during drying, and consequently develop a kiln schedule with the aid of the computer simulation program. An

associated aim was to identify what other properties of the material or the process of the drying could be usefully examined to extend the validity of the computer program currently used to describe the model. It should be pointed out that DRYWOOD is restricted to a single set of kiln conditions chosen by the user at the start of a run and the same restriction was accepted in the design of the experiments so as to avoid known problems such as the effect of cycling humidity on the physical properties of the wood.

2.1 Outline of the Model

The principle of the model is to "divide the net strain into four components which are taken to be separable and separately measurable but linearly additive. The four components of strain are taken to be[4]:

1. Instantaneous strain as obtained from a short term loading test but with some modification in the nonlinear range,
2. Unconfined shrinkage strain taken to be the values of the shrinkage strain at different moisture contents as measured on thin unrestrained specimens presumed to be at a uniform moisture content (taken to be independent of temperature),
3. Mechano–sorptive strain due to the interaction between stress and moisture movement (taken to be independent of temperature), and
4. Mechanical creep, the time dependent effect (a function of time, stress and temperature but independent of moisture content as long as the moisture content remains constant)."

The strain components, except the unconfined shrinkage strain, are calculated as finite increments subject to the restrictions that: a) the net strain is independent of the value of the dimension in the direction across the plank; and b) the net force on the cross–section of the plank is zero.

The program used here is restricted to one dimensional behaviour which is appropriate to the "middle portions of wide planks which are wholly backsawn or wholly quartersawn and far from the middle of the tree." The moisture transport in the program is described as a diffusion process. The moisture distribution is calculated from Fick's equation, in which the diffusion coefficient is taken to be constant and the surface moisture content is calculated as a function of time from an empirical equation[7]. One of the purposes of this investigation is to replace Schaffner's equation with a more widely accepted analysis of heat and mass transfer between the air and the wood including an allowance for the effect of 'dry patches' which appear to be a feature of drying wood and seem to have caused previous failures to describe the process of drying wood by standard techniques of calculation.

2.2 Testing Procedure and Result Discussions

2.2.1. Tests for the Initial Conditions

Timber is a variable material and its physical properties vary greatly according not only to the growth rate of the tree from which the timber was cut, but even from what part of the trunk it was taken. Furthermore, these properties may change considerably from board to board and even within the

same board. It is, therefore, necessary to measure the initial (green) conditions of the timber used for the experiments so that the input parameters to the computer simulation program can be determined. The initial measurements made in this test included the initial moisture content, basic density, moisture distribution through the board thickness, and unconfined shrinkage. The Young's modulus and creep were not measured; published values on the Tasmanian eucalyptus materials were used in the computer program.

1. Measurements of the Initial Moisture Content and Basic Density

The material chosen for this work was from Tasmanian–grown Eucalypt. Quarter–sawn green boards were randomly selected from a sawmill. The selected boards were numbered and wrapped with plastic film to decrease drying while being transferred from the sawmill to the laboratory. Some of the wrapped boards were directly taken to the laboratory for the initial tests, while others were kept in a cool room at about 7 ^{0}C dry–bulb temperature and 80 percent relative humidity (5.5 ^{0}C wet–bulb temperature) for the kiln drying test.

Samples 200 x 30 x 28 mm for initial moisture content and basic density tests were cut from the numbered green boards. The samples were then scraped to remove loose splinters and sawdust. Weighing of the samples was done as soon as they were scraped and the weight of each sample was recorded together with the identifying number of the sample.

The moist (green) volume of each sample was measured by the water displacement method with a Sartorius balance. In this test, the sample was hung by a band and sunk completely into the water–filled glass column on the balance. The difference between the readings from the balance before and after the sample was completely sunk into the water was the mass of the volume of water displaced equal to the volume of the sample. The sample was then oven–dried at a temperature of about 105 ^{0}C. After about 24 hours, the samples were weighed at intervals of 4 hours until there was no further loss in weight, and then removed from the oven for the final weighing to get its oven–dry weight. It should be pointed out that the hot specimen needs to be cooled down in a desiccator before the final weighing to minimize the effect of hot air currents.

Percentage moisture content (dry basis) was expressed as the ratio of the weight of moisture to the oven–dry weight of the sample, while basic density was calculated as the ratio of oven–dry weight of the sample to the green volume. Samples were taken from every board being tested.

The measured moisture content and basic density were plotted against the board number in Figure 2.1, in which points were joined by lines to show where they were and the lines have no other significance. Great variations can be seen from those curves. It was later concluded that the boards being tested were apparently not from the same log. Under this situation, a moisture content of 72 % and a basic density of 650 Kg/m^{3} were chosen as inputs to the DRYWOOD program.

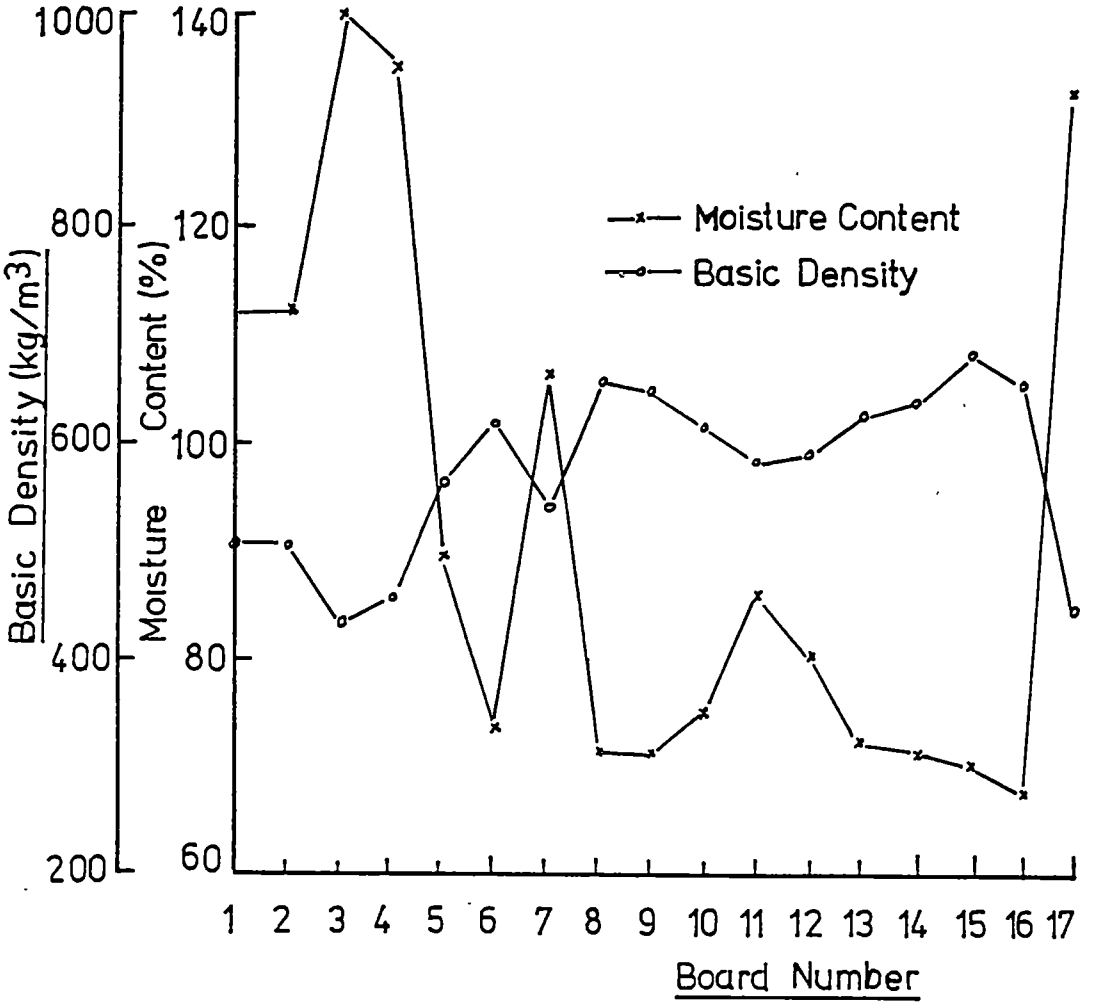

Figure 2.1

Initial Moisture Content and Basic Density

2. Measurement of the Initial Moisture Distribution within One Board

As mentioned earlier, the moisture content inside the timber may vary considerably within the same board. The program, however, uses the condition that the initial moisture content within the same board is uniformly distributed. Thus, the measurements of the moisture distribution through the board thickness are necessary for checking the difference between

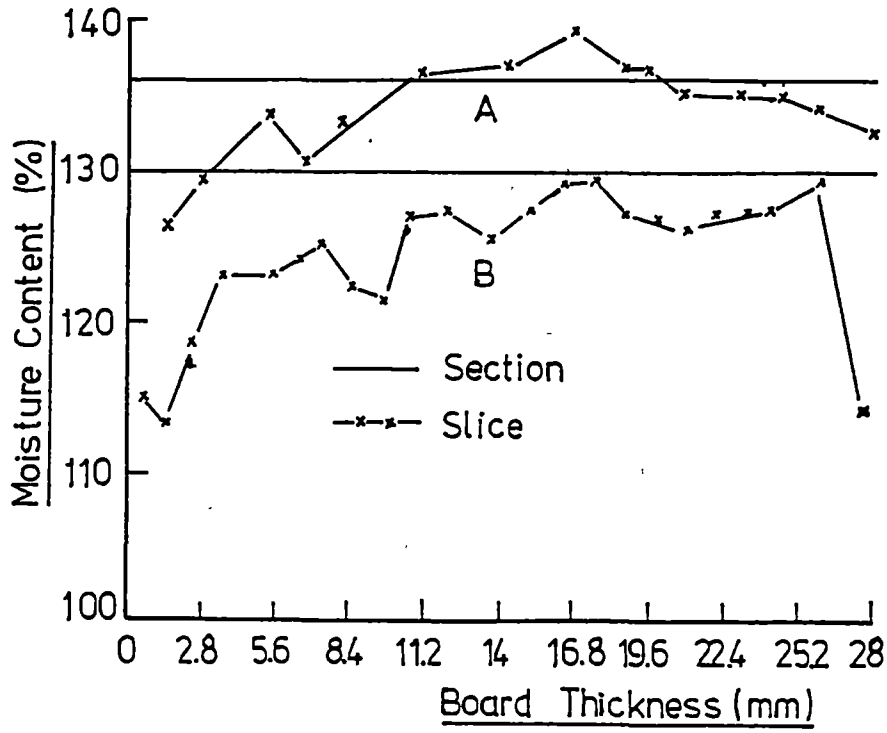

Figure 2.2

Initial Moisture Distribution

the real boards and the program–based condition. Samples 30 x 30 x 28 mm were taken from the middle portions of the corresponding green boards and then sliced with a microtome into thin slices (thickness about 1 to 2 mm). As soon as the slice was taken, it was numbered and weighed on a Projecta balance (sensitivity 0.0001 g). The process of the slicing and weighing was completed as quickly as practicable to minimize the loss of moisture prior to weighing. The thickness of the slice was measured with a micrometer. The reading of the thickness measurement was carefully taken because the slice was sometimes not evenly cut and the adding of all the slices usually exceeded the original thickness of the sample. The numbered slices were then oven–dried to constant weight at about 105 ^{0}C to get the oven–dry weight. To check the errors introduced by slicing, the average moisture content of one neighbouring element was also measured for each sample to be sliced. It

was later recognized that it would be useful to measure the average moisture content of the neighbouring whole sections to check the longitudinal variation of moisture content, but this was not done in this test.

Figure 2.2 shows the results of the measurement from two different boards. The average variation of the measured moisture content within those boards was about 10 percent. The average difference of moisture measurement between slice and section was about 5 percent. Those results were used to make some allowance for differences between the computer program output and the test measurements in the later sections.

3. Measurement of Unconfined Shrinkage

Test samples about 1.5 mm thick were cut from the green boards using a circular–saw. Two markers (thin and short electric wire) were embedded on the face of each green sample in the board width direction. During tests, the samples were allowed to dry in air. They were restrained by metal frames from deforming out of the plane, but not restrained against shrinkage within the plane. The distance between two markers was measured with a travelling microscope and the samples (plus restraining frame) were weighed on the Projecta balance every 30 minutes. The test was conducted until there was no further loss in sample weight, and then the samples were oven–dried so as to find the moisture content at the different stages. The shrinkage (expressed as the ratio of the change in dimension to the green dimension) was plotted against moisture content. The experimental curves were smoothed and two elbow points (knees) from the curve were chosen for use in the computer simulation programs.

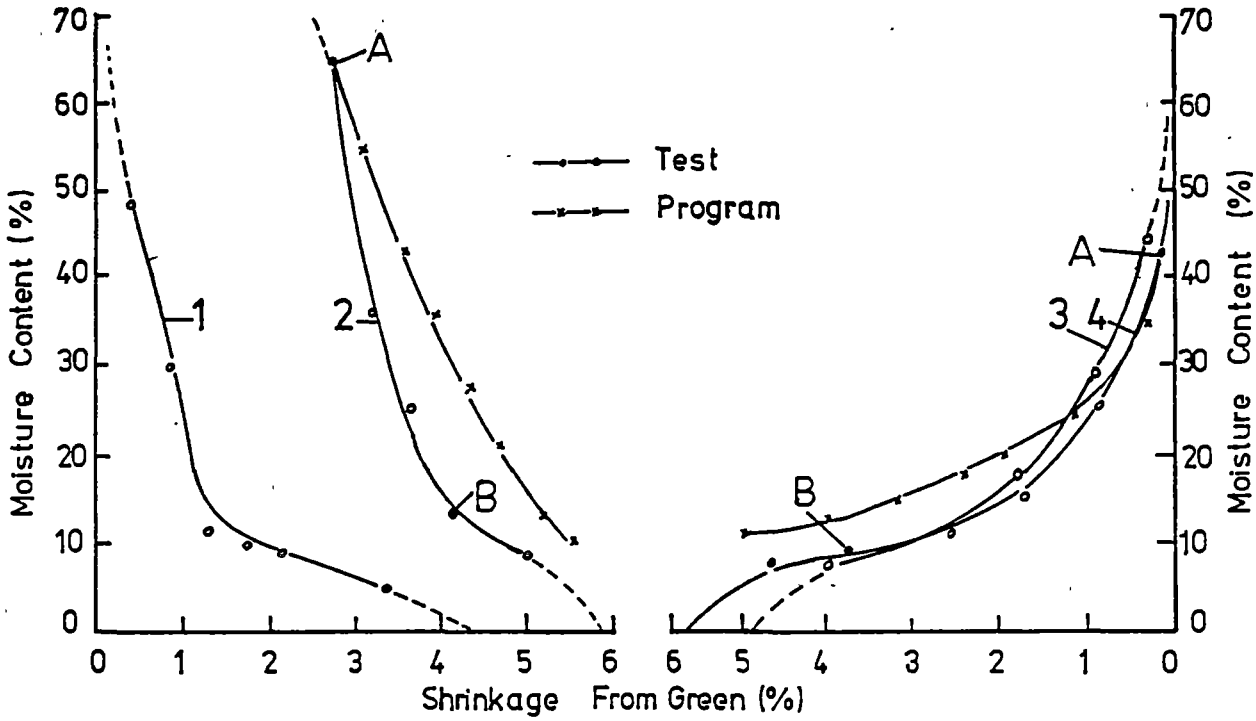

Figure 2.3

Measurement of Unconfined Shrinkage

Figure 2.3 shows the results of the measurement from four different boards, in which curves 1, 3 and 4 show the same pattern of the shrinkage, while curve 2 was later realized to indicate early collapse. Two points A (MC–moisture concentration: 270 Kg/m^3, and US: unconfined shrinkage 0.001), and B (MC:68.9, US:0.038) were chosen from the curve 4 to represent the average condition of the boards, except board 2, as the input to the computer program DRYWOOD.

2.2.2 Computer Simulation

Based on the initial measurements of basic density, moisture content, and unconfined shrinkage, values representing average conditions were chosen as input parameters to the computer program. The program was then run to get a drying schedule under which the boards at the average conditions started to check after about one week. It was hoped that necessary data were collected during this time period to get the moisture distribution and net shrinkage, to check the time at which the first visible crack started on the surface of each board, and to infer the diffusion coefficient from the drying tests at the different stages of the drying process.

The variables to the program were the air temperature, air velocity, and relative humidity. In choosing the conditions, one of the three variables was changed at a time while the other two were kept constant. Mass diffusion coefficient and surface moisture concentration factor (the factor which determines the board surface moisture concentration in the drying process) were initially taken to be those measured by other researchers on Tasmanian Eucalypt materials. Several simulation runs were conducted before the final condition was chosen.

Under the chosen drying conditions, the computer program was run again to simulate the boards which had much different initial moisture content and basic density from those for getting the drying schedule. In this way, crack starting times on those boards were obtained so that observation could be made during the test to compare results from the program with those from the tests.

Table 2.1

Drying Schedule and Computer Output

Drying Schedule:

Air Temperature (°C) : 36
Air Velocity (m/s) : 0.9
Relative Humidity (%) : 42

Computer Output

Board Number	Basic Density Kg/m³	Moisture Content %	Checking Time Day	Hour
8,9,13,14,15	650	72	5	20
6, 10	620	75	3	10
1, 5, 12	590	86	2	15
7	550	105	2	10
1, 2	510	112	2	1
4, 17, 3	450	135	1	20

Table 2.1 shows the chosen schedule and the computer output of the crack starting time for the boards with different moisture content and basic density. The test was conducted under this schedule.

2.2 Kiln Drying Tests

1. Test Arrangements

The tests were conducted in the instrumented kiln recently built by the Timber Research Group of the Tasmanian Timber Promotion Board (TTPB) in the Department of Civil and Mechanical Engineering of the University of Tasmania (Figure 2.4). The kiln was of aluminium skin, in which fan, heater,

vent, and water spray systems were provided for the control of air velocity, temperature, and humidity. The size of the drying chamber was about 900x500x500 mm and 18 boards each 900 x 200 x 28 mm could fit in the chamber at one time, the flow direction being along the boards.

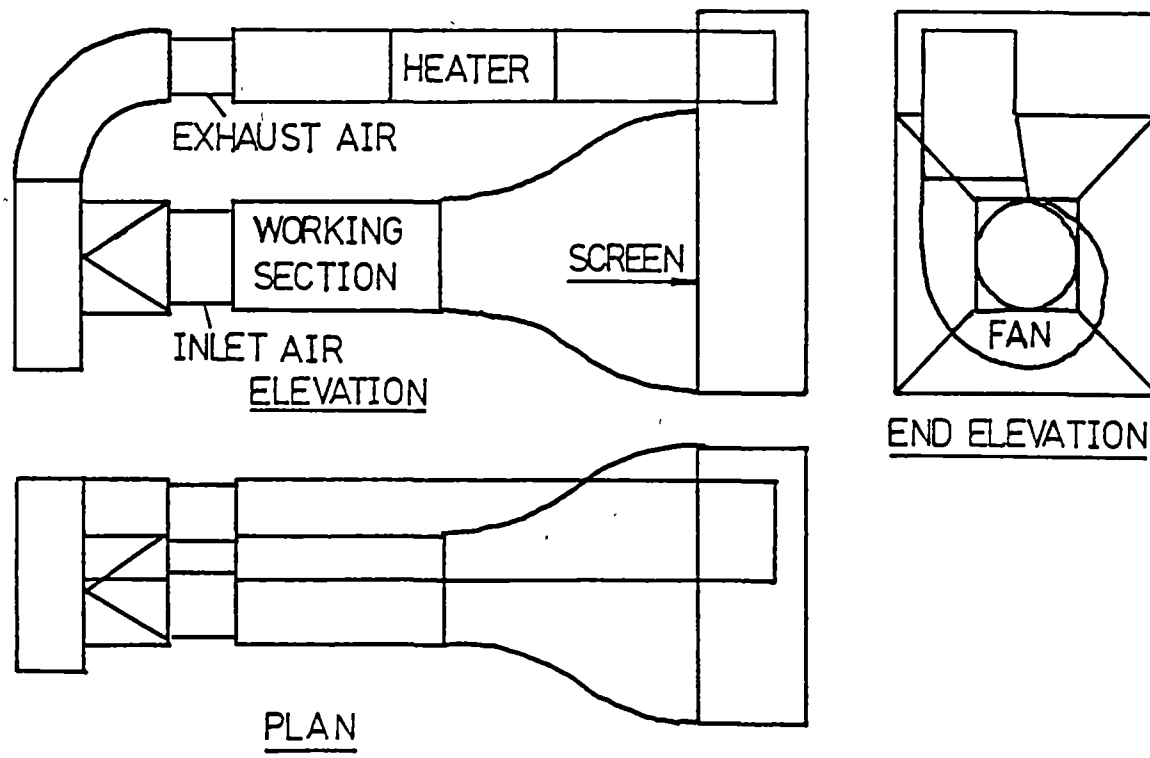

Figure 2.4

Air Conditioned Wind Tunnel

The temperatures of air (dry bulb and wet bulb) in the kiln were measured with AD590 two–terminal temperature transducers at upstream and downstream. Automatic control and data logging system for the temperature and relative humidity were provided in the kiln control system. Automatic control of air velocity, however, was not available and adjustment of air velocity had to be done by hand.

The measurement of the air velocity was done by TESTOVENT 40000 vane anemometer. It was later found that the shape of the detector limited the use of this kind of anemometer in such narrow space as that between two boards. At that stage it was decided to try a DISA constant temperature hot wire anemometer for later runs.

Before the drying started, the boards were taken from the cool room to the kiln. The weight and the size of each green board were measured. On the surface of each board two straight lines perpendicular to the edges of the board were drawn and the board width along each line was measured with a micrometer caliper to get the green dimension. The ends and the edges of each board were coated with a waterproof sealing compound to restrict the movement of the moisture to one direction. The boards were then stacked with 20 mm space between them in such a way that the samples including the boards with different moisture content and basic density were put on the top of the other boards for convenience in removing from kiln during tests.

2. Drying Operation

The drying operation was conducted under the schedule chosen from the computer trials (Table 2.1). The top sample boards were removed from the kiln at a time interval of about 20 hours to measure the weight, and the net shrinkage in the board width. A sample was cut from the end of each sample board every time the sample board was taken out of the kiln. The cut sample was then machined into three parts, in which the middle one was used for the moisture profile test and two others for the average moisture content test.

Surfaces of the boards were checked at about the crack starting time predicted by the computer as shown in Table 2.1. It should be pointed out that unawareness of the fact that at the early stage of crack formation a crack is very fine resulted in failure in observing the crack starting times in this initial test.

When the kiln was first opened, it was found that the automatic control mode should have been changed to the manual and the fan and the heater should have been shut down. The kiln was only recently built and there was no cooling system provided, so it took a long time for the kiln to settle down to the set–conditions when the temperature went up too high, as a result of the heater going on when the boards were taken out for the measurements. On the other hand, the temperature was quickly brought up to the set condition when the kiln was cooled down during sampling.

2.2.4 Checking of the Instrumentation

The accuracy of the sensors used for the measurements of the dry–bulb and wet–bulb temperatures in the kiln must be checked continually in the drying process. To do this, heat and mass balances were made over the air across the timber stack. The balances are based upon the following assumptions:

1. The heat and mass balances are made while the board moisture content is above the FSP, so the board surface was assumed to be equal to the wet bulb temperature of the air in contact with it;

2. Air conditions, i.e. temperature, velocity and humidity profiles in the different air spaces between the boards being dried are the same;
3. In the chosen time interval, the amount of air passing the timber stack is constant as long as there is no air velocity change;
4. Heat loss from the outside of the kiln is ignored as the sensors are well away from the kiln wall.

The inlet and outlet humidities (or mixing ratios) at the board surface and the bulk air can be calculated from the data of dry and wet bulb temperatures at the inlet and outlet positions. Under the assumption that the board surface is at the wet–bulb temperature, the vapour saturation pressure on the board surface was estimated from the following equation[16]

$$P_{satwb} = EXP\left\{-\frac{7511.52}{T} + 89.63121 + 0.023998970\ T - 1.1654551\ x10^{-5}\ T^2 - 1.2910336\ x10^{-8}\ T^3 + 2.0998405\ x10^{-11}\ T^4 - 12.145799\ Ln(T)\right\} \quad (2.1)$$

where, T, the board surface temperature, is equal to wet bulb temperature in ^oK. The wet–bulb humidity at the board surface (Y_w) was obtained as[17]

$$Y_w = 0.62198\ \frac{P_{satwb}}{PT\ -P_{satwb}} \quad (2.2)$$

where PT, the atmospheric pressure, is taken to be 101.325 KPa.

The enthalpy balance between the enthalpy reaching the board surface by heat transfer and that convected away by evaporation gives the following approximate expression (APPENDIX B)

$$C_{py}\,(T_{db} - T_{wb}) = -\,H_{fg}\,(Y_g - Y_w) \tag{2.3}$$

and, from which the humidity in the bulk air is obtained as

$$Y_g = Y_w - C_{py}\,(T_{db} - T_{wb})/\,H_{fg} \tag{2.4}$$

where, C_{py} is calculated from the equation

$$C_{py} = C_{pg} + C_{pw}\,Y_w \tag{2.5}$$

and H_{fg} is estimated from the expression

$$H_{fg} = 2502.1 - 2.4345\,T_{wb} \tag{2.6}.$$

From the data of the change in air humidity and temperature, mass and heat balances over the air were examined. For the mass balance, moisture lost from the timber stack in the chosen time interval must equal the moisture gain of the air passing through the stack at same time, that is,

$$(Y_{gout} - Y_{gin})\,G\,t = (W_1 - W_2) \tag{2.7}$$

in which, G, the air flow rate, is calculated as

$$G = U\,A\,\rho_{mair} \tag{2.8}.$$

ρ_{mair} was calculated as[18]

$$\rho_{mair} = \rho_{dair}\,\frac{1 + Y_g}{1 + 1.609\,Y_g} \tag{2.9}$$

in which, ρ_{dair} was estimated as

$$\rho_{dair} = 1.177 \frac{300}{273.15 + T_{db}} \tag{2.10}$$

For the heat balance, the heat released from air should equal the heat for evaporating moisture at surface temperature, i.e.

$$(T_{ain}-T_{aout})\ G\ C_{py}\ t = (W_1-W_2)\ H_{fg}$$

thus,

$$G\ C_{py}\ t\ (T_{ain}-T_{aout}) / H_{fg} = W_1-W_2 \tag{2.11}$$

in which C_{py} is calculated from Equation (2.5) at the air average temperature ($T_{ad} = (T_{ain} + T_{aout})/2$) and humidity ($Y_{ag} = (Y_{gin} + Y_{gout})/2$), H_{fg} is calculated from Equation (2.7) at average surface temperature ($T_{aw} = (T_{wbin} + T_{wbout})/2$). Equation (2.7) and (2.11) should enable calculation of the moisture loss from the measurements of the air velocity, and wet and dry bulb temperatures. The calculated values were compared with the measured ones in the same time period.

A computer program was written in FORTRAN 77 (APPENDIX E (A)) on the basis of Equations (2.1) to (2.11). Testing of the program was done by randomly choosing five points from a psychrometric chart, then calculating the humidities using dry bulb and wet bulb temperatures at these points, and comparing the calculated values with those from the psychrometric chart. Table 2.2 showed the comparison, which indicated that the program written for calculating humidity from the dry and wet bulb temperatures gave acceptable agreement with the the values obtained from

the psychrometric chart. At that stage, data on dry bulb and wet bulb temperatures from the data logging system was put into program to compare the heat and mass balances over the air in a period of 15 minutes.

Table 2.2

Program Testing

Inlet				Outlet			
Temperature		Humidity		Temperature		Humidity	
DB	WB	Calculated	Chart	DB	WB	Calculated	Chart
40.0	22.1	0.00951	0.00943	50.0	28.0	0.01509	0.0150
35.0	24.0	0.01456	0.01440	35.0	24.0	0.01456	0.0144
30.0	20.0	0.01077	0.01060	40.0	29.0	0.02136	0.0211

Accurate checking of the thermometers requires that the whole stack be weighed at the same time interval as used in the data logging system (15 minutes). However, due to the lack of the automatic weighing system in this initial trial, manual weighing of the whole stack over such short time periods had been proved to be difficult and also to affect the set drying conditions considerably. In this situation, the whole stack was weighed only twice, while the top four sample boards were weighed at every chosen time interval. The ratio of the contribution to the overall moisture lost from the top four boards to that from the whole stack was obtained from the two measurements, which was used to estimate the actual overall moisture change throughout the drying process.

Table 2.3

Output of the Heat and Mass Balances

Inlet			Outlet			Moisture Loss From		
DB	WB	Humidity	DB	WB	Humidity	MB	HB	Test
^{o}C			^{o}C			Kg	Kg	Kg
25.2	26.0	0.01783	34.7	25.8	0.01769	–0.018	0.028	0.020
37.3	25.8	0.01658	36.3	25.6	0.01666	0.011	0.055	0.020
36.5	25.6	0.01658	35.8	25.5	0.01671	0.017	0.039	0.020
36.5	25.8	0.01692	36.0	25.5	0.01662	–0.039	0.028	0.020
36.5	26.0	0.01727	35.8	25.8	0.01722	–0.006	0.039	0.020
36.3	25.5	0.01649	35.4	25.3	0.01654	0.006	0.050	0.020
36.5	26.9	0.01888	35.6	26.8	0.01908	0.027	0.050	0.020
35.6	25.1	0.01611	34.9	24.9	0.01608	–0.005	0.039	0.020
35.6	25.8	0.01731	34.9	25.5	0.01709	–0.028	0.039	0.020
36.9	27.1	0.01907	36.0	26.8	0.01891	–0.021	0.050	0.020
37.1	26.0	0.01701	36.2	25.6	0.01705	0.005	0.050	0.020
37.1	25.8	0.01667	36.2	25.6	0.01671	0.005	0.050	0.020
36.7	26.0	0.01719	35.8	25.5	0.01722	0.005	0.050	0.020
35.2	26.4	0.01854	34.7	26.2	0.01840	–0.018	0.028	0.020
36.7	25.6	0.01649	35.8	25.5	0.01671	0.028	0.050	0.020
36.7	25.8	0.01684	35.8	25.5	0.01671	–0.017	0.050	0.020
36.2	25.8	0.01705	35.4	25.5	0.01688	–0.023	0.044	0.020

Table 2.3 shows the results of mass and heat balances, in which the moisture loss is estimated in a period of 15 minutes. From Table 2.3, the following points were observed:

1. Some negative values of the moisture lost were obtained from the mass balance equation. One of the reasons was probably that the sensors at the inlet and outlet positions were not measuring the same air as the thermometer readings were taken almost at the same instant whereas it took some seconds for the air to travel between them. It is obviously

very difficult to maintain steady conditions for the whole of the air circulating in the kiln. Other reasons are still under investigation.

2. Moisture lost calculated from the heat balance is bigger than those from mass balance equation.
3. Moisture lost estimated from the measurement will be rechecked with the automatic weighing system.

2.2.5 Inferring the Diffusion Coefficient

The method of inferring diffusion coefficients from drying tests has been widely used in the timber drying simulation studies. The basic method involved here is to use the mathematical model of the drying process and then adjust the diffusion coefficient until the solutions from the model fit the measured behaviour.

In this test, data collected in the slicing tests at different drying times were plotted with the moisture concentration as ordinate and the board thickness as abscissa in Figure 2.5. There were obviously differences between the moisture contents at the symmetrical points about the center line; the average value was taken where the difference was big. The half curve at the right hand side was extrapolated to get the moisture concentrations at the board surface from the corresponding moisture distribution curves (points 1 to 5).

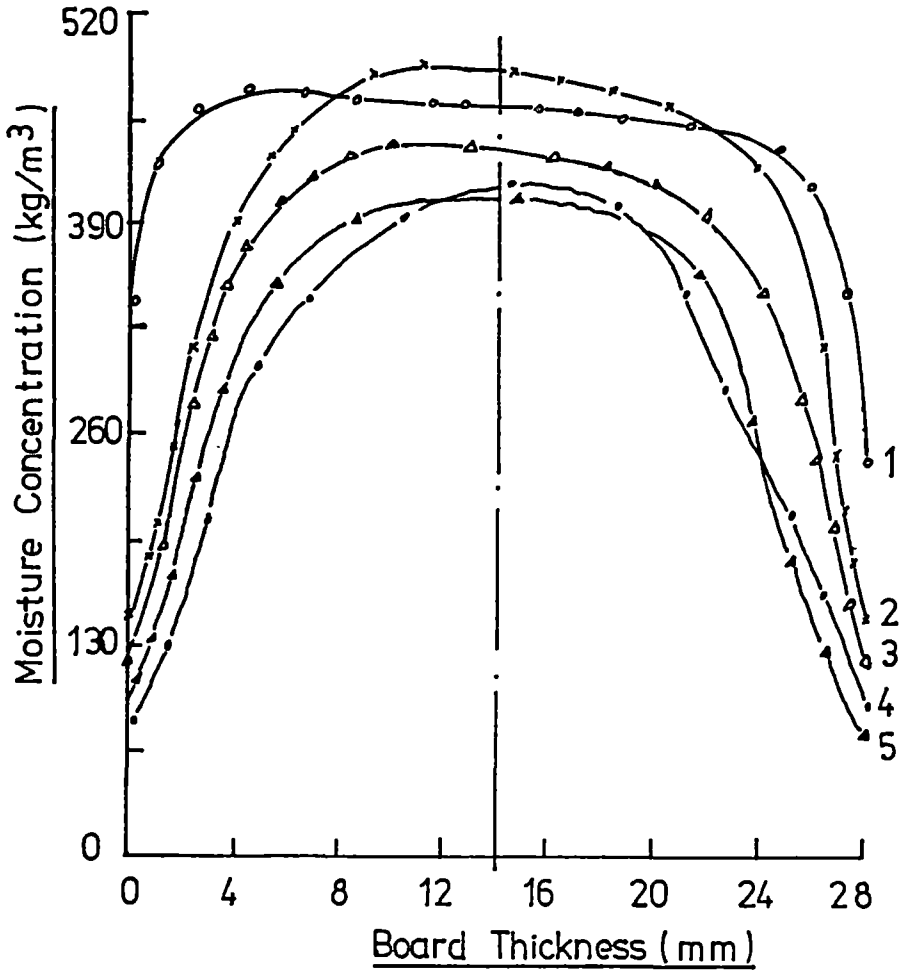

Figure 2.5

Moisture Distribution from Test

The computer program DRYWOOD was run again under the air conditions used in the kiln drying test. The first variable to be changed was the boundary moisture concentration factor, to get the surface condition to fit the extrapolated value. The diffusion coefficient was then adjusted and the moisture profiles from the computer output were plotted and compared with the measured ones. Figure 2.6 shows the comparison of the moisture concentrations at the different positions of the half board

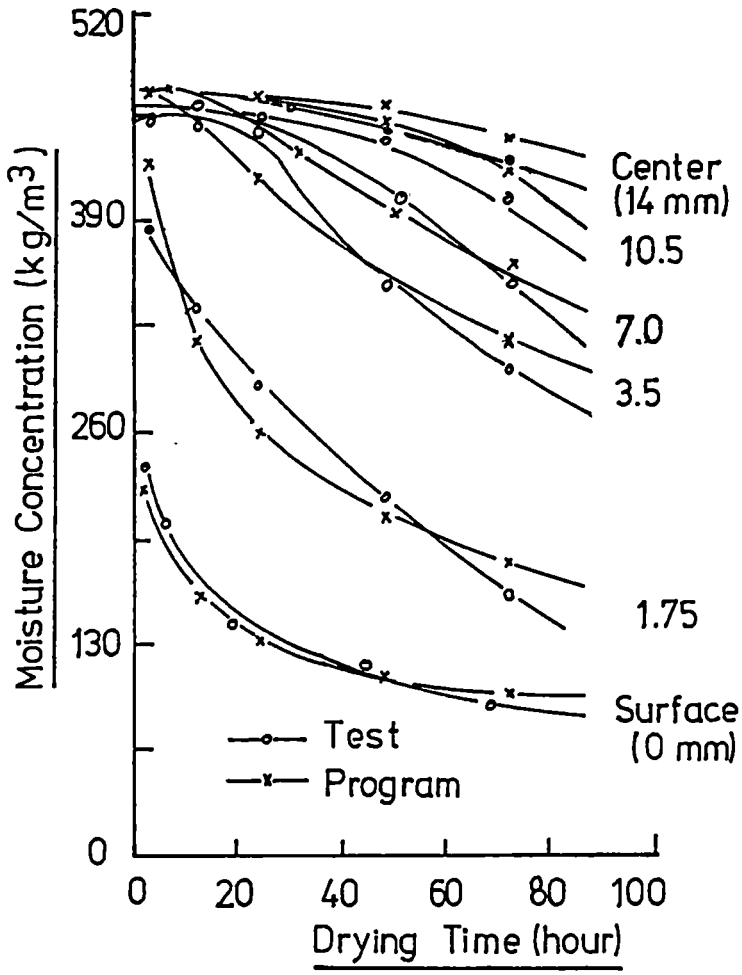

Figure 2.6

Comparison of Moisture Distribution

thickness, in which the curves from the program were obtained with the moisture diffusion coefficient of 3.4×10^{-7} m^2/hr. From Figure 2.6 it can be seen that the difference between the results from test and program was generally within 4 percent moisture content.

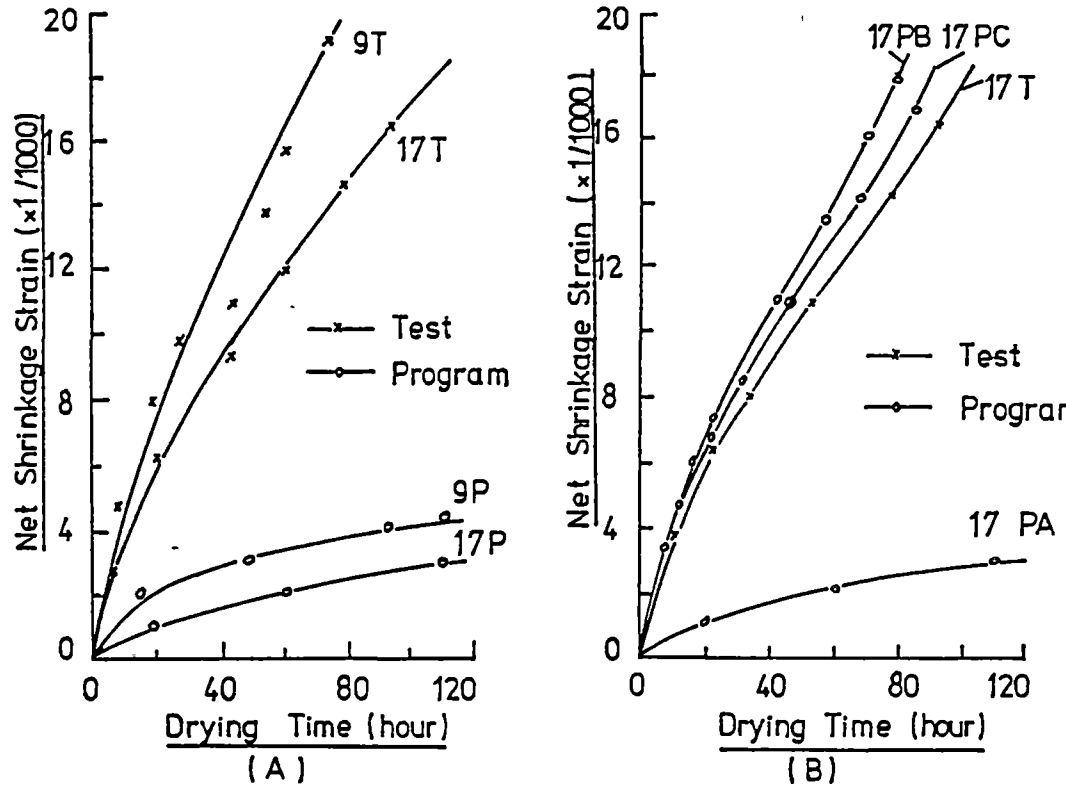

Figure 2.7

Comparison of Net Shrinkage

2.2.6 Net Shrinkage and Average Moisture Content

With the inferred boundary concentration factor and diffusion coefficient as shown in the last section, the program was run again at the drying conditions used in the test. Average moisture content and the net shrinkage strain from the program were recorded.

Net shrinkage strains from the test and program are plotted against drying time in Figure 2.7. It can be seen from Figure 2.7 (A) that the measured net shrinkage (Curves 9T and 17T) is much bigger than that from the computer program (Curves 9P and 17P). Observation of the boards exposed the fact that the boards had badly collapsed during experiments. The program, however, had made no allowance for the collapse, having been based on points A and B of curve 4 in Figure 2.3. Another reason was possibly due to the parameters to calculate the creep and mechano–sorptive strain components being wrong for the boards being tested.

Figure 2.7 (B) shows the comparison of the net shrinkage strains for board 17, in which the strain from the program was obtained from points A and B on curve 2 in Figure 2.3 as the input for unconfined shrinkage (taking account of the collapse). In this case the net shrinkage strain from the program was obviously brought up (from curve 17 PA to curve 17 PB), which was about 16 percent bigger than the measured one (17 T). Curve 17 PC was obtained by adjusting the parameters to calculate the mechano–sorptive strain (compression parameter used in the program being reduced from 5.3 in curve 17 PB to 3.3 in curve PC), which reduced the difference in the net shrinkage strain to about 8 percent. From this it can be concluded that collapse played a major role in the net shrinkage for most of the boards, and once collapse was properly included into the program it gave quite close agreement with measured behaviour. Thus, attention must be paid in the selection of the sample boards to make sure that the chosen boards do not collapse in the drying process as there is still no proper way to model collapse in the DRYWOOD program.

The unconfined shrinkage strains predicted by the DRYWOOD program were also plotted against moisture contents in Figure 2.3 for curves 2 and 4, to compare with the measured ones. It can be seen that the points A and B, which were used to define curves 2 and 4 in the program, were not well chosen as the predicted shrinkage was much bigger than the measured values. This would be another reason why the predicted net shrinkage was bigger than the measured values once curve 2 of Figure 2.3 was input to the program as mentioned above.

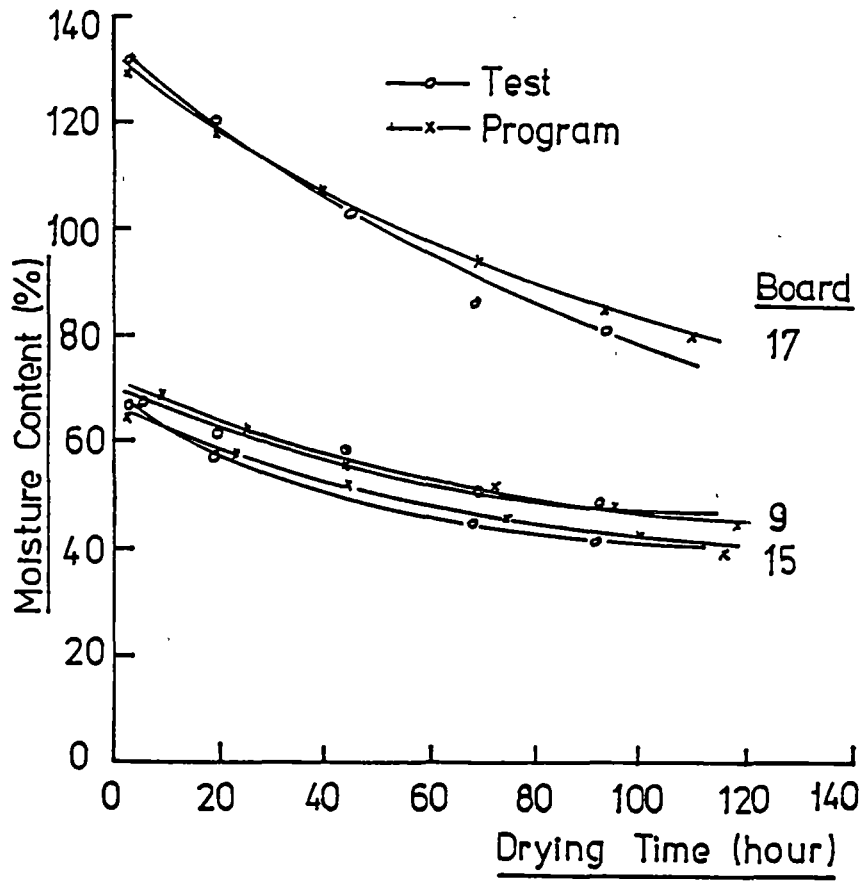

Figure 2.8

Comparison of the Average Moisture Content

It should also be pointed that only one shrinkage curve showed the sign of collapse in this test, while all the sample boards had collapsed in the tests. Thus, more thick samples should be taken for unconfined shrinkage measurements in the next run to get more idea on collapse formation of the board being dried.

Figure 2.8 shows the comparison of the average moisture contents from the test and the program. The difference between the test and the program in this case was within 2 percent moisture content.

2.3 Suggestions for Further Tests

This initial trial exposed many problems both in the equipment and methodology employed for the test. This information allowed us to develop better methodology for subsequent experiments under the present available conditions. On the basis of this initial test, further modification of the experiment was proposed in the following areas:

2.3.1 Selection of the Boards

Due to the great variation of timber's properties, caution must be exercised in selecting the boards at the sawmill. During this initial test, great variation in moisture content (from 70% to 140 %) and basic density (from 450 to 650 Kg/m^3) was encountered with the boards apparently from different logs. This situation resulted in difficulty in choosing the proper drying schedule from the computer program. Thus, it would be more convenient to use the boards from the same log for a run.

Observation of the sample boards indicated that all the chosen sample boards had been badly collapsed. This resulted in difficulty in comparing the net shrinkage from program and test as there is no proper way to model collapse presently in this DRYWOOD program. Therefore, attention must be paid in selection of the sample boards to minimize the possibility of the collapse occurring during tests. In a general sense, it appears from visual observation that the boards with widely separated growth rings are more prone to collapse. Visual observation also showed that the whole problem of collapse was too variable and ill–defined to provide a suitable project for investigation in this exercise.

2.3.2 Sampling and Testing

In taking samples and doing measurements throughout the whole test process, attention would be paid in the following places for the next run:

1. Sample material should be placed in the kiln as near to the 'green–off–saw' condition as practicable to minimize the inside stress development before measurement.
2. Samples for unconfined shrinkage tests should be taken from boards with different moisture contents and basic densities; the maximum thickness of the sample should be controlled to be within 1.0 mm. When collapse shrinkage is suspected, another set of test is required on slices about 2 mm thick , the difference between these curves and those for the thinner slices can help to find the effect of collapse.
3. Samples for moisture profile tests should be taken from about 20 mm inside the end of the board to minimize the effect of the coating

material on moisture diffusion. Samples should be marked on one surface immediately after it was taken from the board, to make sure that slicing is always started from the same surface.

4. The ends of the sample boards should be coated as soon as the sample is taken.
5. The first few slices in the moisture profile test should be taken with the possible minimum thickness for the convenience of extrapolation to the surface moisture content.
6. Observation of crack formation should be done with the help of a magnifying glass. Net shrinkage strain at the observed crack starting time should be recorded for estimating the criterion used in the program of the likely first appearance of surface check.

2.3.3 Data Processing

Data collected from the experiment should be carefully processed both for further use in the tests and for the analysis of the final results. One of the important places to be mentioned in this test is to choose the points for defining the unconfined shrinkage. As the program uses an hyperbola to define the unconfined shrinkage strain, two elbows (knees) have to be carefully chosen from the measured unconfined shrinkage curve.

Extrapolation of the surface moisture concentration from the measured moisture profile is always suspect. Reduction of the thickness of the first few slices may increase the accuracy of the extrapolation.

2.3.4 Net Shrinkage

The test result indicated that the measured net shrinkage was much bigger than the prediction when there was no allowance for collapse. The possible reasons have been already mentioned in the previous section. To cope with this problem, the following suggestions were proposed for the next run:

1. Carefully select the boards being tested to minimize the possibility of the collapse formation;
2. Measure the creep strain component and Young's Modulii;
3. Infer the mechano–sorptive strain component and collapse from the measured net shrinkage and the computer program.

2.3.5 Control and Weighing Systems

Mass balance on the air across the timber stack showed that negative values of the moisture loss from the stack, calculated from the measurement of air temperatures, were sometimes observed. This might indicate that the sensors for measuring wet and dry bulb temperatures at inlet and outlet positions were not accurate. Thus the sensors have to be carefully checked with standard thermometers at these two positions. For more accurate calibration of the thermometers and the measurements of the surface transfer coefficients, an automatic weighing system was installed at the later stages of research.

2.4 Conclusion

It should be pointed out that the initial tests reported here were influenced by such problems as a newly built kiln and first use of the control system. However, test results clearly indicated that based on properly measured initial properties of timber the DRYWOOD program can give quite accurate results in predicting both moisture content change and the net shrinkage strain formation. This confirmed the idea of using the program to increase the rate of understanding of the process of drying timber, and consequently develop new procedures under which timber is dried without drying defects. The tests also exposed areas where further research should be conducted.

CHAPTER 3

AIR FLOW THROUGH A TIMBER STACK

Air flow through a timber stack is one of the many areas involved in the process of timber drying which are still not well documented in the forest products literature. The pattern of air flow so completely determines the heat and mass transfer between the air and the wood that it controls the rate of drying of the wood in the early stages and interacts with the diffusion of moisture within the wood in the later stages. The control of surface checking requires an understanding (at the quantitative level) of how the properties of the drying air interacts with those of the wood to affect the stresses at the surface of the wood.

Greenhill[19] used a vane anemometer to measure the air flow through a timber stack. He reported the effect of rate of air circulation on the rate of drying of timber in narrow stacks, but his measurements are suspect because they indicate a friction factor increasing with Reynolds Number where all other reports indicate a decrease. Sharma and Jain[20] and Jain and Sharma[21] studied the air circulation inside a kiln using an "Alnor" vane velometer by inserting its probe into gaps on the inlet side of the stack. The instruments used in those studies had some limitations, such as the length of time needed to carry out each measurement. Also, the large dimensions of these instruments made it impossible to measure at a sufficient number of positions across the small gap to establish the shape of the boundary layers. Nassif et al[22] measured the air flow profile through a timber stack with a

hot wire anemometer, type DISA 55M. The measurements were conducted at one position of the flow passage under various fan speeds. Although the velocity profiles at that point were reported, no quantitative analysis was made on the measured data. Also, the flow development along the board, turbulence, and pressure drop were not measured.

The necessary step for constructing the equations to describe the heat and mass transfer processes over a board surface requires detailed studies of the air flow. The first step in this discussion was a detailed study of the flow pattern made possible by the small spacial discrimination of modern hot–wire anemometers. The measurements were first conducted with the flow along the board, i.e. roughly perpendicular to the saw marks, whereas in commercial practice the flow is across the boards. This was done because many experimental kilns used this condition so the results are relevant to them. It was anticipated at this stage that broad features of the flow would be much the same in both cases, although the numbers may change. The experiments for finding out the differences between the two cases were described in the later part of the chapter.

3.1 Developing Air Flow in the Space between Two Layers of Flat Boards

Although the equations to describe fluid motion are well described in most modern text books on fluid mechanics[23], their application to the situation of flow through a stack of timber is repeated here for the sake of coherence.

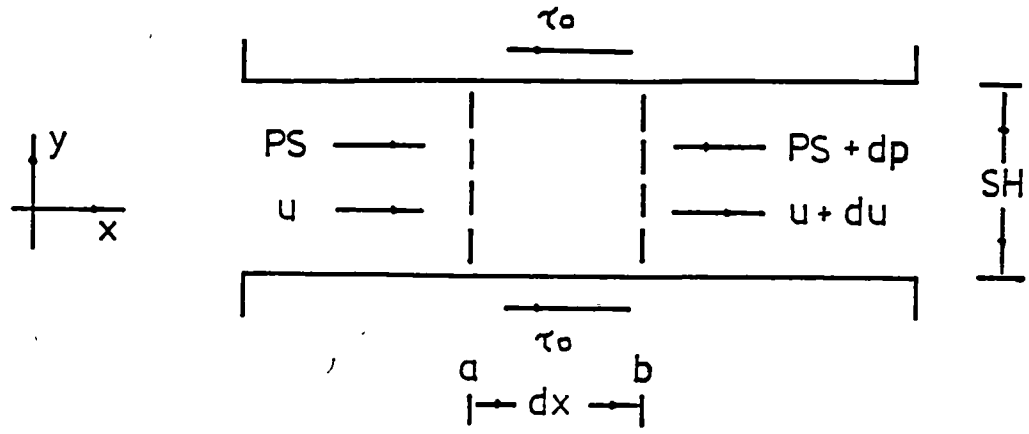

Figure 3.1

Air Flow Between Two Layers of Timber Boards

The flow is assumed to be two–dimensional steady flow and having a boundary layer growing on each timber surface. Consider an element of the flow with unit length normal to the xy plane as shown in Figure 3.1, the total mass flux across the element is given by

$$M = \int_0^{SH} \rho_{mair}\, u\, dy \qquad (3.1)$$

In the presence of boundary layers having a maximum velocity of U in the free stream, it is usually more accurate to direct attention to the velocity deficiency U–u than to the absolute value u. One definition of the displacement thickness (δ^*) is the amount that the wall should be displaced to allow a uniform velocity to have the same mass flux as the actual flow, i.e.

$$M = \rho_{mair}\, U\, (SH - \delta^*)$$
$$= \int_0^{SH} \rho_{mair}\, u\, dy \qquad (3.2).$$

When the flow is incompressible, ρ_{mair} is constant, and δ^* is given by

$$\delta^* = \int_0^{SH} (1 - u/U)\, dy \qquad (3.3)$$

where the value of δ^* includes the growth on both upper and lower surfaces. In the presence of temperature and moisture gradients through the boundary layer, Equation (3.3) must be modified, but Equation (3.2) still applies.

Equation (3.2) is based on mass conservation because no matter is created or destroyed so that M must be the same for all sections along the space when the flow is two dimensional. Thus, the first check on the measured values of velocity is always based on Equation (3.2) because it depends on the first power of the velocity. It should be pointed out that when drying wet timber, there is small change in M due to addition of water vapour evaporated from the boards but this can be easily estimated and the effect is usually very small.

Newton's law that force equals rate of change of momentum applies only to particles so that rate of change must follow a particle path. The general definition of rate of change of momentum of the particle (dx dy) is

$$\frac{d}{dt}(\rho_{mair}\, u\, dx\, dy) = \frac{\partial}{\partial t}(\rho_{mair}\, u\, dx\, dy) + \frac{dx}{dt}\frac{\partial}{\partial x}(\rho_{mair}\, dx\, dy) \qquad (3.4).$$

In steady flow, we have $\partial/\partial t = 0$ and along a particle path $dx/dt = u$ so that rate of change of momentum in incompressible flow is equal to (ρ_{mair} dxdy u $\partial u/\partial x$) for a particle. When this is integrated across the flow passage, we have a momentum flux given by

$$F = \int_0^{SH} \rho_{mair}\, u^2\, dy \qquad (3.5).$$

The change of momentum flux between two sections at a and b shown in Figure 3.1 must be balanced by the forces on the control volume bounded by these sections and timber surfaces.

As is the case with mass flux, it is usually more accurate in the presence of boundary layers to direct attention to momentum flux deficiency rather than the absolute value. If all of the total mass flux in Equation (3.1) had velocity U, the momentum flux would be given by

$$\begin{aligned} F1 &= \int_0^{SH} \rho_{mair}\, u\, U\, dy \\ &= M\, U \end{aligned} \qquad (3.6).$$

Whence the momentum flux deficiency is

$$F1 - F = \int_0^{SH} \rho_{mair}\, u\, (U - u)\, dy \qquad (3.7).$$

Following Von Karman, the momentum flux deficiency thickness (θ) is defined by

$$F1 - F = \rho_{mair}\, U^2\, \theta \qquad (3.8)$$

from which it follows that

$$\theta = \int_0^{SH} (u/U)(1 - u/U)\, dy \tag{3.9}$$

where θ is the sum of the momentum thickness for both surfaces, and then the actual momentum flux is given by

$$F = M\, U - \rho_{mair}\, U^2\, \theta \tag{3.10}$$

In the presence of temperature and moisture gradients a small modification of Equation (3.10) is required, but it appears that this is negligible in this context.

The forces on the control volume arise from the difference in static pressure ($PS_a - PS_b$) and the shear stresses (τ_0) on the timber surface whence we get

$$PS_a\, SH + M\, U_a - \rho_{mair}\, U_a^2\, \theta_a - PS_b\, SH - M\, U_b + \rho_{mair}\, U_b^2 \theta_b - 2\, \tau_0\, dx = 0 \tag{3.11}$$

Equation (3.11) enables the calculation of the surface shear stress τ_0 from the measurements on velocity and static head drop.

3.2 Air Flow Along the Board

3.2.1 Examination of the Uniformity of the Inlet Air Flow

Uniformity of the inlet air flow to the timber stack is one of the major factors which determines whether the flow through the stack is two dimensional or three dimensional. Since the analysis of the board surface

friction, and hence the heat transfer is restricted to the two dimensional case, two dimensional steady flow through the stack must be assured. Also, this is the situation to be aimed at in commercial operation to ensure uniform drying.

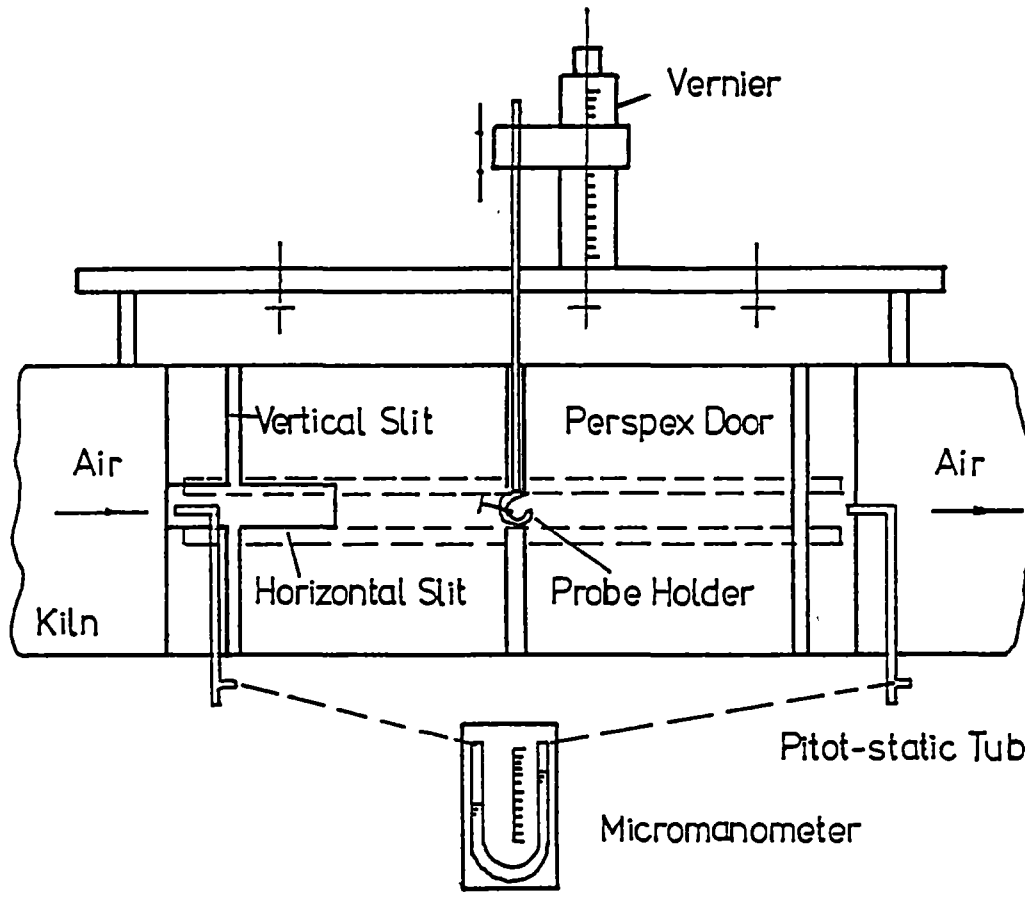

Figure 3.2

Set–Up of Measurements

The inlet air flow was examined by measurement of the variation of the total pressure head at the entrance position (clear of the stack) by a traverse across the middle of the flow in each of vertical and horizontal directions. The total head was measured with a total head tube connected to a Betz micromanometer. The other leg of the micromanometer was open to

atmosphere, so the value of the total head was relative to the atmospheric pressure. The total head tube was held by the probe holder shown in Figure 3.2, in which the tube was moved both vertically and horizontally.

Table 3.1

Examination of the Inlet Air Flow (One Screen)

Distance From	Distance from Tunnel Bottom (mm)				
Tunnel Wall	90	150	200	300	380
(mm)	Total Head (mm water)				
5	–0.20	–0.30	–0.25	–0.30	–0.30
155	–0.22	–0.30	–0.25	–0.22	–0.23
305	–0.25	–0.25	–0.22	–0.23	–0.25
385	–0.25	–0.25	–0.25	–0.27	–0.27
435	–0.25	–0.22	–0.25	–0.27	–0.25

Table 3.2

Examination of the Inlet Air Flow (Two Screens)

Distance From	Distance from Tunnel Bottom (mm)				
Tunnel Wall	50	90	190	290	380
(mm)	Total Head (mm water)				
80	–0.26	–0.26	–0.27	–0.29	–0.29
200	–0.26	–0.27	–0.28	–0.29	–0.29
300	–0.29	–0.29	–0.28	–0.29	–0.29
425	–0.29	–0.27	–0.29	–0.29	–0.29
470	–0.29	–0.29	–0.29	–0.29	–0.29

Note: Negative values of total head indicate pressures less than atmospheric.

Table 3.1 shows the results of the measurement with one layer of wire screen (wire thickness : 0.4 mm and spacing : 1.2 mm) at inlet to the converging section. Table 3.2 shows the result with two layers of screen, which indicates that more uniform inlet air flow was obtained with the addition of the extra screen. The differences in Table 3.2 are very near the limits of sensitivity of the micromanometer.

3.2.2 Measurement Preparation

1. Hot Wire Anemometry Techniques

The technique of hot–wire anemometry for measuring air flows is now well established and widely used. In the present investigation, the hot wire measurements were obtained with a DISA Type 55A01 constant temperature anemometer and locally constructed probes. The mean velocity was obtained from the non–linearized anemometer output voltage using the corresponding calibration curve. The R.M.S. value of non–linearized voltage fluctuations was read from a pointer–type voltmeter on the anemometer.

The hot–wire probes consisted of a 8 micrometer diameter tungsten wire element with a temperature coefficient of resistance of 0.0042 Ω /Ω/^{o}C, spot–welded to 0.5 mm diameter nickel wire prongs. The prongs were sharpened at the ends to reduce flow distortion as much as possible, and flattened slightly to permit a reasonable weld. The supporting prongs were mounted by means of a plastic moulding compound on a 6.5 mm O.D. stainless steel tube probe shaft. Each prong was connected via insulated electrical conductor to a socket soldered to the other end of the shaft, which attached to a co–axial cable lead from the anemometer. Detail of a typical probe is shown in Figure 3.3.

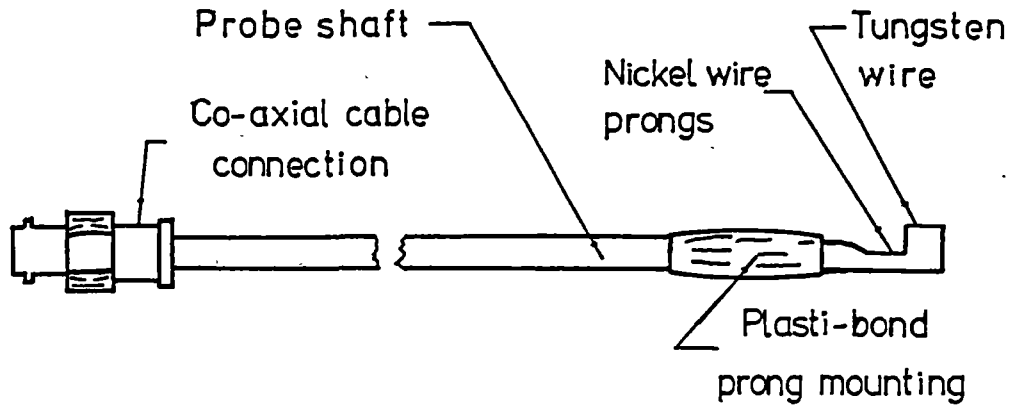

Figure 3.3

Hot Wire Probe

Calibration of hot–wires was carried out in a low turbulence level, closed circuit calibration tunnel designed and constructed at the University of Tasmania. It has a single stage fan with thin circular arc blades driven by a 2 h.p. D.C. motor with continuously variable speed control. Hot wire probes were calibrated in the working section against a pitot–static tube as standard. Velocity head was measured with a BETZ micromanometer (TYPE 250) reading to 0.02 mm of water, which is related to the local air speed (U) by the equation[24]

$$H_{air} = H_w \, \rho_{water} / \, \rho_{mair} = U^2 / (2\,g) \qquad (3.12)$$

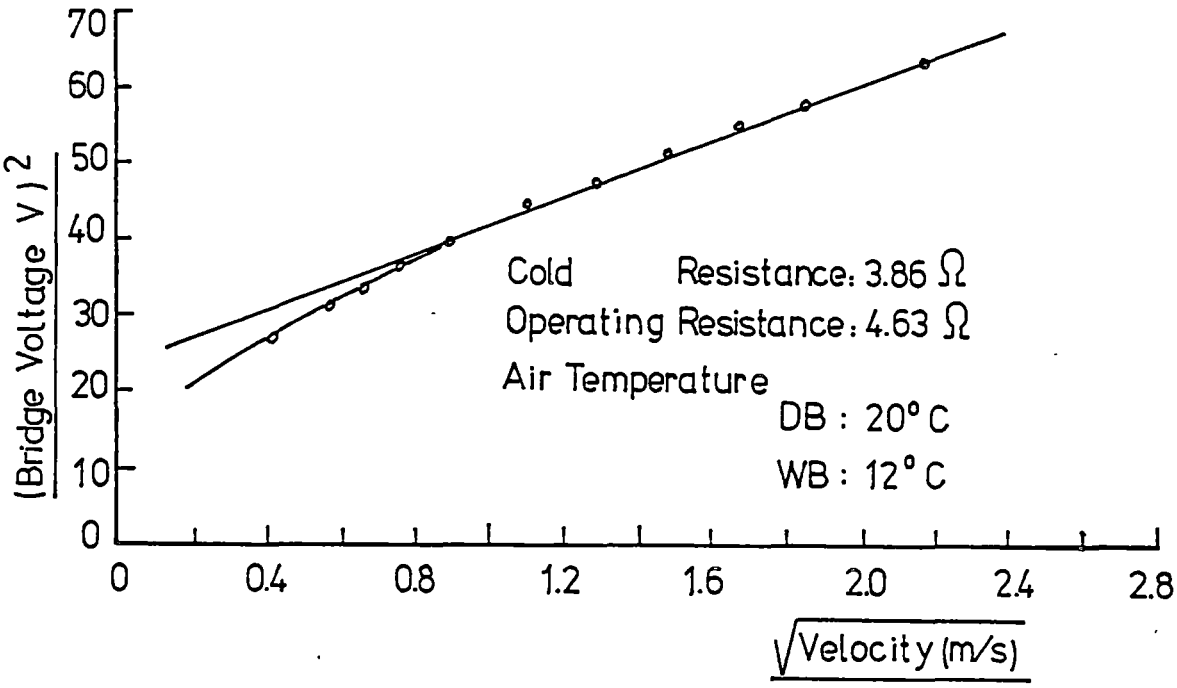

Figure 3.4

Typical Hot–Wire Calibration Curve

The calibration curve was plotted with the bridge voltage squared as ordinate and the square root of flow velocity as abscissa. A typical calibration curve is shown in Figure 3.4. It should be noted that the method of plotting assumes that the heat transfer from the wire to the air is through a laminar boundary layer. At very low velocities, there is a significant contribution from "natural convection" (i.e. buoyancy effect). Because of this, the measured points at very low velocities were linked to form a calibration curve for that region, which was obviously separated from the one extrapolated from the straight line obtained in the higher velocity region. It needs to be mentioned that in this velocity range the reading of the manometer used to calibrate the hot wire probe was suspect because it was

close to the limit of sensitivity, so that the value of velocity would be doubtful.

The anemometer output voltage is subject to significant variation with atmospheric conditions, and to compensate for this a voltage correction (∇V) given by the following expression was applied[25].

$$\frac{\nabla V}{V} = -\left\{ 1.0 - 0.123\left(\frac{\theta}{T_m}\right)\right\} \frac{R_0\ \alpha\ \nabla T}{2(R_w - R_a)} + 0.18\frac{\nabla P}{P} \qquad (3.13).$$

To check the effect of the air draft and the environmental conditions on the hot wire, the calibration of the probe should be checked frequently when measuring in the dirty environment of a timber drying kiln. In measurements reported here, the recalibration of the probe was only done at the end of the measurement and indicated that the above mentioned effects in the present case were negligible.

2. Kiln Preparation

Eighteen kiln–dried boards were chosen for the measurements. To reduce the effect of collapse on the measurement, the boards were reconditioned with steam and then stacked in the kiln with spaces of 20 mm between them. The surface roughness of the boards measured with an optical microscope over a 1.7 mm diameter field was 0.34 mm peak–to–valley with an occasional 'whisker' 0.15 mm long standing up from the surface. The space between the kiln side wall and stack edge was blocked by sponge rubber strips both upstream and downstream to reduce flow in this space.

A perspex door of the drying chamber was made to replace the original one of aluminium. As shown in Figure 3.2, one horizontal slit upstream and three vertical slits upstream (60 mm from the entrance to the stack), middle of the board, and downstream (60 mm from the end of the stack) were cut through the door, so that the probe could be put into the kiln without opening the door. These slits were kept closed by adhesive packing paper where not filled by the probe.

The support shown in Figure 3.2 was built to hold the probe, so that it could be moved in either vertical or horizontal direction. The position of the probe was read from the vernier fixed on the support. It was later found that accurate determination of the distance above the board surface from which the readings of measurement were taken was very important for calculating properties of the boundary layer. Difficulty was, however, encountered in placing the wire close to the surface because the very rough surface of the sawn board broke the wire very easily when the wire was put too close to it. It should be pointed out that changes in boundary layer thickness measurements were so slow at the velocities examined that errors in these did not much affect the final conclusions. Also, the surface of a sawn board is so rough that there seems to be no practical way of defining an equivalent plane as an origin for y.

3.2.3. Measurements in the Entrance Region

The measurements in the entrance region were conducted with the hot wire probe moved in small steps from the leading edge under a fixed free stream velocity. At every chosen distance from the leading edge the hot wire

probe was moved vertically from one surface to another to measure the velocity profile and the turbulence level across the space. It should be pointed out that at the same level above the board surface variation of the anemometer reading across the width of the stack was observed in the measurement. This implies variation of the velocity across the width of the stack, apparently due to variations in thickness of the air gap due to distortions of the boards. To ensure all the measurements were conducted at the same distance from the stack side, a straight line parallel to edge of the stack was drawn on the inner part surface of the chosen boards and measurements were conducted along that line.

Percentage of turbulence was calculated from the measurement of the longitudinal turbulent fluctuation by the method recommended in the instruction manual for the anemometer, i.e.

$$\text{Percentage of Turbulence} = 100\ V_{rms}\frac{4\ V}{V^2 - V_0^2} \qquad (3.14)$$

where V_0 was obtained at the time the hot wire probe was calibrated in the wind tunnel (with the fan off).

Readings of the bridge voltage at free stream velocity of 4.35 m/s were transferred to velocities with the corresponding calibration curve. The velocities were then plotted against the distance from board surface in Figure 3.5 for different cross–sections along the space. It can be seen that after the air enters the space a separated shear layer develops and quickly grows in thickness. At $R_{el} = U\ l/\nu$ about 10000 (where l is the distance from the leading edge) it starts to decrease; and the boundary layer regrows from

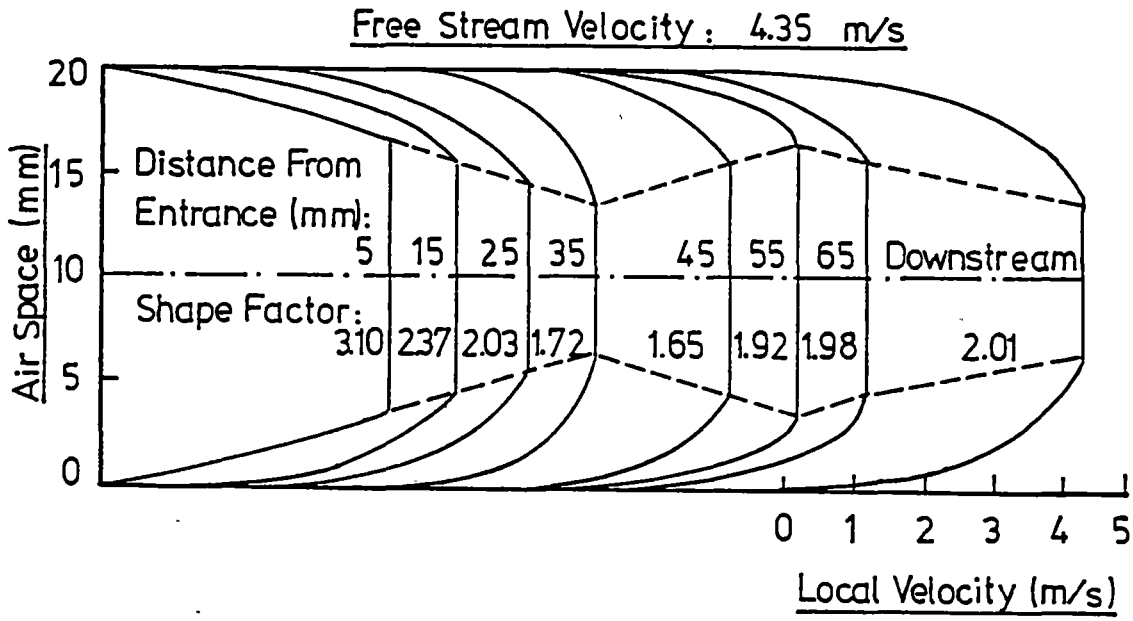

Figure 3.5

Velocity Profiles at Different Distances from Entrance

about R_{el} =17000 until downstream. This implies that the separated shear layer from the end of the board reattaches to the board surface at about R_{el} = 17000. It is not clear from these measurements whether R_{el} is the appropriate non–dimensional number to define the length of the separation bubble.

Based on the measured velocity profiles, values of displacement and momentum thickness were calculated from Equations (3.3) and (3.9) by the trapezoidal method and plotted in Figure 3.6. It can be seen that the same development pattern as the boundary layer shown in Figure 3.5 was observed. The shape factor (H) was calculated from displacement thickness (δ^*) and momentum thickness (θ) as

$$H = \frac{\delta^*}{\theta} \tag{3.15}$$

which is also plotted in Figure 3.6.

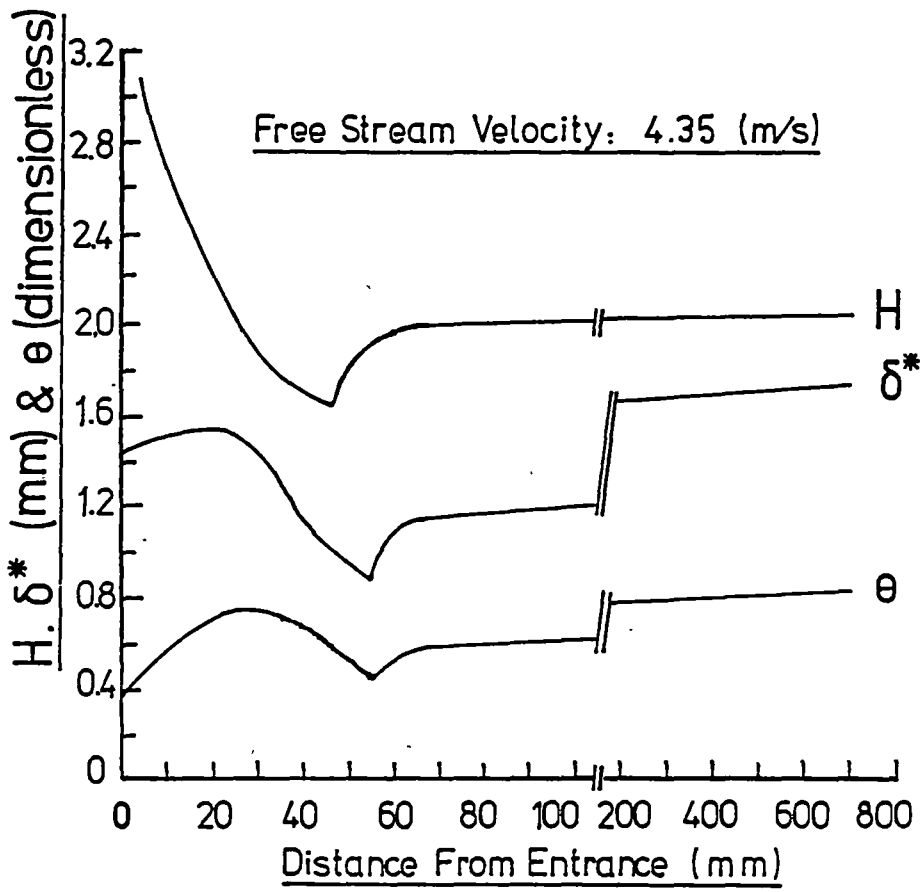

Figure 3.6

Variation of the Boundary Layer Properties

Examination of the variation of the shape factor against distance from the leading edge indicates that the calculated value of H is about 3.0 at $R_{el} = U\,l/\nu = 1400$, which decreases as the flow moves forwards along the board and reaches a minimum value of about 1.7 at R_{el}=17000. Existing literature in the area of fluid mechanics[26] indicates that the laminar separation occurs at the shape factor H about 3.7 for the flow over a smooth plate with

zero pressure gradient. A slightly higher value should be expected under the present situation of the rough surface. Thus, from this point of view, the calculated value of H is far less than the expected one. This difference appears to be caused by the following two reasons : difficulty in defining an origin for y as mentioned earlier, and physical impossibility of using hot wire probe to measure the backwards flow as those occurred in the entrance range because the hot wire has no directional sensitivity.

Measured percentage of turbulence was plotted against distance from the leading edge to about 70 mm in Figure 3.7 for the free stream velocities from 1.21 m/s to 5.5 m/s. From Figure 3.7 it can be seen that percentage of turbulence generally increases with the increase of the free stream velocity.

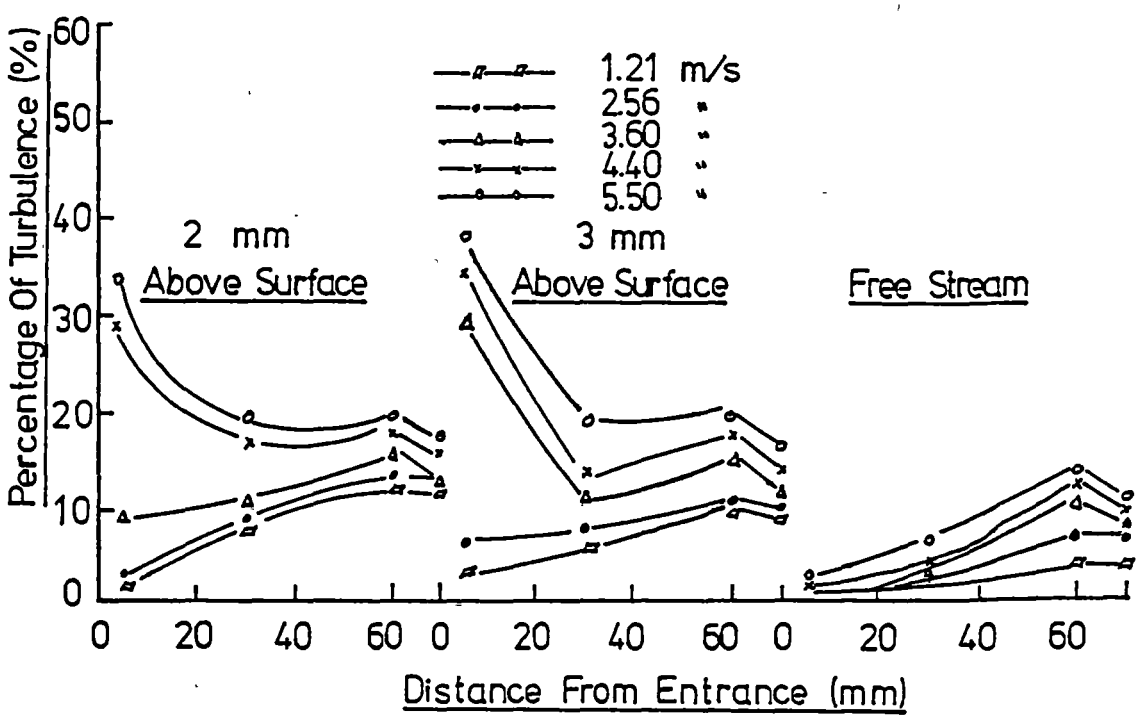

Figure 3.7

Variation of the Percentage of Turbulence in Entrance Area

Examination of the curves for the measurements in the free stream indicates that at the same free stream velocity percentage of turbulence increases as the flow proceeds along the flow passage and reaches a maximum at about 60 mm, i.e. about two board thickness, from the leading edge, then settles down to a smaller value. This reinforces the conclusions reached from the velocity profile measurement that the boundary layer flow reattaches to the surface at about 60 mm from the leading edge.

Measurements at 2 mm and 3 mm above the surface show that quite high turbulent fluctuation exists at the entrance to the flow passage, which reached up to about 30 to 40 percent of the local velocity at high free stream velocities being measured.

3.2.4 Measurements of the Pressure Drop along the Board

Measurements of the differences in static head between upstream and downstream stations were conducted with one BETZ micromanometer and two Pitot–static tubes set at the upstream and downstream stations for different velocities. The set–up of the measurement is shown in Figure 3.2, in which the Pitot static tubes were fixed on the perspex door of the drying chamber with the heads of the tubes facing upstream.

When the flow is parallel to the board surface the static pressure across any cross–section is constant, except for small variations due to turbulence. Thus, the measurement of the static head can be obtained by a single measurement anywhere in the cross–section.

Table 3.3

Measurement of the Pressure Drop

*D–head up–A	down–B	Voltage up–C	Velocity from A	B	C	S–head drop	T–head drop
mm water		V		m/s		mm water	
0.01	0.01	5.70	0.41	0.41	0.43	0.01	0.01
0.09	0.10	6.34	1.23	1.29	1.20	0.09	0.06
0.39	0.40	7.20	2.56	2.59	2.62	0.30	0.20
0.60	0.62	7.40	3.17	3.22	3.17	0.50	0.46
0.86	0.90	7.60	3.79	3.86	3.77	0.70	0.66
1.19	1.20	7.80	4.46	4.48	4.41	0.92	0.90
1.55	1.59	8.00	5.09	5.16	5.10	1.27	1.25
1.95	2.00	8.10	5.71	5.79	5.57	1.60	1.56
2.41	2.49	8.30	6.35	6.46	6.35	1.99	1.92
2.99	3.10	8.48	7.07	7.21	7.02	2.49	2.45

* D–Head: Differential Head,

T–Head: Total Head,

S–Head: Static Head,

Up–upstream, Down–downstream.

To check the accuracy of the measurement, the hot wire anemometer was also set up at at the upstream station to measure the velocity at the place where the static head was measured. Comparison was made between the velocities obtained from the hot wire probe and from the pitot–static

tube (based on the measurement of the differential head). Table 3.3 shows the details of the measurements, from which it is seen that reasonable agreement of the values from the two methods was obtained. The static head drop shown in Table 3.3 is plotted against free stream velocity in Figure 3.8.

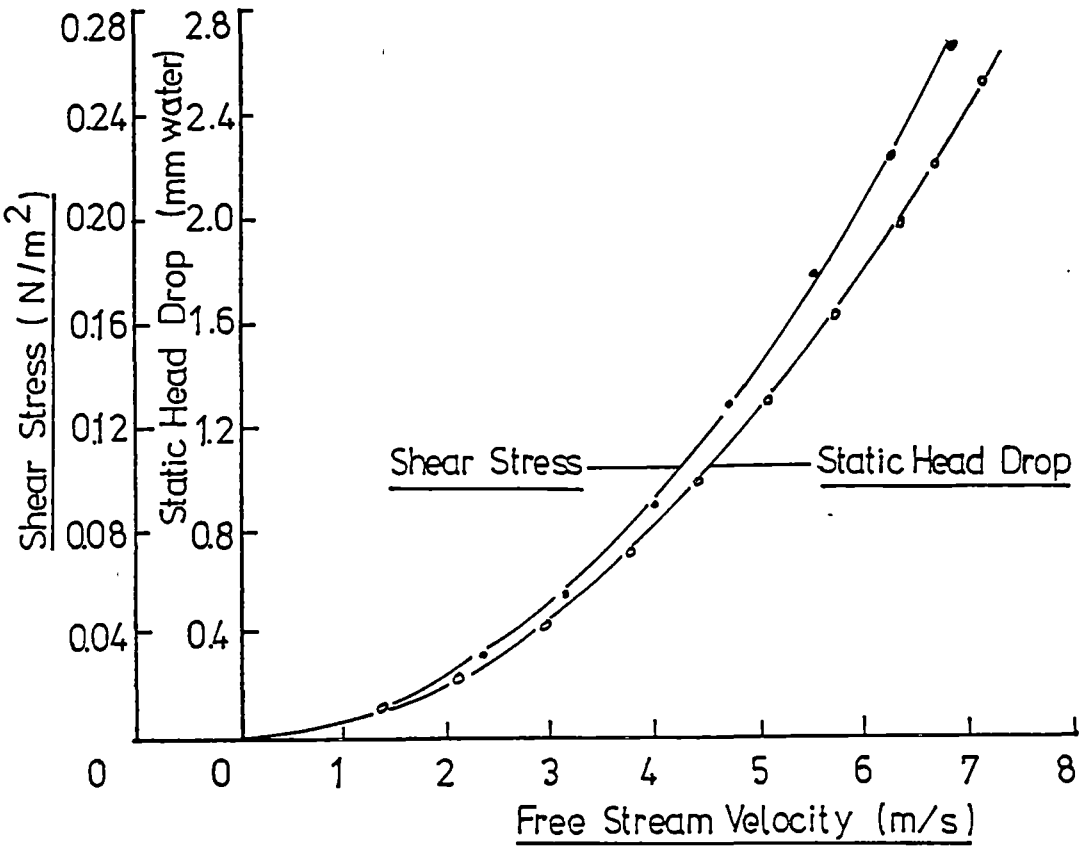

Figure 3.8

Static Head Drop and Surface Shear Stress

3.2.5. Measurements at the Upstream and Downstream Stations

1. Overall Measurements

The air flow development through the air space was measured at an upstream station (60 mm from the leading edge) and a downstream station (60 mm from the end of the stack). The kiln was set at atmospheric conditions with a dry bulb temperature of 11 °C and wet bulb temperature 8 °C. The measurement was conducted from a free stream velocity of 0.60 m/s to about 7 m/s. At each free stream velocity, velocity profiles and turbulence levels across the space were measured.

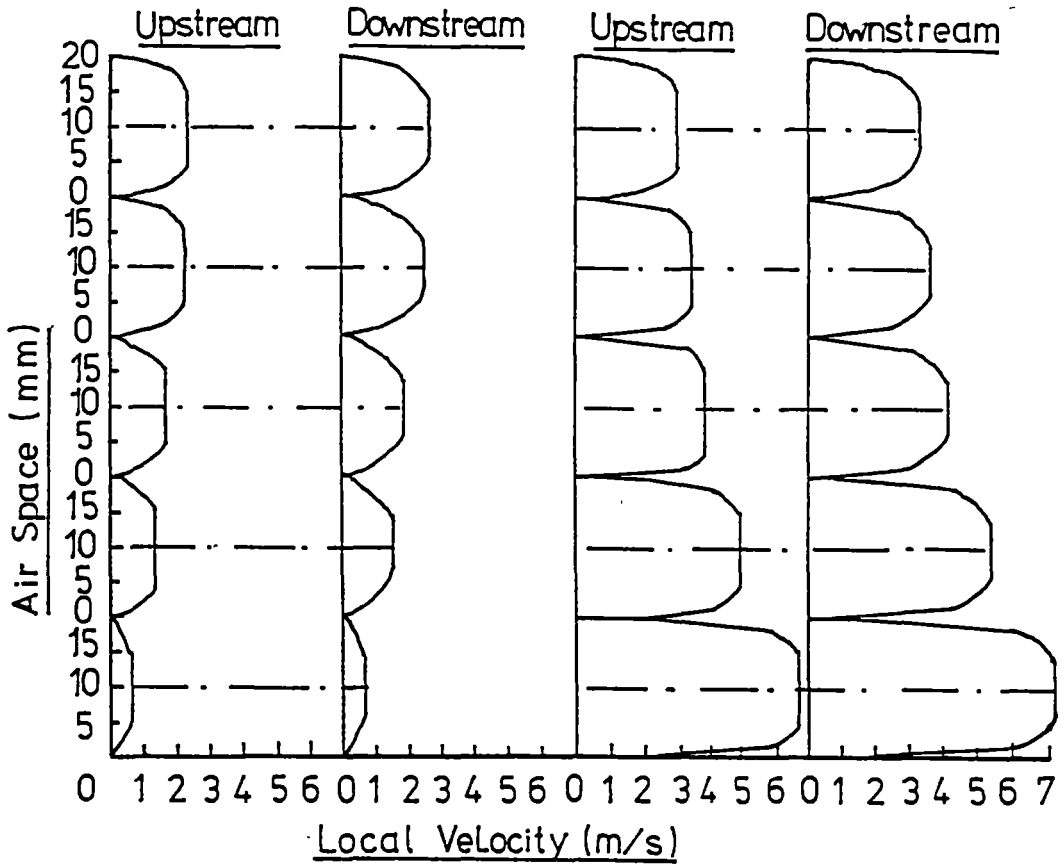

Figure 3.9

Measured Velocity Profiles

Readings of the bridge voltage from the hot wire anemometer were transferred to velocities with the calibration curves such as shown in Figure 3.4, which were then plotted against distance from the board surface in Figure 3.9 to show the boundary layer development from upstream to downstream under different free stream velocities.

Based on the measured velocity profiles, the displacement thickness was determined from Equation (3.3), the momentum thickness from Equation (3.9), and shape factor from Equation (3.16) for the half space. The results are shown in the Table 3.4.

Table 3.4

Boundary Layer Properties at Different Velocities

Velocity		Upstream			Downstream			Mass Flow	
Up*	Down	δ^*	θ	H	δ^*	θ	H	Up	Down
m/s		mm			mm			Kg/m/sx10^{-2}	
0.60	0.60	2.72	1.03	2.64	2.72	1.03	2.64	1.02	1.02
0.96	1.02	2.81	1.07	2.62	3.11	1.24	2.51	1.62	1.64
1.30	1.46	1.42	0.65	2.18	2.11	0.99	2.13	2.62	2.63
1.66	1.82	1.48	0.69	2.12	2.04	0.95	2.15	3.32	3.39
2.20	2.50	1.26	0.61	2.07	1.98	0.97	2.04	4.51	4.70
2.37	2.62	1.24	0.60	2.06	1.58	0.74	2.14	4.87	5.17
3.00	3.35	1.18	0.61	1.93	1.53	0.78	1.95	6.21	6.65
3.42	3.66	1.06	0.53	2.00	1.54	0.79	1.96	7.17	7.26
4.97	5.42	1.04	0.58	1.80	1.14	0.63	1.80	10.5	11.3
6.66	7.24	0.95	0.52	1.81	1.01	0.54	1.87	14.1	15.3

* Up – upstream, Down – downstream.

Examination of Table 3.4 shows that the shape factor keeps at about 2.65 when $R_e\delta^* = U\ \delta^*/\nu < 200$, then decreases from this value with the

increase of the free stream velocity. According to Schlichting[27], the shape factor in the case of a smooth flat plate decreases from about 2.6 in the laminar regime to about 1.4 in the turbulent regime. Thus, for the present case of the rough surface, Table 3.4 implies that the boundary layer flow is laminar when $R_e\delta^*$ is less than 200 (free stream velocity less than 1 m/s), and above this value it transits towards turbulent. It is not clear from the calculation of H that at what free stream velocity the flow becomes fully turbulent as H might be higher than 1.4 for the rough surface.

Comparison of the shape factors at the upstream and downstream stations is made in Figure 3.10 in an attempt to further clarify the flow development. It appears that the calculated value of H is too variable to draw a general conclusion.

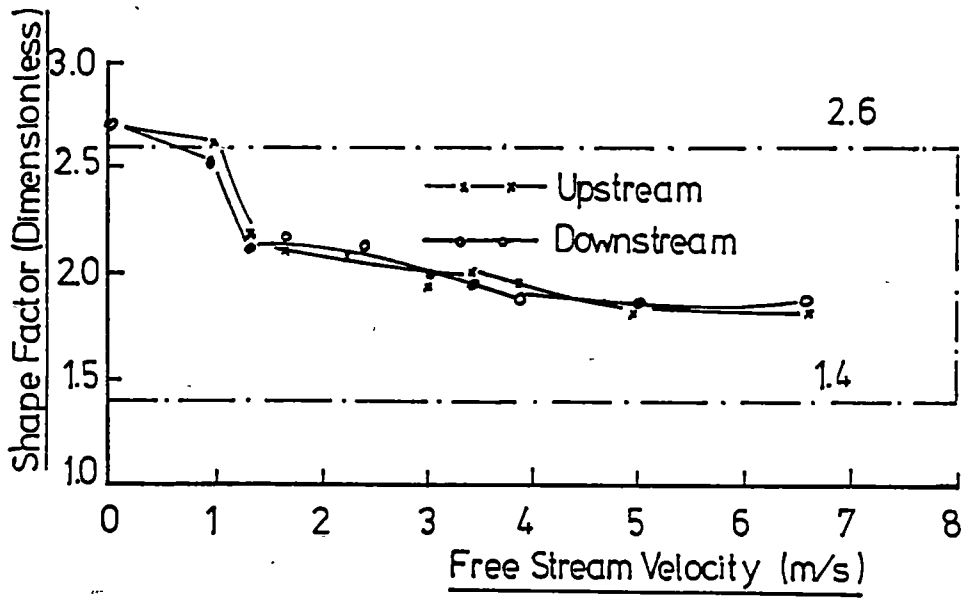

Figure 3.10

Variation of the Shape Factor

A check on the conservation of the mass flow was made by calculating the mass flux at upstream and downstream stations by Equation (3.2) and the result is shown in Table 3.4. It can be seen that the difference of the mass flux between upstream and downstream is very small in the low velocity range, and it slightly increases with the increase of the free stream velocity. This might be partly due to the problem in calculation of the displacement thickness because of the problem of establishing an origin for y, and partly due to variation of the fan speed at high power level which caused variation of the free stream velocity during a measurement (fan speed varies with changes in line voltage which was not controlled). There may also have been some cross–flow effects.

2. Flow at Low Reynolds Number

Under the present situation where a pressure gradient exists along the flow passage, if the boundary layer flow were truly laminar the appropriate equation would be when there is zero acceleration

$$\frac{dp}{dx} = \mu \frac{\partial^2 u}{\partial y^2} \tag{3.16}$$

where, since PS is independent of y, dp/dx is treated as a constant when integrating. The viscosity of air (μ) increases with air temperature and an accurate equation for calculating the viscosity of air is

$$\mu = 3.531 \times 10^{-3} (1.36 + 0.009\ T)/(T + 273.15) \tag{3.17}$$

where T is the air temperature (DB) in °C. Equation (3.16) is the same equation as for Couette flow between parallel walls except that the inner

boundary condition is at the edge of the boundary layer (y=δ) where u=U and the shear stress zero. Integration of this equation gives

$$\mu\, \partial u/\partial y = (dp/dx)\, y + \text{const.} \tag{3.18}$$

where at y=0, $\mu\, \partial u/\partial y = \tau_0$=const, which shows the shear stress varying linearly from τ_0 at the wall. Second integration of the equation gives

$$\mu\, u = \tau_0\, y + 0.5(dp/dx)\, y^2 \tag{3.19}$$

where, at y=0, u=0 so the constant of integration is zero. Equation (3.19) shows a parabola with vertex at the edge of the boundary layer.

A force balance in the space as shown in Figure 3.1 gives

$$SH\ dp/dx = -2\ \tau_0 \tag{3.20}.$$

We have $dp/dx < 0$, so τ_0 is positive in the equation. Then

$$\mu\, u = \tau_0\, y\, (1 - y/SH) \tag{3.21}$$

at y=δ, u=U so Equation (3.21) becomes

$$\mu\, U = \tau_0\, \delta\, (1 - \delta/SH) \tag{3.22}$$

which should be consistent with the linear variation of shear stress, i.e.

$$\tau/\tau_0 = 1 - y/\delta \text{ for } y < \delta$$

$$\text{then } \delta = 0 \text{ until } y = SH/2 \tag{3.23}$$

Differentiation of Equation (3.21) gives

$$\mu\, \partial u/\partial y = \tau_0(1 - 2y/SH)$$

Putting $\tau=\mu\ \partial u/\partial y$ equal to zero at $y=\delta$ gives $\delta=0.5$ SH, so we cannot neglect the $\partial u/\partial x$ term from this point of view. There is contradiction here in that we cannot put $\partial u/\partial y=\tau_0$ at y=0 as well as $\partial u/\partial y=0$ at $y=\delta$.

Table 3.5

Measured Velocity Distribution at Low Reynolds Number*

U (m/s)		1.54			0.96			0.60	
y	u	μu	A**	u	μu	B	u	μu	C
mm	m/s	$kg/s^2 x10^{-6}$		m/s	$kg/s^2 x10^{-6}$		m/s	$kg/s^2 x10^{-6}$	
0.0	0.000	0.00	0.00	0.000	0.00	0.00	0.000	0.00	0.00
0.5	0.300	5.55	8.20	0.140	2.59	3.60	0.079	1.48	2.07
1.0	0.599	11.1	16.9	0.269	4.97	7.50	0.160	2.96	4.26
1.5	0.741	13.7	26.1	0.305	5.64	11.5	0.185	3.42	6.59
2.0	0.879	16.3	35.6	0.339	6.27	15.8	0.210	3.89	9.05
2.5	0.919	16.9	45.7	0.415	7.67	20.4	0.275	5.08	11.6
3.0	0.959	17.7	56.2	0.489	9.04	25.1	0.340	6.29	14.4
3.5	1.070	19.8	67.2	0.579	10.7	30.1	0.390	7.22	17.2
4.0	1.170	21.6	78.6	0.670	12.4	35.3	0.438	8.10	20.2
4.5	1.260	23.3	90.2	0.739	13.7	40.8	0.480	8.90	23.3
5.0	1.350	24.9	102.	0.810	14.9	46.4	0.520	9.60	26.5
5.5	1.450	26.8	115.	0.884	16.3	52.3	0.559	10.4	29.9
6.0	1.540	28.5	129.	0.960	17.7	58.5	0.600	11.1	33.4

* measured at ambient conditions of 20 °C DB and 11 °C WB.

** $A = 0.016\ y + 0.915\ y^2$

$B = 0.007\ y + 0.457\ y^2$

$C = 0.004\ y + 0.261\ y^2$

where y is in metres.

The appropriate non–dimensional form of equation (3.21) appears to be

$$u/u^* = (y\ u^*/\nu)(1-y/SH) \tag{3.24}$$

in which, the friction velocity u^* is defined as

$$u^* = \sqrt{(\tau_0\ /\ \rho_{mair})} \tag{3.25}$$

and ν is the kinematic viscosity in m^2/s and is calculated from the equation

$$\nu = \mu\ /\ \rho_{mair} \tag{3.26}.$$

The fitting of Equation (3.19) with the measured velocity and calculated wall shear stress at the free stream velocities of 1.54, 0.96, 0.6 m/s is shown in Table 3.5 and plotted in Figure 3.11.

Figure 3.11 indicates that the plottings of the measured velocity profiles for free stream velocities of 0.60 and 0.96 m/s come to one curve, while that for 1.54 m/s is obviously different. This implies that at free stream velocity of 1.54 m/s the boundary layer flow is no longer laminar, which confirms the argument made from the calculation of the shape factors that the boundary layer flow was laminar with $R_e\delta^*$ less than about 200.

The fitting of Equation (3.24) to measured velocities is shown in Figure 3.12. It appears that a reasonable fit for the velocities of 0.6 and 0.96 m/s is obtained for regions near the surface. The difference in the outer parts of the boundary layer seems to be due to the fact that Equation (3.21) has its maximum velocity at the middle of the passage whereas we have a fairly well defined boundary layer thickness where the local velocity reaches a free stream value as a maximum.

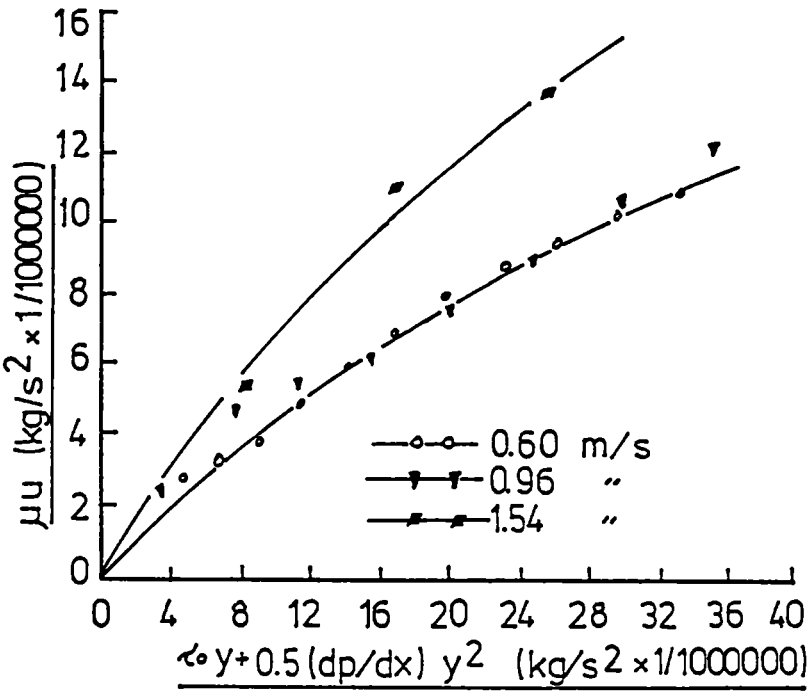

Figure 3.11

Measured Velocity Profiles

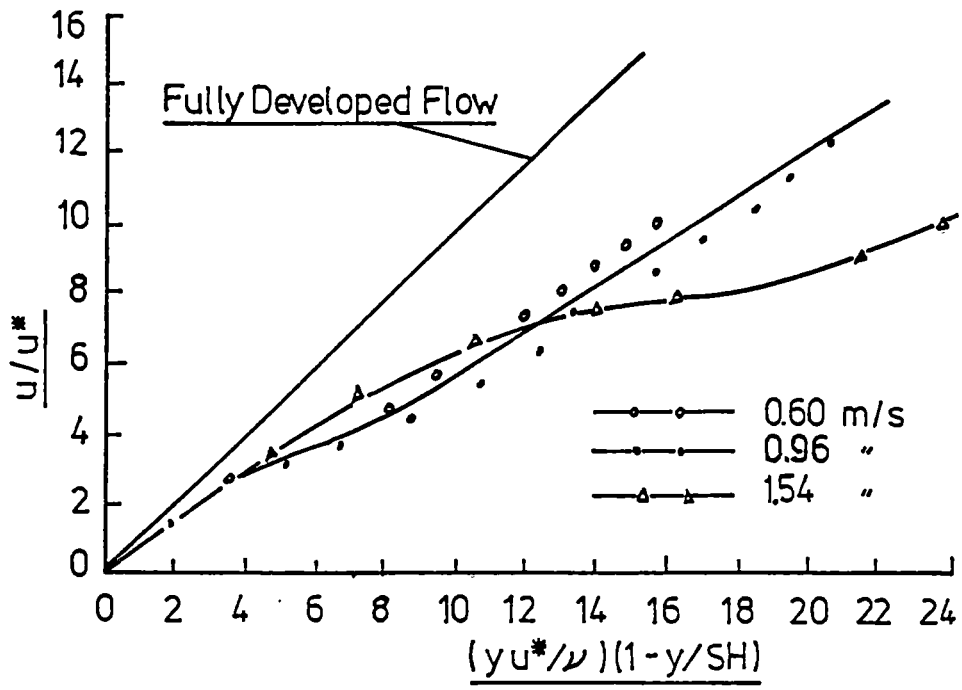

Figure 3.12

Measured Velocity Profiles

There are two other reasons which we might also expect to cause the measured values to differ from Equation (3.21). Firstly, the u du/dx term which has been dropped when writing Equation (3.16) is most likely to be significant in the outer parts of the boundary layer. Secondly, the eddies of transition to turbulence which have caused the separated laminar shear layer to reattach to the surface are dampened more slowly at points far from the wall.

The measured velocities were also processed to compare with Blasius's theory for the laminar boundary flow along a flat plate at zero incidence[27]. The original curve of Blasius's theory was plotted with the value of u/U against ($y\sqrt{[U/(\nu\, x)]}$). Here, x is defined as the distance from the virtual origin of a laminar boundary layer and is calculated from the momentum thickness as

$$\frac{\theta}{x} = \frac{0.664}{\sqrt{(U\,x/\nu)}} \qquad (3.26)$$

Due to the sharp corner of the board, the virtual origin of the laminar boundary layer was shifted to far upstream from the leading edge. Thus, direct measurement of x was impractical. To eliminate the effect of x, the value of u/U was plotted against y/θ in this study which relates to the term ($y\sqrt{[U/(\nu\, x)]}$) by a factor of 1/0.664. Table 6 shows the results of the calculation.

Table 3.6

Comparison of the Velocity Distributions

U(m/s):		1.54		0.96		0.60
θ (mm):		1.066		1.071		1.027
x (mm):		251.0		158.0		91.00
y	η	u/U	η	u/U	η	u/U
0.0	0.000	0.000	0.000	0.000	0.000	0.000
0.5	0.312	0.195	0.310	0.146	0.323	0.133
1.0	0.624	0.389	0.620	0.281	0.646	0.267
1.5	0.936	0.481	0.930	0.318	0.969	0.308
2.0	1.250	0.571	1.240	0.354	1.290	0.350
2.5	1.560	0.597	1.550	0.432	1.610	0.458
3.0	1.872	0.623	1.860	0.510	1.940	0.576
3.5	2.180	0.695	2.170	0.604	2.230	0.650
4.0	2.496	0.759	2.480	0.698	2.580	0.730
4.5	2.810	0.818	2.790	0.770	2.910	0.800
5.0	3.120	0.877	3.100	0.844	3.230	0.867
5.5	3.432	0.938	3.420	0.921	3.550	0.933
6.0	3.744	1.000	3.720	1.000	3.876	1.000

* $\eta = y\sqrt{[U/(\nu\ x)]} = 0.664\ (y/\nu)$ and $\nu = 0.01576\ x10^{-3}\ m^2/s$ at an air temperature of 20 ^oC.

Results shown in the Table 3.6 were plotted to compare the measured velocity distributions and the one obtained from Blasius's theory. It can be seen from Figure 3.13 that the measured values for the free stream velocities of 0.6 and 0.96 m/s ($R_e\delta^*$ less than 200) show reasonable agreement with the Blasius theory for laminar flow, while for a velocity of 1.54 m/s a quite big difference is observed in the early part of the curve.

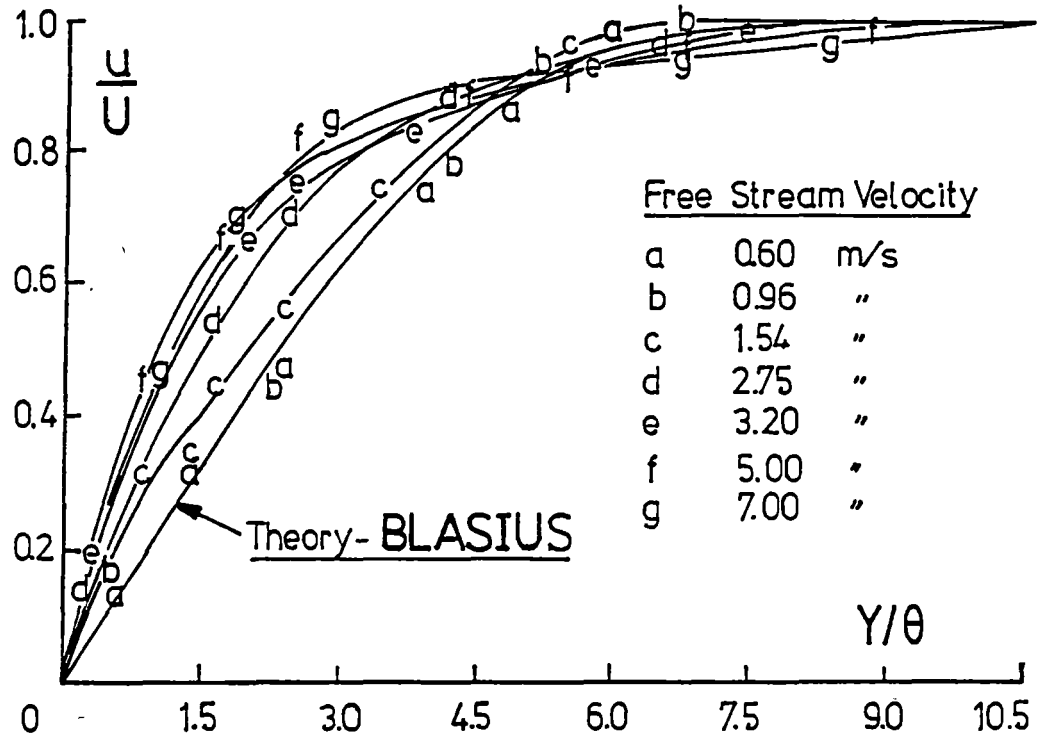

Figure 3.13

Velocity Distribution Over the Board Surface

The close agreement between the measured velocity profiles at low Reynolds number and the Blasius solution for a laminar boundary layer growing with zero pressure gradient seems to indicate that, even at these low values of Reynolds number, the wall shear stress is the quantity that largely determines the velocity distribution.

It is apparent that Equation (3.16) gives a very poor description of the measured velocity distribution. All that can be said about these measurements appears to be that molecular viscosity is an important effect near the surface. The evidence all points to the flow being essentially laminar although unlike any of the expected laminar boundary layers. According to the measurements quoted by Schlichting[27], in the case of the boundary

layer flow over a smooth flat plate transition from laminar to turbulent flow takes place at $(U\ x)/\nu = 300000$, which corresponds to a value of $R_e\delta^* = (U\ \delta^*)/\nu$ about 950. This clearly shows the effect of the board roughness and the entrance flow separation on transition from laminar to turbulent flow in the boundary layer flow in a timber stack.

3. Flow at High Reynolds Number

Figure 3.13 shows the comparison between the measured velocity profiles and that from Blasius's theory for the laminar flow. Obvious differences in the shape of the plots between the measured ones and the theory can be observed for all the free stream velocities greater than about 1 m/s. The difference seems to increase as the free stream velocity increases.

For the free stream velocities above about 1 m/s, the ratio of u/u^* was plotted against LOG $(y\ u^*/\nu)$ in Figure 3.14 to compare the measured velocity profile with the equation established for the turbulent flow in smooth pipe, that is

$$\frac{u}{u^*} = 2.5 \ln (y\ u^*/\nu) + 5.5$$

$$= 5.75 \text{ LOG } (y\ u^*/\nu) + 5.5 \qquad (3.27).$$

Quite large differences were observed for all flows. The reason appears to be that the equation was established for fully developed turbulent flow through a smooth pipe, while we have developing flow over very rough surfaces. The first point in the curve of u/u^* against LOG$(y\ u^*/\nu)$ is always suspect because of the difficulty of fixing the origin of y as already discussed.

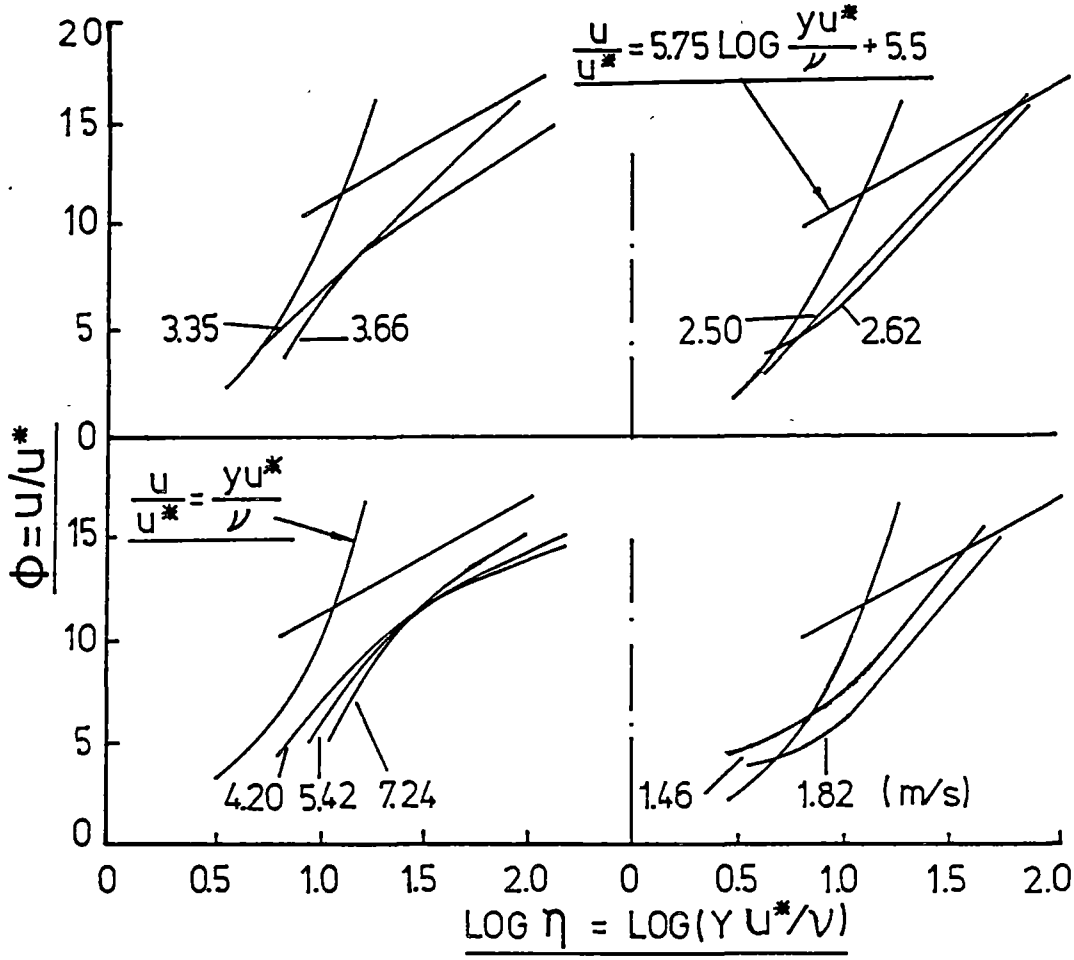

Figure 3.14

Universal Velocity Profile for the Flow along Board

4. Turbulence Measurement

To further identify the flow development, turbulence was measured at each velocity at upstream (about 70 mm from the leading edge) and downstream stations. Percentage of turbulence related to the local velocity (POTl) was calculated by the method described in the section 3.2.3. Figure 3.15 shows the curves of POTl against free stream velocity at 1 mm, 2mm

and 3 mm above the board surface and free stream. From Figure 3.15 it can be seen that POTl is less than about 5 % of the local velocity when the free stream velocity is less than about 1 m/s. As the velocity increases from this value, however, POTl quickly increases and at the free stream velocity of about 1.5 m/s it reaches up to about 15 % of the local velocity at 1 mm and 2 mm above the surface and 10 % at 3 mm. This implies that transition from the laminar to turbulent starts at the free stream velocity of about 1 m/s. According to the turbulent fluctuation measurements quoted by Schlichting[27] for the turbulent boundary layer flow over a smooth plate at zero incidence, percentage of turbulence near the wall reaches up to about 10 % of the free stream velocity at $R_{el}=U\,l/\nu=4.2x10^6$ Thus, this measurement implies that the flow becomes turbulent boundary layer flow with the free stream velocity greater than about 1.5 m/s.

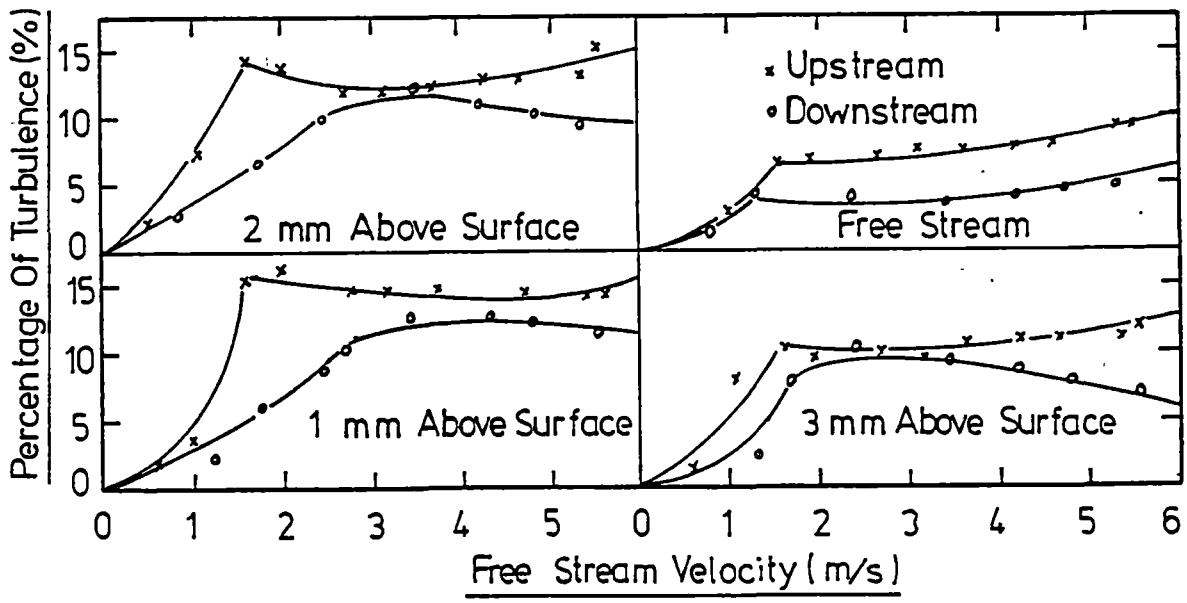

Figure 3.15

Turbulence at Different Free Stream Velocities

From Figure 3.15 it can be seen that the upstream values of POTl in free stream is quite high (up to about 9 % of the free stream velocity). This seems to include some effect of the flow reattachment to the surface in the entrance region.

Figure 3.15 also show that POTl at downstream is less than that at upstream for all the velocities being measured. This appears to indicate that a laminar sub–layer develops from upstream to downstream and eddies created by the roughness elements on the surface of the board are slowly damped by molecular viscosity. It is not clear from these measurements at what critical Reynolds number the eddies grow from upstream to downstream.

5. Calculation of the Friction Factor

Based on the calculated surface shear stress, values of the friction factor were calculated. Two definitions are available for the friction factor, one is based on the free stream velocity defined as

$$f = \frac{\tau_0}{0.5\ \rho_{mair}\ U^2} \tag{3.28}$$

and the other is based on the mean velocity across the air space defined as

$$f = \frac{\tau_0}{0.5\ \rho_{mair}\ U_m^2} \tag{3.29}$$

where U_m is defined as

$$\begin{aligned} U_m &= M/(SH\ \rho_{mair}) \\ &= U\ (SH - \delta^*)/SH \end{aligned} \tag{3.30}.$$

The friction factor based on the free stream velocity is needed for heat and mass transfer calculations, while the other is required for the kiln designer. Thus, both of the friction factors were calculated in this study (Table 3.7), which were then plotted against the Reynolds number based on the space height (SH), i.e.

$$R_{esh} = \frac{U_m \, SH}{\nu} \qquad (3.31).$$

Table 3.7

Calculation of the Friction Factor

F–stream velocity	Shear stress	Friction factor	Mean velocity	Friction factor 1	Friction factor 2	Reynolds number
U	τ_o	u*	U_m	f(U)	$f(U_m)$	R_{esh}
m/s	N/m^2	m/s	m/s			$x10^3$
1.38	0.01198	0.1011	1.12	0.01073	0.0162	1.4
1.74	0.01939	0.1286	1.43	0.01092	0.0162	1.8
2.35	0.03225	0.1685	1.96	0.00996	0.0142	2.5
2.50	0.03612	0.1755	2.14	0.00989	0.0135	2.7
3.16	0.05765	0.2217	2.74	0.00981	0.0131	3.4
3.54	0.07634	0.2551	3.08	0.01038	0.0138	3.9
4.02	0.08910	0.2756	3.90	0.00949	0.0124	4.9
5.20	0.16460	0.3746	4.63	0.00949	0.0131	5.8
6.95	0.26890	0.4788	6.02	0.01037	0.0126	7.6

A relation between U_m and U was fitted from Table 3.7 as

$$U_m = U/1.08 - 0.1996 \qquad (3.32).$$

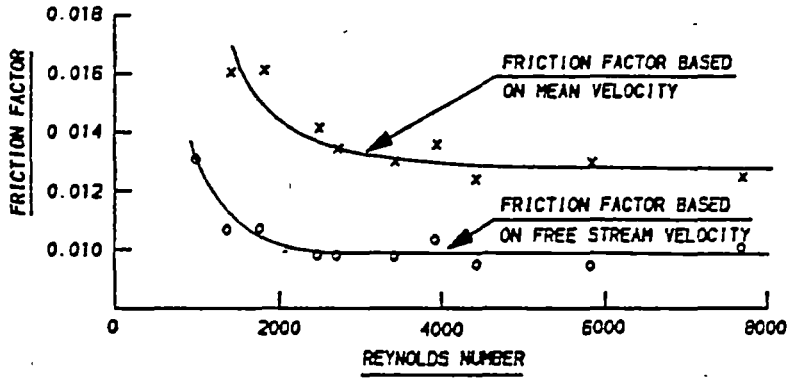

Figure 3.16

Friction Factor for Flow along Board

Figure 3.16 shows the plot of the friction factors against Reynolds number (R_{esh}) defined in Equation (3.31), from which the following functions were fitted for f based on the free stream velocity U

$$f = \begin{cases} A\,(R_{esh} - 2500)^2 + 0.01 & \text{at } R_{esh} \leq 2500 \\ 0.01 & \text{at } R_{esh} > 2500 \end{cases} \tag{3.33}$$

where $A=1.42\text{x}10^{-9}$ and

$$f = \begin{cases} B\,(R_{esh} - 3400)^2 + 0.013 & \text{at } R_{esh} \leq 3400 \\ 0.013 & \text{at } R_{esh} > 3400 \end{cases} \tag{3.34}$$

where $B=1.2\text{x}10^{-9}$ for f based on the mean velocity U_m. Equations (3.33) and (3.34) show general agreement with the same kind of measurement conducted by other researchers on rough pipes.

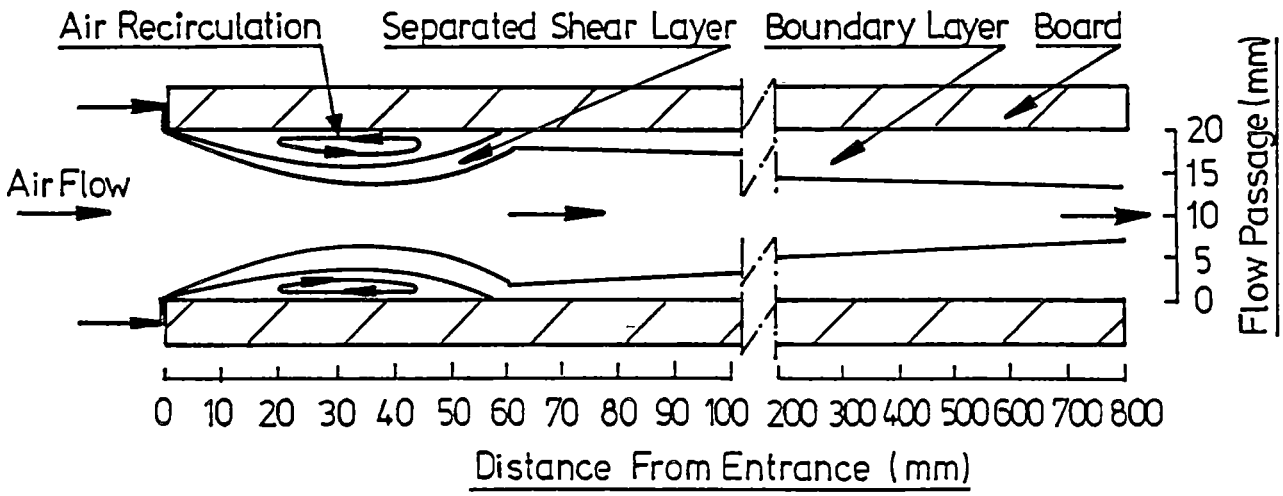

Figure 3.17

Air Flow Development between Two Layers of Sawn Boards

3.2.6 Summary of the Measurements

The measurements described above indicate that air flow along the length of the board in a timber stack is a complicated process and differs from patterns usually obtained. Based upon those measurements, several points can be made:

1). Air flow from far upstream meets the edge of the board at a stagnation point as shown in Figure 3.17. The flow accelerates along the board end and the effect of the surface spreads out the flow into a boundary layer.

2). The boundary layer formed on the edge of the board appears to be laminar for all practical velocities but this laminar boundary flow contains many turbulent fluctuations due to disturbance from the surface of the rough edge of the sawn board.

3). The laminar boundary flow separates from the board surface at the sharp corners of the flow passages, and becomes a separated shear layer which quickly transits towards turbulent flow.

4). As the flow proceeds, the separated shear layer quickly develops in thickness and reaches a maximum at $R_{el} = U\ l/\nu$ about 10000 (U is about 4.7 m/s), then reattaches to the board surface at R_{el} about 17000, which encloses a region of slowly recirculating flow as shown in Figure 3.17. This is the common situation as usually reported. It was assumed to be the same here but was not measured because the hot wire has no directional sensitivity. After R_{el} about 17000, the flow regrows as an attached boundary layer until downstream.

5). At the same free stream velocity, the percentage of turbulent energy in the free stream increases after the flow enters the flow passage, and reaches a maximum at R_{el} about 17000, then settles down to a smaller value.

6). At the same free stream velocity, the percentage of turbulence decreases from upstream station to downstream station.

7). With $R_e\delta^*$ less than about 200 (free stream velocity is less than about 1 m/s), the boundary layer flow from upstream to downstream is laminar.

8). The process of the boundary layer flow transition from laminar to turbulent is fairly fast and from the free stream velocity about 1.5 m/s the flow becomes turbulent boundary layer flow.

9). The friction factor based on the free stream velocity and mean velocity across the flow passage is about 0.010 and 0.013 for R_{esh} greater than about 2500 and 3400 respectively.

3.3 Air Flow Across The Board

Measurements on the boundary layer flow through a timber stack have been made with the flow along the board. The details of the method being used and the experimental results were reported in the last section.

When the flow is across the board as used in the commercial kiln, the boundary layer flow should be expected to be somewhat different because of the difference in the surface resistance to the air flow. Furthermore, as the boards dry, shrinkage gaps appear between edges of the boards. These gaps cause vertical circulation of the air flow. The effect of the vertical flow circulation on the edge drying is expected to be more significant in the case of the flow across the boards.

The purpose of this section is to present the experimental results with the flow across the board. Emphasis was placed on finding the difference in the surface friction between flow along the board and flow across the board at the different stages of the drying process.

3.3.1 Improvement of the Equipment

The first measurements carried out disclosed the need to improve part of the system.

1. Time Stability of the Mean Speed of the Air

In the first installation, the power feeding the motor was supplied by a SLIDER speed controller (TYPE S–260–10); this controller was replaced with the variable speed D.C. drive controller manufactured by ZENER ELECTRIC PTY. LIMITED (Model DC750A). The time stability turned out to be sufficiently improved, so that it was possible to measure the static pressure by direct comparison with the external pressure.

2. Hot wire probe holding equipment

Measurement of the flow development along the flow passage requires the probes to be moved continuously from the upstream station to downstream station. This was done in the previous measurement by shifting the probe holder from the upstream station to downstream station so the measurement could only be made at those two points. For the convenience of these tests, a small trailer was built and one long horizontal slit was cut on the perspex door of the test section, which enable the probe to be continuously moved in a range of about 800 mm.

3.3.2 Timber Stack Set–up

Kiln–dried quarter–sawn boards, 28 mm thick, 480 mm long, and 120 mm wide were stacked in the working section of the air conditioned wind tunnel with a 20 mm high space between two layers of the boards. The stack was so arranged that air flow was across the board surface, i.e. approximately parallel to the saw marks. The space between the kiln side wall and the stack edge was blocked by sponge rubber strips as described earlier.

It should be pointed out that the flow development and the pressure drop along the flow passage largely depend on the state of the surface of the boards, which varies with the state of the saw that cut them, evenness of the board thickness, and the stage of drying of them. Different arrangements were therefore made in measuring the flow development and the pressure drop to simulate the conditions at the different stages of the drying process.

Measurements on the flow development were conducted with the surface of the boards maintained at the same level and the board edges touching. This was done by choosing the kiln–dried boards with the same thickness to reduce the difficulty in moving the hot wire probe along the flow passage. Also, this is the situation expected in the commercial kiln at the early stage of the drying process. This arrangement was similar to the arrangement used for the measurement of the flow along the board so that direct comparison could be made between the two sets of measurements.

The pressure drop measurements were made with the arrangements of the boards being measured:

(a) flat surface level with the edges touching (arranged with the boards having the same thickness);

(b) flat surface level with shrinkage gap between neighbouring boards;

(c) varying surface level with shrinkage gap (arranged with the boards having different thickness).

The last two arrangements were made to simulate the situation expected at the later stage of the drying process and find out the effect of the

shrinkage gaps between the boards and the uneven shrinkage in the board thickness direction on the surface friction. The gap being used was about 5 mm corresponding to 120 mm wide board with about 5 % shrinkage.

3.3.3 Experimental Results

1. Development of the Flow along the Flow Passage

Flow Development along the flow passage was measured by travelling the hot wire probe from the leading edge to the downstream station. Velocity profiles and percentages of turbulence at different Reynolds numbers (R_e) were measured at chosen cross–sections.

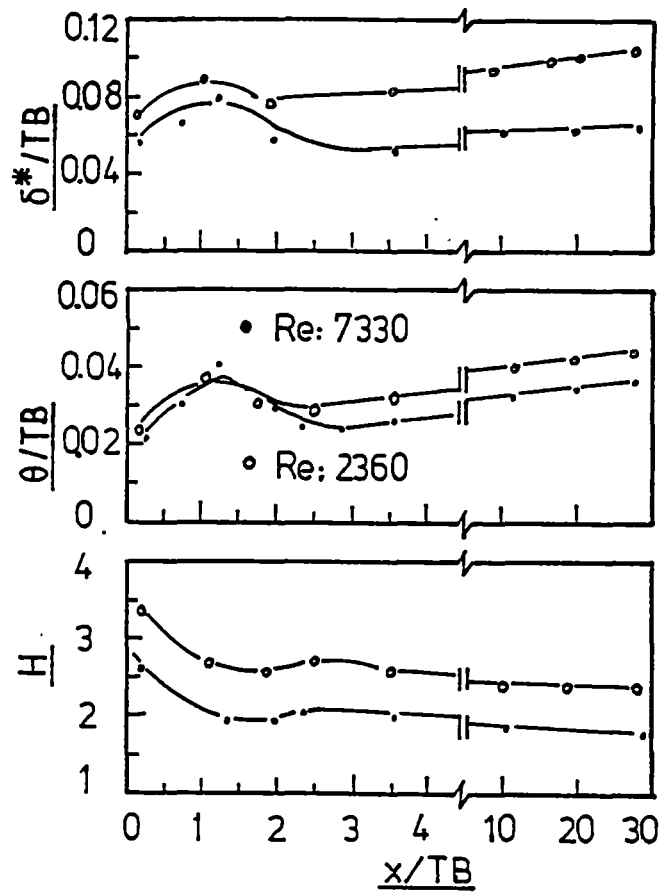

Figure 3.18

Variation of the Boundary Layer Properties

Figure 3.18 shows the variation of the calculated boundary layer displacement and momentum thickness and shape factor plotted against the board thickness. Quite big variation in all three parameters was observed in the range from the leading edge to the point about 3 times the board thickness, from which it was deduced that the flow pattern near the leading edge was much the same as previously reported.

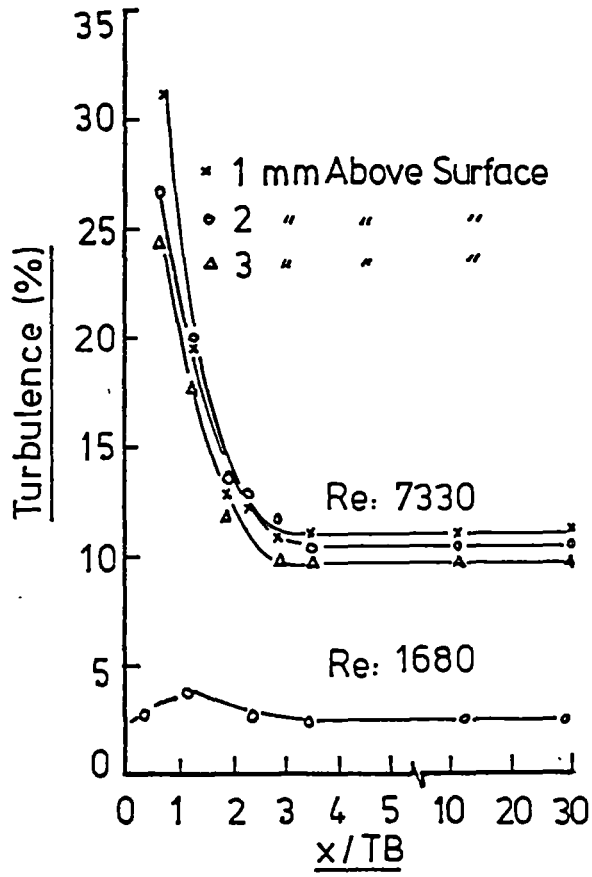

Figure 3.19

Variation of the Percentage of Turbulence

Figure 3.19 shows the variation of the percentage of turbulence along the flow passage. It can be seen that the peak turbulence for the case of high R_e was at the point close to the leading edge, while for the case of the low R_e it was at the point further inside the flow passage (about one board

thickness). Both of the curves seem to indicate that the percentage of turbulence settles down to a constant value after the point about 2.5 to 3 times the board thickness downstream of the leading edge, i.e. after reattachment.

Determination of the reattachment point with a tuft made from thin threads failed because the very rough surface of the board always stuck the thread when it was put close to the surface. At that stage it was decided to use smoke visualization. Two different kinds of smoke were tried in the measurement, one was generated by dry ice and warm water, the second was by light machine oil with a smoke generator. The smoke was injected to the flow passage with a pitot tube at the leading edge. Separation was observed under all the free stream velocities being measured and the point of the reattachment appears to lie between 2.5 and 3 times the board thickness. Ota and Itasaka[28] reported the measurement on the length of the separation bubble over a smooth flat plate and indicated that the flow reattachment occurs at about 4 to 5 times the plate thickness downstream of the leading edge. This difference is thought to be due to the difference between the flow separated after passing the smooth edge of a flat plate in Ota and Itasaka's measurement and the very rough edge of a sawn board in the present case.

2. Flow Pattern and Friction Factor at Different Free Stream Velocities

1). Flow Pattern

Measurement of the redeveloped flow downstream of reattachment was made at upstream station (about 100 mm from the leading edge) and downstream station (100 mm upstream of the trailing edge) under various

free stream velocities. Velocity profile, percentage of turbulence, and the pressure drop along the flow passage were made over a nearly straight surface of the boards for each free stream velocity. Table 3.8 shows the boundary layer properties calculated from the measured data.

Table 3.8

Boundary Layer Properties at Different Velocities

Velocity* up**	down	Upstream δ^*	θ	H	Downstream δ^*	θ	H	M–flow up	down	Static drop
m/s	m/s		mm			mm		$k_g/m/s$ x10 $^{-2}$		mm H_2o
0.34	0.40	2.99	1.17	2.55	3.25	1.29	2.52	0.56	0.63	0.008
0.85	1.04	2.28	0.87	2.62	3.07	1.17	2.61	1.54	1.68	0.042
1.30	1.48	2.10	0.84	2.49	2.35	1.04	2.25	2.41	2.66	0.082
1.69	2.02	2.11	1.07	1.98	2.23	0.99	2.24	3.12	3.60	0.160
2.40	2.75	1.96	0.99	1.97	2.12	1.01	2.08	4.50	5.00	0.280
2.86	3.24	1.62	0.79	2.07	1.97	0.95	2.07	5.63	6.08	0.405
3.85	4.40	1.40	0.73	1.92	1.69	0.91	1.86	7.84	8.55	0.750

* Free stream velocity;

** Up – upstream, Down – downstream.

Calculated shape factors at various free stream velocities are shown in Figure 3.20, from which it can be seen that the shape factor reduces quite quickly in the range of the velocities from about 1 to 2 m/s, then gradually deceases to about 1.9 at a velocity of 4.13 m/s.

Measured percentage of turbulence was calculated based on the local velocity and is also shown in Figure 3.20. Comparison with those for the flow along the board shows that at the higher velocity range the turbulence close to the surface was reduced about 2 to 3 percent in the present case.

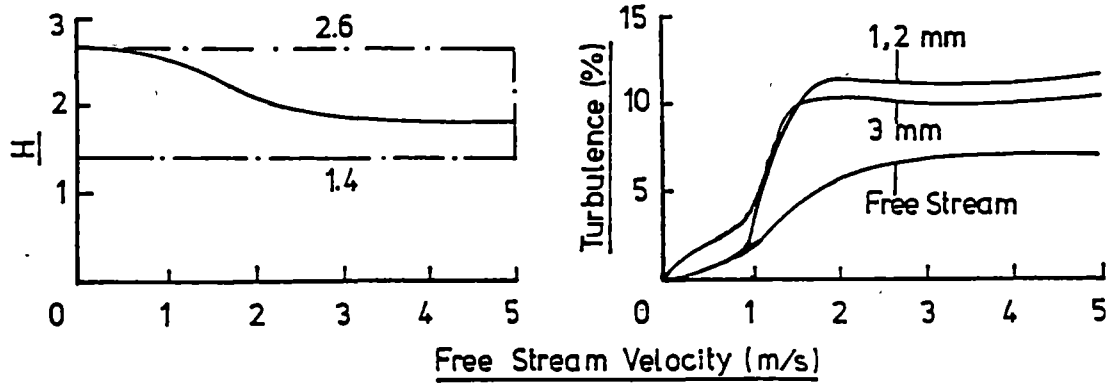

Figure 3.20

Shape Factor and Turbulence at Different Velocities

Curves in Figure 3.21 show comparison of the measured velocity profiles at three low free stream velocities and those from Equations (3.19) and (3.24).

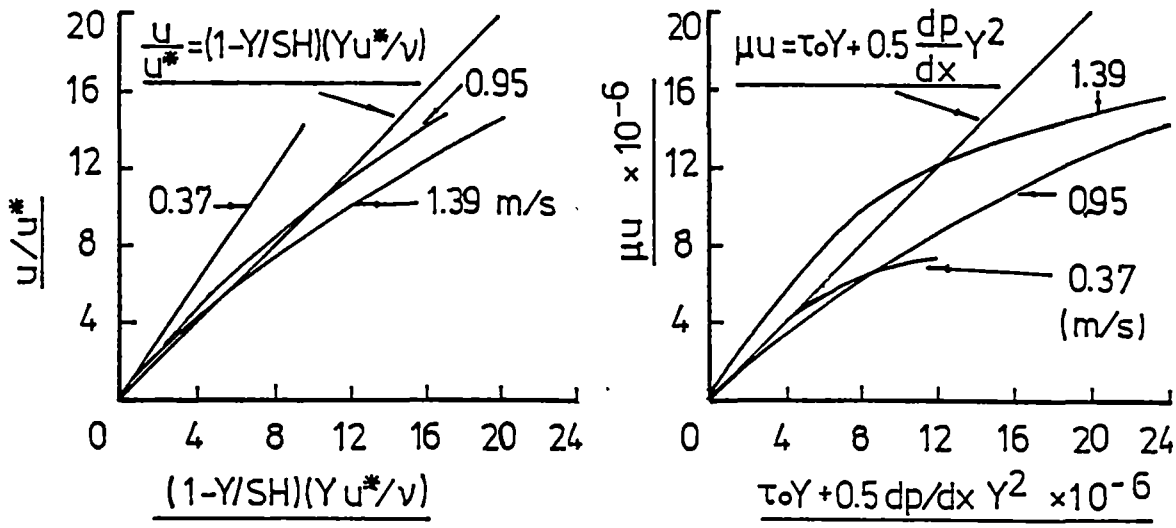

Figure 3.21

Measured Velocity Profiles for the Flow across Board

The measured velocity profiles at the higher free velocities were plotted in Figure 3.22 to compare with Equation (3.27). Examination of Figure 3.22 indicates that in the range close to the board surface the relationship

$$\frac{u}{u^*} = \frac{u^* y}{\nu} \tag{3.35}$$

can be seen from the measured velocity profiles under the two low free stream velocities. At two high velocity runs, however, the laminar sublayer portion of the curve disappeared. It can be also seen that as the free stream velocity increased, the measured velocity profile at the outer part of the boundary layer fell off and the shape of the velocity profile tended to become parallel to that from the formula. The significant difference between the measured velocity profiles and the formula in most of the boundary layer seems to indicate that the boundary layer flow is essentially in the transition range between laminar and turbulent in the velocity range measured.

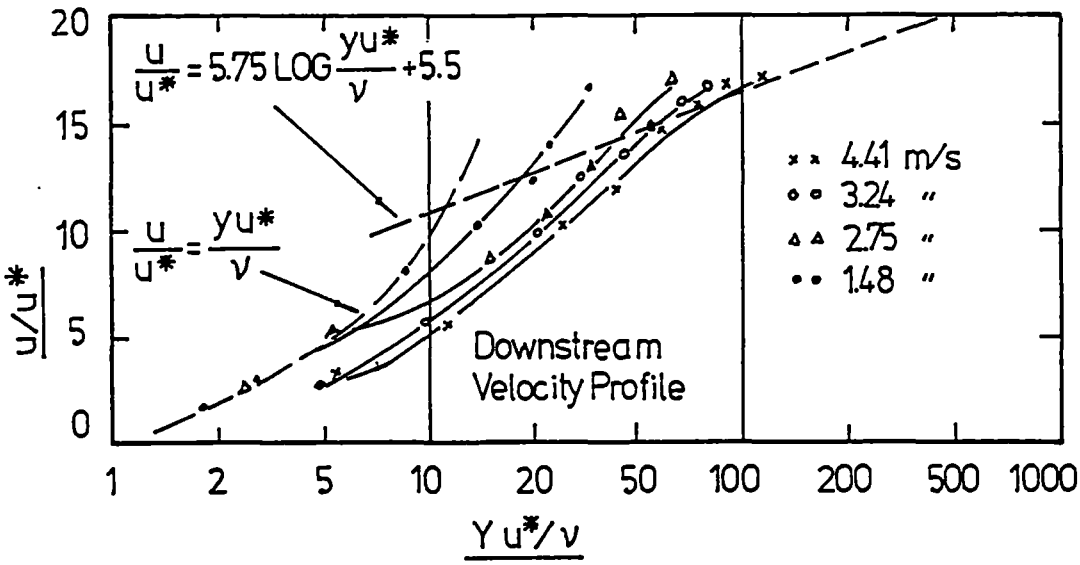

Figure 3.22

Universal Velocity Profile for the Flow across Board

The variation of the Clauser parameter G[29]

$$G = \frac{U}{u^*}\left(\frac{H-1}{H}\right) \tag{3.36}$$

at the downstream station under various free stream velocities is shown in Figure 3.23. This parameter is considered to be a significant measure of the departure of the turbulent boundary layer from the fully developed flow condition. From Figure 3.23 it can be seen that G is reduced from about 11 at a velocity of about 1 m/s to about 7.5 at a velocity of about 4.5 m/s, which is higher than the accepted value of 6.8 for a fully developed constant pressure boundary layer.

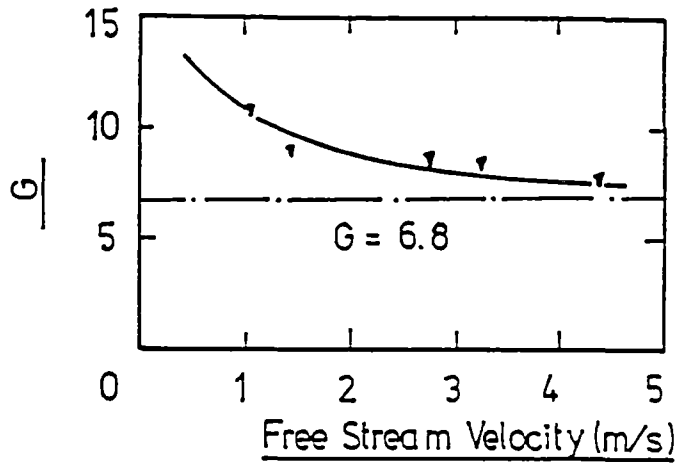

Figure 3.23

Clauser Parameter

Comparison of the measured velocity profiles at the downstream station with the Clauser's equilibrium velocity profile (G=6.8) is shown in Figure 3.24. Apparent departure from the fully developed condition can be seen in the velocity range measured.

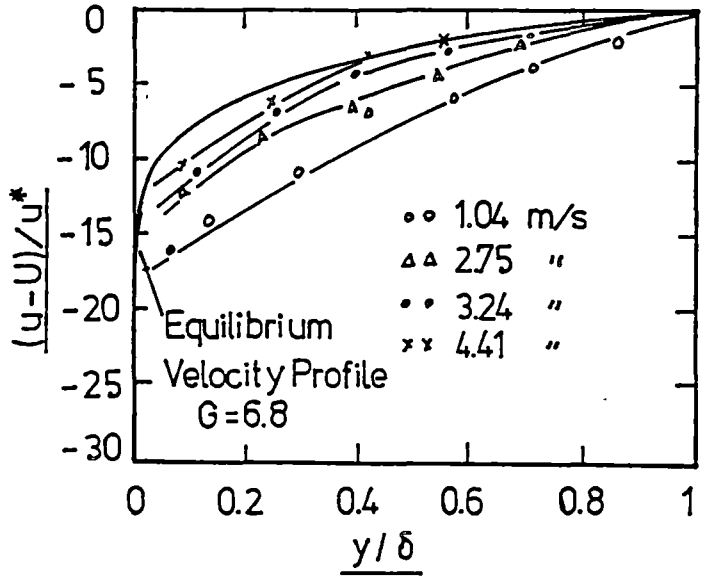

Figure 3.24

Measured Velocity Profiles for the Flow across Board

Thus, on the basis of the above arguments, it can be concluded that the boundary layer flow is essentially laminar up to a free stream velocity about 1.5 m/s, at the higher velocities the flow tends towards turbulent, but does not reach the fully developed condition in the velocity range measured.

2). Surface Friction

Figure 3.25 (A) shows the measurement on the static head drop over a flow passage about 700 mm long. Comparison of the pressure drop with that for the flow along the board indicates that at the same free stream velocity the present pressure drop is less than that for the flow along the board. Repeated measurements on the pressure drops shows the same sort of profile. The explanation for this situation might be that with the flow along the board, the flow was essentially perpendicular to the saw mark, while the flow

across the board was nearly parallel to the saw marks. When the surface of the boards within one layer was maintained at the same level, the saw marks provided more resistance to the air flow than in the case of the flow along the board.

Table 3.9

Calculation of the Friction Factor

F–stream velocity	Shear stress	Friction velocity	Mean vel.	Friction factor 1	2	Reynolds number	
U	τ_0	u*	U_m	f(U)	$f(U_m)$	R(U)	$R(U_m)$
m/s	N/m^2	m/s	m/s			x 1000	
0.37	0.0009	0.028	0.26	0.0115	0.0231	0.47	0.33
0.95	0.0042	0.060	0.69	0.0080	0.0149	1.21	0.88
1.39	0.0089	0.087	1.09	0.0079	0.0151	1.76	1.38
1.86	0.0154	0.115	1.43	0.0076	0.0130	2.36	1.82
2.58	0.0304	0.161	2.04	0.0078	0.0125	3.27	2.59
3.05	0.0437	0.193	2.51	0.0080	0.0118	3.87	3.19
4.13	0.0779	0.258	3.45	0.0078	0.0117	5.24	4.01

Based on the present experimental data, the surface shear stress and the friction factor were calculated and presented in Table 3.9 and Figure 3.25 (B, C).

From Figure 3.25 (C) it can be seen that the friction factor based on the free stream velocity has been reduced from 0.01 for the flow along the board to about 0.008 for the flow across the board at higher free stream velocities. It should be pointed out that the calculation of the heat and mass transfer described in Chapter 4 was based on the higher value of the friction factor, i.e. 0.01.

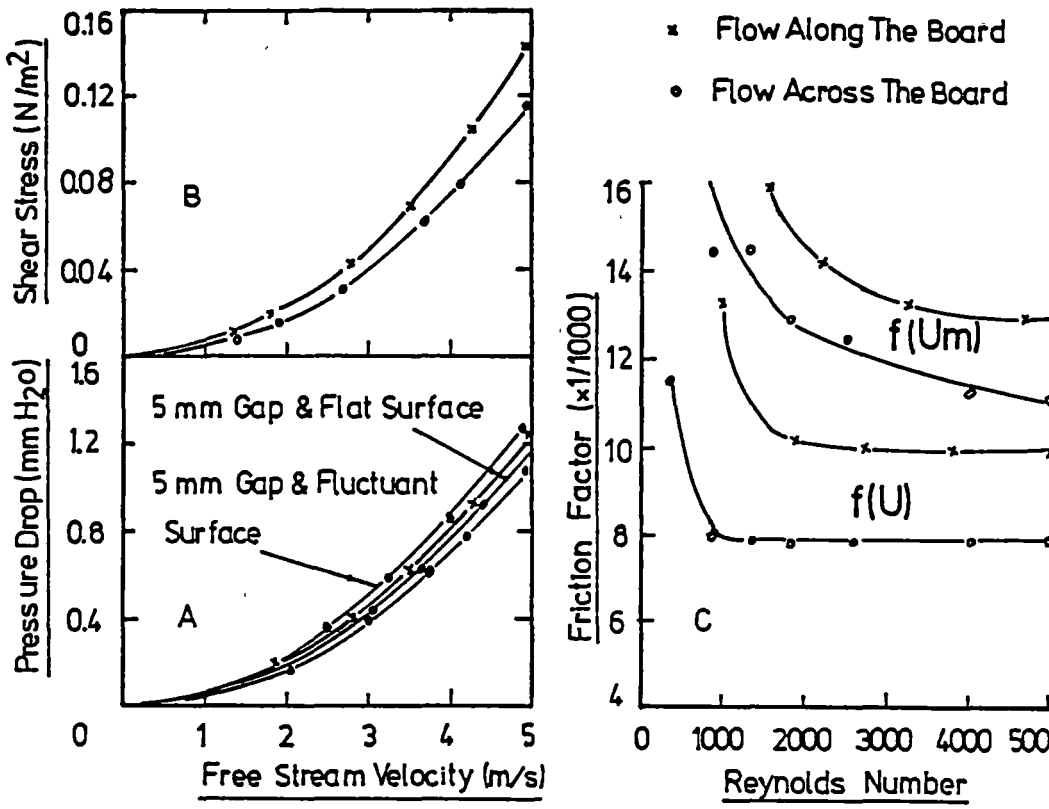

Figure 3.25

Pressure Drop, Surface Shear Stress and Friction Factor

The calculated friction factor was fitted to the following functions:

$$f(U) = \begin{cases} A\,(R_{esh}(U_m)-1000)^2 + 0.008 & R_{esh}(U_m) \leq 1000 \\ 0.008 & R_{esh}(U_m) > 1000 \end{cases} \qquad (3.37)$$

where $A=8.7\times10^{-9}$, and

$$f(U_m) = \begin{cases} B\,(R_{esh}(U_m)-5000)^2 + 0.011 & R_{esh}(U_m) \leq 5000 \\ 0.011 & R_{esh}(U_m) > 5000 \end{cases} \qquad (3.38)$$

in which $B = 25\times10^{-9}$.

The relation between the free stream velocity and the mean velocity was fitted as

$$U = 1.25\ U_m \qquad (3.39).$$

3. The Effect of the Shrinkage Gap

The pressure drops along the flow passage with 5 mm gap between the boards are shown in Figure 3.25 (A). Surprisingly, when the surface of the boards was maintained at the same level the static pressure drop was only slightly increased above that for the case of board edges touching. The possible reason for this situation might be that the flow passage was relatively short (only about 700 mm long) and four 5 mm wide gaps along the flow passage only made a small effect on the overall pressure drop. Also, the edges of the boards were not exactly straight and there must have been some gaps even when they were close together.

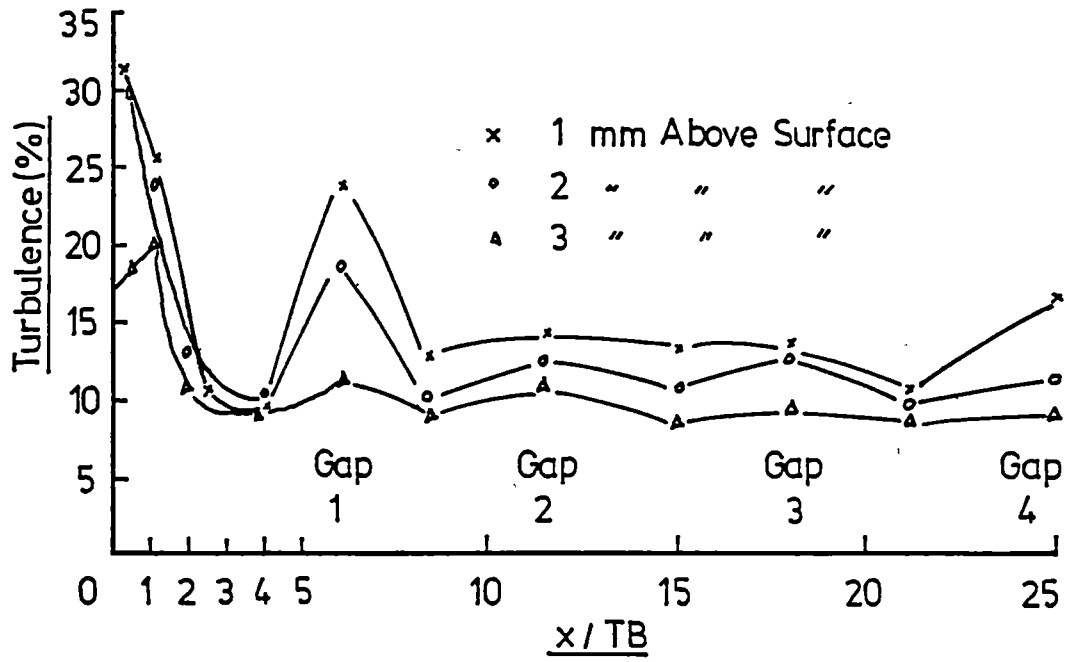

Figure 3.26

Variation of Turbulence along the Flow Passage (R_e:5330, Gap: 5 mm)

When the surface level was varying, however, extra resistance from the fluctuated edges of the boards caused a quite big increase in the pressure drop, which gives a surface friction factor based on the free stream velocity about 0.012 at the high velocity range.

Variation of the measured percentage of turbulence along the flow passage with about 5 mm gap between the boards is shown in Figure 3.26. Four peak points along the flow passage can be seen at the centres of the four gaps, which would certainly imply that vertical air circulation occurs in the gap between two boards, thus edge drying at the latter stages of the drying process should be expected.

For the present purpose, since there is no significant change in pressure drop with the 5 mm gap between the boards, the measurements on the velocity profiles have been excluded.

3.3.4 Summary of the Measurements

The boundary layer flow across the board surface is essentially similar to the flow along the board and thus similar conclusions apply to the both cases.

The surface friction largely depends on the state of the board surface. With the surface of the boards maintained at approximately the same level, the saw marks offer more resistance to the air flow in the case of flow along the board under the present test conditions, although in practice saw marks may change through a wide angle.

A 5 mm wide gap between neighbouring boards makes only a small effect on the overall pressure drop when the surface of the boards was maintained at the same level. The fluctuation of the surface level of the boards due to the uneven shrinkage in the board thickness direction plays a more important role in increasing the surface friction to the air flow. From this point of view, collapse should be expected to increase the friction factor and thus speed up the heat and mass transfer process.

The shrinkage gaps between the edges of the boards cause vertical air circulation, and consequently edge drying.

4.4 Conclusions

Measurements of the velocity profiles as shown in the last two sections show general development of the boundary layer from upstream to downstream at various free stream velocities. Those results are useful in industry for the design of new kilns because they indicate how closely boards can be spaced (i.e., thickness of the racking sticks). The flow pattern must be essentially the same while there are two well defined boundary layers. For a stack of 1.3 m wide, the recommended minimum thickness of racking sticks appears to be about 16 mm.

Calculation of the shape factor shows that despite restrictions on the value of momentum thickness because of the inability to define an origin for y, the calculated values of the shape factor are close enough to the expected values to provide a useful guide to the flow pattern. Experimental analysis of the surface friction shows that, although the change in momentum thickness has very little effect on the friction factor, the detailed study is needed to understand the heat and mass transfer processes over the surface of the board.

CHAPTER 4

DEVELOPMENT OF A HEAT AND MASS TRANSFER MODEL FOR DRYING OF TASMANIAN EUCALYPTS

Wood drying involves a process in which wood properties should be studied from the time they are still live trees. The first problem is to assign an initial temperature and moisture content to a sawn board. Unfortunately, there is not much idea of such properties as the variation of temperature and moisture content across a log, which has been subject to changes from various sources such as effect of direct sunlight and chemical changes as it grew as a tree. After it was felled, it lay as a log subject to daily variations in air temperature until it was presented to the saw.

The act of sawing damages most of the fibres near the surface of the newly sawn board and adds energy to it thereby increasing its temperature. As soon as the newly sawn surface is exposed to the atmosphere it starts to dry out. In the early stages there may be some contribution of enthalpy from the wood towards the "latent heat" required to evaporate moisture from the new surface. Any such contribution lowers the temperature of the surface of the wood and thus there is more transfer of heat from the air. When the wood is at the wet bulb temperature of the air all the heat required to evaporate the moisture must come from the air.

The simple model of drying is based on the the concept of "free water" and "bound water" sharply separated by a fibre saturation point (FSP). In this model, the evaporation rate from the wood surface is the same as from a

free water surface while the wood is above FSP; the gradient of moisture concentration within the wood adjusts itself so that the rate of movement of water towards the surface equals that evaporated and convected away by the air. If the temperature of the wood surface remains constant at the wet bulb temperature of the air the flux of moisture across the surface remains constant and the surface moisture concentration decreases with the square root of time.

The very limited amount of experimental evidence that is available indicates that this is a too much simplified picture. The range of time over which square root drying occurs seems to be quite small. It appears that either the estimates of surface temperature are wrong or that the wood surface is subject to dry patches. No comprehensive studies of the interaction between moisture transport in the wood and that in the air seem to have been reported in the literature. Measurements of surface temperature of the wood reported here throw some light on this problem.

When the moisture concentration at the wood surface drops below FSP, the surface moisture concentration and the surface temperature adjust themselves along the sorption isotherm. It is not at all clear as how to handle the problem of dry patches where some fraction of the area of surface is moving along the sorption isotherm while the the remainder is drying like a free water surface if this situation exists. Most of the available experimental evidence is irrelevant to the present problem because it was obtained from tests in which surface checking started fairly soon (i.e. within a day or two) after the surface MC reached FSP. Surface checks appear as wet lines under a magnifying glass and the drying rate is higher than with an unchecked

surface. The main aim of research at the University of Tasmania has been to eliminate surface checking because it decreases the market value of the final product so we are interested only in the drying rate of an unchecked surface.

The measurements of air flow through a timber stack so far indicate that a boundary layer is formed in the air adjacent to the board and gradients of velocity, moisture concentration and temperature are set up within this layer. These gradients result in convection of moisture by the air away from the surface of the wood. The rate of convection depends upon the velocity of the air relative to the board in the free stream (i.e. outside the limits of the boundary layer), the difference in moisture concentration and temperature across the boundary layer and the pattern of the distribution of these three variables across it. This pattern depends on whether the flow is laminar, in transition or turbulent and whether the walls are aerodynamically smooth, in transition from smooth to rough or wholly rough.

There are well proven theoretical arguments which give useful predictions of heat, mass and momentum transfer across boundary layers under various of these conditions, but our measurements of velocity distribution do not fit any of the standard solutions. Even when the flow is nominally laminar the relatively large roughness of the sawn surface appears to introduce enough disturbance into the air to cause appreciable differences between measured and theoretically predicted values of friction factors.

In this situation, it appears that the best that can be done is to depend on the Reynolds analogy which states that the mechanism of transport by the eddies of turbulent flow of momentum, heat and mass (water vapour) is

the same for all three properties. The velocity, temperature, and moisture concentration in the turbulent regimes are then all expected to have similar distributions. Very near the wall the effects of molecular viscosity, conduction and diffusion are expected to dominate the transport of the respective properties. It is not known how much the very rough surface of a sawn board affects this.

The studies reported in this chapter were therefore arranged with the aim to clarify these questions.

4.1. Analysis Of Momentum, Heat, And Mass Transfer Over The Surface Of Sawn Timber Boards

The knowledge of turbulence is so limited that it is very difficult to determine analytically the velocity and temperature distributions. By means of an analogy between heat, mass and momentum transfer, however, predictions have been made of heat and mass transfer coefficients from friction factor data. Details of this similarity and discussion of its degree of approximation in laminar flow over smooth surfaces can be found in any modern text book on heat and mass transfer. For the present purpose only a brief introduction is made.

4.1.1 Reynolds Analogy

On the basis of experimental studies of turbulent flow, Reynolds[30] proposed that for turbulent flow, both momentum and heat transfers occur

by an analogous mechanism. This observation is readily extended to include mass transfer.

The general transfer equations can be written to include both molecular and eddy diffusivities as

Mass transfer:

$$N_a = -(D + E_d)\left.\frac{\partial C}{\partial Y}\right|_{Y=0} = k_c\,(C_w - C_a) \tag{4.1}$$

Heat transfer:

$$q = -(\kappa + E_h)\left.\frac{\partial(\rho\ c_p\ T)}{\partial Y}\right|_{Y=0} = h\,(T_w - T_a) \tag{4.2}$$

Momentum transfer:

$$\frac{\tau}{U} = -(\nu + E_v)\left.\frac{\partial(\rho\ u/U)}{\partial Y}\right|_{Y=0} = \frac{f\ \rho}{2}\,U \tag{4.3}$$

Equations (4.1) through (4.3) relate the fluxes to a driving force and diffusivity. Since we are considering transfer from the surface of the board, the driving force is equal to the difference between the temperature (T) or concentration (C) at the surface (T_w, C_w) and the free stream (T_a, C_a). A summary of the remaining terms presented in the equations above is given in Table 4.1.

Table 4.1

Definition of Terms Used to Describe the

Analogy between Heat, Mass, and Momentum Transfer

Variables	Mass transfer	Momentum transfer	Heat transfer
Potential	C	$\rho\, u/U$	$\rho\, c_p\, T$
Flux	N_a	τ/U	q
Molecular diffusivity	D	ν	κ
Eddy Diffusivity	E_d	E_v	E_h
Convective coefficient	k_c	$f\,\rho/2$	h

With the introduction of the groups of the variables

$$\pi = \frac{u}{U} = \frac{T - T_w}{T_a - T_w} = \frac{C - C_w}{C_a - C_w} \tag{4.4}$$

the Reynolds analogy is obtained readily by writing Equations (4.2) through (4.3) in dimensionless form, i.e.

Mass transfer:

$$\left.\frac{\partial\, \pi}{\partial\, Y}\right|_{Y=0} = \frac{k_c}{D + E_d} \tag{4.5}$$

Heat transfer:

$$\left.\frac{\partial\, \pi}{\partial\, Y}\right|_{Y=0} = \frac{h}{\rho\, c_p\, (\kappa + E_h)} \tag{4.6}$$

Momentum transfer:

$$\left.\frac{\partial \pi}{\partial Y}\right|_{Y=0} = \frac{f\ U}{2\ (\nu + E_h)} \tag{4.7}$$

The analogy between momentum and heat transfer is obtained by combining Equations (4.6) and (4.7) to give

$$\frac{f\ U}{2\ (\nu + E_v)} = \frac{h}{\rho\ c_p\ (\kappa + E_h)} \tag{4.8}$$

In the turbulent region the eddy diffusivities are much larger than the molecular diffusivity. If the assumption is made that the eddy diffusivities for momentum and heat transfer are approximately equal, ν and κ can be neglected, and the Reynolds analogy results in

$$\frac{f}{2} = \frac{h}{\rho\ c_p\ U} = St \text{ (Stanton number)} \tag{4.9}$$

Thus, the heat transfer coefficient is expressed as

$$h = f\ \rho\ c_p\ U\ /\ 2 \tag{4.10}$$

The Reynolds analogy for mass transfer is obtained by combining Equations (4.5) and (4.7). Thus

$$\frac{f}{2} = \frac{k_c}{U}\left(\frac{\nu + E_v}{D + E_d}\right) \tag{4.11}$$

In turbulent flow the molecular properties can be neglected since they are much less than the eddy terms. Following the assumption that mass, momentum, and heat are transferred by the same mechanism for turbulent flow, and assuming that the eddy diffusivities are approximately equal, we obtain the Reynolds analogy given as

$$\frac{k_c}{U} = \frac{h}{\rho\, c_p\, U} = \frac{f}{2} \tag{4.12}$$

Thus, the mass transfer coefficient can be expressed as

$$k_c = h / (\rho\, c_p) = f\, U / 2 \tag{4.13}$$

The expression above can be used to predict turbulent heat and mass transfer data for fluids which have Prandtl and Schmidt numbers close to unity. For Prandtl ($P_r = \nu/\alpha$) or Schmidt ($S_c = \nu/D$) numbers significantly different from 1, however, the Reynolds analogy predicts values substantially different from those observed in practice. This difference is thought to arise from the boundary conditions at the solid surface where the effects of turbulent eddies are small and molecular effects become important. Also, the boundary layers for the various properties have different thicknesses in laminar flow.

4.1.2 Prandtl Analogy

To apply the analogy approach to fluids with Prandtl or Schmidt numbers not close to unity, Prandtl[31] suggested that the flow be divided into two regions. One is near the wall, where flow is expected to be laminar and transport occurs by a molecular mechanism, and the other is the turbulent region, which can be described by the Reynolds analogy. Prandtl's analogy takes into account the variation with the Prandtl or Schmidt numbers and has the form

$$\frac{h}{c_p\ U\ \rho} = \frac{K_c}{U}$$

$$= \frac{f}{2}\left[\frac{1}{1 + 5(S_c \text{ or } P_r - 1)\ (f/2)^{0.5}}\right] \qquad (4.14)$$

4.1.3 Chilton–Colburn j–factor

Chilton–Colburn[32] observed that by replacing the term $[1+5(S_c$ or $P_r-1)(f/2)^{0.5}]$ of the Prandtl analogy by $S_c^{2/3}$ or $P_r^{2/3}$ an improvement could be obtained in the correlation of heat and mass transfer data. Thus the equation becomes

$$[h/(U\ c_p\ \rho)]\ P_r^{2/3} = f/2 \qquad (4.15)$$

and

$$(k_c/U)\ S_c^{2/3} = f/2 \qquad (4.16)$$

where the first terms are defined as the Chilton–Colburn j–factor, jh and jd respectively. Thus we have

$$j_h = \frac{h}{U\ c_p\ \rho} P_r^{2/3} = \frac{N_u}{R_e\ \ P_r^{1/3}} = \frac{f}{2} \qquad (4.17)$$

and,

$$j_d = \frac{k_c}{U} S_c^{2/3} = \frac{S_h}{R_e\ \ S_c^{1/3}} = \frac{f}{2} \qquad (4.18)$$

The Chilton and Colburn j–factor approach provides reasonable correlation of experimental data for flow past smooth flat plates.

It should be pointed out that both Prandtl and j–factor equations are based on the assumption of a laminar sublayer near the wall, which can be

described by universal velocity profile equations. Measurements on the flow so far show that the boundary layer flow over a sawn timber board is quite different from those described by the universal velocity profile equations. Thus, the applicability of those equations to the present situation must be suspect.

4.2. The Development Of The Mathematical Model

4.2.1. General Assumptions

In the construction of the mathematical model to describe the heat and mass transfer process in the drying of Tasmanian Eucalypt timber, the following assumptions have been made:

1. The moisture and heat flow through the wood is restricted to the one dimensional case.
2. Moisture movement inside wood is a diffusion process in which the diffusion coefficient is independent of the moisture content and the driving force is taken to be the moisture concentration as in true molecular diffusion.
3. All of the moisture evaporation takes place at the surface of the board and moisture movement between the board surface and the surrounding air is by a mass transfer process through a boundary layer in the air.
4. Equilibrium exists between the moisture content at the board surface and the film of air adjacent to the surface so that a suitable sorption isotherm can be used to estimate the board surface conditions.

5. The initial temperature of the board is taken as the wet bulb temperature of the air. When the external drying schedule changes, the board temperature remains constant throughout the board; an almost immediate temperature change to the new wet bulb temperature occurs throughout the board because heat is transferred through the wood so very much faster than moisture.

4.2.2. Model Formulation For Mass Transfer

Research into the drying phenomena has been extensively conducted in the area of heat and mass transfer. Peck[33] discusses capillary theory applied to the drying of a solid using brick as an example and partitions the mathematical analysis into three periods:

a). the constant rate period when the entire surface is kept wet by capillarity and surface evaporation determines the drying rate;

b). the first falling rate period when capillary action is not sufficient to keep the surface uniformly wet; and

c). the receding front drying period during which the liquid surface recedes into the solid.

However, the drying of wood is more complex than can be explained by capillarity alone. Skaar[34] pointed out that wood contains free water in cells and capillaries connecting the cells as well as water bound within the cellulose walls and lignin matrix around the cells. Both free water and bound water are removed during drying. Direct observation confirms that no free water exists at the wood surface at the time the boards reach the kiln, so a constant rate model does not apply[13]. Experimental results on wood

reported in the literature[34,2] show that the receding front model does not directly apply either. Recalling the literature indicates that both vapour pressure and concentration gradient based diffusion models have been successfully used to model the moisture transport in wood, although there are many apparently sound theoretical arguments against the validity of these models under these conditions.

1. The Diffusion Equation

Wet timber loses moisture from all surfaces in the process of drying. However, in kiln drying, the boards are placed edge to edge, and because there is only small vertical air circulation, loss from the narrow edge surfaces is small compared to losses from the wide surfaces. Moisture losses from the board ends are also insignificant because of the relatively small surface areas in relation to the transport distances. Board ends were coated in these tests as they are in some industrial applications. Therefore, moisture loss is assumed to be chiefly from the top and bottom surfaces, for which the one–dimensional model oriented in this dominant direction is taken as sufficient for studying the process.

To describe the unsteady–state, one dimensional movement of moisture through wood, Fick's second law of diffusion

$$\frac{\partial\, MC}{\partial\, t} = \frac{\partial}{\partial Y}\left[D(Y,MC,T)\,\frac{\partial\, MC}{\partial Y}\right] \qquad (4.19)$$

has been often used in the forest products literature.

The diffusion coefficient, D, can in general vary with location in the board, Y, moisture concentration, MC, and temperature T. The variation of D with Y is influenced by difference in the wood structure such as the distribution of heartwood and sapwood and growth ring orientation in the same board as well as other local effects. Ray cells conduct moisture more easily than longitudinal cells[35] so that diffusion is influenced by the angle (a function of Y) that the wood rays make with the Y–axis of the board. But, assuming that there is no systematic variation in the distribution of heartwood, sapwood, and growth–ring angle with respect to the Y–axis within the boards that make up a typical kiln charge, D, on the average is modelled as independent of Y.

The dependence of the diffusion coefficient on the moisture concentration of the wood should be expected. The diffusion coefficient is a measure of the ease of conductance of moisture through wood. Activated molecules diffuse from site to site along the cellulose molecules and, in doing so, pass through the molecular–dimensional interstices between them or along the surfaces of fibres. As the cellulose molecules are drawn together in shrinkage during desorption, the available space for the diffusion is reduced, and the conductance of the system is expected to be reduced accordingly. For Tasmanian eucalypt materials, however, extensive experiments so far have indicated that a constant value seems to give useful results as close to values obtained by slicing as can be justified by experimental error. For this reason, D is taken as independent of the moisture content in this study.

Bramhall[36] reported results from a series of experiments in which D was plotted against temperature for constant moisture content, from which it

was found that the relationship between D and the absolute temperature T is of the form

$$D = DR \exp(-E/RT) \tag{4.20}$$

Diffusion cell tests conducted by Schaffner[7] show that a similar relationship could be found for the Tasmanian eucalypts, in which E/R was best fitted to be about 3800 (1/K). Thus, for Tasmanian eucalypt, Equation (4.20) can be rewritten as

$$D = DR \exp(-3800/T) \tag{4.21}$$

which is used in this study.

If D is independent of Y and MC, Equation (3.1) reduces to

$$\frac{\partial MC}{\partial t} = D(T) \frac{\partial^2 MC}{\partial Y^2} \tag{4.22}$$

Successful solution of Equation (4.22) has resulted in good estimates of the moisture distribution inside the board at different times.

2. Initial and Boundary Conditions

To solve the equation (4.22), one initial condition and two boundary conditions are needed. The initial condition is usually given by

$$MC = MC_0 \text{ at } t = 0, \text{ all } Y \tag{4.23}$$

which denotes an initially uniform moisture distribution throughout the board.

One boundary condition is given by

$$dMC / dY = 0 \text{ at } Y = Y_{mid}, \text{ all } t \qquad (4.24)$$

which denotes a symmetrical moisture profile located along the centre line of the board.

The second boundary condition accounts for the surface condition and its determination depends upon whether the surface moisture content is above or below FSP.

(1). The Surface Boundary Condition at Moisture Contents above FSP

In the over–simplified drying model, the surface of the wood is assumed to be in equilibrium with saturated air while it is above FSP. Under this assumption, if no dry patches form, the surface temperature of the wood remains constant at the wet–bulb temperature of the air until the surface dries down to FSP. The moisture concentration in the air in contact with the wood is that of the saturated air at the wet–bulb temperature (C_{wb}) and remains constant at this value. The moisture concentration of the air at the edge of the boundary layer must remain the same as that of the incoming air (C_a) and determined by the dry–bulb temperature and relative humidity of the air. According to this argument the difference between the moisture concentration in the air at the surface of the wood and that in the free stream remains constant whilst the moisture concentration in the wood at its surface remains above FSP. The flux of moisture (FM_o) from the wood into the air would then be constant, which can be calculated from the Reynolds analogy between mass transfer and surface friction, i.e.

$$FM_o = \frac{1}{2} f U (C_{wb} - C_a) \qquad (4.25)$$

Available experimental results indicate that this over–simplified model does not apply completely to the drying of eucalypt materials because nearly all the "free water" in eucalypts is held inside fibres. Nevertheless it remains a useful starting point for discussion. It appears that in most eucalypt materials the pits (that in most timbers are seen as holes in fibre walls) are occluded (i.e. covered over) so that for those fibres not ruptured by the saw the 'free water" can escape only by diffusion through the fibre walls which is a very slow process. No established method of handling the problem of dry patches could be found in the literature so we have assumed that it is equivalent to a reduction in the effective area available for moisture transport to the air and have introduced a surface mass transfer area ratio (φ) which is initially set at 1.0 then adjusted by trial until there is agreement between predicted values and experimental measurements. This coefficient must also account for the dry patches that appear on the surfaces of boards in the early stages of drying when the rest of the surface appears to the naked eyes to be wet. Such dry patches seem to be the result of the variability in the properties of the material.

While the moisture vapour concentration near the board surface remains at C_{wb}, the moisture flux from the board surface remains constant and the enthalpy transferred from the air is all required to evaporate the water (the latent heat of vaporization). It is assumed, for the purpose of this analysis, that the whole of the heat and mass transfer between the air and the wood takes place at the surface of the board. This assumption is open to questions, but have so far been justified by the good agreement obtained between computed and measured conditions.

After one hour or so (even less if the surface is in direct sunlight) the truly free water from within torn fibres at the same surface is all evaporated and φ starts to decrease from 1.0. This implies that the effective surface area for evaporating moisture decreases. The total flux of moisture from the board surface then drops from its highest possible value as described by Equation (4.25), so less enthalpy is used in evaporating, leaving an excess to raise the temperature of the wood. Since each board has, effectively, two surfaces when we neglect edge drying, then the surface area per cubic meter of wood is given by 2/TB, where TB is the thickness of the board. The enthalpy balance over the board surface is then given by

$$FH_o = FM_o\, H_{fg}\, \varphi + \frac{TB}{2} (\rho\, C_p)_{wood} \frac{dT}{dt} \qquad (4.26)$$

which enables calculation of the board temperature rise.

Equation (4.26) is based on the assumption that heat is transferred so rapidly through the wood and the rate of rise of surface temperature so slow that the rise in surface temperature is approximately equal to the rise in average temperature. The argument for this assumption comes from the belief that most of "free water" is held within fibres. A plausible description of the movement of the moisture in eucalypt materials has this free water moving by diffusion either to the surfaces of the board or to the surfaces of large vessels. This latter moisture can then evaporate and move towards the surfaces of the board under gradients of partial pressure where they exist. If this argument is correct some of the evaporation and consequent heat transfer occurs within the board. However, as indicated above, it appears unlikely that there is sufficient difference between the two results to resolve the difference between the two points of view.

As soon as the surface temperature (T_w) rises above the wet bulb temperature (T_{wb}), the vapour pressure in the air in contact with the surface decreases below the saturated value (P_{satwb}) which corresponds to the wet bulb temperature. This means that the moisture concentration in the air at the surface must also decrease and so the flux of moisture from the surface as given by Equation (4.25) also decreases. Since we deal with air and water system where the Lewis number is about 1[17], it is probably near enough to take the moisture concentration as varying linearly with the temperature so that

$$\frac{(C_w - C_{wb})}{(C_a - C_{wb})} = \frac{(T_w - T_{wb})}{(T_a - T_{wb})} \qquad (4.27).$$

The final solution requires simultaneous solution of the above equations and entails a knowledge of the moisture distribution within the wood at each time step in order to estimate its thermal capacity $(\rho\ C_p)_{wood}$. However, as mentioned above and shown by the measurements presented here, the rate of change of temperature of the surface of the board in ordinary commercial practice of drying eucalypt materials while the moisture content at the middle of the board is above FSP is so slow that we can ignore the dependence between diffusion coefficient and temperature and estimate the moisture distribution separately. It should be remembered that both calculation and experiment in this study were carried out at nominally constant dry bulb temperature of the air.

The vapour concentrations of C_{wb} and C_a in Equation (4.25) were determined from the following approach. Firstly, the saturated water vapour

pressure (P_{sat} in P_a) in air at the absolute temperature T was calculated from the equation

$$P_{sat} = 1.005\ EXP\left(22.3286 - \frac{1}{T}(2881.0 + \frac{1}{T}(5.07\ x10^5 - \frac{1}{T}2.925\ x10^7))\right) \qquad (4.28).$$

This is an empirical fit to data from steam tables based on the observation that $LN(P_{sat})$ is nearly linear with 1/T over a wide range. The factor 1.005 is an allowance for real gas effects of water vapour, usually stated as varying between 0.4 % and 0.6 %. The partial pressure of the dry air is then expressed as

$$P_{dair} = P_{mair} - P_{sat} \qquad (4.29)$$

where P_{mair} is the barometric pressure in Pa and is usually taken as constant in the drying calculations.

With wet bulb and dry bulb temperatures given, the usual practice is to calculate P_{sat} at the wet bulb temperature (P_{satwb}) where RH=1.0. The mixing ratio at the wet bulb temperature is then calculated as

$$r_{wb} = 0.622\frac{P_{satwb}}{P_{dair}} = 0.622\frac{P_{satwb}}{P_{mair} - P_{satwb}} \qquad (4.30).$$

An approximate equation was used to calculate mixing ratio at the dry bulb temperature, that is

$$r_{wb} - r_{db} = 0.905\ (T_{db} - T_{wb})/H_{fg} \qquad (4.31).$$

It is common to put

$$H_{fg} = 2502.1 - 2.4\ T \tag{4.32}$$

where T is in ^{0}C.

Since dry air is very nearly an ideal gas at most conditions, the density of the dry air was calculated as

$$\rho_{dair} = \frac{M_a}{R}\frac{P_{dair}}{T}$$

$$= 3.485\text{x}10^{-3}\frac{P_{dair}}{T} \tag{4.33}$$

where R is the universal gas constant (8.3143 Pa m^3/mole K) and T is in ^{0}K. The moisture concentrations are thus calculated as

$$C_{wb} = r_{wb}\ \rho_{dair}$$

and

$$C_a = r_{db}\ \rho_{dair} \tag{4.34}.$$

It should be pointed out that the value of ρ_{dair} changes through the boundary layer. However, since only a small temperature gradient exists in the boundary layer, we should be able to ignore the variation of ρ_{dair}.

(2). The Surface Boundary Condition At Moisture Contents Below FSP

When the moisture concentration at the wood surface drops below FSP, the moisture concentration and temperature at the surface are assumed to adjust themselves along a sorption isotherm.

Literature contains detailed research on the adsorption of the water with wood. Simpson[37] has shown that a number of theories of Type II (or multilayer) adsorption can describe sorption data for wood, and that they provided reasonable mechanistic interpretation of how wood takes up water. In contrast to work on adsorption, little effort has been made to describe theoretically the equilibrium moisture contents obtained by desorption. Instead, the kinetics of this process has been of greater interest, and numerous models describing desorption rates have been proposed[34,38,2,39]. In this study, the model proposed by Nelson[39] was chosen, which relates equilibrium moisture content with the Gibbs free energy change and has the basic form

$$\nabla G = -(RT/M_w)\, \mathrm{Ln}(P_{vap}/P_{sat}) = -(RT/M_w)\, \mathrm{Ln}(RH) \qquad (4.35)$$

Nelson fitted Kelsey's data[40] with

$$\begin{aligned} \mathrm{Ln}(\nabla G) &= \mathrm{Ln}(\nabla G_o)\,(1 - EMC/FSP) \\ &= A\,(1 - EMC/FSP) \end{aligned} \qquad (4.36).$$

There seems to be no systematic variation of A and the fourth figure of A in Nelson's table 1 is far from the mean so that the average of the first three was used, i.e. 5.116.

With $R/M_w = 0.11$ for water, where $R = 8.3143 \times 10^7$ ergs/mole/K = 1.9858 cal/mole/K, we get

$$\mathrm{Ln}\Big((-0.11 * T_{wk})\, \mathrm{Ln}(RH)\Big) = 5.116*(1.0 - MCS/FSP) \qquad (4.37)$$

in which, MCS is the moisture concentration in wood at surface, and T_{wk} is the surface temperature in ^{0}K.

A possible problem with this equation is that it gives RH about 0.97 when EMC = FSP at room temperature. In order to put RH=1.0 when EMC=FSP, Equation (4.37) was modified as

$$\mathrm{Ln(RH)}=\left(\mathrm{EXP(5.116*(1-EMC/FSP))-1.0}\right)/(-0.11*T_{wk}) \tag{4.38}$$

In practice, it appears that RH=0.97 is not physically sustainable so that the gap at EMC=FSP has not been the computational hazard as first appeared, although it remains as a worry with iterative solutions. The expressions

$$\mathrm{EMC=FSP*}\left(1.0-\mathrm{Ln}(-0.11*T_{wk}*\mathrm{Ln(RH)})/5.116\right) \text{ and}$$

$$\mathrm{RH=EXP}\left(\mathrm{EXP(5.116*(1-EMC/FSP))}/(-0.11*T_{wk})\right) \tag{4.39}$$

appear to be well-balanced passing through EMC=FSP in ordinary drying but look to need some modification when modelling cycling of humidity or reconditioning with steam.

Solution of Equation (3.20) requires both surface moisture content and temperature to be known. For this, the previous change in moisture content DQS is used in the computer program of APPENDIX E (B) as a first estimate of the surface moisture content, i.e. $PQS_2=QS_1+DQS$. RH and C_w are then calculated which give a new estimate of the surface moisture flux at the end of the time step. The average value of the surface flux over the time step is taken as the value for the constant flux solution. It should be pointed out that because of the rise in board surface temperature when the surface moisture concentration is above FSP, RH at the surface drops from 1.0 to a

value which depends on the rise of the surface temperature (RH_{fsp}). Thus, the first estimated value of RH after FSP must lie in the range from RH_{fsp} to RH_a. This leaves a gap between 1.0 to RH_{fsp} which can not be described by the sorption isotherm. At the present calculation, the value of RH in this gap was taken as constant at RH_{fsp}, then decreased along the sorption isotherm. RH_{fsp} can be estimated from the moisture vapour concentration (C_w) and the board surface temperature (T_{wk}) as

$$RH_{fsp} = \frac{P_{vap}}{P_{satw}} = \frac{461.3 C_w \, T_{wk}}{P_{satw}} \qquad (4.40).$$

To put the difference between the estimated PQS_2 and calculated QS_2 values of the surface moisture content within the specified accuracy, a variable DIFF is defined as $DIFF = QS_2 - PQS_2$, and, on going out of the loop, the values of PQS_2, QS_2 and DIFF are renamed as

$$PPQS = PQS_2,\ PQS_2 = QS_2, \text{ and } PDIFF = DIFF \qquad (4.41).$$

After the first round of iteration the value of QS_2 is used as the next trial and a new QS_2 is calculated as

$$QS_2 = PPQS - PDIFF*(PQS_2 - PPQS)/(DIFF - PDIFF) \qquad (4.42)$$

which is a linear interpolation calculated to put the next value of DIFF equal to zero.

Since the surface temperature (T_w) of the board increases from the wet bulb temperature (T_{wb}) at this stage of the drying, the calculation of the surface temperature (T_w) and saturated vapour pressure (P_{satw}) at this temperature in each time step is needed to get the partial vapour pressure ($P_{vap}=RH*P_{satw}$), and thus the moisture concentration C_w of the air.

4.2.3 Model Formulation for the Heat Transfer

The heat transfer process involved in wood drying consists of two parts, namely, convective heat transfer over the boundary layer and conduction heat transfer inside the board. Because only a small temperature gradient exists across the board in the low temperature drying of timber, investigations on the heat transfer process are not as widely conducted as that for the moisture transfer. Kollman[41] shows that the variation in temperature throughout the board is of the order of two degree Celsius and he thus concluded that heat transfer can be ignored in the moisture model. Luikov[42], however, in a comprehensive review paper of theoretical work on drying of capillary–porous bodies suggests that both heat and moisture transport should be included in the drying models. Bramhall[36] and Wengert[43] stated that moisture transport in wood is driven by the vapour pressure gradient including heat transfer in their models and the models coefficients were adjusted to obtain good fits to average moisture data. Since the surface temperature change largely affects the moisture transfer process in drying of eucalypt material as described earlier, study on both kinds of heat transfer is necessary for understanding the process of drying.

1. Enthalpy Balance at the Board Surface

The temperature distribution inside the board can be determined by considering the enthalpy balance at the board surface and heat conduction inside the board. For the enthalpy balance, it is necessary to consider the factors involved in the influx and efflux of both sensible heat and latent heat. Heat entering the surface which is not offset by heat leaving must remain

and increase the temperature of the board. Reservations about these assumptions have been expressed but the argument between measurement and calculation that appears in what follows indicates that errors in these assumptions are within the range of expected errors in measurement.

(1). Heat Flux Convected Towards Wood

Since a temperature gradient exists between the air flow and the wood surface, heat convects towards that surface. The amount of heat transferred from the air flow can be estimated by the Reynolds analogy between heat transfer and the surface friction, that is

$$FH_o = \frac{1}{2} f \rho_{mair} C_{py} U (T_a - T_w) \tag{4.43}$$

where, C_{py}, the specific heat of the moist air, is expressed as

$$C_{py} = C_{pg} + C_{pw} r_{db} \tag{4.44}.$$

In Equation (4.44), C_{pg} and C_{pw} are functions of the average value of the dry bulb and wet bulb temperatures, i.e. $TDW=0.5(T_{db}+T_{wb})$, and empirical equations were fitted from the table provided by Keey[17] as

$$C_{pw} = \begin{cases} 1.86 + 8.33\text{x}10^{-5}\ TDW & 0^0<TDW\leq 60^0C \\ 1.91 + 2.5\text{x}10^{-3}(TDW-60) & 60^0<TDW<100^0C \end{cases} \tag{4.45}$$

and

$$C_{pg} = \begin{cases} 1.0037 + 5.0\text{x}10^{-5}\ TDW & 0^0<TDW\leq 52^0C \\ 1.0063 + 8.6\text{x}10^{-5}(TDW-52) & 52^0<TDW<100^0C \end{cases} \tag{4.46}$$

(2). Activation Energy of Diffusion

In terms of physics, the activation energy is the energy which a molecule receives to break the hydrogen bond holding it to other molecules in the liquid state or to sorption sites in hygroscopic materials[36]. Because hydrogen bonds are involved in both cases, the value of activation energy of diffusion above FSP should equal that of evaporation from a free liquid surface, and this is expressed fairly well by Equation (4.32) where T becomes the average timber surface temperature over the time interval.

As wood dries below FSP increased energy is required to break the hydrogen bonds; this is the heat of wetting. Bramhall[36] proposed an empirical equation based on the data published by Weichert[44], in which the heat of wetting is expressed as a function of moisture content in the form of

$$H_w = 1172.3\ EXP(-0.15\ M_i) \qquad (4.47)$$

where M_i is the average surface moisture content over each time step in percent. Thus, the activation energy of diffusion is expressed as

$$\begin{aligned} H_{ae} &= H_{fg} + H_w \\ &= 2502.1 - 2.4\ T_{wa} + 1172.3\ EXP(-0.15\ M_i) \end{aligned} \qquad (4.48).$$

(3). Net Heat Flux for Heating the Board

As moisture evaporates from the board surface, it carries with it the activation energy of diffusion, this, together with the sensible heat which moves in response to a temperature gradient, constitutes the total heat flux

into the board. It is this amount of heat which is actually used to increase the temperature of the board. The net heat flux for heating the board is thus expressed as

$$\begin{aligned} DFH &= FH_o - H_{ae} \\ &= FH_o - (H_{fg} + H_w)\, FM_o\, \varphi \end{aligned} \qquad (4.49).$$

Determination of DFH requires the estimation of the surface temperature over each time step. This is done by assuming the surface temperature rise equal to the rise in average temperature as described earlier.

2. Conduction of Heat Inside the Board

Under the assumption that there is no moisture evaporation inside the board, heat conduction in the board due to the incoming net heat flux can be described by Fourier's equation in the one dimensional form, i.e.

$$\frac{\partial H}{\partial t} = K \frac{\partial^2 T}{\partial Y^2} \qquad (4.50).$$

The thermal conductivity (K) of wood varies with the basic density, fractional void volume filled with air, and the moisture content. Maclean[45] measured the thermal conductivity of many samples of wood with a large range of moisture contents and specific gravities. He presented an empirical equation which gave the best agreement with his experimental data:

$$K = 10 \times 10^{-4} [\, \rho\, (5.18 + 0.096\, M) + 0.57\, V_s)] \qquad (4.51)$$

where K is thermal conductivity of wood in cal/(cm s C), ρ is the basic density in g/cm^3, M is the moisture content in percent, V_s is porosity as a fraction.

At moisture contents above 40 %, a significant portion of the moisture is free water in the lumens, which apparently contributes more than the bound water to the over–all thermal conductivity. Therefore, the factor 0.096 in Equation (4.51) is replaced by 0.131:

$$K = 10x10^{-4} [\rho (5.18+0.131M) + 0.57 V_s)] \qquad (4.52).$$

Siau[46] proposed that porosity can be calculated as

$$V_s = 1 - \rho (0.667 + 0.01 M) \qquad (4.53).$$

When Equation (4.53) is substituted into Equations (4.51) and (4.52) their forms may be simplified to

$$K = 10x10^{-4} [\rho (4.80 + 0.090 M)+0.57] \text{ cal/(cm s C)} \qquad (4.54)$$

for M<40 %, and

$$K = 10x10^{-4} [\rho (4.80+0.125 M)+0.57] \text{ cal/(cm s C)} \qquad (4.55)$$

for M> 40 %. To convert the unit cal/(cm s C) to KJ/(m hr. C) above equations for K should be multiplied by a factor of 1504.

Since $\partial T=\partial(\Sigma H)/(\rho_{wood}\ C_{pwood})$, the change of temperature per unit volume is equal to the change of heat content divided by the product of specific heat (C_{pwood}) and density (ρ_{wood}) of the moist wood. The rate of change of temperature is then

$$\frac{\partial T}{\partial t} = \frac{1}{(\rho C_p)_{wood}} [\, K \frac{\partial^2 T}{\partial Y^2} \,] \qquad (4.56).$$

The specific heat of moist wood was calculated by treating wood as an additive mixture of dry cell wall substance and water. Skaar[34] stated that the specific heat of the dry wood increases significantly with temperature similar to other organic materials. He tabulated the results of six investigations in which an average value for dry wood was (0.268 + 0.0011 T) cal/g/C, where T=Celsius temperature. Skaar also discussed a small increase in the specific heat of bound water with moisture content between 5 % and FSP, but, for simplicity, the value of 1.0 cal/g/C is assumed for both bound and free water. Then the specific heat of moist wood is calculated as

$$C_{pwood} = (0.286 + 0.0011\ T + 0.01\ M)/(1 + 0.01\ M) \tag{4.57}$$

where T is in ^{0}C, M in percent, and C_{pwood} in cal/g/C. To convert C_{pwood} to KJ/Kg/C, Equation (4.57) becomes

$$C_{pwood} = 4.1868(0.286 + 0.0011\ T + 0.01\ M)/(1 + 0.01\ M) \tag{4.58}$$

Solution of Equation (4.56) requires the moisture distribution inside the board to be known over each time step. Once again, we ignore the dependence between temperature and diffusion coefficient and estimate moisture distribution separately.

4.2.5 Solution Strategy of the Governing Equations

The finite difference approximation has been often used to solve the diffusion equation in the forest products literature. This has been due partly to the increasing interest in numerical analysis, and partly due to the

possibility of solving non–linear boundary conditions by the use of computer. The methods involve superimposing a grid with a finite number of intersections or points over the cross–section of a body and the unknowns are evaluated at each grid point. A possible problem associated with this solution is that the obtained moisture and temperature distributions between two grid points might be different from the real conditions, because finite difference approximations fit parabolas to three neighboring points to obtain the second derivatives. Under some conditions these parabolas "overshoot" and give misleading results. For this reason, analytical solutions are used to solve the governing equations in this study.

For the equation of linear flow of heat, Carslaw and Jaeger[47] proposed several analytical solutions under different boundary conditions. Since we assumed that the moisture diffusion coefficient is independent of the moisture concentration, the equation of diffusion is the same as that of conduction of heat. Thus the solutions are valid for both cases and combination of these solutions was used in this study to describe the moisture and temperature distribution across the board.

1. Constant Flux Solution

With the boundary condition of constant heat flux from the solid surface and zero initial temperature, Carslaw and Jaeger's solution of the linear heat flow equation has the form

$$v = \frac{FH_0}{K} \int_Y^{\infty} \operatorname{erfc} \frac{Y}{\sqrt{(4\ \kappa\ t)}}\, dY$$

$$= \frac{2\ FH_o\ \sqrt{(\kappa\ t)}}{K}\ \text{ierfc}\ \frac{Y}{\sqrt{(4\ \kappa\ t)}}$$

$$= \frac{2\ FH_o}{K}\left\{\sqrt{\left(\frac{\kappa t}{\pi}\right)}\ \exp\left(-\frac{Y^2}{4\ \kappa t}\right) - \frac{Y}{2}\ \text{erfc}\ \left(\frac{Y}{\sqrt{(4\ \kappa t)}}\right)\right\} \tag{4.59}$$

where v is the temperature of the solid at point Y. For the case of the moisture diffusion with a constant diffusion coefficient, Equation (4.59) takes the following form after allowing for the difference between diffusion and heat transfer,

$$Q = 2\ FM_o\left\{\sqrt{\left(\frac{t}{\pi D}\right)}\ \exp\left(-\frac{Y^2}{4Dt}\right)\right.$$

$$\left. -\frac{1}{2}\ \frac{Y}{D}\ \text{erfc}\ \sqrt{\left(\frac{Y}{4Dt}\right)}\right\} \tag{4.60}$$

in which,

$$\text{erfc}\ x \qquad = 1 - \text{erf}x$$

$$= \left\{\frac{2}{\sqrt{\pi}}\right\}\int_x^{\infty} \exp(-\xi^2)d\xi \tag{4.61}$$

and,

Q is the moisture concentration deficiency, i.e. decrease below the initial value. Under these conditions the surface value of Q (named as QS) is given by

$$QS = 2\ FM_o\ \sqrt{\left(\frac{t}{\pi\ D}\right)} \tag{4.62}.$$

The numerical evaluation of the error function for small values of x is quite straightforward because the series expansion for $\exp(-x^2)$ is uniformly convergent and so can be integrated term by term. The series expansion for $\exp(-\xi^2)$ is

$$1 - \xi^2 + \frac{\xi^4}{2!} - \frac{\xi^6}{3!} \ldots\ldots \tag{4.63}$$

whence term by term integration with respect to ξ gives the series

$$\text{erf}\xi = \xi - \frac{\xi^3}{3} + \frac{\xi^5}{2!\ 5} - \frac{\xi^7}{3!\ 7} \ldots\ldots \tag{4.64}.$$

The ratio of the (n)th term to the (n–1)th term (taking the first term ξ as at n=0 so that the next term has n=1) is

$$-\xi^2 \frac{2n-1}{n(2n+1)} \tag{4.65}$$

then,

$$\text{erf}\,(x) = \frac{2}{\sqrt{\pi}} \int_0^x \exp(-\xi^2)\, d\xi$$

$$= \frac{2}{\sqrt{\pi}} * \text{sum of series} \tag{4.66}$$

and

$$\text{ierfc}\,(x) = -x\ \text{erfc}\,(x) + \frac{1}{\sqrt{\pi}} \exp(-x^2) \tag{4.67}$$

in which $x = \frac{Y}{\sqrt{4Dt}}$.

Thus, Equation (4.60) can be rewritten as

$$
\begin{aligned}
Q &= 2\,FM_o\sqrt{\left(\frac{t}{D}\right)}\ \text{ierfc}\ x \\
&= 2\,FM_o\sqrt{\left(\frac{t}{D}\right)}\left\{\frac{1}{\sqrt{\pi}}\exp(-x^2)\right. \\
&\qquad \left. -x\left(1-\frac{2}{\sqrt{\pi}} * \text{sum of series}\right)\right\} \\
&= C\left(\frac{1}{2}\,\text{TORPI}\exp(-x^2) - x\,(1-\text{TORPI} * \text{sum of series})\right)
\end{aligned}
\tag{4.68}
$$

where

$$
C = 2\,FM_o\sqrt{\left(\frac{t}{D}\right)}
$$

$$
\text{TORPI} = \frac{2}{\sqrt{\pi}} \tag{4.69}.
$$

It should be pointed out that when x becomes greater than 6 ierfcx for mass transfer becomes very small so it is taken as zero in the actual calculation.

2. Laplace's Solution

Moisture concentrations at other drying times were obtained by Laplace's solution to the diffusion equation, which has the form

$$
mc(Y,t) = \frac{1}{\sqrt{(4\ \pi Dt)}}\int_{-\infty}^{\infty} mc'\ \exp\left\{\frac{-(Y-Y')^2}{4Dt}\right\} dY' \tag{4.70}
$$

where, $mc'=mc'(Y',0)$ is the initial value at point Y' and zero time. The problem of the integration limits appeared in the equation for the present situation is discussed in the next section.

Values of mc′ were described by fitting parabolas to the natural logarithms of values of mc′ at finite intervals of Y, which is equivalent to fitting error functions to actual values of mc′ and avoids the overshoot that is obtained by the more common practice of fitting parabolas to the actual values of mc′. The equation for mc′ then becomes

$$mc'(Y',0) = mc'o \exp\left(A_c(Y-Y')^2 + B_c(Y-Y')\right) \tag{4.71}$$

where mc′o is the initial value at Y′=0. Whence the equation (4.71) is rewritten as

$$\begin{aligned} mc &= \frac{mc'o}{\sqrt{(4\ \pi Dt)}} \int_{-\infty}^{\infty} \exp\left\{\frac{-(Y-Y')^2}{4Dt}\right\} \exp\left((A_c(Y-Y')^2+B_c(Y-Y')\right) dY' \\ &= \frac{mc'o}{\sqrt{(4\ \pi Dt)}} \int_{-\infty}^{\infty} \exp\left((B_c(Y-Y')\right) \exp\left(-(\frac{1}{4Dt} - A_c)(Y-Y')^2\right) dY' \end{aligned} \tag{4.72}$$

The first term in the integrand is expanded as the well known series for the exponential whence the whole integral is evaluated term by term using well known results to yield the series solution for mc in the form

$$mc = \frac{mc'o}{\sqrt{1-4A_cDt}}(1 + z_1 + z_2 + z_3 + ...) \tag{4.73}$$

in which the ratio of successive terms is given by

$$\frac{z(n)}{z(n-1)} = \frac{B^2}{4n(\frac{1}{4Dt} - A_c)} \tag{4.74}.$$

3. Solution for the Heat Transfer Equation

The constant flux solution mentioned above is for a semi–infinite plane. It is valid under the present condition for mass transfer because the diffusion coefficient is so small that $\text{ierfc}\left\{\frac{Y}{\sqrt{(4\ Dt)}}\right\}$ drops to a very small values when y=2 mm or so and t is in a step of one hour so that what happens at the surface during an hour has very little effect on the internal points.

With the heat transfer, however, the diffusion coefficient D is replaced by $\alpha = \kappa/(\rho\ C_{pwood})$ which is at least 1,000 times as great so that the ierfc solution dies out very much more slowly, e.g., $\alpha = 4\ x10^{-4}\ m^2/hr.$ gives $\sqrt{(4\alpha t)} = 0.04$ so at y = 20 mm, $\left\{\frac{Y}{\sqrt{(4\ \alpha t)}}\right\} = 0.5$ then $\text{ierfc}\left\{\frac{Y}{\sqrt{(4\ \alpha t)}}\right\} =$ 0.1996. This means that for 28 mm thick boards the ierfc solution has an appreciable value at the other side of the board and does not satisfy the boundary condition, that is, the condition of symmetry about the centre of the board.

The appropriate solution for the one–dimensional Fourier's equation in the region $0 < x < l$ (here l is equal to TB/2) with the boundary conditions of zero initial temperature, constant heat flux FH_o into the board at x=l, and no flow of heat over x=0 has the following form[47]

$$v = \frac{2\ FH_o\ \sqrt{\kappa\ t}}{K} \sum_{n=0}^{\infty} \left\{ \left(\text{ierfc}\ \frac{(2n+1)l-x}{\sqrt{4\ \kappa t}} + \text{ierfc}\ \frac{(2n+1)l+x}{\sqrt{4\ \kappa t}} \right\}. \tag{4.75}$$

The value at the board surface is obtained with x = 1 as

$$v = \frac{2\,FH_0\sqrt{\kappa t}}{K}\sum_{n=0}^{\infty}\left\{\text{ierfc}\frac{nl}{\sqrt{4\,\kappa t}} + \text{ierfc}\frac{(n+1)l}{\sqrt{4\,\kappa t}}\right\}$$

$$= \frac{4\,FH_0\sqrt{\kappa t}}{K}\left\{\text{ierfc}(0) + \text{ierfc}\frac{2l}{\sqrt{4\,\kappa t}} + \text{ierfc}\frac{4l}{\sqrt{4\,\kappa t}} + \text{ierfc}\frac{6l}{\sqrt{4\,\kappa t}} + \ldots\ldots\right\} \tag{4.76}$$

Accordingly, the value at the centre is obtained with x=0 as

$$v = \frac{2\,FH_0\sqrt{\kappa t}}{K}\sum_{n=0}^{\infty}\left\{2\,\text{ierfc}\frac{(2n+1)l}{\sqrt{4\,\kappa t}}\right\}$$

$$= \frac{4\,FH_0\sqrt{\kappa t}}{K}\left\{\text{ierfc}\frac{l}{\sqrt{4\,\kappa t}} + \text{ierfc}\frac{3l}{\sqrt{4\,\kappa t}} + \ldots\ldots\right\} \tag{4.77}$$

The method for evaluating the error function (ierfc x) was discussed in detail above and the same principle is applied here. It should be pointed out that since the above equations involve the series of the error function the calculation becomes very much slower.

4.3 Computer Program

The proposed mathematical model was programmed in TURBO PASCAL to compare the model with the experimental results. The program is included in APPENDIX E (B) which can be divided into following three main phases.

4.3.1. Data Input

The input of the data was arranged in two parts:

1. those that were either fixed by the geometry of the kiln such as the board spacing or by the nature of the wood being dried such as the board thickness, moisture content at the fibre saturation points, and reference value of the diffusion coefficient.

2. those that related to the specific experimental run such as air temperature, flow velocity, slice thickness, green and oven–dry weight of each slice. Data related to the specific experimental run were fed in as raw figures. The remainder of the data, which describes the physical properties of the wood and its relationships with the surrounding air such as surface friction factor, heat and mass transfer coefficient were established in the program.

4.3.2. The Calculation Phase

The theoretical calculation of the moisture and temperature changes starts with interpolating data from the initial slicing measurements (APPENDIX C) and calculating the air properties to establish the initial conditions of the calculation. To ensure the integration to be convergent and cover the effect of the Laplace's solution of the governing equations in the infinite region, the board is evenly divided in a step

$$DYEVEN = TB/(NSL+1) \tag{4.78}$$

where NSL is taken from the slicing measurements. One hour time step is also subdivided into

$$DTIME = \frac{1}{ROUND\left\{\left(\frac{16.0 \quad DR}{DYEVEN^2}\right)\right\}} \tag{4.79}$$

which ensures that the effect of neighbouring points on the point under observation is small enough to allow the use of $-\infty$ and ∞ as limits in Equation (4.70). Integration of the governing equations is made over each DYEVEN and DTIME and the results are printed out every hour. For moisture transfer, at the third hour from the start the error function (constant flux) solution of Equation (4.68) is used to get sufficient moisture differences between the surface and the first two points inside the board to allow fitting parabolas as described in section 4.2.5 (2), then the calculation is shifted to use the Laplace solution in which the surface value is set by the square root drying equation (4.62) over each time step. The surface mass flux was assumed to be near enough constant over the time interval DTIME. The calculation continues until the time at which the first set of slicing measurements was made. At this time the computer interpolates the measured data and compares the interpolated surface value with that calculated theoretically. When the difference is big the program adjusts the coefficient φ and restarts the calculation from the very beginning. Comparison of the interpolated and calculated surface moisture content is made throughout the whole drying process (at specified time intervals) and φ is adjusted accordingly.

Heat transfer calculation starts from the point where φ decreases from 1.0. When the external drying schedule changes, air properties, diffusion coefficient, heat, and mass flux are re–estimated for the new drying

conditions. Theoretical calculation of the moisture and temperature change is made under the new conditions.

4.3.3 Result presentation

The calculated results are presented in the form of calculated values and tables of profiles of the variables. Variation of the moisture content and temperature with drying time and across the board thickness are also plotted graphically.

4.4 Performance Evaluation of the Proposed Model

The requirement of the heat and mass transfer model is to predict moisture and temperature distributions needed for the ultimate development of an optimum drying schedule. Thus, performance evaluation of the proposed model should be treated as an element in the drying–schedule optimization procedures. The operational mode for the model in these procedures is first to optimize or statistically fit the model to a set of data (moisture and temperature distribution curves) from a specified drying run of the same species, moisture content, and thickness. This optimized version of the model would then be used to predict or simulate the moisture and temperature distributions needed to generate an optimum schedule for drying a kiln charge of the same species. The first step in the evaluation, then was to determine whether or not the model could be made to fit the experimental data sufficiently well to be used as a basis for the moisture–distribution prediction needed for the drying schedule optimization.

4.4.1. Test Arrangement

Tests for evaluating the performance of the model were conducted in the experimental kiln described earlier. The boards were entirely quarter–sawn Tasmanian eucalypt materials and chosen from a sawmill at "green off–saw" conditions. Caution was taken in selecting the boards to ensure that all the boards were from the same log in order to improve the chance that sample boards would be representative of the whole stack.

As soon as the boards were transported to the laboratory, one sample was taken from the middle part of each board for green property tests. The ends and edges of the boards were coated with the waterproof sealing compound to restrict the moisture transfer process to the one dimensional case. The boards were then stacked in the kiln. Based on the previous measurement of the unconfined shrinkage, the drying condition was initially chosen from the program DRYWOOD as 15 ^{0}C dry bulb temperature, 12.5 ^{0}C wet bulb temperature, and 0.7 m/s air velocity. The schedule was so chosen that the boards being tested were set under a controlled condition rather than being stored in a cool room as was done in the previous run.

Initial tests including measurements of the average moisture concentration, basic density, moisture distribution across the thickness of the board, and unconfined shrinkage were conducted and the results are shown in Figures 4.1 and 4.2. It can be seen from Figure 4.1 and 4.2 that the initial conditions for the boards being tested were nearly uniform so that one typical board could be chosen to represent the average conditions of the kiln charge.

With the new measurements of the green properties of the boards, a drying schedule was chosen again by trial using the computer program DRYWOOD so that the boards could be dried without surface check formation in about three weeks. Since the unconfined shrinkage for these boards (Figure 4.2) was smaller than that from the previous measurements, a higher temperature drying schedule (35 ^{0}C DB temperature, 29 ^{0}C WB temperature, and 0.7 m/s air velocity) was used for the rest of drying. During the whole drying process, sample boards were removed from the kiln at various time intervals for measurements of the net shrinkage, average moisture content, and moisture distributions.

The surface temperature of the boards was directly measured by a copper–constantan thermocouple and a Cambridge Potentiometer (TYPE 44228). The thermocouple was stuck onto the surface of the board, and leads connected to the potentiometer so that measurements could be made without opening the door of the kiln. One thermocouple was also set up to measure the air temperature at the upstream station so comparison between the measured air temperature and the controlled dry bulb temperature could be made to check on each other.

4.4.2 Results and Discussions

To compare the results from tests and computer simulation, the surface mass transfer area ratio and the reference value of the diffusion coefficient were adjusted by trial to get the best fit between the two sets of data. With the moisture content at FSP taken from the adsorption curve, i.e. 0.25 and

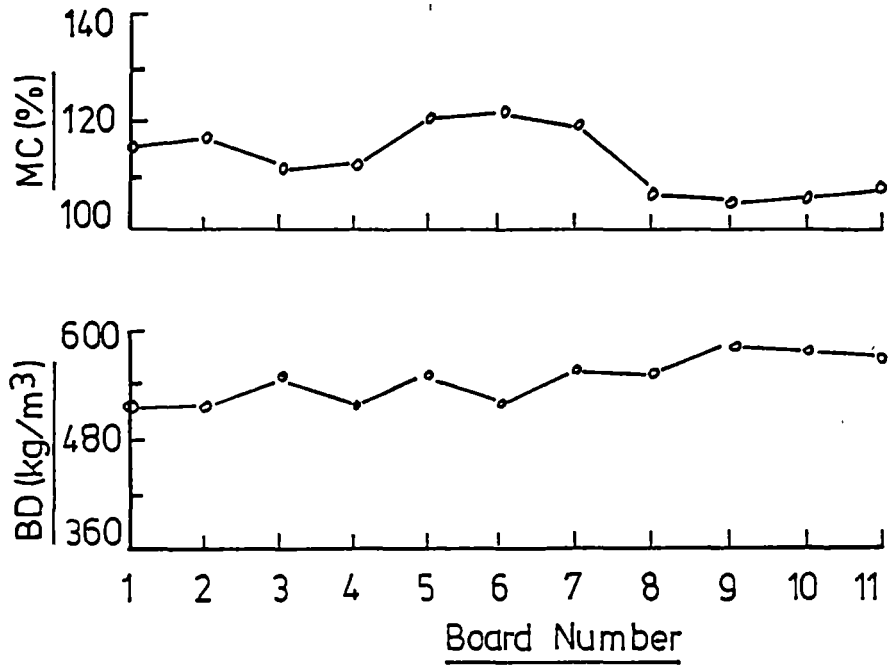

Figure 4.1

Initial Moisture Content (MC) and Basic Density (BD)

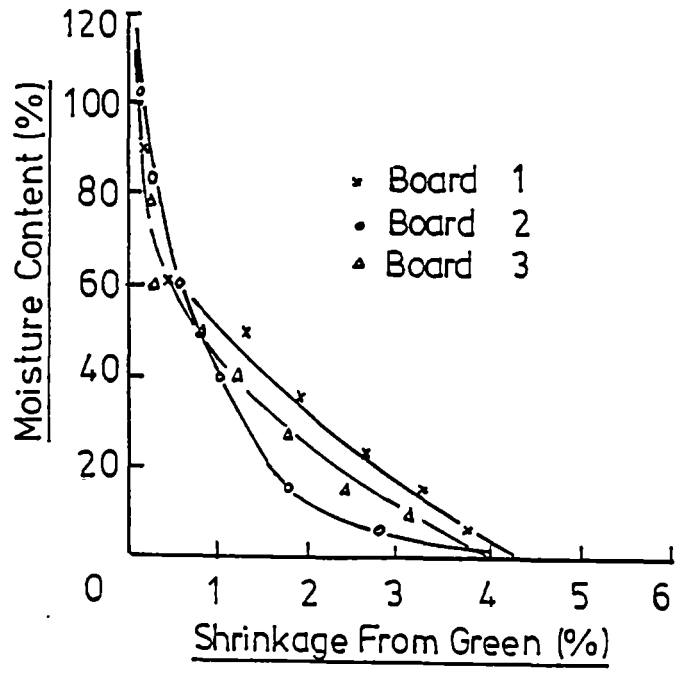

Figure 4.2

Unconfined Shrinkage

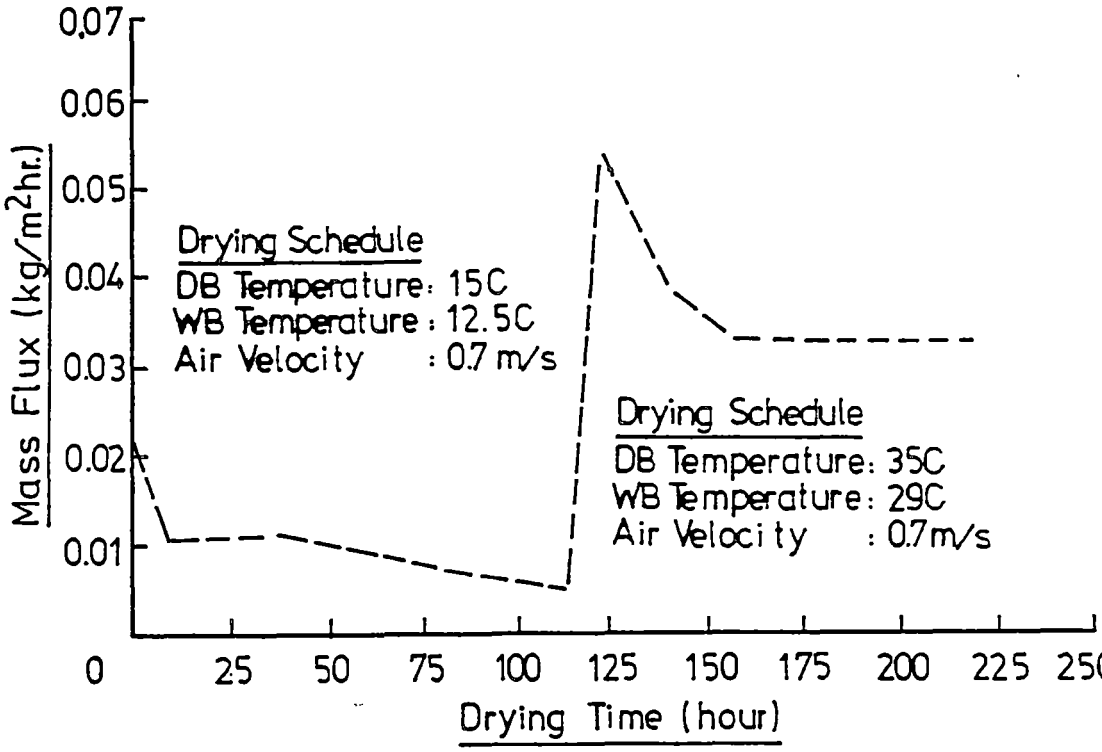

Figure 4.3

Evaporation Rate from Board Surface

the reference value of the diffusion coefficient equal to 8.1 $x10^{-7}$ $m^2/hr.$, the results for a typical board of the kiln charge are reported in Figures 4.3 to 4.9. Figures 4.3, 4.4 and 4.5 show the variations of the net surface mass flux FM_o, surface mass transfer coefficient φ and average temperature of the board with the drying time respectively. From Figures 4.3 and 4.4 it can be seen that, to match the measured moisture profile from the first slicing measurement at 45 hours, φ is required to start with a value of about 0.6 and discussion of this low value of φ is made later. This implies that at that stage of drying the effective area of the evaporation has to be reduced about 40 percent of the total value in order to make proper allowance for the restricted movement of the free water and the formation of dry patches on the wet

surface of the board. The reduction of the effective surface area results in the decrease of the total mass flux (φ FM_0) coming out from the surface, and thus causes excess heat left inside the board to increase the temperature of the board (Figure 4.5). As a result of the temperature increase, the net mass flux FM_0 decreases as shown in Figure 4.3. A proper balance between the board temperature, φ, and FM_0 is then maintained by the measured moisture profile. When the drying schedule changes, the net mass flux FM_0 increases to a higher value and new balances are formed and maintained by the new measurements of the moisture distribution.

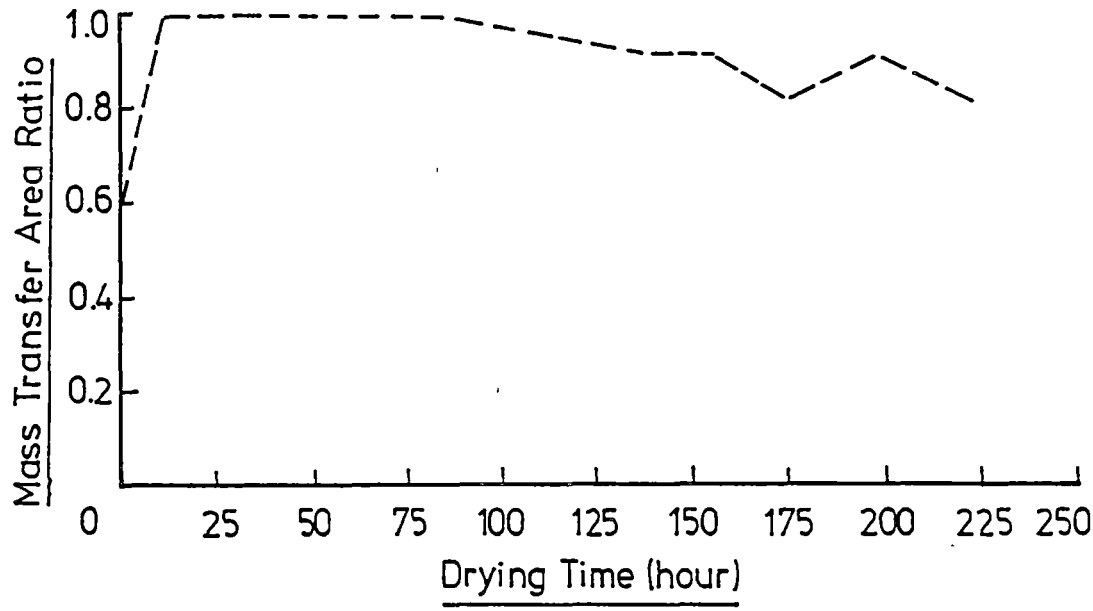

Figure 4.4

Variation of Computed Surface Mass Transfer Area Ratio

It should be pointed that the fitted variation of the area ratio φ differs from the expected pattern at the early stages of drying. This part of curve was obtained by balancing the calculated moisture distribution with the measurement at 45 hours, which is subject to the errors from the slice measurement and variation of the moisture content inside the board. Thus,

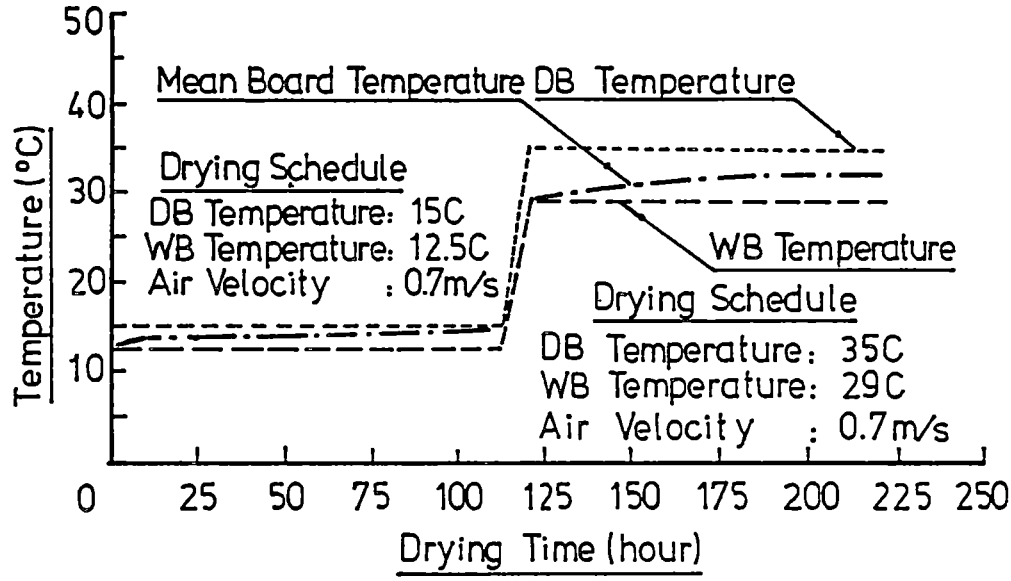

Figure 4.5

Drying Schedule and Mean Board Temperature

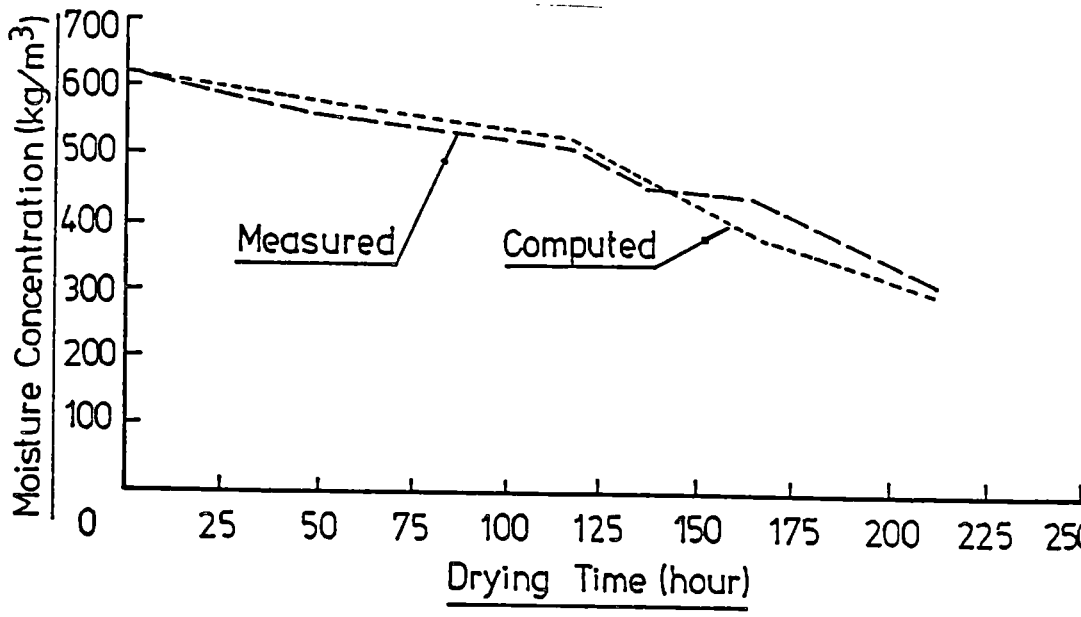

Figure 4.6

Computed and Measured Mean Moisture Concentration

to eliminate this problem, more measurements should be taken at the beginning of drying. Also, the present calculation was based on uniform initial moisture and temperature distribution across the board. This was done because of lack of data on these properties of the wood, but, addition of these effects to the present model is straight forward when appropriate data become available.

From Figure 4.5 it can be seen that the average temperature rose about 1.5 ^{0}C in the first 10 hours, which seems to be rather too quick compared with later changes. It is due to the reduction of the coefficient φ at the beginning of the drying, which causes more heat used to contribute to the temperature rise of the board. It may also have been due to an incorrect estimate of the initial temperature of the board. The average temperature at the end of the drying was substantially constant at about 33 ^{0}C, i.e. about 2 degrees below the dry bulb temperature, which appears to indicate that a proper balance was established between the air and the board. Figure 4.6 shows the comparison of the average moisture concentrations. Under this condition it can be seen that the difference between the calculated and measured values is within 10 Kg/m^3 moisture concentration which is equivalent to about 2 percent moisture content, except for one point at about 164 hours. This discrepancy can not be explained.

The interpolated and calculated values of the surface moisture concentration are shown in Figure 4.7. Examination of Figure 4.7 indicates that less than 2 percent moisture content difference between the measured and calculated values can be observed throughout the whole drying process.

Figure 4.7 also shows that the surface moisture content dropped quite slowly at the initial drying schedule (low temperature and high humidity), but after the drying schedule was changed it quickly decreased and reached close to EMC at about 170 hours.

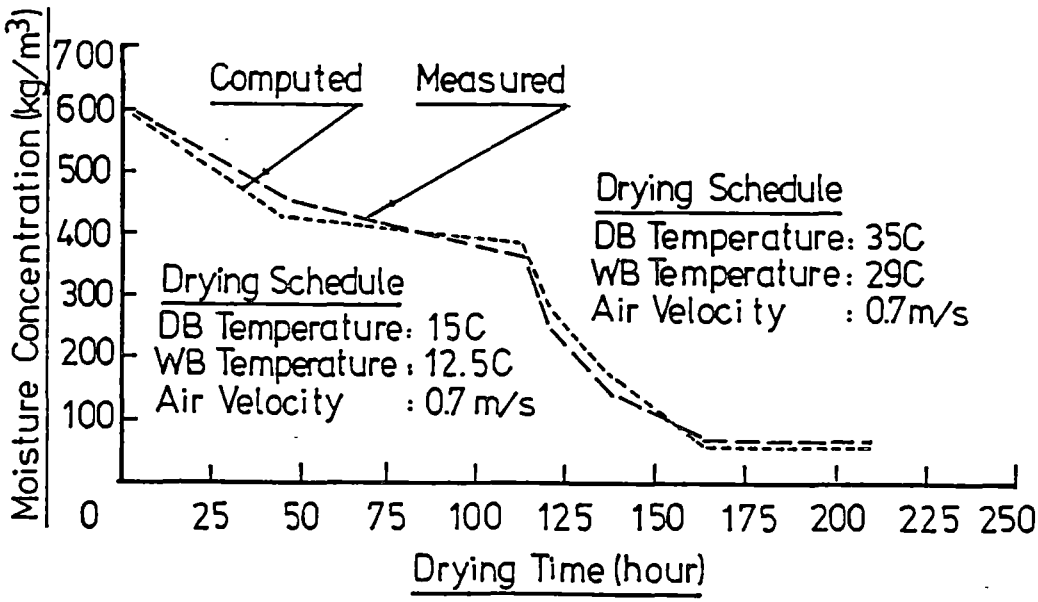

Figure 4.7

Moisture Concentration at Board Surface

Both the calculated and measured surface moisture concentration curves seems to expose the fact that the wood surface is not at EMC during the greater part of drying although several published descriptions of moisture diffusion and evaporation indicate that it is. In fact, the surface cannot be at EMC until drying is complete. Otherwise there would be no driving potential for the moisture transport through the surface boundary layer.

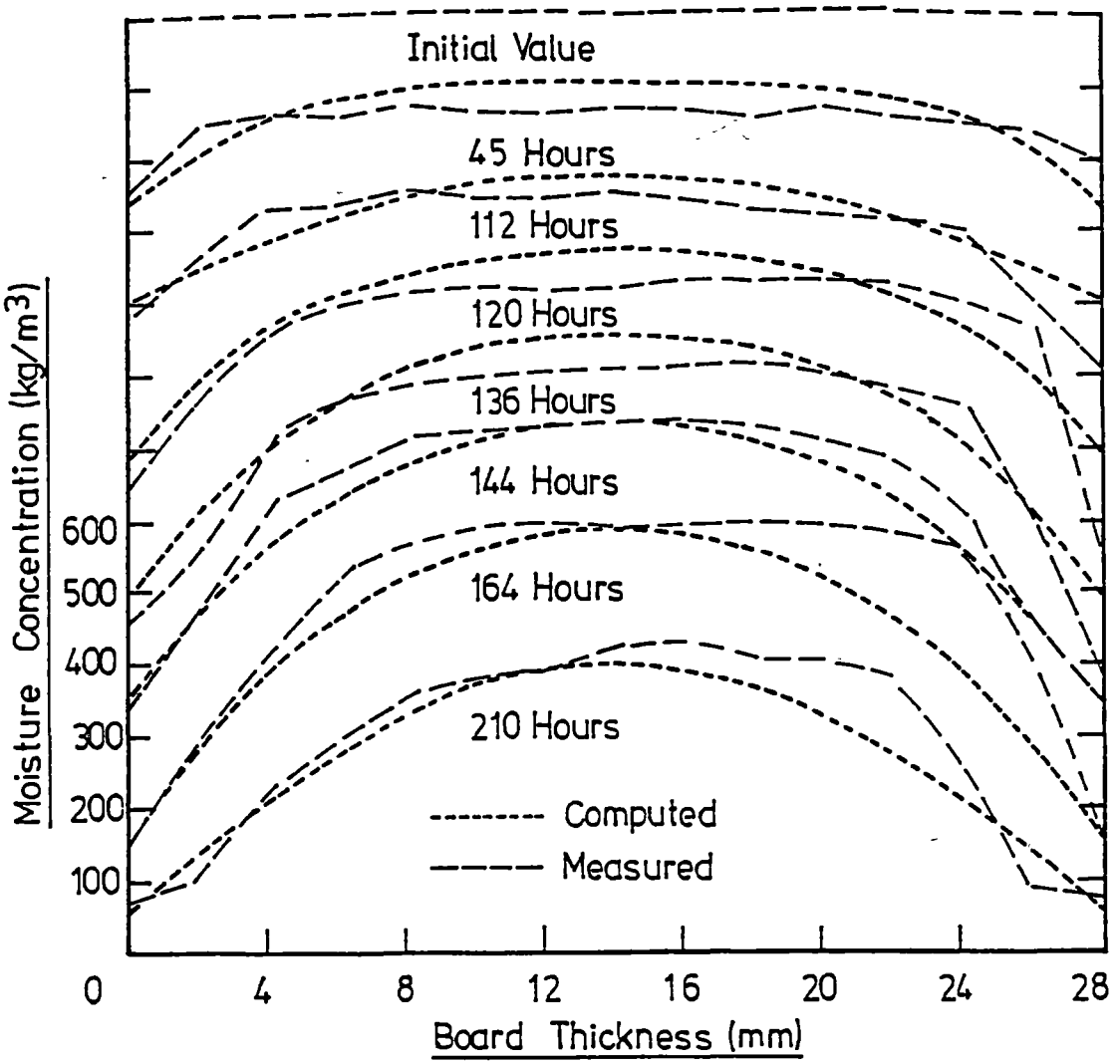

Figure 4.8

Moisture Concentration Profiles in Board

Figure 4.8 shows the moisture distributions across the board thickness at different times of drying. About 10 percent moisture content difference between the measured and calculated values is observed in the center part of the board at the early stage of drying. This seems to indicate that the diffusion coefficient used at that stage of drying was a little small. Also, the measured moisture concentrations from slices tend to be less than the real

condition as moisture is lost from thin slices very quickly at the high moisture content and no allowance was made for the moisture lost during slicing measurement. Close agreement between the calculated and experimental values of the moisture profile at later stages of drying seems to confirm that the moisture transfer process can be modelled with a diffusion coefficient independent of the moisture content in drying of eucalypt materials.

Table 4.2 shows the temperature measurements by the thermo–couples. Comparison of the measured air temperature and the controlled dry bulb temperature indicates that the results from both methods are quite close to each other (within 1 ^{0}C). From Table 4.2 it can be seen that after the drying schedule was changed (at 112 hours from the start), it took about 3 hours for the surface temperature to reach up to the new wet bulb temperature of the air.

Calculated temperature profiles inside the board and measured surface values were plotted in Figure 4.9. Due to the small wet bulb depression involved in the initial drying schedule (2.5 ^{0}C), the development of the temperature gradient inside the board is more clearly observed in the high temperature schedule. As shown in Figure 4.9, the surface temperature gradually increased from the wet bulb temperature of 29 ^{0}C, and reaches about 34 ^{0}C at 210 hours. The temperature rise in the center of the board was only within 2.0 ^{0}C. The average temperature rise within an hour of drying time was about 0.05 ^{0}C for the board surface and 0.02 ^{0}C for the

Table 4.2

Temperature Measurement by the Thermo–couples

Drying Time	Ambient Temperature	Control Temperature		Measured* Temperature			
		DB	WB	Air		B–Surface	
				Voltage	Temp.	Voltage	Temp.
hour	°C	°C	°C	mv	°C	mv	°C
0	11.0	15.0	12.5	0.14	3.64	0.06	1.56
45	10.5	15.5	12.8	0.21	5.50	0.11	2.86
113	11.5	34.5	29.2	0.88	22.4	0.55	11.6
115	13.5	34.7	29.3	0.82	20.9	0.69	17.6
120	13.0	35.1	29.4	0.79	20.2	0.74	18.9
136	10.0	34.9	28.8	0.95	24.2	0.89	22.6
144	15.5	34.7	29.4	0.72	18.4	0.67	17.2
164	16.5	35.1	28.8	0.70	17.9	0.63	16.2
210	16.2	35.2	29.0	0.71	18.2	0.66	16.9

* measured surface and air temperatures equal to the sum of the ambient temperature and the temperature from thermocouple.

center of the board. From Figure 4.9 it can also be seen that the measured surface values are in general agreement with the calculated ones. Calculated temperature profiles inside the board were not checked directly by measurement. However, the principle of the mathematical model appears to be sound, and the calculated values of the surface temperature are close to experimental values. The calculated profile is also expected to be reasonable.

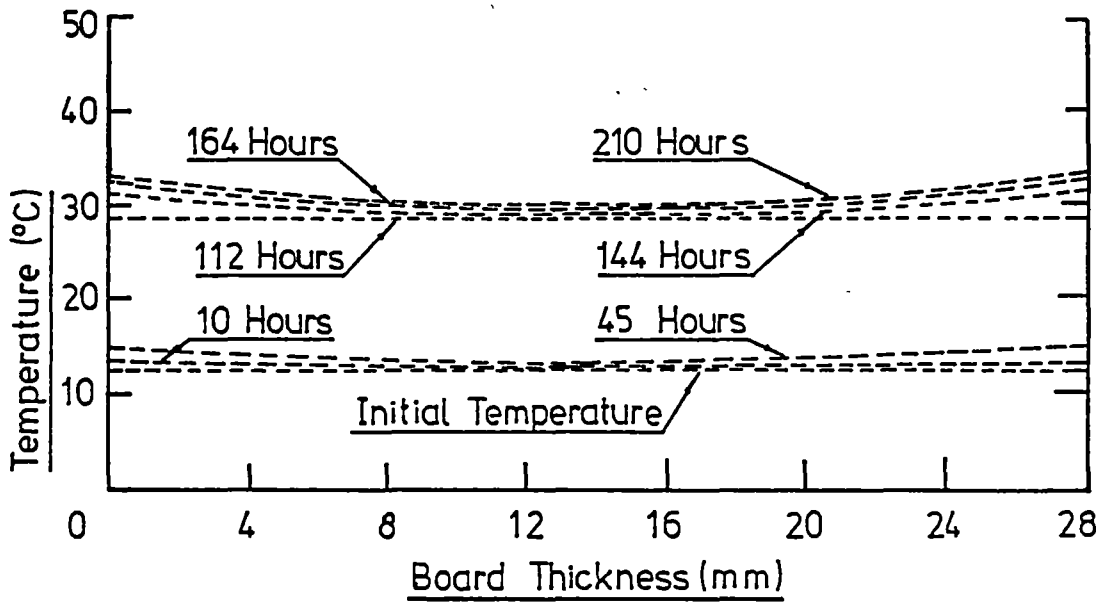

Figure 4.9

Temperature Profiles in Board

With the same data file, the moisture content at FSP that was used (i.e. 0.25 from the adsorption curve) was replaced by that from desorption curve, i.e. 0.30 and the program was run again. There seemed to be no significant difference in the overall drying behaviour that could be observed between the two cases.

4.5. Conclusions

The primary aim of the study was to investigate the heat and mass transfer process over the rough surface of the sawn board in the drying of Tasmanian eucalypt materials. Emphasis was placed on developing the theoretical model so that prediction of the drying behaviour of large populations of the boards could be made.

The over–simplified drying model of "free–water" and "bound–water" separated by a fibre saturation point was tested and proved to be unsuitable for modelling the process of drying eucalypt materials because of the restricted movement of the free water and the formation of the dry patches on the wet surface of the sawn board. An approach was thus proposed to handle this problem and its effect on the board temperature increase while the surface moisture concentration is still well above FSP. A mathematical model for predicting the moisture and temperature changes in the drying of eucalypt material was developed on the basis of detailed measurements on the boundary layer flow, in which the Reynolds analogy was found to give close prediction of the heat and mass transfer coefficients from the measured surface friction data.

The introduction of the surface mass transfer area ratio φ was shown necessary to get good results from the model. Adjustment of φ, however, has to be done by trial and no simple way of predicting it was found in this study. Experiments for measuring moisture and temperature change were conducted and the results were compared with simulation from the mathematical model, which shows that the model is working as it was hoped.

CHAPTER 5

THE DRYING OF THE TASMANIAN EUCALYPTS

Early drying tests conducted on the Tasmanian eucalypt materials confirmed the idea of using the computer program to quickly develop a drying schedule under which the boards being tested were dried without checking formation. During these tests, sufficient data were collected to enable a general test procedure to be outlined and a heat and mass transfer model of the drying process to be developed. For the previous runs, however, the tests were stopped shortly after the drying was started. This next run was to be of longer duration.

The measurements on the air flow so far indicate that the surface friction largely depends on the state of the surface of the boards which varies with the nature of the boards and their drying history, as well as the condition of the saws. With the chosen boards, however, it is not clear how the surface friction varies quantitatively through a complete drying process. Also, no experimental evidence can be found in the forest product literature about the effect of the temperature and humidity gradient on the boundary layer flow through the timber stack.

The heat and mass transfer model developed previously has been restricted to the one–dimensional case. This was done with the belief that the moisture was mainly transferred from the wide surfaces of the board as typically boards are 3 to 4 times as wide as they are deep; as well, the boards are stacked with their narrow faces in contact at the beginning of the drying.

In the real drying process, however, the one dimensional model for modelling the drying behaviour of the whole board is only valid for the beginning of the drying. This is due to the fact that the boards shrink during drying and shrinkage gaps appear between the edges of the boards. The previous measurements on the air flow across the boards have indicated that the gaps between the boards cause vertical air flow circulation. As a result, drying from the narrow surfaces of the board (edge drying) should be expected as soon as the shrinkage gaps appear. The problem of edge drying is commercially important because it is the cause of surface checks on the backsawn edges of quartersawn boards. However, there seems no experimental data which has been reported to show the effect of the edge drying on the overall drying behaviour of the whole board.

This study was, thus, carried out to dry the timber from its green state to the complete dry conditions so that the theory developed from the previous tests could be applied all the way from green to EMC. During the tests measurements on the velocity profiles and pressure drop were made at the different stages of the drying process. Because the process of drying was so slow in the later stages that it was thought desirable to see if these tests would give a lead into the effects of edge drying. For doing this, an attempt was made to separate the total water loss into two parts, namely from the wide surface and from the edges so that some new information on the edge drying might come to light.

5.1 Analytical Background

The primary objective of this chapter is to present the experimental results obtained. However, certain analytical techniques are required merely to evaluate the obtained data. It should be pointed out that since there is no stress at the corners of the boards to restrain shrinkage in the process of drying, it is higher there and equal to the unconfined shrinkage strain at the corners so the gap between edges of neighbouring boards not only varies with time, but also with distance from the wide surface (Figure 5.1). This situation must lead to the variation of the mass flux across the edge. Also, there is not any guidance from the literature about the pattern of air flow within this gap so we have no idea of the mechanism of transport of water vapour from drying through the edges to the main air stream. Thus, any analytical solution can only give a rough idea of the problem.

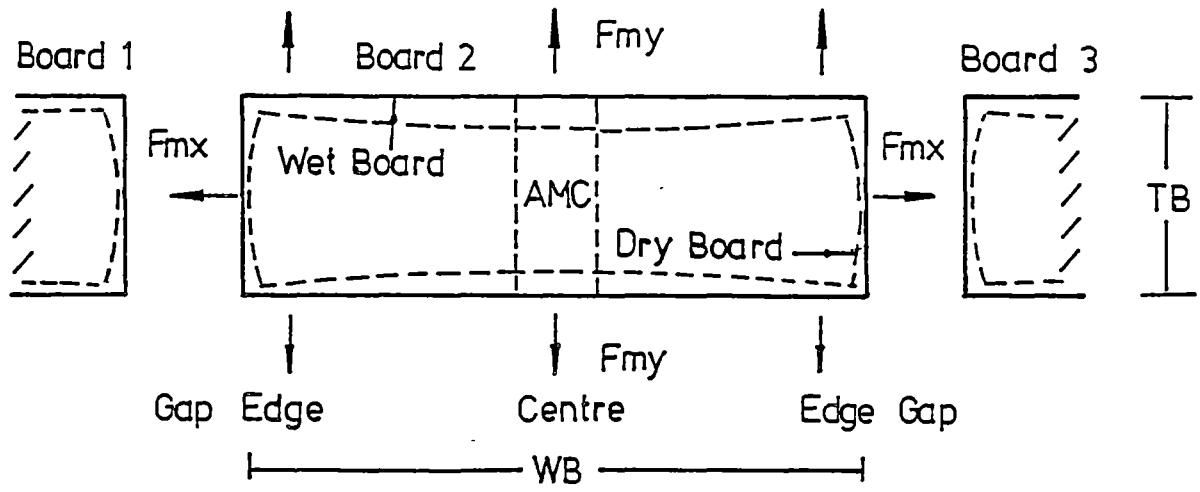

Figure 5.1.

Diagram Illustrating Edge Drying

In the process of timber drying, the moisture leaves the surfaces of the board in the way shown in Figure 5.1 if the small amount of drying from the ends of the board is ignored. Thus, to model this process precisely, two dimensional mass transfer must be taken into consideration. Since the timber is assumed to be an anisotropic solid, modelling of the drying process is often done using an equation similar in form to Fick's second law, as follows:

$$\frac{\partial\, MC}{\partial\, t} = \frac{\partial}{\partial\, x}\left(Dx \frac{\partial\, MC}{\partial\, x}\right) + \frac{\partial}{\partial\, y}\left(Dy \frac{\partial\, MC}{\partial\, y}\right) \tag{5.1}$$

where the coordinate of x and y is shown in Figure 5.2.

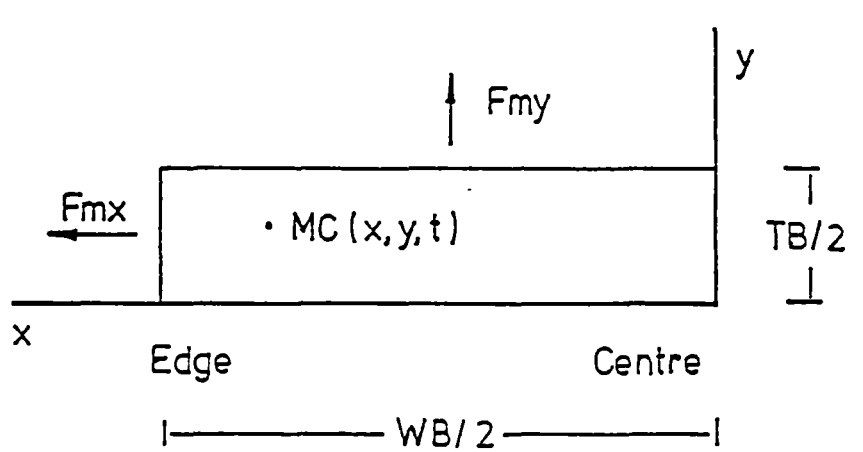

Figure. 5.2.

Two–dimensional Moisture Transfer in Drying Timber

A transformation to rectangular coordinates ξ and η can be found which reduces Equation (5.1) to

$$\frac{\partial\, MC}{\partial\, t} = D_{xx} \frac{\partial^2 MC}{\partial\, \xi^2} + D_{yy} \frac{\partial^2 MC}{\partial\, \eta^2} \tag{5.2}$$

These new axes are called the principal axes of diffusion and the coefficient D_{xx} and D_{yy} are the principal diffusion coefficients. If the further transformation is made

$$\xi 1 = \xi \sqrt{(D/D_{xx})},$$
$$\eta 1 = \eta \sqrt{(D/D_{yy})} \tag{5.3}$$

where D may be chosen arbitrarily, Equation (5.2) becomes

$$\frac{\partial\, MC}{\partial\, t} = D\left(\frac{\partial^2 MC}{\partial \xi_1{}^2} + \frac{\partial^2 MC}{\partial \eta_1{}^2}\right) \tag{5.4}$$

which has the same form as that for the isotropic material. Thus, this transformation reduces problems on the anisotropic material to the solution of corresponding problems on the isotropic material, or when it is bounded by planes perpendicular to the principal axes of diffusion. As mentioned earlier, timber is an anisotropic material with three principal property directions, namely longitudinal, tangential, and radial. In practice, the board is usually sawn from a log in the way that its length coincides with the longitudinal direction and its cross–section is oriented somehow in the R–T plane. The two orientations of major interest are known as backsawn and quartersawn. If the radius from the centre of the tree is large with respect to the board dimensions, then growth rings are essentially linear over the cross section. That is, the directions of the principal axes of diffusion are invariant over the cross section and are at right–angles to one–another. Thus, for perfectly backsawn and quartersawn boards, a further simplification may be made, in which the x and y axes coincide with the principal directions of diffusion.

The diffusion coefficient may be a function of x, y, MC and the temperature of the wood. In this study, the diffusion coefficient was taken to be independent of the moisture concentration MC, but different for the two directions x, y and varying with the temperature of the wood. Experimental result from Schaffner's measurement[7] on the diffusion coefficient in Tasmanian Eucalypt shows that in the principal directions of diffusion, the relationship

$$\frac{\text{Tangential Diffusion Coefficient}}{\text{Radial Diffusion Coefficient}} = 0.7 \tag{5.5}$$

is a good fit at all moisture concentrations. This relationship has been adopted for this study. The analytical solution of Equation (5.4) is available from such books as Carslaw and Jaeger[47] and Crank[48]. They show that the solution of Equation (5.4) when subject to certain initial and boundary conditions is given by

$$mc = MC(x,t)\, MC(y,t) \tag{5.6}$$

where MC(x,t) is the solution to the simple equation

$$\frac{\partial\, MC}{\partial t} = D \frac{\partial\, MC}{\partial\, x^2} \tag{5.7}$$

The initial condition in which the above simplification can be made is given as

$$MC(x,y,0) = MC_0 \text{ at } t=0, \text{ all } x, y \tag{5.8}$$

which denotes an initially uniform moisture content throughout the board.

The boundary conditions are given as

$$MC(x,y,t) = EMC \text{ at } x=WB/2,\ y=TB/2,\ \text{all } t \tag{5.9}$$

which assumes that the surfaces of the board comes to EMC as soon as the drying starts and remains at this value for all time thereafter. This assumption is rather crude, particularly during the early stages of drying. However, there seems no other practical ways to deal with the boundary conditions which will give an analytical solution for two dimensional diffusion equation. An attempt was made to show the effect of the edge drying and the validity of the assumption made about the surface boundary conditions by comparing the calculated values with the experiments.

It is shown later in the chapter that an attempt was made in the process of the experiments to separate the total water loss from the board into two parts, namely, from wide surfaces and from the edges. This was done with the intention that the mass fluxes from the wide surfaces and the edges as functions of the drying time could be obtained, which then leads to the solution of the two dimensional diffusion equation. However, the separation has not been successful as the variation of the moisture content along the length of the board leads to unrealistic value of the mass flux (Figure 5.6). The variability of the material is so high that, in the early stages of drying, it was not uncommon to find that the measurements from slices indicated that moisture was moving in through the edges rather than out.

Under the assumption that the surface comes to EMC as soon as the drying starts, one of the analytical solutions for the one dimensional diffusion equation has the form of

$$\frac{MC - EMC}{MC_o - EMC} = \frac{4}{\pi}\left[\cos\left(\frac{\pi\ y}{TB}\right)\exp\left\{-D\ t\left(\frac{\pi}{TB}\right)^2\right\}\right.$$

$$-\frac{1}{3}\cos\left(\frac{3\ \pi\ y}{TB}\right)\exp\left\{-9Dt\left(\frac{\pi}{TB}\right)^2\right\}$$

$$+\frac{1}{5}\cos\left(\frac{5\ \pi\ y}{TB}\right)\exp\left\{-25Dt\left(\frac{\pi}{TB}\right)^2\right\}$$

$$\left.-.....\right\} \qquad (5.10)$$

where, y has a value from -(TB/2) to (TB/2). The right hand side of Equation (5.10) is known as a Fourier series.

The average moisture content inside the board at any particular time can be obtained by integrating the above equation as

$$\frac{AMC-EMC}{MC_o-EMC} = \frac{1}{TB}\int_{TB/2}^{-TB/2}(\text{Series y})\,dy$$

$$= \frac{8}{\pi^2}\left[\exp\left\{(-D\ t\left(\frac{\pi}{TB}\right)^2\right\}\right.$$

$$\left.+\frac{1}{9}\exp\left\{-9Dt\left(\frac{\pi}{TB}\right)^2\right\}\right.$$

$$+\frac{9}{25}\exp\left\{-25Dt\left(\frac{\pi}{TB}\right)^2\right\}$$

$$+.....\Bigg] \tag{5.11}$$

The solution of the two dimensional diffusion equation (5.4) is thus obtained as

$$\frac{MC - EMC}{MC_0 - EMC} = [\text{Series x}]\,[\text{Series y}] \tag{5.12}$$

for the moisture concentration at the point (x,y,t), and,

$$\frac{AMC-EMC}{MC_0-EMC} = \left\{\frac{1}{WB}\int_{WB/2}^{-WB/2} \text{Series x}\,dx\right\}\left\{\frac{1}{TB}\int_{TB/2}^{-TB/2} \text{Series y}\,dy\right\} \tag{5.13}$$

for the average moisture concentration inside the board.

The equations (5.12) and (5.13) were programmed for the boards to be either perfectly quartersawn or backsawn and the program was coupled in the one–dimensional computer program developed in Chapter 4. By adjusting the diffusion coefficient and φ, the one–dimensional part of the program provides the best fit of the calculated moisture distributions and those from the measurement of the central part of the board. The two–dimensional part of the program then works to show the effect of the edge drying.

5.2. Experiments

The experiments were conducted in the experimental kiln described earlier. The initial trial was made with the backsawn boards in an attempt that they could be successfully dried without any predrying treatment. This trial was, however, not successful as the present design of the kiln control system does not allow very low fan speeds (for safety of the heating element), say 0.5 m/s wind speed. Also, there was no cooling system provided which is needed to reduce the temperature of ambient air in the early stages of the drying, as was required by the solution of the DRYWOOD program for backsawn materials. Thus, even at minimum or no heating conditions, the backsawn boards were still checked at the second day. As a result, the experiment had to be stopped as the heat and mass transfer from the checked surfaces are much different from the unchecked ones.

Quartersawn boards cut from one single log were selected for the second trial. Samples from the centre part of the boards were cut for the tests of the green properties as soon as the boards were taken to the laboratory for the selection of the drying schedule. Only the ends of the board were coated with the water–proof sealing compound so that the moisture inside the wood could move in the other two directions during drying. The boards were then stacked in the kiln so that the air flow was across the boards and the racking space was chosen as 20 mm high. During drying, measurements on the velocity profile and pressure drop were made at different stages of the drying process to assess the variation of the surface friction. Also, about 20 mm long samples were cut from one end of the sample boards at a time interval of about 24 hours in the early stages and 48 hours in the later stages of drying.

Three small samples with the size of 20 x 20 x 28 mm (one from the outer part, and the other two from the central part of the board) were taken to measure the average moisture contents and the moisture distribution in the central part of the board. The freshly sawn end was re–coated before replacing in the stack. The space cut for sampling was filled by a dummy board to ensure even flow through the stack. Care was taken to mark the position of the sample boards so that the spaces between the boards were not affected by moving the boards for sampling.

The sample board was weighed and the total average water loss rate from the board over the time period was estimated as

$$TWL = \frac{W_1 - W_2}{t_1 - t_2} \tag{5.14}$$

where, 1 and 2 denote two points of the measurement. By assuming that the moisture in the centre of the board was transferred only in the y–direction and the measurements from the sample cut at the end of the boards can represent the average conditions of the whole board, the water loss rate from the wide surface of the board was then obtained as

$$WWL = \frac{(AMC_1 - AMC_2)\, W_1 \left(\frac{1}{1+AMC_1}\right)}{t_2 - t_1} \tag{5.15}$$

where, AMC_1 and AMC_2 are the average moisture content at the central part of the board at times t_1 and t_2 respectively.

Thus, the mass flux from the edges was estimated as

$$F_{mx} = \frac{TWL - WWL}{2\ TB\ (LB\ -\ n\ SL)} \qquad (5.16).$$

5.3. Results and Discussions

Based on the measurement of the boundary layer properties, the surface friction factor was estimated. Table 5.1 shows the values at about 100 hours from the drying start. It should be pointed out that in order to prevent the formation of the surface checking, a low free stream velocity (0.8 m/s) was used in the experiments. Under this velocity, the measurement on the variation of the boundary layer properties and the pressure drop at different stages of the drying process is subject to large uncertainty as there was insufficient accuracy of measurement to justify any change. Thus, it had to be taken as constant in the experiment.

Table 5.1

Measurement of the Surface Friction

Hot Wire Reading Correction Factor	$V_a = (1 + 0.0338)\ V_0$					
Boundary Layer Properties	upstream			downstream		
	U m/s	δ^* mm	θ mm	U m/s	δ^* mm	θ mm
	0.81	2.4	0.97	0.85	2.54	1.15
Pressure Drop			0.035	mm water		
Friction Factor			0.0116			

The one dimensional part of the program was run over a period of 700 hours with a constant surface friction factor of 0.0116. The comparison of the moisture concentrations between the calculated values and the measured ones from the centre of the board is shown in Figure 5.3, for which the reference value of the diffusion coefficient was fitted as a constant value of 3.5×10^{-7} m^2/s.

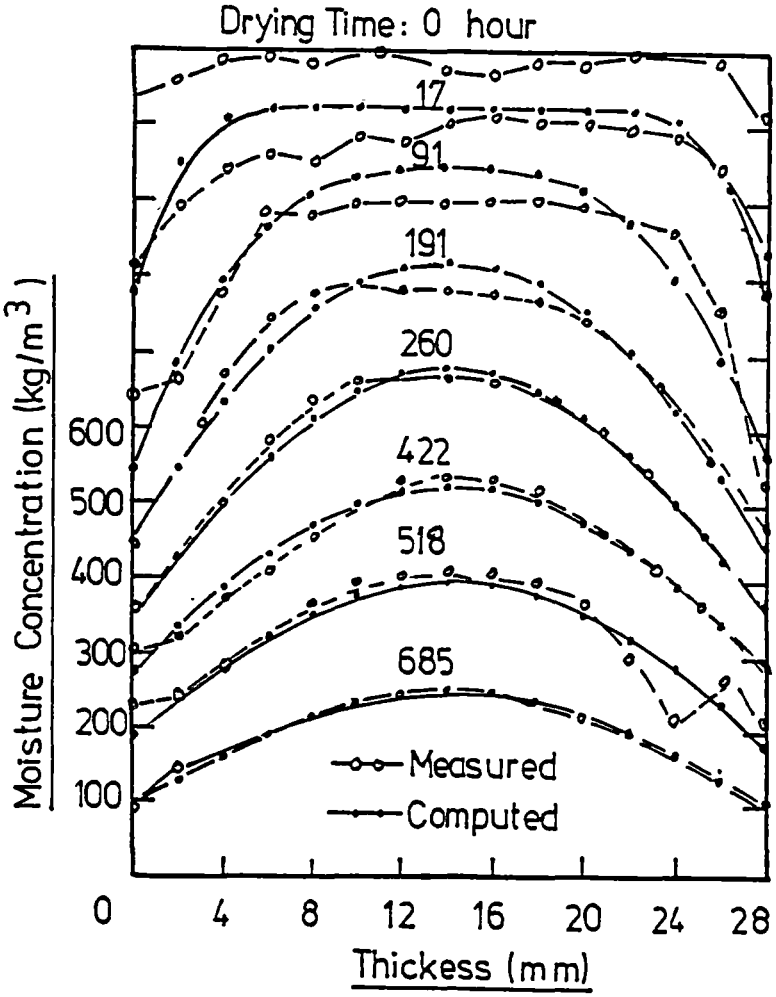

Figure 5.3

Comparison of Moisture Concentration

Figure 5.4 shows the variation of the measured average moisture contents at the outer and central parts of the board. From Figure 5.4 it can be seen that the amount of difference in the average moisture contents of the two parts is very small at the beginning of the drying. This difference gradually increases and reaches to a maximum value at about 300 hours, then decreases until zero at the complete dry condition. This pattern of variation would imply that at the beginning of the drying, since only a small gap exists between the edges of two neighbouring boards, the drying from the edges is relatively small and the moisture content inside the board tends to be uniform across the width of the board. As the drying proceeds, however, a

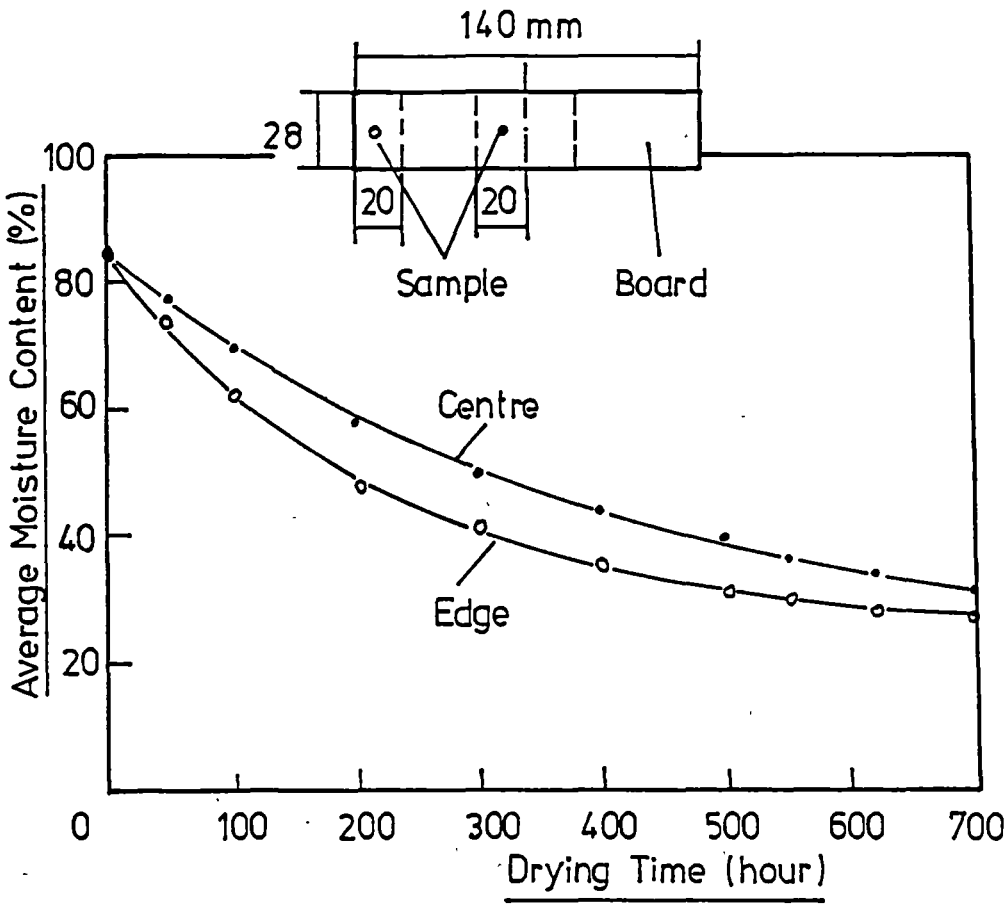

Figure 5.4

Variation of Average Moisture Contents Across the Board

shrinkage gap appears and increases in width both in time and in direction across the board as indicated by Figure 5.1, the drying from the edges then increases. At the later stages of the drying, the drying rate from the outer part of the board becomes slower than that from the central part and the difference in the average moisture contents then decreases until the complete dry conditions.

The calculated average moisture concentrations under two dimensional conditions are shown in Figure 5.5 together with the measured values. The initial moisture concentration of the board was 502 Kg/m^3 and the equilibrium moisture concentration corresponding to the conditions used (30°C, 78 percent relative humidity) was 91 Kg/m^3. Since the calculation is

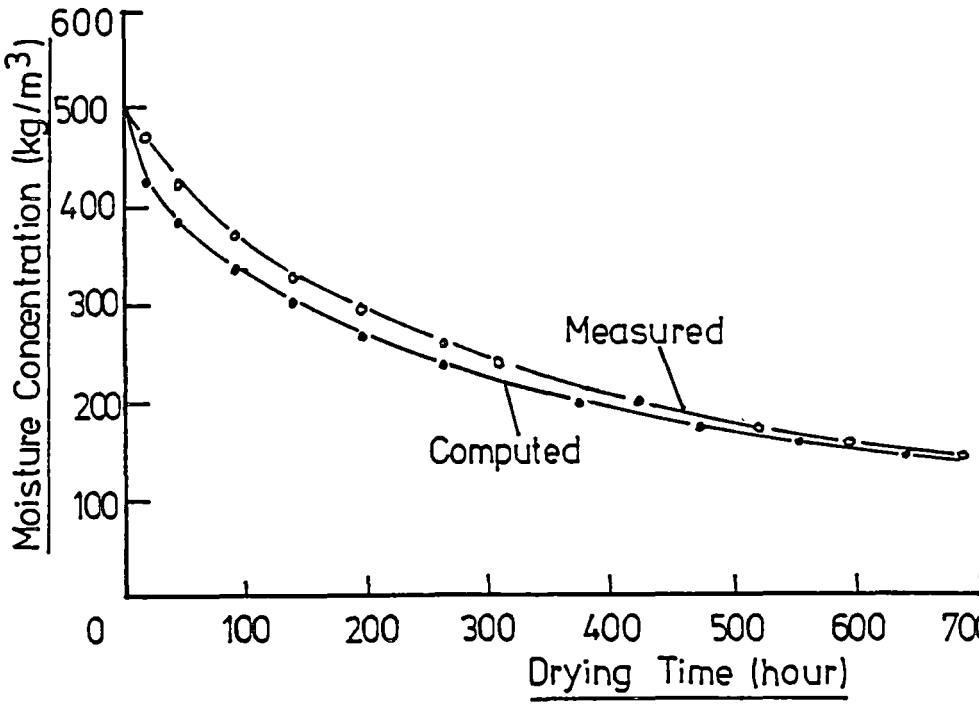

Figure 5.5.

Computed and Measured Moisture Concentrations

based on the assumption that the surface comes to EMC as soon as the drying starts, which provides a steeper moisture gradient between the surface and inside the board, the calculated values are smaller than the measured ones at the early stages of the drying process. The difference, however, decreases with the increase in the drying time and after about 450 hours the two values are nearly equal. This clearly indicates that the calculation based on the assumption that the surface comes to EMC as soon as drying starts, which is widely used in the forest product literature, would over-estimate moisture loss at the early stages of the drying. The program used for one-dimensional drying does not use this assumption and gives much better agreement with very little additional calculation.

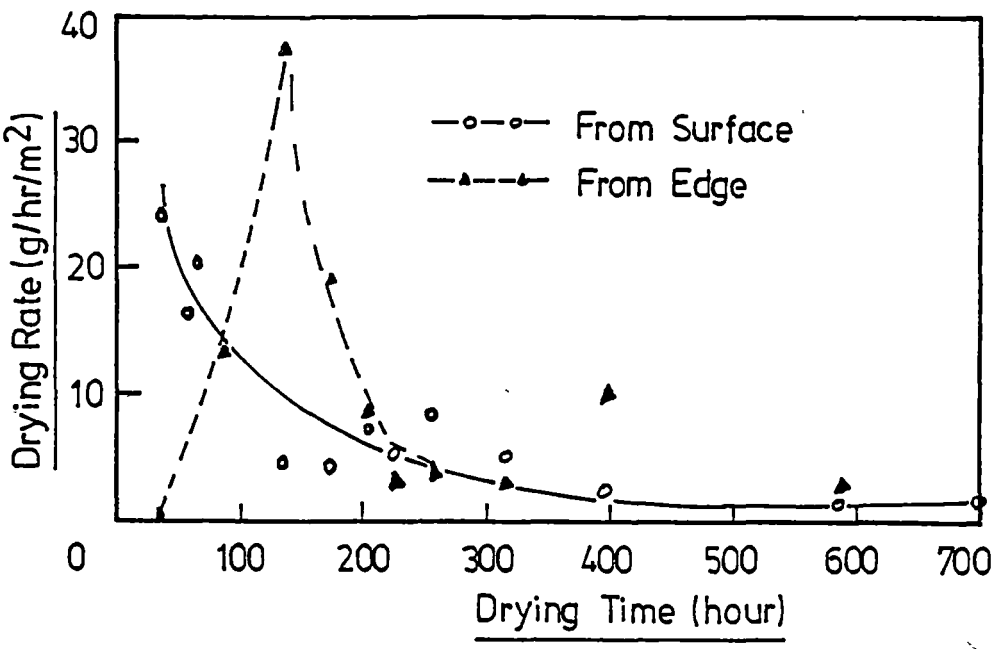

Figure 5.6.

Measured Drying Rates from Surface and Edge

Two dimensional moisture distributions calculated from the mass transfer simulation at the different drying times are shown in Table D5.1 in APPENDIX D for a quadrant of a drying board. It can be seen from Table D5.1 that the effect of the edge drying increases toward the centre of the board with the increase in the drying time. At the later stages of the drying process this effect reaches up to 40 to 50 mm inside the board, which leads to a substantial variation of the moisture contents across the width of the board. The separation of the mass flux from the wide surfaces and edges as calculated from the measurement is shown in Table D5.2 (A and B) and Figure 5.6. It can be seen from Table D5.2 (B) that the surface water loss (WLS) calculated from the measurement of the average moisture content in the centre part of the board is subject to errors associated with the variation of the moisture content inside the board, which in turn affects the calculation of the water loss from the edges. As a result, the separated mass flux is imprecise and the obtained values seem too variable to be used for solution of the two dimensional diffusion equation. Thus, other approaches to the problem have to be considered. It appears that a study of edge drying effects should be based on tests on sections that are more nearly square.

5.4 Conclusions

Quartersawn Tasmanian eucalypt timber was dried without surface checking formation from the green to the complete dry conditions. Sufficient data was collected in the process of experiments to test the one dimensional heat and mass transfer model developed previously.

The effect of the edge drying due to the shrinkage gap were shown by measuring the average moisture content from the the samples taken from the different parts of the board. The separation of the water loss from the wide surface and edges was made, but the result so obtained was imprecise and subject to the errors associated with the variation of the moisture content along the length of the board.

The two dimensional diffusion equation was solved analytically by assuming the surface comes to EMC as soon as the drying starts. The validity of such assumption for the drying of the Tasmanian eucalypts was shown by comparing the calculated values of the average moisture content with those from the experiments.

CHAPTER 6

THE MECHANO–SORPTIVE EFFECT IN THE DIRECTION PERPENDICULAR TO GRAIN

Wood is not an ideal elastic material, which means that when subjected to a prolonged loading it undergoes increasing distortion. This increase in distortion under load can be caused under both constant and changing moisture conditions of the wood. The former is known as mechanical creep, while the latter is known as mechano–sorptive effect.

CSIRO tests on beams have shown that mechanical creep is almost independent of moisture content so long as the moisture content remains constant, but is strongly dependent on temperature and time. The effect of a change in load on a beam takes about a day to settle down to a new deflection at loads less than about half the ultimate load. At higher loads beams creeped to failure.

When the moisture content changed in a loaded beam the effects of volume change due to change of moisture content and that due to stress interacted in the mechano–sorptive effect. This change occurs almost as rapidly as the change in moisture content. Since moisture changes of wood may occur as a consequence of normal daily and seasonal variations in environment, the effects of deformation so induced are recognized as of very substantial practical significance in structural situations. Particularly, that is because the deformations involved with extensive and repeated cyclical moisture changes may be up to many times greater than those arising from initial loading at same imposed stress level. Consequently, the mechano–sorptive effect can cause aesthetically unacceptable deflection of beams and columns, and may seriously reduce strength.

6.1 Literature Review

6.1.1 Mechano–sorptive Effect

The history of investigations into the effect dates back to World War II. Literature available indicates that Lawniczak[49] first showed that in wood strained to a given extent, the rate of the subsequent stress relaxation was increased if moisture content of the wood was allowed to change. Armstrong and Kingston[50] reported that the rate and extent of deflection of wooden beams under bending load was considerably greater if moisture content changes occurred at the same time. To explain this, Armstrong and Kingston first suggested that the enhanced deflection of beams accompanying moisture content changes may have arisen from additional stresses created in the beams by moisture gradients associated with the moisture content change.

Christensen[51] showed that in specimens of wood which are made thin enough, the rate of change in vapor pressure is not controlled by diffusion of moisture through the wood but by a much slower mechanism, thought to be associated with relaxation of swelling stresses. Since moisture is able to diffuse into these thin samples more rapidly than it can be incorporated into the swelling structure, the moisture content of the wood is presumed to be changing nearly uniformly throughout. By using sufficiently small specimens to study the effect of changing moisture content on bending of wood under load, Armstrong and Christensen[52] showed that the enhanced deformation still occurred and hence was associated with the moisture content change itself and not primarily with stresses arising from moisture gradients.

In order to describe this phenomenon more fully, Armstrong and Kingston[53] extended their observations into wood under bending, compressive, and tensile loading while subjected simultaneously to various sequences of moisture content change. It was found that a reduction in moisture content causes enhanced deformations under bending, compressive, shear, and tensile loading, whereas an increase in moisture content, except when it is the first moisture change, causes only a small increase or even a reduction in deformation. With cycling of moisture content, a resultant continuing increase in deformation occurs, reaching a value much greater than the corresponding initial deflection at constant moisture content. When the first change in moisture content is an increase, deformations in wood in bending and tension increase markedly, even after allowance is made for swelling. The largest changes in deformation arise in wood in compression; intermediate values arise in tension. It was also shown that the rates of change in deformation is dependent upon the rate of change in moisture content, and the magnitude of the final deformation is unaffected by the rate of change but is dependent upon the amount of the change in moisture content. The deformation is not therefore directly time–dependent.

The effect is seen in hardwoods from the green state to the air–dry condition, but in softwoods there appears to be almost no change from green to FSP then it appears to be related to the unconfined shrinkage curve which, itself, is almost linearly related to moisture content between FSP and air–dry condition. No reasonable explanation has been advanced for this difference in behavior between the two types of species. All existing hypotheses seem to run into contradictions before the argument is far advanced because of the near linearity of the ratio right from the green state

in hardwoods and the almost zero values above fibre saturation point in softwoods. This difference has been observed in both wetting and drying tests.

The bulk of mechano–sorptive effect is retained after the removal of stress. A large part of the deformation due to this effect is, however, recoverable after removal of the primary activating force when the wood is taken through another moisture cycle. Subsequent tests have shown that some beams crept to failure at about 1/3 the ultimate load (when measured at initial loading) after cycling humidity.

Tests in bending on reconstituted wood such as hardboard and particle–board have also been carried out[54,55], and although differences in behaviour have been observed during absorption and desorption of moisture, all workers have found a large and progressive increase in the total deformation of beams of reconstituted wood during moisture content cycling.

A suggested qualitative explanation of the phenomenon has been advanced in terms of a dynamic interaction between water and wood substance during water movement and the contribution of secondary bonding, including hydrogen bonding, to the strength of wood[56,57]. It is suggested that under the bias of an external force and in the interval between the breaking and reformation of hydrogen bonds during moisture movement in a desorption process, the molecular chains undergo displacement in the direction determined by the external force because of temporary weakening of the molecular system. It should be pointed out that those explanations have the common proposal that moisture movement from one sorption site to

another affects the hydrogen bond systems in the amorphous regions between and within the cellulose chains in the wood cell and that this movement of water molecules is facilitated by conditions of sorption. Usually, the moisture content of the wood changes under these conditions; however, it is possible to cause water molecules to move through wood without changing the moisture content, and under this condition enhanced deformation should also occur if temporary bond rupture during moisture movement is the source of the mechanism.

Armstrong[58] conducted experiments on a hollow compression specimen of wood which was designed to enable a moisture gradient to be maintained through the specimen without causing a change in moisture content of the material. He demonstrated that strain was not affected by the movement of water through wood as long as the moisture distribution remained constant. From the results of these experiments, he proposed that the phenomenon could be explained in terms of 'displacement between the cellulose chains of the wood substance, under the bias of an external force, following changes in the macromolecular configurations initially motivated by volume change in wood during sorption of water. Without this motivation no relative displacement occurs between units of the molecular system, even though water molecules move through the system and exchange with those present between hydroxyl groups of adjacent cellulose'.

Further study conducted by Armstrong[59] on the collapsible and non–collapsible species of wood showed that the effect coincides with the abnormal shrinkage (collapse) and normal shrinkage of the wood, thus provided further evidence to support his explanation of the mechanism of

mechano–sorptive behaviour in wood. Quantitative evidence is, however, needed to show that distortions in the cell wall which accompany collapse of the cell during loss of free water cause volume changes in wood substance. No such evidence is yet available.

It needs to be noted that the arguments mentioned above have been based on considerations at the molecular level of hydrogen bonding in cellulose. Hiski Kippo[60], however, has raised the idea of reconfiguration of long chain polymers in the hemi–cellulose and perhaps in other components (e.g. polymeric lignins). It is suggested that the celluloses are mechanically much stronger than hemicellulosics and solvents (e.g. water) and do not swell the crystalline regions of wood. Hemicellulosics, however, are weaker and can become highly swollen. During a drying process one side of an amorphous region is likely to become depleted in water before the other, leaving 'solvent holes' in the swollen amorphous regions, into which polymer chains can take up new positions. In such a scenario, the main feature of the mechano–sorptive effect can be accounted for and is associated with a change in moisture content. The explanation, however, does not account for other effects, e.g. difference between hardwood and softwood reported above.

6.1.2 Effect of Temperature on Creep Responses of Wood

The influence of temperature on creep of wood when its moisture content is maintained constant has been conducted both at constant temperature and cyclic temperature change conditions. Stamm[2] made a general reference to the fact that a temperature increase had a plasticising effect on the reaction of the cell wall. Davidson[61] demonstrated that, for

two softwoods and one hardwood species at moisture contents in the range from 18 % to 20 %, the rate of creep increased with temperature level (held constant). Comparable rate increases occurred with each 10 ^{0}C step from 20 to 50 ^{0}C, but there was a much larger rate increase with the step from 50 to 60 ^{0}C. It was suggested that the latter might be explained if 'some of the hydrogen bonds in the wood cellulose were broken at those higher temperatures'.

In bending tests on small water saturated wooden beams of Japanese cedar, Kitahara and Yukawa[62] showed that when the temperature was raised within the range of 20 ... 50 ^{0}C during a creep experiment, the creep response was greater than when the temperature was maintained constant at the highest level throughout the test. With the same species and moisture conditions, Arima[63] made tests in compression perpendicular to the grain, at temperature levels from 20 to 75 ^{0}C. In that case there were similar initial rate changes with temperature steps, but a substantial increase in creep rate at the higher temperatures; most of the latter seemed to be stimulated at 60 ^{0}C. Similar creep responses of hoop pine to temperature were demonstrated by Kingston and Budgen[64], for the range from 20 to 50 ^{0}C.

In practice, however, the changes in temperature of wood are taking place simultaneously with changes in moisture content. During those changes, such phenomena as thermal expansion or contraction, swelling or shrinkage, changing rates of heat and mass transfer, and possible changes in the microstructure of the wood arise in the loaded specimen. All those

internal phenomena and the interactions between them contribute to the complex changes in dimension that cannot be predicted from simple shrinkage and thermal expansion data. Also, possible combinations of changing temperatures and moisture content are infinite. Thus, a general treatment of this problem is very difficult. It is known that the creep during those conditions is usually greater than the creep in constant temperature or moisture content, but no common theory for such a behaviour is available.

6.1.3 Statement of Objectives

The evidence presented so far has indicated that the deformations of wood under the influence of the loading and the environmental conditions are greatly affected when the moisture content is increased and decreased. However, there is no general agreement or general trend that is clear about this effect. Thus, further investigations on the effects of such factors as direction of loading with respect to the grain of the wood, temperature, and applied stress level will be necessary before the mechanism of the phenomena can be understood, and before a knowledge of the phenomena can be intelligently applied in practical problems.

The experiments described in this chapter were thus made to show such an effect under bending conditions. Various tests were conducted with stresses applied in the direction across grain at different temperature and moisture levels.

6.2 Apparatus and Experimental Methods

6.2.1 Creep Test Apparatus

1. Testing Rig

The creep testing rig (Figure 6.1) was constructed from 316 stainless steel, to prevent corrosion while testing in humid conditions. The test rig fits into an insulated temperature and humidity controlled box fitted with an air circulation fan and two 325 watt, 240 volt heaters.

An externally mounted Linear Variable Displacement Transducer (LVDT) with an extended core rod measures the wood specimen deflections.

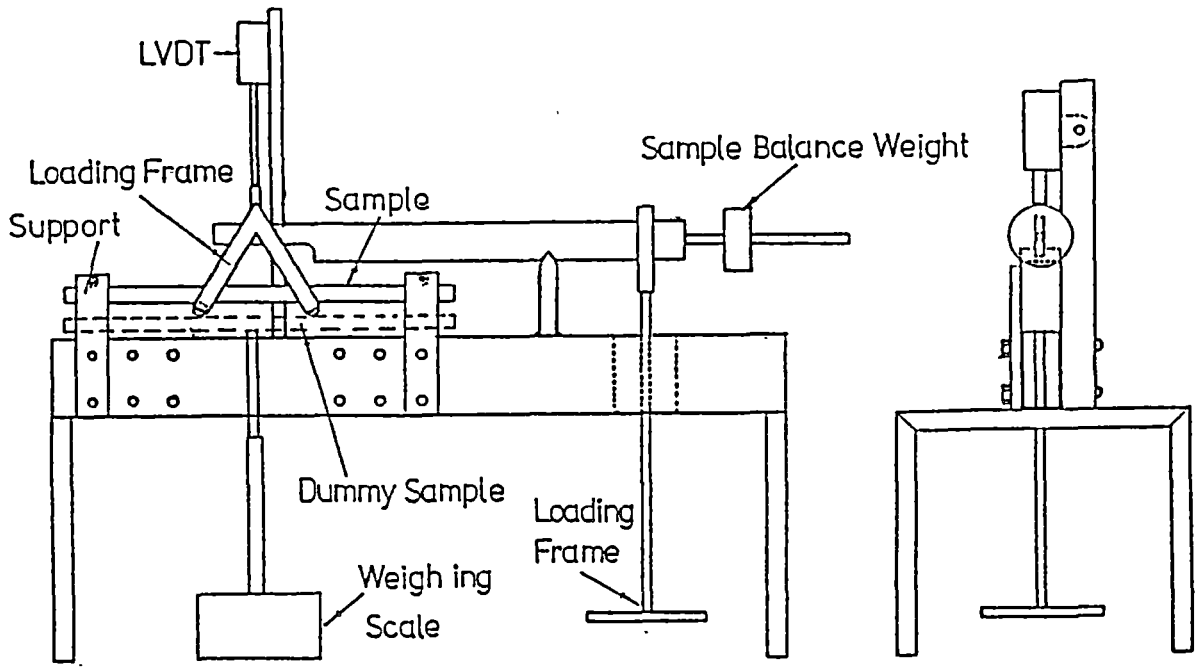

Figure 6.1

Set–up of the Testing Rig

The hanger can be extended through the bottom of the control box for the option of changing loads during a test without altering the inside environment of the control box.

Moisture content measurement was made by measuring the dummy sample placed at the same level with the sample under test. To reduce the effect of opening the door of the test chamber on the internal controlled air conditions, a weighing system, connected with the balance outside the control box, was built so that the weight of the dummy sample could be read outside the control box.

2. Data Acquisition and Control Equipment

A Hewlett–Packard 3421A data Acquisition and Control unit is used to monitor wet and dry bulb temperatures, time, LVDT output voltage and LVDT supply voltage, as well as controlling heating and air circulation in the box.

The 3421A is software controlled by either a HP 86 computer or HP 41C programmable calculator with a thermal printer. The 3421A has a resolution of 100 μV with an accuracy of plus and minus 0.003 % for DC voltage and a resolution of 0.02 ^{0}C for thermocouple measurement.

The LVDT, a Schaetvitz 500HR–DC, has a linear range of plus and minus 12 mm, with an output of 0.3 v/mm and linearity of plus or minus 0.40 %.

A: LVDT Supply and Output Voltage

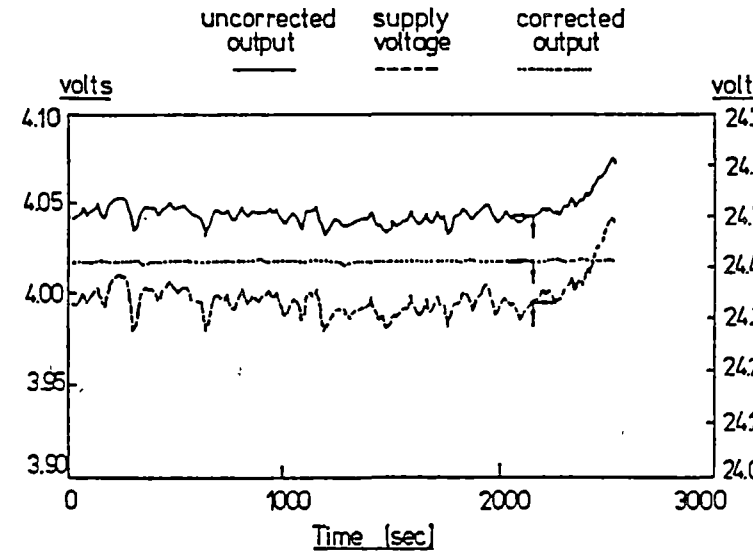

B: Corrected Output Voltage vs Core Displacement

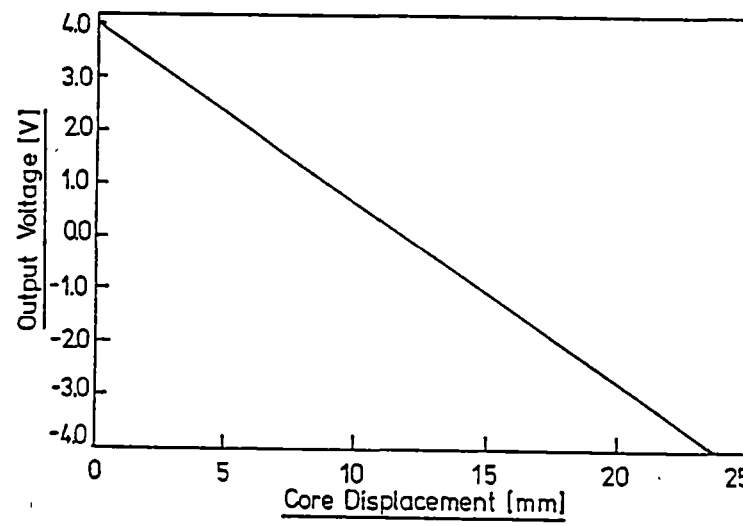

C: Corrected Output Voltage vs Core Displacement

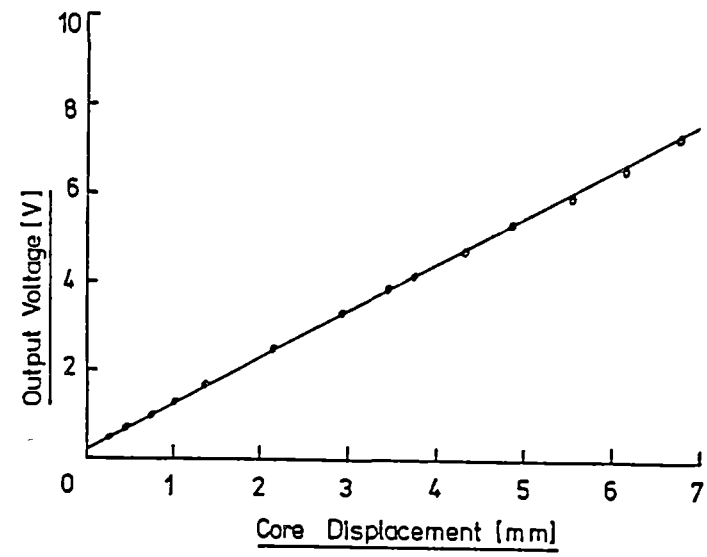

Figure 6.2 Calibration of the LVDT

3. Calibration of the LVDT

Variation in the supply voltage was seen to influence displacement reading with the LVDT output voltage fluctuating with the supply voltage. A multivariable linear relationship was established between LVDT output voltage and the supply voltage and displacement.

Figure 6.2 (A) shows corrected and uncorrected LVDT output voltages for a constant LVDT position. Also shown is the supply voltage. From Figure 6.2 (A) it can be seen that the corrected LVDT output has resolution of about 0.003 V which corresponds to a linear displacement resolution of 0.01 mm. The estimated error in measured deflection is ± 0.1 mm (± 0.7 % of LVDT linear range).

Figure 6.2 (B) is the calibration curve of the LVDT against the dial gauge, which shows the line of best fit through 7 data points. Figure 6.2 (C) is the calibration curve after amplification of the output voltage of LVDT.

6.2.2 Experimental Methods

Experiments were conducted with the beams of the size of 240 BY 10 BY 10 mm. When under test, the beam was simply supported and sustained loads were applied to the radial faces of the beam. The resulting bending stresses were in the order of one–half or less of the short term ultimate stresses for the green wood. The humidity of the testing chamber was controlled by saturated salt solutions and the moisture content of the dummy beam and the deflection rate were measured.

Creep tests with dry beams were made under each stress and temperature condition. It was assumed that creep for the green beams of the same timber has the same order as that for dry beams when their moisture contents are controlled constant. Separation of the creep from the mechano–sorptive effect was made by the deduction of creep from the total deformation over the same time period.

Data was logged into disk once every minute for first 30 minutes, then every 15 minutes, in which the first reading was taken as the zero deflection position. The load was applied about 5 seconds before the second reading (instantaneous deflection) appears on the screen to reduce the creep effect on the initial deflection.

6.3 Result Analysis and Discussions

6.3.1 Broad Behaviors

Tests for the broad behaviors of the effect were made with the kiln–dried beams preconditioned to about 15 % moisture content before the tests. A constant temperature of 60 ^{0}C and nominal stress of 11 % ultimate of the green wood were used in the tests. The data were presented as multiples of the initial deflections measured on application of the sustained loads.

Figure 6.3 shows the deformation rates under both constant and changing moisture conditions and the effect of the changing RH on the recovery. It can be seen that the deflection of the beam maintained at constant moisture content of 5 % increased at a gradually decreasing rate to 1.35 times the initial deflection during the test period of 20 hours.

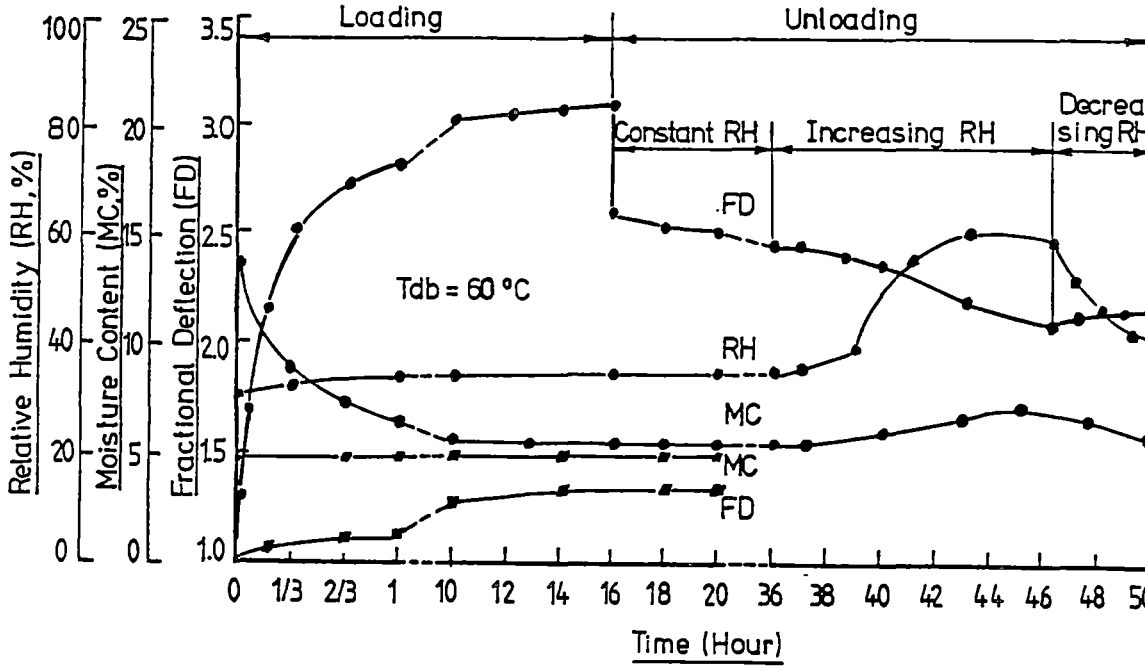

Figure 6.3

Broad Behavior of the Mechano–sorptive Effect

The deflection of the beam allowed to dry from the moisture content of 14 % increased to 3.15 times the initial value over a period of 16 hours, in which the fractional deflection increased to 2.8 in the first hour while the moisture content decreased from 14 % to 6.5 %.

At about 16 hours, the beam was unloaded to allow the recovery. It can be seen from Figure 6.3 that only a small decrease of 0.17 in the fractional deflection occurred after the beam had been unloaded for 20 hours at nearly constant RH condition. However, a further recovery of 0.35 occurred in less than 10 hours when the beam was allowed to absorb moisture and a 5–hour desorption process did not cause any further recovery.

A replot of the loading part of the curve in Figure 6.3 with the fractional deflection (corrected for creep) against average moisture content of the beam is shown in Figure 6.4. It can be seen that a nearly straight line was fitted between moisture content and fractional deflection.

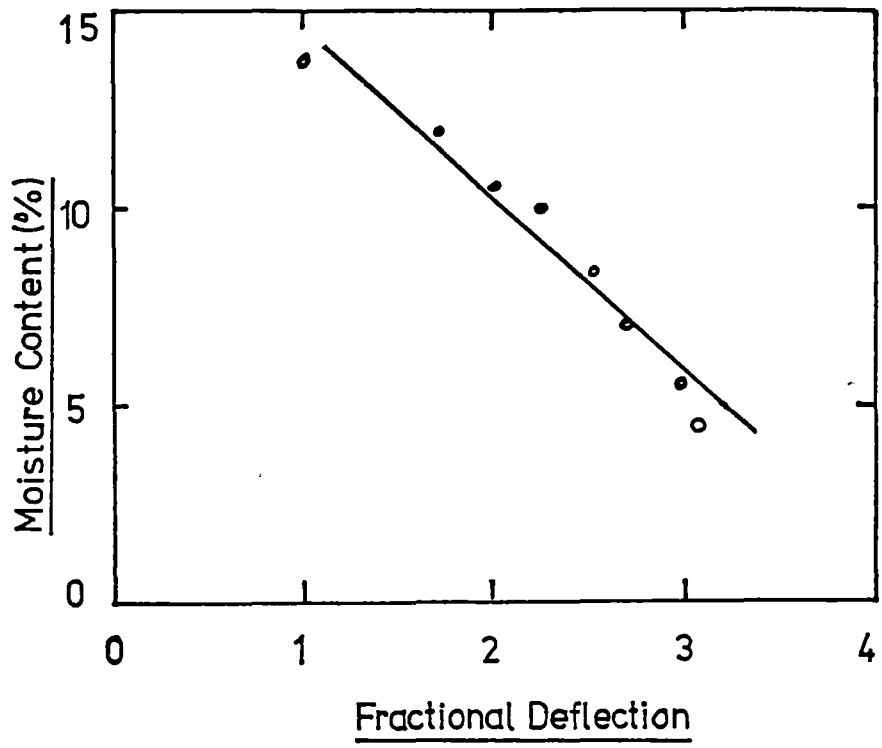

Figure 6.4

Mechano–sorptive Data

The effect of cycling the change in humidity on the deformation rate of the beam is shown in Figure 6.5. It can be seen that each desorption process leads to an increase in the fractional deflection and each absorption process leads to a reduction of fractional deflection. The total deflection reached 2.8 times the initial value after three cycles of the humidity.

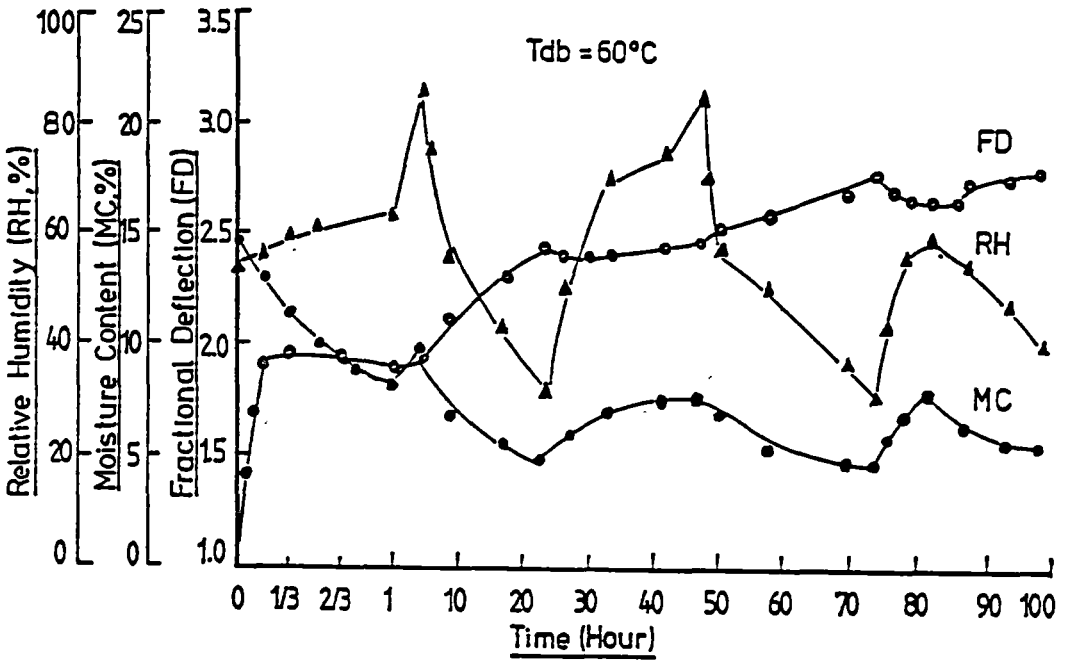

Figure 6.5

Effect of Cycling the Change of Humidity

on the Fractional Deflection

It can thus be concluded that the broad behavior of the effect in the direction across grain is much the same as those reported in the direction along grain[53], although the actual number is somewhat different.

6.3.2 Effect of the Loading Level

The effect of loading level on the deformation of the beam was demonstrated with the green beams cut from a billet of regrowth Peppermint eucalypt timber (most likely to be either E. pulchella or E. tendiramis). The tests were made under five different loading conditions, namely 6, 8, 13, 22, and 44 % of short term ultimate stress for green wood. In all those tests, the moisture content of the beams was allowed to change from

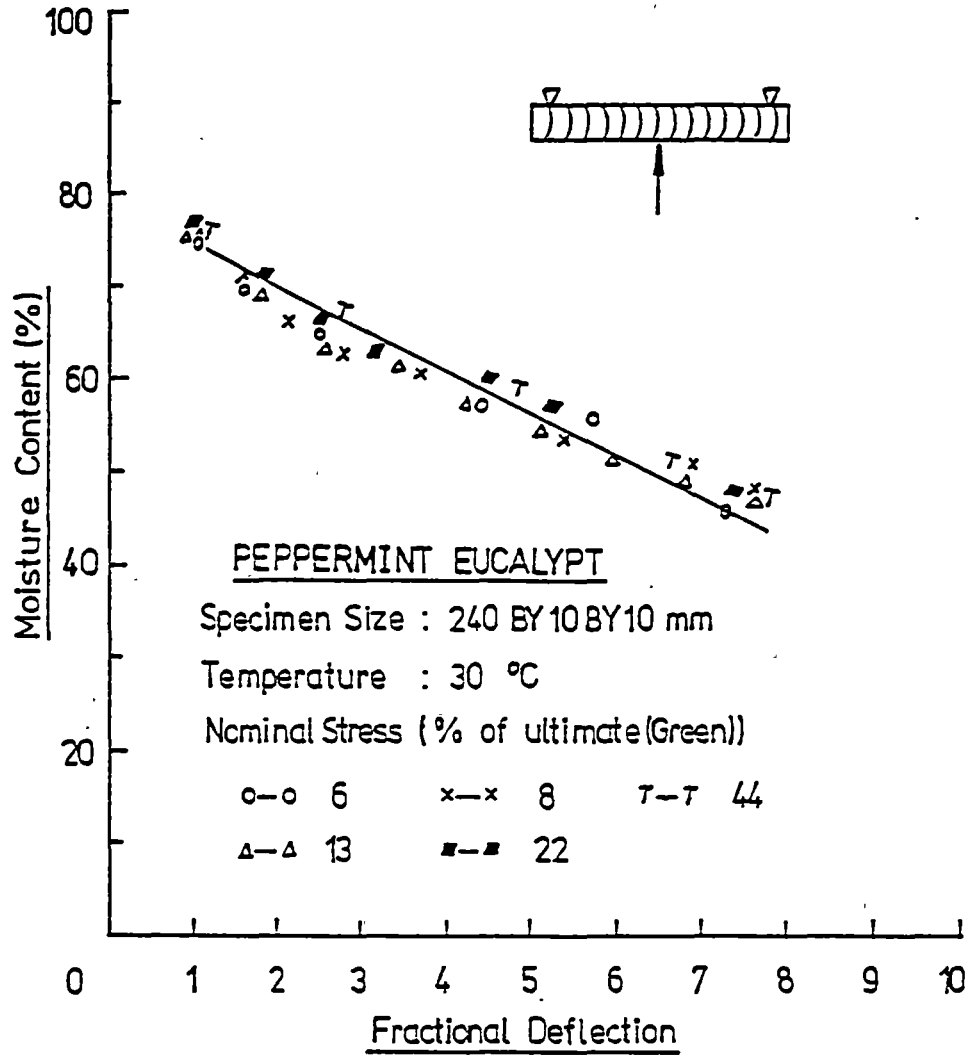

Figure 6.6

Effect of the Loading Level on the Deformation

about 78 to 46 % and the temperature of the test chamber was set constant at 30 °C. The result shown in Figure 6.6 indicates that with the decrease of the moisture content from 78 to 46 % the deflection increases to about 7.5 times the initial value. This amount of fractional deflection is much bigger than those reported by Armstrong and Kingston[53] where the load was applied along the grain (on the tangential faces). It can be seen that there

seems no any noticeable effect either on the rate or the total change of deformation when the nominal stress was changed from 6 to 44 %. Also a nearly straight line was fitted between the change of the average moisture content and fractional deflection for all tests.

6.3.3 Effect of the Initial Moisture Content and Loading Directions

The total magnitude of the mechano–sorptive deformation is strongly dependent on the amount of drying that has been taken place before sustained loads are applied. Figure 6.7 shows the measurements at two different initial moisture conditions in the direction across grain. Due to the limit of the LVDT, the test at higher initial moisture content had to be stopped at about 45 % moisture content. Comparison of the two curves clearly indicates that partially drying of the timber before sustained load applied can greatly reduce the final deflection of the wood. It is thus of practical benefit to permit drying in structure timber prior to the application of service loads.

Observation of the two curves also shows that the deformation occurs throughout the whole moisture content range and the linear relationships could be fitted between the average moisture content and the mechano–sorptive effect. However, most of the deformation occurs during removal of the free water. This can be seen from the curve for the lower initial moisture content of 48 %. As the average moisture content decreases from 48 to 30 %, the net increase of the fractional deflection is about 6.5, while for the moisture content decrease from 30 to 5 % the net increase of the fractional deflection is only 1.9. The shape of the fitted line changes at about 30 % moisture content which is generally believed to be roughly the FSP.

Further tests with the beams cut along the grain from the same timber board are also presented in Figure 6.7, in order to establish whether this sudden change of slope (which does not seem to have been reported elsewhere) was due to the species of material or the direction of loading. It can be seen that with moisture content decreasing from about 78 % to 5 %, the fractional deflection almost linearly increases to about 7.5. Comparison of

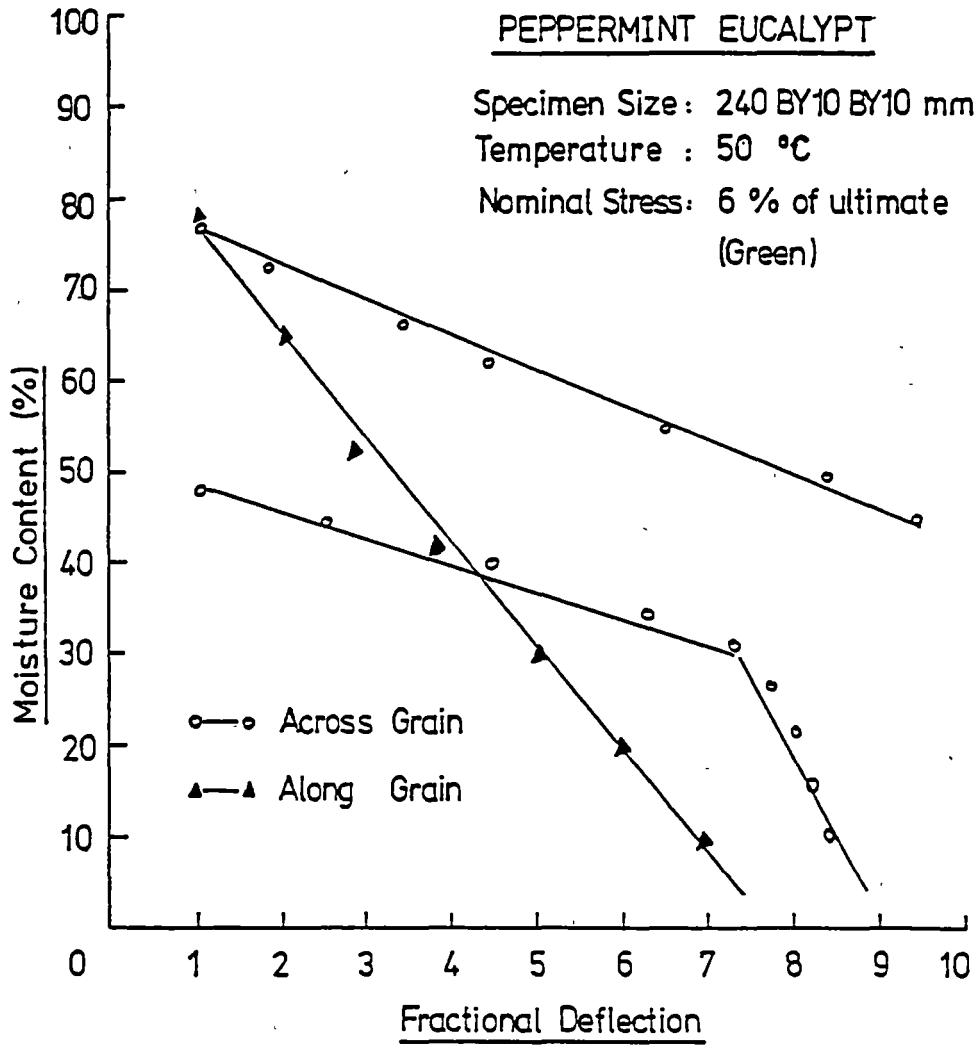

Figure 6.7

Effect of Initial Moisture Content and Loading Direction

the results from the two loading directions indicates that change of loading direction from along the grain to across grain results in much more increase in the final magnitude of the deformation. Also, only one linear relation which could be fitted over the whole moisture content range would suggest that change of the linearity of the lines at about 30 % moisture content in the direction across grain was caused by the direction of loading, not by the species of timber used for tests.

Therefore, it may be suggested that one straight line for describing the mechano–sorptive effect over the whole moisture content range would be not sufficient in the direction across grain. Also, any mathematical expression for describing this effect must take into account the initial moisture contents of wood and the loading direction as the change in the initial moisture content and loading direction results in changes in the shape of moisture content–fractional deflection plot.

6.3.3 Effect of the Temperature

Tests to show the effect of temperature on the mechano–sorptive effect were made under two moisture content ranges, namely 78 to 46 % and 48 to 18 % at the constant temperatures of 30, 40, 50, 60, 70 and varying temperatures from 30 to 70 ^{0}C. The results are shown in Figure 6.8.

At the moisture content range from 78 to 46 %, it can be seen that the final fractional deflection gradually increases from 7.5 at 30 ^{0}C to 12 at 70 ^{0}C. This indicates that an increase in the temperature results in increases not only in the rate of deformation, but also in the final magnitude of the

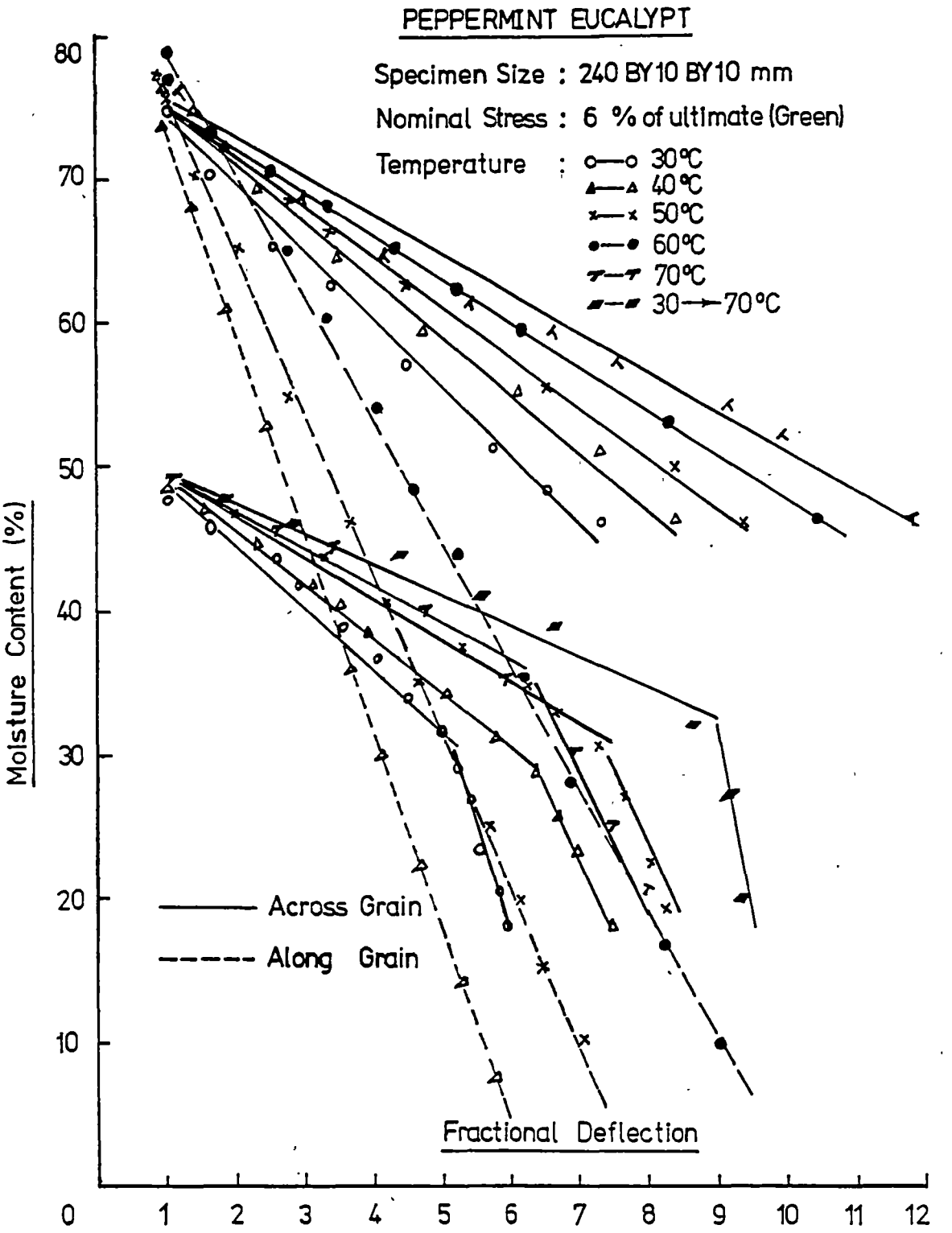

Figure 6.8

Effect of the Temperature on the Deformation

fractional deflection. This is different from usually reported behavior that the total change in deformation is dependent upon the size of the moisture content change and not the rate of change in a given moisture content step. Thus, the temperature must contribute to the increase of the final deformation.

Similar effect of the temperature was observed for the moisture content changing from 48 to 18 %. The linearity of the moisture–deflection plot started to change at about 30 % moisture content under all temperature conditions, and thus confirms the observation mentioned earlier that there is a large change at about FSP. However, it should be noted that the slopes of the line after FSP do not appear to vary significantly with temperature.

With the temperature gradually increasing from 30 to 70 ^{0}C, both the rate and the final magnitude of the deformation exceeds that at the highest constant temperature of 70 ^{0}C as also shown on Figure 6.8.

Figure 6.8 also presents three test curves in the direction along the grain for the purpose of comparison. Although slight differences in the initial moisture contents of the beams were observed, the increase of the total fractional deflection from about 6 at 40 ^{0}C to 7.5 at 50 ^{0}C, and to 9.5 at 60 ^{0}C clearly indicates a temperature effect on the deformation.

A replot of the total fractional deflection against temperature over the moisture content range from 78 % to 46 % is shown in Figure 6.9, from which it can be seen that the total fractional deflection almost linearly increases with the increase of the temperature in the tests across the grain.

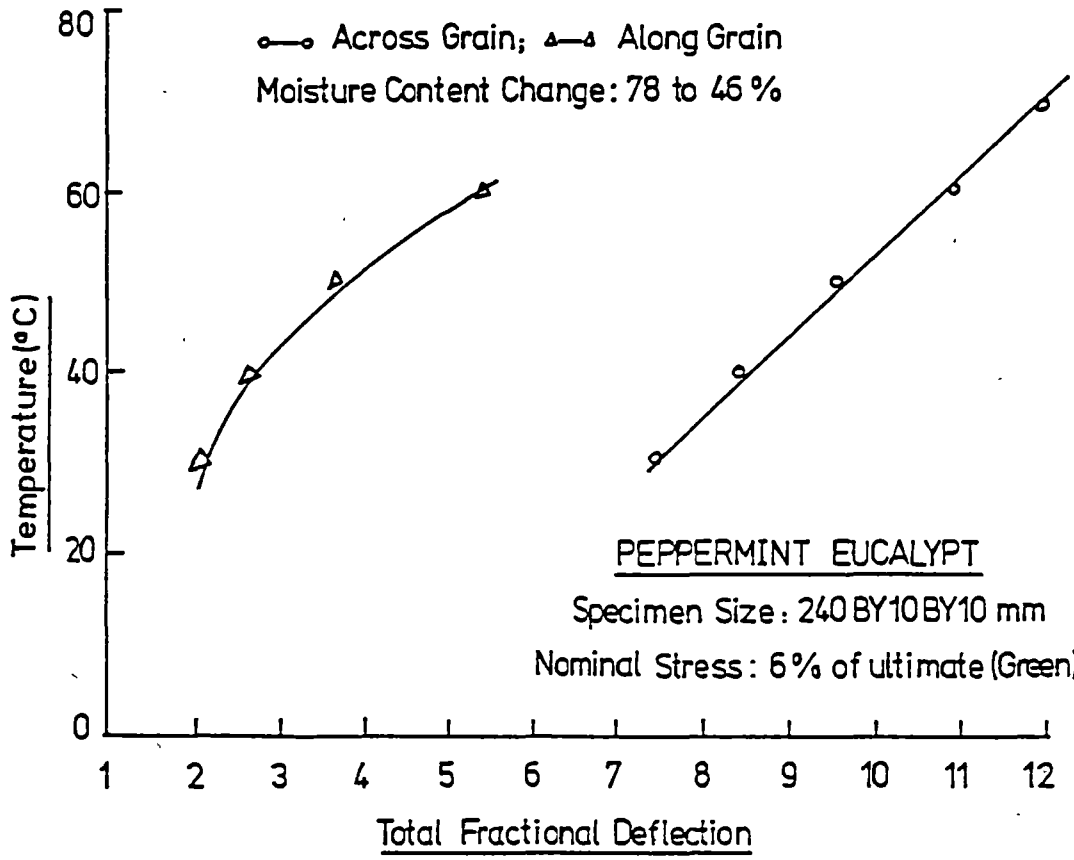

Figure 6.9

Temperature – Total Fractional Deflection Plot

6.4. Conclusions

A literature survey on the mechano–sorptive effect was made. Under bending conditions, the general behavior of the deformation and the effect of cycling the change in humidity on the deformation and recovery were shown experimentally, the results being much the same as reported elsewhere.

Nominal bending stresses applied on the radial faces of the wood were shown to have no effect on the fractional deflections up to about 44 % of ultimate for the green wood. Change of the loading directions from along

grain to across grain results in much greater increase in the final magnitude of the deflection.

The relationship between the fractional deflection and the average moisture content of the wood was found to be nearly linear over the whole moisture content range, but the slope of the line is different for the bound water and free water when the stresses were applied across the grain. The slope of the line also appears to be dependent upon the the initial moisture content and the temperature of the wood.

Several questions need to be answered before further conclusions are reached about the effect. Some of these are listed as follows:

1. The evidence indicates that eucalypt materials show the mechano–sorptive effect (MSE) from green, whereas softwoods appear to have no MSE. What anatomical differences are likely to cause this difference?

2. Is the high value of MSE in the direction across the grain more consistent with microscopic effects like changes of hydrogen bonds as elsewhere proposed or by realignment of curved long–chain polymers as proposed by Hiski Kippo[60]?

3. Do the similarities in various aspects of the structure give some reasons for the sudden changes at FSP for both softwoods and some eucalypts such as Peppermint used in the tests?

CHAPTER 7

CONCLUSION

The work presented herein was directed towards the drying of Tasmanian eucalypt timber so as to be almost free of checks. Such material can then be sold for high quality furniture where the market value is highest. In the process of investigation, emphasis was placed on providing experimental evidence for the basic transport processes involved and the drying properties of the wood so that a theoretical model could be developed to predict the drying behaviour of large populations of the boards.

The study started with an overall investigation of problems of drying timber. Preliminary attempts were made to relate the experimental measurements to the predictions from the existing computer simulation program DRYWOOD. Some of the sources of difference between two cases and the experimental methodology employed were analyzed.

Detailed measurements were made of the boundary layer flow over the rough surface of sawn boards using hot wire anemometry. A general account on the flow through the space between two layers of flat plates was given in order to calculate the boundary layer properties for demonstrating the structure and development of the boundary layer. Measurements of velocity profile and turbulence level were conducted at various distances from the leading edge. To observe the flow reattachment to the board surface at the entrance region, smoke was injected to the flow passage near the leading edge.

The boundary layer formed on the vertical edge of the board was found to be laminar. The effect of the sharp corner at the leading edge separates the flow from the board surface so that the flow becomes a separated shear layer after it enters the flow passage. This separated shear layer is unstable to eddies from the rough surface of the board and increases quickly in thickness. At the point about one and half times the board thickness it reaches a maximum, then reattaches to the surface at the point about three times the board thickness which encloses a region of slowly recirculating flow; after this it redevelops as an attached boundary layer flow. The redeveloped boundary layer flow was found to transit from laminar to turbulent at a free stream velocity outside the developing boundary layer of about 1 m/s.

The surface shear stress and friction factor were calculated from the measurements of static head drop and the boundary layer properties. It was found that the surface friction largely depends on the state of the board surface. A slightly larger value of the friction factor was found in the case of the flow along the board where the flow was roughly perpendicular to the saw marks under the present test conditions. It was thus anticipated that the angle between the saw teeth marks and the flow played an important role in the variation of the surface friction factor, although in practice those marks may change through a wide angle. Less than 5 mm shrinkage gap between the edges of the boards made only a small increase in the overall pressure drop, but the gap did cause vertical air flow circulation, and consequently the edge drying. Functions were fitted between the measured friction factor and free stream velocity for the purpose of the heat and mass transfer calculation.

With the experimental evidence of the surface temperature change, the simplified drying model based on the concept of "free–water" and "bound–water" sharply separated by a Fibre Saturation Point (FSP) was proved to be of limited value for the drying of Tasmanian Eucalypts. The trouble for the argument was found to be the restricted movement of free water in eucalypt materials and the formation of dry patches on the surfaces of drying boards. A surface mass transfer area ratio was introduced to handle the problem and its effect on the surface temperature change even when the surface moisture content is still well above FSP.

A coupled heat and mass transfer model was constructed with the aid of the Reynolds analogy among heat, mass and momentum transfers. In the model, the transfer of moisture within the wood was assumed to be a diffusion process in which the diffusion coefficient is independent of the moisture content and the driving force is the moisture concentration as in true molecular diffusion. For the solution of the unsteady–state diffusion equation, mass flux from the board surface at any given time was estimated by considering effects of the introduced surface mass transfer area ratio and the board temperature rise.

The process of heat transfer was modelled by considering convection heat transfer to the board surface and heat conduction inside the board. On the belief that most free water in eucalypt material is held inside fibres and can escape only by diffusion through the fibre walls, all heat and moisture transfers between the wood and the air were assumed to take place at the surface of the board. For the solution of the Fourier equation, heat flux from the board surface over each time step was estimated by taking the surface temperature rise equal to the rise in the average temperature of the board.

A technique was used to interpolate moisture content at the edges of the slices taken from experiments for checking the validity of the model. The principle is on the ground that analytical solutions of the Fourier equation most conveniently occur as sums of error functions, so that parabolas were fitted to the logarithms of moisture concentration deficiencies at three neighbouring points which is equivalent to fitting a simple sum of error functions to the measured values. Experiments were conducted to test the proposed mathematical model, in which measurements were made of the moisture and temperature change in the sample boards at different drying times. Detailed comparison of moisture and temperature profiles with experiments demonstrated very satisfactory agreement between measurement and calculation with a diffusion coefficient independent of the moisture content.

To test the theory from green to EMC right across the board, experiments were made to dry quarter–sawn material from its green to the complete dry condition. In the process of experiments an attempt was also made to show the effect of edge drying. This was done by weighing a sample board and taking slices from the center of the board hoping that separation of the mass flux from the edge and the wide surface could be made by comparing the board average moisture content estimated from the overall weight loss of the board and from slicing measurements at the center of the board. The variability of the initial distribution of moisture even within any particular board prevented any useful measurement of the effect of edge drying by this method.

A critical literature survey on the mechano–sorptive effect was made as entry to the subject. Preliminary tests under bending condition were conducted with stresses applied perpendicular to grain on the radial faces of the beams. The tests indicate that the relationship between the mechano–sorptive effect and average moisture content is nearly linear over the whole moisture content range, but the slope of the line is different for the bound water and free water. The slope of the line also appears to be dependent upon the initial moisture content and temperature of the wood. Comparison of the results obtained with the stresses applied along and across grain indicates a large increase of the mechano–sorptive effect in the direction across the grain.

REFERENCES

1. McMillen J.M. 1958, Stresses in wood during drying. For. Prod. Lab. Rept. NO. 1652, USDA For. Serv., Madison, Wis.
2. Stamm A.J. 1964, Wood and Cellulose Science. Ronald New York
3. Kawai S., K. Nakato, and T. Sadoh 1979, Computation of drying stresses resulting from moisture gradients in wood during drying II Numerical calculation. Mokuzai Gakkaishi 25(4):272–283
4. Oliver A.R. 1984, Shrinkage and creep in drying timber, 21st. For. Prod. Res. Conf. Paper E13, Australia
5. Skaar C. 1954, Analysis of methods for determining the coefficient of moisture diffusion in wood. For. Prod. J. 4(6):403–410
6. Hart C.A. 1977, Effective surface moisture content of wood during sorption. Wood Sci. 9(4):196–201
7. Schaffner R. D., 1981 Fundamental aspects of timber seasoning. M. Eng. Sci. thesis, Uni. of Tas.
8. Nadler K.C., E.T. Choong, and D.M. Wetzel 1985, Mathematical modelling of the diffusion of water in wood during drying. Wood and Fiber Sci. 17(3):404–423
9. Schniewind A.P. 1968, Recent progress in the study of rheology of wood. Wood Sci. Technol. 2: 188–206
10. Grossman P.V.A. 1986, Requirements for a model that exhibits mechano–sorptive behaviour. Wood Science and Technology 10:163–168
11. Ashworth J.C. 1979, Design of drying schedules for kiln–drying of softwood timber, Developments in drying. Sci. Press, New York

12. Morgan K., H.R. Thomas and R.W. Lewis 1982, Numerical modelling of stress reversal in timber drying. Wood Sci. 15(2):139–149

13. Lessard R.A., D.E. Limbert, J.L. Pokoski, and J.L. Hill 1982, A stress model for lumber drying control. J. Dynamic System, Measurement, and Control. 104, 283–289

14. Rice R. W. and R. L. Youngs 1987, A mass transfer approach to simulating drying stresses and predicting check formation, Paper presented at the international conference on wood drying, Skelleftea, Sweden

15. Oliver A.R., Mills R. and K. Ralph 1986, Pascal Program DRYWOOD, Tasmania Timber Promotion Board.

16. Wilhelm L.R. 1976, Numerical calculation of psychrometric properties in SI Units, Transaction of the ASAE: 318–325

17. Keey R.B. 1978, Introduction to industrial operations, PERGAMON PRESS

18. Wexler A. 1965, Humidity and moisture, measurement and control in science and industry, Volume 3, Fundamental and Standards, Reinhold publishing corporation, N.Y.

19. Greenhill W.L. 1936, The measurement of the flow of air through timber seasoning stacks, J. Coun. Sci. Ind. Res. (Aust.) 9:128–134.

20. Sharma, S.N. and P.K. Jain 1977, Air circulation in an overhead cross–shaft internal fans kiln, J. Timber Dev. Assoc. (India): 23(4): 8–21

21. Jain P.K. and S.N. Sharma 1981, Studies on air circulation in a new design of side–mounted fan kiln, J. Timber Dev. Assoc. (India) : 17(3): 12–25

22. Nassif N.M., P.N. Alexiou and H. Wiedemann 1984, Air flow profile through a timber stack inside a kiln, 21st For. Prod. Res. Conf. (Aust.)

23. Duncan W.J., A.S. Thom and A.D. Young 1981, Mechanics of fluids, Edward Arnold (Printers) Ltd.

24. Ower E. and R.C. Pankhurst 1966, The measurement of air flow, Pergamon Press

25. Walker G. J. 1971, An investigation of the boundary layer behaviour on the blading of single–stage axial–flow compressors, Ph.D thesis, University of Tasmania

26. Dean R. B. 1978, Reynolds number dependence of skin friction and other bulk flow variables in two–dimensional rectangular duct flow, ASME J. of Fluid Engineering, 100:215–223

27. Schlichting H. 1960, Boundary layer theory, McGraw Hill

28. Ota T. and M. Itasaka 1976, A separated and reattached flow on a blunt flat plate, ASME J. of Fluid Engineering, 98:79–86

29. Clauser F.H. 1956, The turbulent boundary layer, Advances in Applied Mechanics, 4:1–51

30. Reynolds O.1901, Scientific papers of Osborne Reynolds, Vol. 2, Cambridge University Press, London

31. Prandtl L. 1910, Phys. Z., 11, 1072

32. Chilton T. H. and A. P. Colburn 1934, Mass transfer (adsorption) coefficients, prediction from data on heat transfer and fluid friction. Ind. Eng. Chem., 26, 183–a87

33. Peck R.E., K. C. Vyas and R. Toei 1977, Capillary theory applied to drying. AIChE Symposium Series, 73(163)

34. Skaar C. 1972, Water in wood. Syracuse University Press, New York

35. Simpson W. T. 1973, Relation of comparative diffusion rates of Oak Ray and surrounding tissue to check formation, Wood and Fiber, 5(1):34–40

36. Bramhall G. 1979, Mathematical model for lumber drying I. Principles involved, Wood Science, 12(1):14–21

37. Simpson W. T. 1979, Sorption theories for wood, Proc. Symp. on wood moisture content–temperature and humidity relationships, Blacksburg, VA. For. Prod. Lab., WI.

38. Siau J. F. 1971, Flow in wood, Syracuse Univ. Press, Syracuse, NY

39. Nelson R. M. 1983, A model for sorption of water vapor by cellulosic materials, Wood and Fiber, 15(1):8–22

40. Kelsey K. E. 1957, The sorption of water vapor by wood, Aust. J. Appl. Sci., 7:160–175

41. Kollman F. F. P. and N. A. Cote 1968,. Principle of wood science and Technology solid wood, Springer–Verlag, Berlin

42. Luikov A.V. 1975, Systems of differential equations of heat and mass transfer in capillary–porous bodies, Int. J. of heat and mass transfer, 5(8):1–14

43. Wengert E. M. 1976, Predicting average moisture content of wood in a changing environment, Wood and Fiber, 7(4):264–273

44. Weichert L. 1963, Holz als Roh–und Werkst. 21(8):290–300

45. Maclean J. D. 1941, Thermal conductivity of wood. Heating, piping, and air conditioning 13:380–391

46. Siau J. F. 1984, Transport processes in wood, Springer–verlag Berlin Heidelberg New York Tokyo

47. Carslaw H. S. and J.C. Jaeger 1959, Conduction of heat in solids, Clarendon Press (2nd ed.)

48. Crank J. 1975, The mathematics of diffusion, Clarendon Press, Oxford

49. Lawniczak M. 1959, Study of the effect of moisture content in wood on relaxation of stresses imparted in preliminary bending. Folio forestalia polonica (1B) 103. CSIRO Austral.,Transl. No. 5099

50. Armstrong L.D. and R.S.T. Kingston 1960, Effect of moisture changes on creep in wood. Nature (London) 185(4):869–870

51. Christensen G.N. 1960, Austr. J. Appl. Sci. 11:295

52. Armstrong L.D. and G.N. Christensen 1961, Influence of moisture changes on the deformation of wood under stress. Nature 191(4791):869–870

53. Armstrong L.D. and R.S.T. Kingston 1962, The effect of moisture content changes on the deformation of wood under stress. Austr. J. Appl. Sci. 13: 257–276

54. Bryan E. L. and A.P. Schniewind 1965, Strength and rheological properties of particle–board as affected by moisture content and sorption. For. Prod. J. 15(4):143–148

55. Saue D.J. and J.G. Haygreen 1968, Effects of sorption on the flexural creep behaviour of hardboard. For. Prod. J. 18(10):57–63

56. Gibson E.J. 1965, Creep of wood: role of water and effect of a changing moisture content. Nature 206(4980):213–215

57. Bethe E. 1969, Holz als Roh– und Werkstoff 27(8):291–303

58. Armstrong L.D. 1972, Deformation of wood in compression during moisture movement. Wood Sci. 5(2):81–86

59. Armstrong L. D. 1983, Mechano–sorptive deformations in collapsible and non–collapsible species of wood. J. Inst. Wood Sci., 9:206–211

60. Hisk Kippo 1987, Personal Communication

61. Davidson R.W. 1962, The influence of temperature on creep in wood. For. Prod. J. 12(8):377–381

62. Kitahara K. and K. Yukawa 1964, The influence of the change of temperature on creep in bending. J. Japan Wood Res. Soc. 10(5):308–314

63. Arima T. 1967, The influence of high temperature on compressive creep of wood. J. Jap. Wood. Res. Soc. 13(2):36–40

64. Kingston R.S.T. and B. Budgen 1972, Some aspects of the rheological behaviour of wood. IV. Non–linear behaviour at high stresses in bending and compression. Wood Sci. Technol. 6:230–238

65. Wilke R.C. and D.T. Wasan 1965, A new correlation for the psychrometric ratio, AICHE–ICHE Symp. Series 6(21–26)

66. Sherwood T.K., R.L. Pigford and C.R. Wilke 1975, Mass transfer, McGraw Hill, New York

APPENDIX A
NOMENCLATURE*

SYMBOL	SIGNIFICANCE	UNIT	OCCURRENCE
A	area of the flow passage	m^2	(2.8)
A_c	constant		(4.71)
AMC	average moisture content	%	(5.11)
B_c	constant		(4.71)
C	vapour concentration	Kg/m^3	(4.4)
C	psychrometric coefficient		(B6)
C_a	vapour concentration in the free stream	Kg/m^3	(4.1)
c_p	specific heat of the air	kJ/Kg/C	(4.2)
C_{pg}	specific heat of the dry air	kJ/Kg/C	(2.5)
C_{py}	specific heat of the moist air	kJ/kg/C	(2.3)
C_{pw}	specific heat of the moisture vapour	kJ/Kg/C	(2.5)
C_w	vapour concentration in the air near the board surface	Kg/m^3	(4.1)
C_{wb}	vapour concentration in the air at the wet bulb temperature	Kg/m^3	(4.25)
C_{pwood}	specific heat of the moist wood	kJ/Kg/C	(4.56)
D	Molecular diffusivity	m^2/hr	(4.1)
D	diffusion coefficient	m^2/hr	(4.20)
D	coefficient (0.622)		(B2)
DR	reference value of the diffusion coefficient	m^2/hr	(4.20)
dt	time interval	hr	(4.26)

*— Except where otherwise specified, the symbols used in the thesis have the meanings specified in the table.

dT	average temperature rise of the board	^{0}C	(4.26)
E	activation energy of diffusion	kJ/Kg	(4.20)
E_d	eddy diffusivity for mass transfer	m^2/hr	(4.1)
E_h	eddy diffusivity for heat transfer	m^2/hr	(4.2)
E_v	eddy diffusivity for momentum transfer	m^2/hr	(4.3)
EMC	equilibrium moisture concentration	Kg/m^2	(4.36)
F	momentum flux	Kg/s^2	(3.5)
f	friction factor		(3.28)
FM_o	mass flux	Kg/m^2/hr	(4.25)
FH_o	heat flux	kJ/m^2/hr	(4.26)
FSP	moisture concentration at fibre saturation point	Kg/m^3	(4.36)
G	the air flow rate	Kg/s	(2.8)
G	Clauser parameter		(3.36)
H	shape factor		(3.15)
h	heat transfer coefficient	kJ/(m^2hrC)	(4.2)
H_{ae}	activation energy of diffusion	kJ/kg	(4.48)
H_{air}	differential head	mm air	(3.12)
H_{fg}	heat of evaporation	kJ/Kg	(2.6)
H_w	differential head	mm water	(3.12)
H_w	heat of wetting	kJ/Kg	(4.47)
j_d	j–factor for mass transfer		(4.18)
j_h	j–factor for heat transfer		(4.17)
K	thermal conductivity of the wood	kJ/(mhrC)	(4.52)
k_c	mass transfer coefficient	Kg/m^2/hr	(4.1)
LB	length of the board	m	(5.16)
M	mass flux	Kg/m/s	(3.1)
M	moisture content in wood	%	(4.53)
M_a	molecular weight of dry air		(4.33)
MC	moisture concentration in wood	Kg/m^3	(4.19)
MC_o	initial moisture concentration in board	Kg/m^3	(4.23)

M_i	moisture content at the surface of the board	%	(4.47)
M_w	molecular weight of the water		(4.35)
n	number of samples taken		(5.16)
N_a	mass flux	$Kg/m^2/hr$	(4.1)
NSL	number of slices		(4.78)
Nv	drying rate	$Kg/m^2/hr$	(B1)
P	ambient atmospheric pressure	Pa	(3.13)
P_{dair}	partial pressure of the dry air	Pa	(4.29)
P_{mair}	barometric pressure	Pa	(4.29)
P_r	Prandtl number		(4.14)
PS_a	static pressure at the point a	mm water	(3.11)
PS_b	static pressure at the point b	mm water	(3.11)
P_{sat}	saturated vapor pressure	Pa	(4.28)
P_{satwb}	saturated vapour pressure at T_{wb}	Pa	(2.1)
PT	atmospheric pressure (101.325)	kPa	(2.2)
P_{vap}	partial pressure of water vapour	Pa	(4.35)
q	heat flux	$kJ/m^2/hr$	(4.2)
Q	moisture concentration deficiency	Kg/m^3	(4.60)
QS	surface moisture concentration deficiency	Kg/m^3	(4.62)
QS_1	surface moisture concentration at the beginning of each time step	Kg/m^3	(4.41)
QS_2	surface moisture concentration at the end of each time step	Kg/m^3	(4.41)
R	universal gas constant		(4.20)
R_a	wire resistance at ambient temperature T_a	Ω	(3.13)
R_e	Reynolds number (U TB/ν)		
R_{el}	Reynolds number (U l/ν)		
$R_e\delta^*$	Reynolds number (U δ^*/ν)		
R_{esh}	Reynolds number (U_m SH/ν)		(3.31)
RH	relative humidity	%	(4.35)

RH_a	relative humidity of the air in free stream	%	(4.40)
RH_{fsp}	relative humidity of the air near the wood surface at FSP	%	(4.40)
R_o	wire resistance at ambient temperature T_o	Ω	(3.13)
R_w	wire resistance at temperature T_w (constant)	Ω	(3.13)
r_{wb}	mixing ratio at the WB temperature		(4.31)
r_{db}	mixing ratio at the DB temperature		(4.31)
S_c	Schmidt number		(4.14)
S_h	Sherwood number		(4.18)
SH	Flow passage height	m	(3.1)
SL	length of the sample	m	(5.16)
S_t	Stanton number		(4.9)
t	time	hr	(4.19)
T	temperature of the board	°C	(4.19)
T_a	air temperature in free stream	°C	(4.4)
T_{ain}	inlet air temperature	°C	(2.11)
T_{aout}	outlet air temperature	°C	(2.11)
TB	board thickness	m	(4.26)
T_{db}	dry bulb temperature of the air	°C	(2.3)
T_g	air temperature in free stream	°C	(B1)
T_m	mean film temperature $(1/2(T_{wire}+T_{air}))$	°C	(3.13)
T_s	temperature of the timber surface	°C	(B1)
T_w	temperature of the board surface	°C	(4.27)
T_{wa}	average temperature of the board	°C	(4.48)
T_{wb}	wet bulb temperature of the air	°C	(2.3)
T_{wk}	board surface temperature	°K	(4.37)
u	local velocity in the boundary layer over the board surface	m/s	(3.1)
u*	friction velocity	m/s	(3.24)
U	free stream velocity	m/s	(3.2)

U_m	mean velocity	m/s	(3.30)
V	bridge voltage	V	(3.13)
v	temperature	°C	(4.59)
V_o	bridge voltage at zero flow velocity	V	(3.14)
V_{rms}	root mean square value of bridge voltage fluctuation	mV	(3.14)
W	weight of the board	Kg	(2.11)
WB	board thickness	m	(5.13)
x	coordinate in the width direction of the board		(5.1)
Y	coordinate in the thickness direction of the board		(4.19)
Y_g	humidity of the air in free stream		(2.4)
Y_s	humidity of the air near timber surface		(B1)
Y_{mid}	Y–direction coordinate of the half board thickness	m	(4.24)

GREEK LETTERS

ρ_{dair}	density of the dry air	Kg/m^3	(2.9)
ρ_{mair}	density of the moist air	Kg/m^3	(2.9)
δ^*	displacement thickness	m	(3.2)
θ	momentum thickness	m	(3.8)
β	velocity coefficient		(B3)
τ_o	board surface shear stress	N/m^2	(3.11)
ρ_{water}	density of water	Kg/m^3	(3.12)
∇P	difference in atmospheric pressure	mm water	(3.13)
∇T	difference in ambient temperature	°C	(3.13)

∇V	difference in bridge voltage	V	(3.13)
θ	temperature difference between the wire and ambient air	^oC	(3.13)
α	temperature coefficient of resistance (taken as 0.0042)	$\Omega/\Omega/C$	(3.13)
μ	viscosity of air	Kg/m/s	(3.16)
δ	Boundary layer thickness	m	(3.22)
ν	kinematic viscosity of air	m^2/s	(3.24)
κ	thermal diffusivity	m^2/hr	(4.2)
ρ	density	Kg/m^3	(4.2)
τ	shear stress	N/m^2	(4.3)
ν	momentum diffusivity	m^2/hr	(4.3)
π	variable		(4.4)
∇G	Gibbs free energy change	cal/g	(4.35)
ρ_{wood}	density of the moist wood	Kg/m^3	(4.56)
π	constant (3.141593)		(4.59)
ξ	variable		(4.63)
φ	surface mass transfer coefficient		(4.26)

APPENDIX B

DERIVATION OF THE EQUATION (2.3)

Consider the layer of moisture–laden gas next to a wet timber surface. Throughout this layer there will be changes in temperature and humidity as shown in Figure B1

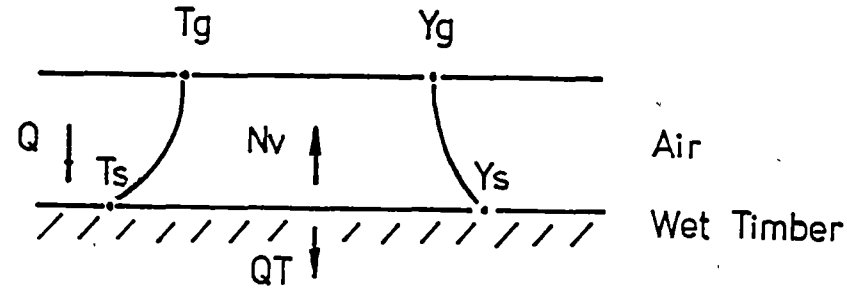

Figure. B1 Humidity and Temperature Profiles Near the Surface of a Wet Timber

The total heat transfer QT into the timber surface is given by the difference between that conducted through the air due to temperature difference across it Q and the enthalpy converted away by the movement of moisture, that is:

$$QT = Q - N_v H_{fg}$$
$$= h (T_g - T_s) - \phi k_c (Y_s - Y_g) H_{fg} \qquad (B1)$$

where ϕ is the so called humidity potential coefficient[17] and is calculated as

$$\phi = \frac{D}{(D + Y_s)} \tag{B2}$$

in which, for air–water system $D = M_w/M_a = 0.622$.

Chilton and Colburn[32] suggested the simple form of the analogy between the heat and mass transfer coefficients, which assumes turbulent flow of air over the swept surface, i.e.,

$$\begin{aligned} J_d &= k_c \frac{S_c^{2/3}}{G_t} \\ &= \beta J_h \\ &= \beta h \frac{P_r^{2/3}}{c_p G_t} \end{aligned} \tag{B3}$$

where, G_t is the total air flow per unit cross section and β is close to unity. c_p may be related to the humid heat C_{py} by the identity

$$\begin{aligned} c_p &= \frac{(C_{pg} + C_{pw} Y)}{(1 + Y)} \\ &= \frac{C_{py}}{(1 + Y)} \end{aligned} \tag{B4}$$

Thus, Equation (B1) becomes

$$QT = h \left((T_g - T_s) - \beta L_u^{2/3} \phi (Y_s - Y_g) \frac{H_{fg}}{c_p} \right) \tag{B5}$$

here L_u is the Luikov number and equal to (P_r/S_c). For water evaporating into air Luikov number is about 1.170 at 25 °C air temperature[65].

The initial distribution of temperature within a board as it leaves the saw cannot be determined, but it appears that under most commercial conditions, the temperature of the wood must soon be reduced to the wet bulb temperature of the air. Thus, in this test, it was taken that the timber surface remains at the wet bulb temperature while doing heat and mass balances. Under this assumption, QT in Equation (B5) is equal to zero, which means that all the heat reaching the timber surface is used to evaporate the moisture. Equation (B5) for this case becomes

$$(T_g - T_s) = \beta L_u^{2/3} \phi (Y_s - Y_g) \frac{H_{fg}}{c_p}$$

$$= -\beta L_u^{2/3} D \frac{1 + Y_s}{D + Y_s} \frac{H_{fg} (Y_g - Y_s)}{C_{py}}$$

$$= -C \frac{H_{fg} (Y_g - Y_s)}{C_{py}} \qquad \text{(B6)}$$

where,

$$C = \beta L_u^{2/3} D \frac{1 + Y_s}{D + Y_s} \qquad \text{(B7)}$$

is called the psychrometric coefficient. For the air–water system the value of C varies from 1.10 when $Y_s = 0.01$ to 1.05 when $Y_s = 0.1$ if the experimental value of 1.0 is taken for β[17]. However, the value of the psychrometric coefficient for air–water system is normally taken to be unity, the approximation being within the scatter of published data. Sherwood and co–authers[66] quote values ranging between 0.95 and 1.12 for measurements on the evaporation of water in wetted–wall columns.

Therefore, Equation (B6) in practice reduces to the expression

$$(T_g - T_w) = - H_{fg} (Y_g - Y_w) / C_{py} \qquad (B8)$$

for the state conditions (T_w, Y_w) next to the wet bulb for water evaporating into air.

APPENDIX C

A TECHNIQUE FOR INTERPOLATING MOISTURE CONCENTRATIONS AT THE EDGES OF SLICES

Examination of any proposed mathematical model for the calculation of the moisture distribution inside a timber board largely depends on accurate comparison of predicted values from the model and actual measurements from slices. Problems were, however, encountered to get the values at the edges of each slice by simply fitting the measured curves with the naked eye. It was clear that the surface value thus obtained was subject to large error, which turns out to be a very serious problem as the surface moisture content is important for analyzing the heat and mass transfer process. A technique was therefore developed to overcome this problem and get these values by interpolating and extrapolating the measured values from slices. The principle is on the grounds that analytical solution of the Fourier equation most conveniently occur as sums of error functions, so parabolas were fitted to the logarithms of moisture concentration deficiencies at three neighbouring points. This is equivalent to fitting a simple sum of error functions to the measured values.

The moisture content obtained from slice measurements is initially taken as the value at the center of each slice. As shown in Figure C1, three slices were taken in turn to form a parabola of the form

$$L = L_2 + B\,(Y-Y_2) + A\,(Y-Y_2)^2 \qquad (C1)$$

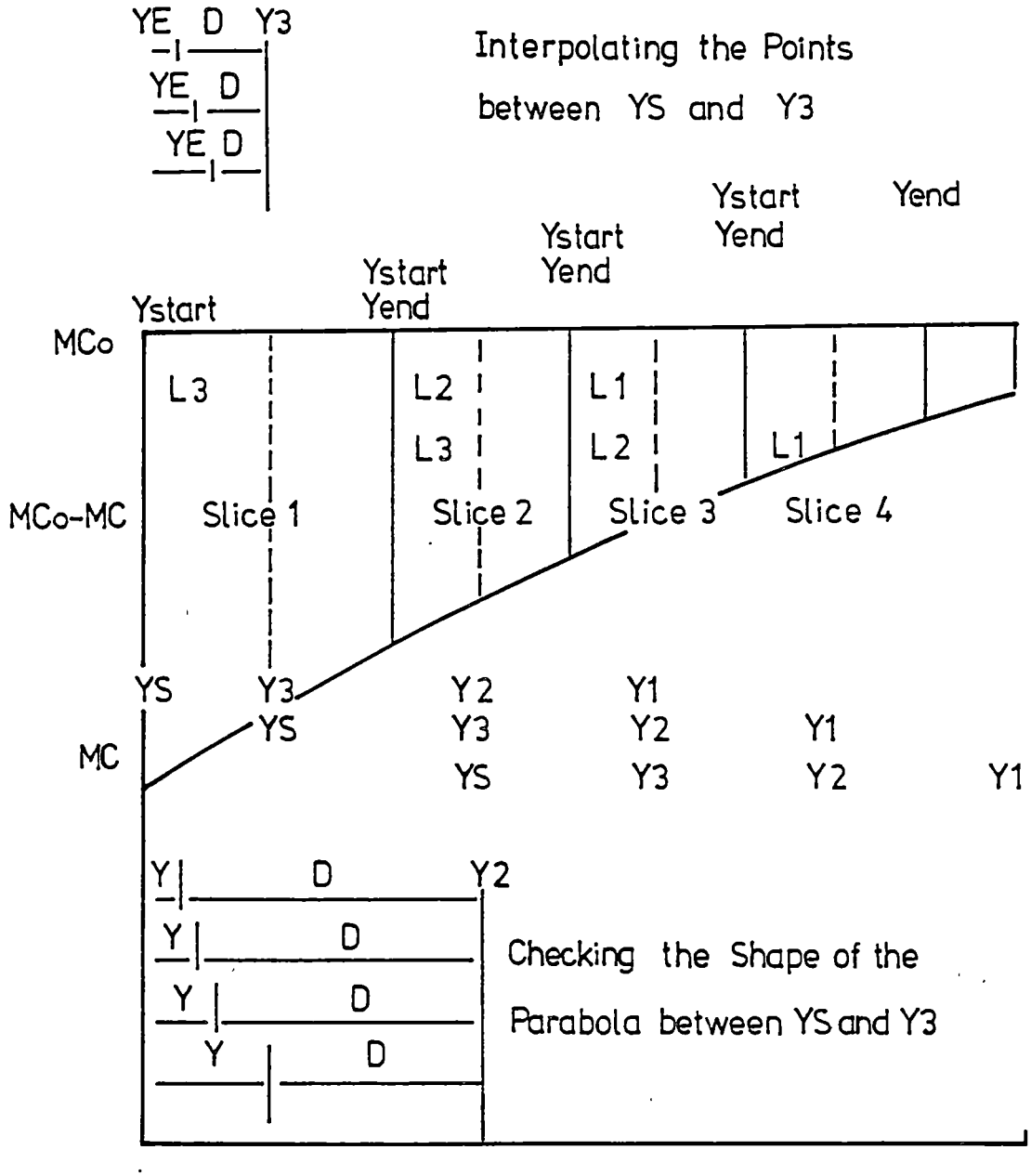

Figure. C1. Diagram Illustrating The Interpolation Of Moisture Concentration At Edges Of Slices

where

$$A = (D_1 - D_2)/(Y_1 - Y_3)$$

$$B = D_1 + A\,(Y_2 - Y_1) \qquad (C2)$$

and

$$D_1 = (L_1 - L_2)/(Y_1 - Y_2)$$

$$D_2 = (L_2 - L_3)/(Y_2 - Y_3) \qquad \text{(C3)}$$

In the above equation, Y ,Y_1, Y_2, Y_3 denote the distances from the surface at the point to be interpolated and the centres of three different slices respectively. L, L_1, L_2, L_3 are the logarithms of moisture deficiencies.

In every three slices taken, the second one (Y_2 and L_2) is used to examine the shape of the parabola between YS and Y_3 as defined by Equation (C1). The method used is to increase Y in Equation (C1) in a step

$$DDY = 0.1\ (Y_{start} - Y_{end}) \qquad \text{(C4).}$$

At every point of Y, the moisture content is calculated as

$$MC(i) = MC_o - EXP(L) \qquad \text{(C5).}$$

This calculation is repeated 10 times (until Y_{end}) and the summation of MC(i) and $\left(MC(i)\ (Y(i)-Y_2)\right)$ is made as

$$SUM_1 = \sum_{i=1}^{10} MC(i) \quad \text{and} \quad SUM_2 = \sum_{i=1}^{10} \left(MC(i)\ (Y(i)-Y_2)\right) \qquad \text{(C6)}$$

so that SUM_1 is a measure of the area under the curve of moisture concentration against Y and SUM_2 an equivalent measure of the moment of that area about Y_2.

The value of the centroid of the area SUM_1 is then obtained as

$$Y_2 + \frac{SUM_2}{SUM_1}$$

and is compared with Y_3. The program then takes

$$\begin{aligned} Y_3 &= Y_2 + \frac{SUM_2}{SUM_1} \\ D2 &= \frac{L_2 - L_3}{Y_2 - Y_3} \\ A &= \frac{D_1 - D_2}{Y_1 - Y_3} \\ B &= D1 + A\,(Y_2 - Y_1) \end{aligned} \qquad \text{(C7)}$$

and restarts the calculation until the absolute value of $\left(Y_3-(Y_2+SUM/SUM_1)\right)$ is less than the specified accuracy, say 10^{-6}. This process shifts the point at which the average moisture content of each slice is plotted away from the middle of the slice to a better measure of where the average value might be as guided by measurements on neighboring slices.

Interpolation of the moisture contents starts from the surface (YS) in a step defined by a specified YE with the parabola

$$L = L_3 + D\,(B + A\,D) \qquad \text{(C8)}$$

where $D=YE-Y_3$, A and B are the previously defined values which satisfy the specified accuracy. The interpolation is continued until Y becomes greater than Y_3, then in going out of the loop the calculation is shifted further inside to include another point (slice) and a new parabola is fitted.

The calculation continues until the half board thickness is reached, then restarts from the other surface. This process allows much more reassuring values for values of moisture concentration extrapolated to the surface than curves fitted by eye.

The computer program was written with the thickness, green weight, and oven–dry weight of each slice as input parameters and the computer interpolates moisture content across the thickness of the board in any specified interval (taken as $\frac{\text{Board Thickness}}{\text{Slice Number} + 1}$) in this study).

APPENDIX D

RESULTS FROM CHAPTER 5

Table D5.1.

Two Dimensional Moisture Distribution For a Quadrant of a Drying Board at Different Drying Times

Drying Times : 1 hour

x =	0	2	6	10	20	30	40	50	60	70
y= 0	91	91	91	91	91	91	91	91	91	91
2	91	470	501	501	501	501	501	501	501	501
4	91	471	502	502	502	502	502	502	502	502
6	91	471	502	502	502	502	502	502	502	502
8	91	471	502	502	502	502	502	502	502	502
10	91	471	502	502	502	502	502	502	502	502
12	91	471	502	502	502	502	502	502	502	502
mm14	91	471	502	502	502	502	502	502	502	502

Drying Times : 50 hours

x =	0	2	6	10	20	30	40	50	60	70
y= 0	91	91	91	91	91	91	91	91	91	91
2	91	167	212	222	231	231	231	231	231	231
4	91	230	312	331	347	347	347	347	347	347
6	91	273	381	405	426	426	426	426	426	426
8	91	297	419	446	470	470	470	470	470	470
10	91	308	437	465	490	490	490	490	490	490
12	91	312	443	473	498	498	498	498	498	498
mm14	91	314	445	475	500	500	500	500	500	500

Drying Times : 200 hours

x =	0	2	6	10	20	30	40	50	60	70
y= 0	91	91	91	91	91	91	91	91	91	91
2	91	111	129	136	156	161	161	161	161	161
4	91	130	165	179	219	227	228	228	228	228
6	91	147	198	218	275	286	287	287	287	287
8	91	162	224	249	320	335	336	336	336	336
10	91	173	244	273	355	371	372	372	372	372
12	91	178	256	287	375	393	395	395	395	395
mm14	91	181	260	292	382	401	402	402	402	402

Drying Times : 400 hours

x =	0	2	6	10	20	30	40	50	60	70
y= 0	91	91	91	91	91	91	91	91	91	91
2	91	99	107	111	124	130	132	132	132	132
4	91	107	123	130	157	168	171	172	172	172
6	91	114	138	148	185	201	206	207	207	207
8	91	121	149	162	209	229	236	237	237	237
10	91	126	159	173	227	251	258	259	259	259
12	91	129	164	180	239	264	271	273	273	273
mml4	91	130	166	182	242	269	276	277	278	278

Drying Times : 600 hours

x =	0	2	6	10	20	30	40	50	60	70
y= 0	91	91	91	91	91	91	91	91	91	91
2	91	95	99	100	108	112	115	115	116	116
4	91	99	107	110	125	134	138	139	139	139
6	91	103	114	119	141	152	158	160	160	160
8	91	106	119	127	153	169	175	178	178	178
10	91	108	124	132	163	180	188	190	191	191
12	91	109	127	135	168	188	196	199	199	199
mml4	91	110	128	136	171	191	199	202	203	203

Drying Times : 700 hours

x =	0	2	6	10	20	30	40	50	60	70
y= 0	91	91	91	91	91	91	91	91	91	91
2	91	94	97	98	104	107	109	109	109	109
4	91	97	102	105	116	123	126	128	128	128
6	91	99	107	111	127	137	142	144	144	144
8	91	101	111	117	137	149	155	158	158	158
10	91	103	115	120	144	158	165	168	168	168
12	91	104	117	122	147	164	171	174	175	175
mml4	91	104	118	123	149	165	173	176	177	177

Table D5.2.

Measurement of the Mass Flux (A)

No.	Time	Board weight 1	2	Average M.C.	M.C. in center	Water weight	Wood weight	Water loss
i	DT(i)	$BW_1(i)$	$BW_2(i)$	AMC(i)	MCC(i)	$W_a(i)$	$W_o(i)$	$W_l(i)$
	hour	g	g	%	%	g	g	g
1	0	2146.0	2146.0	85.0	85.0	986.0	1160.0	
								16.0
2	30	2130.0	2046.0	83.6	82.5	932.0	1110.0	
								54.0
3	47	1992.3	1911.7	79.1	73.8	844.0	1070.0	
								14.6
4	54	1897.1	1831.6	77.5	70.4	780.0	1032.0	
								50.1
5	74	1781.5	1715.9	70.9	75.0	712.0	1044.0	
								51.2
6	99	1664.7	1596.3	65.8	70.9	634.0	963.0	
								34.5
7	121	1561.8	1497.0	62.2	67.2	574.0	922.9	
								32.0
8	143	1465.0	1385.4	58.7	65.9	512.4	872.9	
								31.3
9	167	1354.1	1293.9	55.1	62.3	495.7	834.2	
								22.9
10	191	1271.0	1206.1	52.3	60.8	414.0	792.1	
								21.7
11	215	1184.4	1119.5	49.5	58.6	371.0	748.8	
								16.8
12	242	1102.7	1048.1	47.3	56.6	337.0	711.1	
								22.0
13	266	1026.7	980.00	44.4	48.3	301.2	678.7	
								4.50
14	290	975.5	911.60	43.7	50.5	277.2	634.4	
								22.4
15	335	889.9	823.90	40.2	47.4	236.0	587.9	
								43.0
16	452	780.9	727.70	32.8	44.1	179.8	547.8	
								12.4
17	500	715.3	656.50	30.5	40.9	153.7	502.8	
								11.5
18	548	645.0	598.90	28.3	36.4	132.0	466.9	
								11.6
19	623	587.3	543.50	25.8	34.7	111.4	423.1	
								9.40
20	715	534.1		23.6	31.0			

Table D5.2

Measurement of the Mass Flux (B)

Time	Water loss total	surface	edge	Area surface	edge	Time step	Drying rate surface	edge
	WLT	WLS	WLE	AS	AE		Ras	Rae
hour	g	g	g	m^2	m^2	hour	$g/m^2/hr$	
0				0.1344	0.0269			
	16	16	0			30	3.97	0
30				0.1308	0.0263			
	54	54	0			17	24.2	0
47				0.1272	0.0258			
	15	15	0			7	16.8	0
54				0.1236	0.0252			
	50.1	50.1	0			20	20.3	0
74				0.1200	0.0246			
	51.2	42.8	8.4			25	14.3	13.7
99				0.1164	0.0241			
	34.5	35.6	—			22	—	—
121				0.1128	0.0235			
	32.0	12.0	20.0			22	4.80	38.7
143				0.1092	0.0229			
	31.3	31.4	—			24	—	—
167				0.1056	0.0224			
	22.9	12.5	10.4			24	4.90	19.3
191				0.1020	0.0218			
	21.7	17.4	4.3			24	7.10	8.21
215				0.0984	0.0213			
	16.8	14.8	2.0			27	5.60	3.10
242				0.0948	0.0207			
	22.0	19.9	2.1			24	8.75	4.23
266				0.0912	0.0202			
	4.50	22.4	—			24	—	—
290				0.0876	0.0197			
	22.4	19.7	2.7			45	4.99	3.05
335				0.0840	0.0190			
	43.0	19.4	23.6			117	1.98	10.6
452				0.0804	0.0185			
	12.4	17.5	—			48	—	—
500				0.0768	0.0179			
	11.5	22.6	—			48	—	—
548				0.0732	0.0174			
	11.6	7.9	3.7			75	1.44	2.8
623				0.0696	0.0168			
	9.40	15.7	—			92	—	—
715				0.0660	0.0162			

Notes on Table D5.2 (A):

W_a – Weight of Water Left in Board;

W_o – Weight of Dry Wood Left in Board;

W_l – Weight of Water Lost.

$$AMC(i) = \frac{W_aB(i-1) - WL(i)}{W_ob(i-1)};\ WL(i) = BW_2(i) - BW(i+1);$$

$$W_aB(i) = BW_2(i)\frac{AMC(i)}{1 + AMC(i)};\ W_oB(i) = BW_2(i) - W_aB(i)$$

Notes on Table D5.2 (B):

AS – Area of Surface; AE – Area of Edge;

Ras – Drying Rate from Surface; Rae – Drying Rate from Edge;

WL – Water Loss.

$$WLS = \Big(MCC(i-1) - MCC(i)\Big)\ W_oB(i-1);$$

$$WLE = WLT - WLS$$

APPENDIX E

COMPUTER PROGRAMS

A: Program HMBALA in Fortran–77

```
      PROGRAM HMBALA
C.
C.  THIS PROGRAM IS WRITTEN FOR CALIBRATING THE NEWLY
C.  BUILT KILN IN THE C & M ENGINEERING DEPARTMENT
C.
      DIMENSION VELO(100),TIME (100),TDB1(100),TDB2(100)
      DIMENSION TWB1(100),TWB2(100),DW1(100),DW2(100)
      DIMENSION DW3(100),W1(100),W2(100),PDAIR(100)
      DIMENSION PMAIR(100),GAIR(100),YGIN(100),YGOUT(100)
      DIMENSION YAG(100),HTC(100),YAW(100),AHVS(100)
      DIMENSION HVS1(100),HVS2(100),YW1(100),YW2(100)
      REAL NV(100),MTC(100)
      OPEN(6,FILE='PRN')
      OPEN(3,FILE='C:HMBALA.DAT')
      READ(3,*)(VELO(I),TIME(I),TDB1(I),TDB2(I),
     * TWB1(I),TWB2(I),W1(I),W2(I),I=1,20)
C.
C.  COMMON EQUATIONS FOR HEAT AND MASS BALANCE
C.
      DO 100 I=1,20
      SPNO=10.
      WIKI=0.5
      SPHI=0.025
      BW=0.23
      BL=0.85
C.  CALCULATE THE SPACE AREA
      AREA=SPNO*WIKI*SPHI
C.  CALCULATE THE DENSITY OF THE DRY AIR
      PDAIR(I)=1.177*300.0/(273.15+TDB1(I))
C.  CALCULATE THE INLET HUMIDITY OF THE BULK AIR
      TS1=TWB1(I)
65    TDT=TDB1(I)-TWB1(I)
      CALL PYCHY(TS1,TDB1(I),TDT,YWI,YG1)
      YW1(I)=YWI
      YGIN(I)=YG1
C.  CALCULATE THE DENSITY OF THE MOIST AIR
      PMAIR(I)=PDAIR(I)*(1.+YGIN(I))
C.  CALCULATE THE AIR FLOW RATE
      GAIR(I)=PMAIR(I)*VELO(I)*AREA
C.  CALCULATE THE OUTLET HUMIDITY OF THE BULK AIR
      TS2=TWB2(I)
66    TDT=TDB2(I)-TWB2(I)
      CALL PYCHY(TS2,TDB2(I),TDT,YWO,YG2)
      YW2(I)=YWO
      YGOUT(I)=YG2
      YAW(I)=YW1(I)+YW2(I)
```

```
C.
C. DO THE MASS BALANCE
C.
      DW1(I)=(YGOUT(I)-YGIN(I))*GAIR(I)*TIME(I)
C.
C. DO THE HEAT BALANCE
C.
      TDIN=TDB1(I)
      TDOUT=TDB2(I)
      TADB=(TDIN+TDOUT)/2.
      TAWB=(TWB1(I)+TWB2(I))/2.
      TADW=(TADB+TAWB)/2.
      CPG=CPGD(TADB)
      CPW=CPWD(TADB)
      YAG(I)=(YGIN(I)+YGOUT(I))/2.
C. HEAT CAPACITY AT THE AVERAGE AIR TEMPERATURE
      CPY=CPG+CPW*YAG(I)
C. TOTAL ENTHALPY REQUIRED FOR THE MOISTURE LOST
      CPWW=CPWD(TADW)
      HVS=HVSD(TADW)
      HVST=HVS+CPWW*(TADB-TAWB)
C. HEAT BALANCE
      DW2(I)=(TDIN-TDOUT)*GAIR(I)*CPY*TIME(I)/HVST
C.
C. CALCULATE THE MOISTURE LOSS FROM THE MEASUREMENT
C.
      DW3(I)=W1(I)-W2(I)
C.
C. CALCULATE THE SURFACE TRANSFER COEFFICIENTS
C.
C. CALCULATE THE DRYING RATE
      BSA=BL*BW
      NV(I)=DW3(I)/(BSA*TIME(I))
C. CALCULATE HEAT TRANSFER COEFFICIENT
      HVS1(I)=HVSD(TWB1(I))
      HVS2(I)=HVSD(TWB2(I))
      AHVS(I)=(HVS1(I)+HVS2(I))/2.
      HTC(I)=NV(I)*AHVS(I)/(TADB-TAWB)
C. CALCULATE MASS TRANSFER COEFFICIENT
      MTC(I)=NV(I)/(YAW(I)-YAG(I))
100   CONTINUE
C.
C. WRITE OUT THE OUTPUT
C.
      WRITE(6,10)
10    FORMAT(28X,'INPUT VARIABLES'/75('*'))
      WRITE(6,11)
11    FORMAT(2X,'INLET db',4X,'INLET wb',4X,'OUTLET db',
     * 4X,'OUTLET wb',3X,'INLET',4X,'OUTLET'/2X,'TEMPERATURE'
     * ,2X,'TEMPERATURE',2X,'TEMPERATURE',2X,
     * 'TEMPERATURE',2X,'HUMIDITY',2X,'HUMIDITY'/75('*'))
      DO 15 N=1,20
      WRITE(6,12)TDB1(N),TWB1(N),TDB2(N),
           (6,12)TWB2(N),YGIN(N),YGOUT(N)
```

```
15    CONTINUE
12    FORMAT(4X,F5.2,7X,F5.2,9X,F5.2,8X,F5.2,7X,F7.5,4X,F7.5)
      WRITE(6,14)
14    FORMAT(75('*'))
      WRITE(6,1)
1     FORMAT(/21X,'HEAT-MASS BALANCE OUTPUT'/75('*'))
      WRITE(6,2)
2     FORMAT(2X,'M-LOSS FROM',4X,'M-LOSS FROM',5X,
           'M-LOSS FROM'
     * ,4X,'H-TRANSFER',4X,'M-TRANSFER'/2X,'M-BALANCE
           KG',3X,
     * 'H-BALANCE KG',3X,'MEASUREMENT
           KG',2X,'COEFFICIENT',3X,
     * 'COEFFICIENT'/75('*'))
      DO 3 J=1,20
      WRITE(6,4) DW1(J),DW2(J),DW3(J),HTC(J),MTC(J)
3     CONTINUE
      WRITE(6,5)
5     FORMAT(75('*'))
4     FORMAT(2X,F7.3,8X,F7.3,8X,F7.3,10X,F7.4,8X,F7.4)
      CLOSE(6)
      CLOSE(3)
      STOP
      END
C.
C. START THE SUBROUTINE AND FUNCTION STATEMENTS
C.
C. THE SUBROUTINE IS TO CALCULATE THE HUMIDITY OF AIR
      SUBROUTINE PYCHY(TS,TD,TDT,YW,YG)
      PT=101.325
      A=4.18684
      HFG=597.31
      TA=TS+TD
      PSWB=P(TS)
      YW=0.62198*PSWB/(PT-PSWB)
      CPG=CPGD(TA)
      CPW11=CPWD(TS)
      CPW12=CPWD(TD)
      CPF=CPFD(TS)
      CPY=CPG+CPW11*YW
      HVSDD=A*HFG+CPW12*TD-CPF*TS
      YG=YW-CPY*TDT/HVSDD
75    RETURN
      END
C.
C. THE FUNCTION IS TO CALCULATE THE LATENT HEAT
C.
      FUNCTION HVSD(T)
      HVSD=2502.1-2.4345*T
      RETURN
      END
C.
```

```
C. THE FUNCTION IS TO CALCULATE HEAT CAPACITY OF
   DRY AIR
C.
      FUNCTION CPGD(T)
      A=4.18684
      CPGD=(0.2402+3.83E-06*T)*A
      RETURN
      END
C.
C. THE FUNCTION IS TO CALCULATE HEAT CAPACITY
   OF VAPOUR
C.
      FUNCTION CPWD(T)
      A=4.18684
      CPWD=A*(0.440904-0.00016*T)
      RETURN
      END
C.
C. THE FUNCTION IS TO CALCULATE WB SATURATION
   PRESSURE
C.
      FUNCTION P(T)
      T=273.15+T
      P=EXP(-7511.52/T +89.63121+0.023998970*T-1.1654551E
     * -05*T**2.-1.2810336E-08*T**3.+2.0998405E-11*T**4.-
     * 12.145799*LOG(T))
      RETURN
      END
C.
C. THE FUNCTION IS TO CALCULATE CPF
C.
      FUNCTION CPFD(T)
      A=4.18684
      A1=4.119E-04
      A2=8.117E-06
      A3=-6.052E-08
      CPFD=A*(1.0074+A1*T+A2*T**2.+A3*T**3.)
      RETURN
      END
```

B: Program HMMODEL in Turbo–Pascal

```
PROGRAM HMMODEL
(*THIS PROGRAM IS WRITTEN TO CALCULATE MOISTURE AND
  TEMPERATURE DISTRIBUTIONS INSIDE A TIMBER BOARD
  UNDER ITS DRYING CONDITION*)
CONST
    PI=3.14159265;
  (*NUMBERS OF BOARDS, SECTIONS,SLICES & REGIMES[0..N]*)
    NB=5; NS=7; NSL=13; NR=5;
  (*NUMBER OF WORKSPACES FOR PROCESSING DATA *)
    NWM=14;
  (*NUMBER OF WORKSPACES FOR MOISTURE PROFILE
                              0.5*(NSL–1)*)
    NW=6;
  (*NUMBER OF NODES (NW+1)*)
    NN=7; NX=7; NY=7;
  (*WIDTH OF BOARDS AND THICKNESS*)
    WB=0.14; TB=0.0280;
  (*WIDTH OF SPACING *)
    WS=0.018;
  (*MASS TRANSFER COEFFICIENT*)
    HSCF=1.0;
  (*FIBRE SATURATION POINT FACTOR*)
    FSPF=0.25;
    ENDTIME=700;
  (*REFERENCE DIFFUSION COEFFICIENT*)
    DR=0.35E–6;
  (*TEMPERATURE AT WHICH DR OBTAINED (DEG.C)*)
    TEMP1=40.0;
  (*NUMBER OF CHANGES IN KILN CONDITIONS AFTER START*)
    N1=5;
  (*BAROMETRIC PRESSURE, MOIST AIR, PA*)
    PMOIST=101835.0;
  (*PRINT DATA TRUE OR FALSE*)
    PRINTFILE = FALSE;

VAR

  A,AMCC,AMCM,B,B1,C,CW,CWB,CMID,CPG,CPW,CPY,D,D1,
  D2,DC, D C1,DC2,DTEMP,DITEMP,DDY,DMC,DQS,DQ1,DT,
  DTIME,DY,DY2,D0,DXEVEN,EMC,F,FH,FHO,DFH,
  FOURD,FSP,FR,FT,F0,F01,F02,HW,HFG,HDDY,HDY,IERFCX,
  ERFX,IDY,IDY2,IS4PIDT,I4DT,I4PID,INVN,INVT,INVTWB,
  INT,INVTW,ISPID,L,L0,L1,L2,L3,MC,MCS,MC0,MC1,MC2,
  MC3,MU,MUL,N3,PDRY,PDIFF,PID,PSAT,PSATWB,PSATW,
  PVAP,Q,QS1,QS2,R,RDB,RWB,REW,RHA,AMCT,AMCT2,RH,
  RHSURF,RHO,RHODRY,RHOWET,SPI,ST,STOPID,SYMID,SUM,
  T,TORPI,T1,TDB,TEMP,TERM,TERM1,TK,TKW,TKWB,TWW,
  VEL,VELM,X,X2,Y,YS,Y0,Y1,Y2,Y3,YMID,YEND,
  YEVEN,YSTART,DYEVEN,HSC :REAL;
  NUMBERPOINTS,TFACTOR,I,IIT,IT,II,ITA,IT1,ITIME,
  I1,J,K,M,N,NTIME :INTEGER;
```

```
    ATH,AWET,ADRY     :ARRAY[0..NSL,0..NSL] OF REAL;
    ATIME             :ARRAY[0..NR] OF INTEGER;(*REGIMES*)
    ADBT,AWBT,AVEL    :ARRAY[0..NR] OF REAL;
    ALN,AMCW,AMCI,AY,AYMID,AQ  :ARRAY[0..NWM] OF REAL;
    ARHO              :ARRAY[0..NB] OF REAL;
    ATIMES            :ARRAY[0..NSL] OF INTEGER;
    MAMC              :ARRAY[0..NSL] OF REAL;
    FTIMES            :ARRAY[0..NWM] OF INTEGER;
    IMC,CPT,VS,KTC,TW,TDC:ARRAY[0..NN] OF REAL;
    QSXY              :ARRAY[0..NX,0..NY] OF REAL;
    NAMES             :ARRAY[0..NSL] OF STRING[20];
    NAMET             :ARRAY[0..NSL] OF STRING[20];
    INFILE: TEXT;
    KEY :STRING[1];

{$i E:\TURBO\GSXLIB.PAS}

(*GSXLIB.PAS CONTAINS A SET OF GRAPHICS PROCEDURES
  WHICH ARE USED TO PLOT THE CALCULATED RESULTS
  GRAPHICALLY*)

VAR

    XX,YY,OO,PP,UU,QQ,RR,SS,TT, TT1,TT2,TT3: QARRAY;

    NAME :QSTRING20; NAME1 :QSTRING20;

PROCEDURE GETPSAT(TEMP: REAL; VAR TK,INVT,PSAT: REAL);
(*THIS PROCEDURE IS TO CALCULATE THE SATURATION
  VAPOUR PRESSURE*)
BEGIN
  TK : =TEMP+273.15; INVT := 1.0/TK;
  PSAT := 1.005*EXP(22.3286–INVT*(2881.0+INVT*
        (5.0751E5–INVT*2.925E7)))
END;

PROCEDURE VAPCON(INVT : REAL);
(*THIS PROCEDURE IS TO CALCULATE THE VAPOUR
  CONCENTRATION*)
BEGIN
  PDRY := PMOIST–PVAP; R := 0.622*PVAP/PDRY;
  RHODRY := 3.485E–3*PDRY*INVT;
  C := R*RHODRY
END;
```

```
PROCEDURE WOODP;
(*THIS PROCEDURE IS TO CALCULATE WOOD THERMAL
  PROPERTIES*)
VAR
  I :INTEGER;
BEGIN
  FOR I := 0 TO NN DO
  BEGIN
    CPT[I] := 4.1868*(0.266+0.00116*TW[I]+AQ[I]/RHO);
    {IF AQ[I]>0.4*RHO THEN
    KTC[I] := 0.782E-3*RHO+1.97E-3*AQ[I]+0.086*VS[I]
    ELSE KTC[I] := 0.782E-3*RHO+1.45E-3*AQ[I]+0.086*VS[I];}
    IF AQ[I]>0.4*RHO THEN
    KTC[I] := (RHO*1E-03*(4.80+12.5*AQ[I]/RHO)+0.57)*0.151
    ELSE KTC[I] := (RHO*1E-03*(4.80+9.0*AQ[I]/RHO)+0.57)*0.151;
    TDC[I] := KTC[I]/((RHO+1000.0)*CPT[I])
  END
END;



PROCEDURE DIFFC(DC: REAL);
(*THIS PROCEDURE TO DEFINE VARIABLES CONTAINING DC*)
BEGIN
  PID := PI*DC; I4PID := 0.25/PID; STOPID := SQRT(DTIME/PID);
  I4DT := 0.25/(DC*DTIME); IS4PIDT := 0.5/SQRT(PID*DTIME)
END;



PROCEDURE IERFC(X :REAL);
(*THIS PROCEDURE CONTAINS THE ERROR FUNCTION
  SOLUTION*)
VAR
  N,N2  :REAL;
  I     :INTEGER;
BEGIN
  TORPI := 2.0/SPI; X2 := SQR(X);
  TERM := X; N := 1.0; SUM := TERM;
  WHILE ABS(TERM)>1.0E-6 DO
  BEGIN
    N2 := N+N; TERM := TERM*(-X2)*(N2-1.0)/((N2+1.0)*N);
    SUM := SUM+TERM; N := N+1.0
  END;
  ERFX := TORPI*SUM;
  IERFCX := 0.5*TORPI*EXP(-X2)-X*(1.0-ERFX);
  IF IERFCX<0.0 THEN IERFCX := 0.0
END;
```

```
PROCEDURE IMDT;
(*THIS PROCEDURE IS TO CALCULATE THE MOISTURE
  CONCENTRATION AT THE BEGINNING OF THE DRYING*)
VAR
  I    :INTEGER;
BEGIN
  Y := 0.0;
  FOR I := 0 TO NN DO
  BEGIN
    X := Y/SQRT(4.0*DC1*DTIME);
    C := (F01+F02)*HSC*SQRT(DTIME/DC1);
    IF X >6.0 THEN IERFCX := 0 ELSE IERFC(X);
    IMC[I] := C*IERFCX;
    AQ[I] := AQ[I]-IMC[I];
    Y := Y+DYEVEN
  END;
  QS1 := AQ[0]
END;


PROCEDURE TEMPD;
(*THIS PROCEDURE IS TO CALCULATE TEMPERATURE
        DISTRIBUTION INSIDE THE BOARD*)
VAR
  CC,DCC,XN1,XN2,XN,AX1,AX2,AX :REAL;
BEGIN
  CC := 1.0; DCC :=-1.0/NN;
  FOR I := 0 TO NN DO
  BEGIN
    DITEMP := 0.0;
    XN := 0.5*TB/SQRT(4.0*TDC[I]*DTIME);
    C := 2.0*DFH*SQRT(DTIME/((RHO+1000.0)*CPT[I]*KTC[I]));
    FOR J := 0 TO 5 DO
    BEGIN
      XN1 := ((2.0*J+1)-CC)*XN; XN2 := ((2.0*J+1)+CC)*XN;
      IF XN1 > 6.0 THEN AX1 := 0.0 ELSE
      BEGIN
        IERFC(XN1); AX1 := IERFCX
      END;
      IF XN2 > 6.0 THEN AX2 := 0.0 ELSE
      BEGIN
        IERFC(XN2);
        AX2 := IERFCX
      END;
      AX := AX1+AX2; DITEMP := AX+DITEMP
    END;
    CC := CC+DCC; TW[I] := TW[I]+C*DITEMP
  END
END;
```

```
PROCEDURE SETQS;
(*THIS PROCEDURE IS TO SET MOISTURE CONCENTRATION AT
  SURFACE*)
VAR
  I1                    :INTEGER;
  DIFF,PPQS,PQS2,RHS: REAL;
BEGIN
  DQS := MC0-QS1;
  ST := PID*SQR(DQS/((F01+F02)*HSC));
  QS2 := MC0-DQS*SQRT(1.0+DTIME/ST);
  I1 := 0; PQS2 := QS2;
  F02 := F01; DQS := QS2-QS1;
  IF (QS2<FSP) THEN
  BEGIN
    GETPSAT(TWW,TKW,INVTW,PSATW);
    PVAP := 461.3*CW*TKW;
    RHS := PVAP/PSATW;
    REPEAT
      RH := EXP((EXP(5.116*(1.0-QS2/FSP))-1.0)/(-0.11*TKW));
      IF PRINTFILE THEN WRITELN('RH=',RH:10,' ');
      IF RH>1.0 THEN RH := 1.0;
      IF RH>RHS THEN RH := RHS;
      IF RH<RHA THEN RH := RHA;
      PVAP := RH*PSATW;INVTW := 1/TKW;
      VAPCON(INVTW); I1 := I1+1; CW := (C+CW)/2.0;
      IF CW<CMID THEN CW := CMID;
      F02 := F*VEL*(CW-CMID);
      IF F02>F01 THEN F02 := F01;
      IF F02=0.0 THEN F02 := F01;
      F02 := (F02+F01)/2.0;
      IF PRINTFILE THEN  WRITELN('CW=',CW:9,'  RH=',
      RH:6:3,'  F01=',F01:9,'  F02=',F02:9);
      F0 := F01+F02;
      D := -F0*HSC*STOPID; DIFF := D-DQS;
      D1 := DIFF-PDIFF;
      IF (I1=1) THEN
      BEGIN
        QS2 := QS2+DIFF/30.0
      END ELSE IF ABS(D1)>1.0E-5 THEN
      BEGIN
        QS2 := PPQS-PDIFF*(PQS2-PPQS)/(D1*30)
      END;
      IF QS2<EMC THEN QS2 := EMC;
      DQS := D; PDIFF := DIFF; PPQS := PQS2; PQS2 := QS2;
      IF PRINTFILE THEN  WRITELN(D:8:3,'=D  ',
      QS2:8:3,'=QS2  ',DIFF:10,'=DIFF')
    UNTIL ABS(DIFF/DQS)<1.0E-5
  END;
  AQ[0] := QS2; F01 := (F02+F01)/2.0; QS1 := QS2;
END;
```

```
FUNCTION POWER(A,N :REAL) :REAL;
VAR
  INTN,I  :INTEGER;
  P       :REAL;
BEGIN
  {POWER := EXP(LN(A)*N); THIS EQUATION IS FASTER BUT
  ONLY FOR POSITIVE A,IT DOES WORK ON FRACTIONAL N}
  INTN := ROUND(N); P := 1.0;
  FOR I:= 1 TO INTN DO P := P*A;
  POWER := P
END;


PROCEDURE FTWOMD;
(*THIS PROCEDURE IS TO CALCULATE MOISTURE
  CONCENTRATION DISTRIBUTION UNDER TWO
  DIMENSIONAL CONDITIONS *)
VAR
  FX1,FX2,FX3,FX4,FX5,FY1,FY2,FY3,FY4,FY5,
  FX,FY,FXY,Y11,X11,AC :REAL;
  I,J,N                :INTEGER;
BEGIN
  X11 := WB/2.0;
  FOR I := 0 TO NX DO
  BEGIN
    FX5 := 0.0; AC := -1.0;
    FOR N := 0 TO 20 DO
    BEGIN
      FX1 := POWER(AC,N)/(2*N+1);
      FX2 := COS((2*N+1)*PI*X11/WB);
      FX3 := EXP(-SQR(2*N+1)*DC2*ITIME*SQR(PI/WB));
      FX4 := FX1*FX2*FX3;
      FX5 := FX5 + FX4
    END;
    FX := FX5*4.0/PI; IF FX>1.0 THEN FX := 1.0;
    Y11 := TB/2.0;
    FOR J := 0 TO NY DO
    BEGIN
      FY5 := 0.0;
      FOR N := 0 TO 20 DO
      BEGIN
        FY1 := POWER(AC,N)/(2*N+1);
        FY2 := COS((2*N+1)*PI*Y11/TB);
        FY3 := EXP(-SQR(2*N+1)*DC1*ITIME*SQR(PI/TB));
        FY4 := FY1*FY2*FY3;
        FY5 := FY5 + FY4
      END;
      FY := FY5*4.0/PI; IF FY>1.0 THEN FY := 1.0;
      Y11 := Y11-DYEVEN;
      FXY := FX*FY;
      QSXY[I,J] := (MC0-EMC)*FXY+EMC;
```

```
    END;
    X11 := X11-DXEVEN
  END
END;


PROCEDURE FTWOAM;
(*THIS PROCEDURE IS TO CALCULATE AVERAGE MOISTURE
  CONCENTRATION UNDER TWO DIMENSIONAL CONDITIONS*)
VAR
  KKX,KKY,KKDX,KKDY,EX,EE1,
  EEX,EY,EE2,EEY,EXY  :REAL;
  I                   :INTEGER;
BEGIN
  EX := 0.0; EY := 0.0;
  KKDX := DC1*ITIME/SQR(TB/2.0);
  KKDY := DC2*ITIME/SQR(WB/2.0);
  KKX := -(KKDX*SQR(PI))/(4.0);
  KKY := -(KKDY*SQR(PI))/(4.0);
  FOR I := 0 TO 6 DO
  BEGIN
    EE1 := EXP(SQR(2*I+1)*KKX)/SQR(2*I+1);
    EX := EX + EE1
  END;
  EEX := 8.0*EX/SQR(PI);
  FOR I := 0 TO 6 DO
  BEGIN
    EE2 := EXP(SQR(2*I+1)*KKY)/SQR(2*I+1);
    EY := EY + EE2
  END;
  EEY := 8.0*EY/SQR(PI); WRITELN('KKDY,EEY',KKDY,EEY);
  EXY := EEX*EEY; WRITELN('EXY',EXY);
  AMCT := (MC0-EMC)*EXY+EMC;
  AMCT2 := (MC0-EMC)*EEX+EMC;
END;


PROCEDURE SURFTEM;
(*THIS PROCEDURE IS TO CALCULATE AVERAGE TEMPERATURE
  OF THE BOARD*)
VAR
  MCI,DIFFT,MI:REAL;
  I           :INTEGER;
BEGIN
  FH := FHO*(TDB-TWW);
  WOODP;
  IF (ITIME<45) AND (HSC=1.0) THEN DTEMP := 0.0 ELSE
  BEGIN
    HFG := 2502.0-2.4*TWW;
    HW := 1172.3*EXP(-15.0*AQ[0]/RHO);
    MI := (HFG+HW)*HSC*F01;
    DFH := FH-MI;
    DTEMP := (DFH*2.0*DTIME)/((RHO+1000.0)*TB*CPT[0]);
    IF DTEMP<0.0 THEN DTEMP := 0.0;
```

```
    IF DTEMP>(TDB-TWW) THEN DTEMP := 0.0
  END;
  TWW := TWW+DTEMP; IF TWW>TDB THEN TWW := TDB;
  FH := FHO*(TDB-TWW);
  HFG := 2502.0-2.4*(TWW-DTEMP/2.0);
  DFH := FH-(HFG+HW)*HSC*F01; IF DFH<0.0 THEN DFH := 0.0
  TEMPD
END;


PROCEDURE SUMS(VAR INT :REAL);
(*THIS PROCEDURE IS TO SUM SERIES FOR INTEGRALS
  OF ERFS*)
BEGIN
  SUM := TERM;
  REPEAT
    TERM := TERM*MUL/N3; N3 := N3+2.0; SUM := SUM+TERM
  UNTIL (ABS(TERM) < 1.0E-5);
  INT := SUM
END;


PROCEDURE IDMC;
(*THIS PROCEDURE IS TO INTEGRATE CHANGES IN MOISTURE
  CONCENTRATION,FITS PARABOLAS TO LOGS I.E. ERFS TO
  M.CONC.*)
VAR
  I,I1          : INTEGER;
  PL1,PL2,R2    : REAL;
BEGIN
  MC3 := AQ[0]; MC2 := AQ[1]; L3 := LN(MC3);
  L2 := LN(MC2); I := 1;
  FOR I1 := 2 TO NN DO
  BEGIN
    MC1 := AQ[I1]; L1 := LN(MC1); B := 0.5*(L1-L3)*IDY;
    A := 0.5*(L1-L2-L2+L3)*IDY2; R2 := I4DT-A;
    TERM := 0.5*SPI/SQRT(R2); MUL := 0.5*SQR(B)/R2; N3 := 2.0;
    SUMS(DMC); MC := MC2*2.0*DMC*IS4PIDT;
    MC3 := MC2; MC2 := MC1; L3 := L2; L2 := L1;
    AQ[I] := MC; I := I+1
  END;
  A := (L3-L2)*IDY2;
  AQ[NN] := MC2*IS4PIDT*SPI/SQRT(I4DT-A);
  SETQS; SURFTEM;
  IF AQ[0]>FSP THEN
  BEGIN
    CW := (TWW-TEMP)*(CMID-CWB)/(TDB-TEMP)+CWB;
    F01 := F*VEL*(CW-CMID); F02 := F01;
  END
END;
```

```
PROCEDURE NEWTEMP(I :INTEGER);
(*THIS PROCEDURE IS TO SET UP THE DRYING SCHEDULE*)
VAR
  DF,E1,FF,F1,RE    : REAL;
BEGIN
  IF PRINTFILE THEN WRITELN('NEW TEMPERATURE');
  VEL := AVEL[I]; TEMP := AWBT[I]; TWW := TEMP;
  GETPSAT(TEMP,TKWB,INVTWB,PSATWB);
  DC1 := D0*EXP(-3800.0*INVTWB); DC2 := DC1/0.7;
  DIFFC(DC1);PVAP := PSATWB; VAPCON(INVTWB);
  RWB := R; CWB := C;
  IF PRINTFILE THEN WRITElN('TWB=',TEMP:6:1,'
      PSAT=',PSATWB:10);
  HFG := 2502.0-2.4*TEMP; TDB := ADBT[I];
  RDB := RWB-0.905*(TDB-TEMP)/HFG;
  GETPSAT(TDB,TK,INVT,PSAT);
  PVAP := RDB*PMOIST/(0.622+RDB); PDRY := PMOIST-PVAP;
  RHODRY := 3.485E-3*PDRY*INVT;
  RHOWET := RHODRY*(1+RDB)/(1+1.609*RDB);
  RH := PVAP/PSAT; RHA := RH; CMID := RDB*RHODRY;
  EMC := FSP*(1.0-LN(-0.11*TK*LN(RH))/5.116);
  VELM := VEL/1.08-0.1996;
  MU := 1.172E-5+5.3E-8*TEMP; REW := VELM*RHOWET*WS/MU;
  IF (REW>2500.0) THEN FF := 0.01 ELSE
  FF := 1.42E-9*SQR(REW-2500.0)+0.01; FF := 0.012;
  F := FF/2;
  IF PRINTFILE THEN WRITELN('FRICTION FACTOR
  (F/2=WALL SHEAR STRESS/(RHO*U*U))=', F:10);
  F := 3600*F;
  F01 := F*VEL*(CWB-CMID); F02 := F01;
  IF TDB>52.0 THEN CPG := 1.0063+8.60E-5*(TDB-52.0)
  ELSE CPG := 1.0037+5.0E-5*TDB;
  IF TDB>60.0 THEN CPW := 1.91+2.50E-3*(TDB-60.0)
  ELSE CPW := 1.86+8.33E-5*TDB;
  CPY := CPG+CPW*RDB;
  FHO := 1800*FF*VEL*RHOWET*CPY;
  FOR I := 0 TO NN DO TW[I] := TEMP;
  IF PRINTFILE THEN WRITELN('SURF.FLUX=',F01:9,'
      KG/(S.M*HR)  DTIME=',DTIME:5:2,' HRS');
  IF PRINTFILE THEN WRITE(' TDB=',TDB:6:1,'  PSAT=',PSAT:10);
  IF PRINTFILE THEN WRITELN('  RH=',RH:6:3,'
      RHO(DRY AIR)=',RHODRY:6:3,' KG/C.M');
  IF PRINTFILE THEN WRITE('EMC=',EMC:8:3);
  IF PRINTFILE THEN WRITELN(' REYNOLDS NUMBER=',REW:7:1,'
                DIFFUSION COEFFICIENT=',DC1:7);
  IF PRINTFILE THEN WRITE('WALL VAPOUR CONC.=',CW:9,
      ' KG/C.M  MID VAPOUR CONC.=',CMID:9);
  IF PRINTFILE THEN WRITELN('  KG/C.M');
  IF PRINTFILE THEN WRITELN
END;
```

```
PROCEDURE PRINT;
(*THIS PROCEDURE IS TO PRINT OUT THE CALCULATED
  RESULTS*)
VAR
  I,NI    : INTEGER;
BEGIN
  SUM := 0.5*AQ[0]; YEVEN := 0.0; NI := 2*NN;
  FOR I := 1 TO NN DO SUM := SUM+AQ[I];
  SUM := SUM-0.5*AQ[NN]; AMCC := SUM/NN;
  IF PRINTFILE THEN WRITELN('AVE.M.CONC.=',AMCC:8:3,
      'KG/C.M AT',ITIME:5,' HOURS');
  IF PRINTFILE THEN WRITELN('DISTRIBUTION OF MOISTURE');
  BEGIN
    FOR I := 0 TO NN DO
    BEGIN
      IF PRINTFILE THEN WRITE(AQ[I]:8:3,' ');
      OO[I+1] := AQ[I]; OO[NI-I+1] := AQ[I]
    END;
    FOR I := 0 TO NI DO
    BEGIN
      IF PRINTFILE THEN WRITE(YEVEN:8:3,' ');
      PP[I+1] := YEVEN; YEVEN := YEVEN+DYEVEN
    END;
  END
END;


PROCEDURE PARABOLA(J :INTEGER);
(*THIS PROCEDURE IS TO SET UP THE PARABOLA FOR
  INTERPOLATION*)
VAR
  I                    : INTEGER;
  SUM1,DIFF,SUMM : REAL;
BEGIN
  L1 := ALN[J]; Y1 := AYMID[J]; D1 := (L1-L2)/(Y1-Y2);
  DDY := 0.1*(YEND-YSTART); A := (D1-D2)/(Y1-Y3);
  B := D1+A*(Y2-Y1);
  REPEAT
    SUM1 := 0.0; SUMM := 0.0; Y := YSTART+0.5*DDY;
    FOR K := 1 TO 10 DO
    BEGIN
      D := Y-Y2; L := L2+D*(B+A*D);
      MC := MC0-EXP(L);
      SUM1 := SUM1+MC; SUMM := SUMM+MC*D; Y := Y+DDY;
    END;
    Y := Y2+SUMM/SUM1;
    DIFF := Y-Y3; Y3 := Y; D2 := (L2-L3)/(Y2-Y3);
    A := (D1-D2)/(Y1-Y3); B := D1+A*(Y2-Y1);
  UNTIL ABS(DIFF)<5E-04;
  YSTART := YEND; L3 := L2; L2 := L1; YS := Y3;
  Y3 := Y2; Y2 := Y1; D2 := D1
END;
```

```
PROCEDURE INTERP(I1 :INTEGER);
(*THIS PROCEDURE IS TO INTERPOLATE M.CONC. AT EDGE OF
  THE SLICE*)
BEGIN
  D := YEVEN-Y3;
  L := L3+D*(B+A*D);
  Q := EXP(L);
  AMCI[I1] := MC0-Q; YEVEN := YEVEN+DYEVEN
END;


PROCEDURE MODDATA(I : INTEGER);
(*THIS PROCEDURE IS TO SET UP THE INTERPOLATION
  PROCEDURE AND PRINT OUT THE MOISTURE
  CONCENTRATIONS AT THE EDGES OF SLICES*)
VAR
  I1,J,K,NM1                : INTEGER;
  SDY,MCM,SUM1,SUM2  : REAL;
BEGIN
  Y := 0.0; SUM := 0.0; AY[0] := Y;
  FOR K := 0 TO NSL DO
  SUM := SUM+ATH[I,K]/1000.0;
  MUL := TB/SUM; SUM := 0.0; MCM := 0.0;
  FOR K := 0 TO NSL DO
  BEGIN
    SDY := MUL*ATH[I,K]/1000.0; Y1 := Y+SDY;
    AYMID[K] := 0.5*(Y+Y1);
    Y := Y1; AY[K+1] := Y; D := ADRY[I,K];
    MC := RHO*(AWET[I,K]-D)/D;
    AMCW[K] := MC;
    IF (I=0) AND (MC>MCM) THEN MC0 := MC;
    MCM := MC0;
    SUM := SUM+MC*SDY
  END;
  IF (I=0) THEN MC0 := MC0+7.0 ELSE MC0 := MC0; I1 := 1;
  FOR K := 0 TO NSL DO
  BEGIN
    Q := MC0-AMCW[K];
    ALN[K] := LN(Q)
  END;
  REPEAT
    Y1 := AYMID[I1]; I1 := I1+1
  UNTIL Y1>YMID; NM1 := I1; AMCM := SUM/TB;
  IF PRINTFILE THEN WRITELN('MEASURED VALUES OF
      MOISTURE CONCENTRATION AT', ATIMES[I]:5,' HOURS');
  IF PRINTFILE THEN WRITELN('MEAN
      VALUE=',AMCM:8:3,'KG/C.M');
  YSTART := 0.0; YEVEN := 0.0; L3 := ALN[0]; L2 := ALN[1];
  Y3 := AYMID[0]; Y2 := AYMID[1]; D2 := (L2-L3)/(Y2-Y3); I1 := 0;
  FOR J := 2 TO NM1 DO
  BEGIN
    YEND := AY[j-1]; PARABOLA(J); AYMID[J-2] := YS;
```

```
    WHILE YEVEN<Y3 DO
    BEGIN
      INTERP(I1); I1 := I1+1
    END
  END;
  NM1 := NM1-2; DYEVEN := -DYEVEN;
  L3 := ALN[NSL]; I1 := NSL-1; L2 := ALN[I1]; Y3 := AYMID[NSL];
  Y2 := AYMID[I1]; D2 := (L2-L3)/(Y2-Y3); K := NSL-2;
  YEVEN := TB; YSTART := TB; I1 := NSL+1;
  FOR J := K DOWNTO NM1 DO
  BEGIN
    YEND := AY[J+2]; PARABOLA(J); AYMID[J+2] := YS;
    WHILE YEVEN>Y3 DO
    BEGIN
      INTERP(I1); I1 := I1-1
    END
  END;
  DYEVEN := -DYEVEN; YEVEN := 0.0; I1 := 0;
  IF PRINTFILE THEN WRITELN('VALUES FROM SLICES
      INTERPOLATED VALUES');
  IF PRINTFILE THEN WRITELN('YMID M.CONC. YEVEN
      M.CONC.');
  ASSIGN(INFILE,'NAME.DAT');
  REWRITE(INFILE);
  FOR J := 0 TO NWM DO
  BEGIN
    IF J=NWM THEN Y := TB+1.0E-6  ELSE Y := AYMID[J];
    WHILE YEVEN<Y DO
    BEGIN
      IF PRINTFILE THEN WRITELN('    ',YEVEN:8:5,
          '  ',AMCI[I1]:8:5);
      XX[J+1] := YEVEN; YY[J+1] := AMCI[I1];
      WRITELN(INFILE,XX[J+1],YY[J+1]);
      IF J+1 > NUMBERPOINTS THEN NUMBERPOINTS := J+1;
      YEVEN := YEVEN+DYEVEN; I1 := I1+1;I := I+1
    END;
    IF YEVEN<TB THEN IF PRINTFILE THEN
      WRITELN(AYMID[J]:8:5,' ',AMCW[J]:8:3)
  END;
  CLOSE(INFILE)
END;


(*MAIN PROGRAM*)
(*MAIN PROGRAM IS TO LINK UP ALL THE PROCEDURES AND
  DATA FILE*)
BEGIN

  NAMES[0] := 'SLICE0'; NAMES[1] := 'SLICE1'; NAMES[2] := 'SLICE2';
  NAMES[3] := 'SLICE3'; NAMES[4] := 'SLICE4'; NAMES[5]:='SLICE5';
  NAMES[6] := 'SLICE6'; NAMES[7] := 'SLICE7'; NAMES[8] := 'SLICE8';
```

```
NAMES[9] := 'SLICE9'; NAMES[10] := 'SLICE10';
NAMES[11] := 'SLICE11'; NAMES[12] := 'SLICE12';
NAMES[13] := 'SLICE13';NAMET[0] := 'QING0';
NAMET[1] := 'QING1'; NAMET[2] := 'QING2';
NAMET[3] := 'QING3'; NAMET[4] := 'QING4'; NAMET[5] := 'QING5';
NAMET[6] := 'QING6'; NAMET[7] := 'QING7'; NAMET[8] := 'QING8';
NAMET[9] := 'QING9'; NAMET[10] := 'QING10';
NAMET[11] := 'QING11'; NAMET[12] := 'QING12';
NAMET[13] := 'QING13';

ASSIGN(INFILE,'QWU.DAT');
RESET(INFILE);
FOR I := 0 TO 5 DO READ(INFILE,ATIME[I]);
FOR I := 0 TO 5 DO READ(INFILE,ADBT[I]);
FOR I := 0 TO 5 DO READ(INFILE,AWBT[I]);
FOR I := 0 TO 5 DO READ(INFILE,AVEL[I]);
FOR I := 0 TO 5 DO READ(INFILE,ARHO[I]);
FOR I := 0 TO 13 DO READ(INFILE,ATIMES[I]);
FOR I := 0 TO 13 DO READ(INFILE,MAMC[I]);
FOR I := 0 TO 14 DO READ(INFILE,FTIMES[I]);
FOR I := 0 TO 13 DO
  BEGIN
    FOR J := 0 TO 13 DO READ(INFILE,ATH[I,J]);
    READLN(INFILE);
  END;
FOR I := 0 TO 13 DO
  BEGIN
    FOR J := 0 TO 13 DO READ(INFILE,AWET[I,J]);
    READLN(INFILE);
  END;
FOR I := 0 TO 13 DO
  BEGIN
    FOR J := 0 TO 13 DO READ(INFILE,ADRY[I,J]);
    READLN(INFILE);
  END;
CLOSE(INFILE);
I := 0; J := 0; K := 0;


I := 0; RHO := ARHO[I]; HSC := HSCF;
FSP := FSPF*RHO; YMID := TB/2.0; PDIFF := 0.0;
ISPID := 1.0/SQRT(PI*DR); DYEVEN := TB/(NSL+1.0);
DY := DYEVEN; IDY := 1.0/DY; DY2 := SQR(DYEVEN);
IDY2 := 1.0/DY2; SPI := SQRT(PI); DXEVEN := WB/70.0;
D0 := DR*EXP(3800.0/(TEMP1+273.5));
NUMBERPOINTS := 0;
NAME := NAMES[I];
MODDATA(0);
ASSIGN(INFILE,'NAME.DAT');
RESET(INFILE);
FOR I := 1 TO 15 DO READ(INFILE,XX[I],YY[I]);
CLOSE(INFILE);
```

```
  QOPEN(NAME);
  QAXES(0,0.028,0,600,0.0,0.0,0.002,100,
  'THICKNESS (m)','M-CONCENTRATION(kg/m^3)');
  QPLOT(XX,YY,NUMBERPOINTS,3,4);
  QMARK(XX,YY,NUMBERPOINTS,2,2,1);
  READLN(KEY); QCLOSE;
  I1 := 0; DTIME := DY2/(32.0*DR);
  NEWTEMP(I1);
  IF DTIME>1.0 THEN BEGIN DTIME := 1.0; NTIME := 1 END
  ELSE BEGIN NTIME := ROUND(1.0/DTIME); DTIME := 1.0/NTIME
END;
  FOR I := 0 TO NN DO AQ[I] := MC0;
  FOR I := 0 TO NX DO
  BEGIN
    FOR J := 0 TO NY DO
    BEGIN
      QSXY[I,J] := MC0
    END
  END;
  I1 := I1+1;ITA := 1; M := 0; II := 1;IT := 0;
  UU[1] := IT; {VV[1]:=AMCM; }TT1[1] := TEMP; TT2[1] := TEMP;
  TT3[1] := TDB; {WW[1]:=AMCM; } QQ[1] := IT; RR[1] := F01;
  SS[1] := HSC; TT[1] := HSC*F01;
  FOR ITIME := IT+1 TO ENDTIME DO
  BEGIN
    FOR I := 1 TO NTIME DO
    BEGIN
      IF (ITIME<2) AND (I=1) THEN
      BEGIN
        IMDT
      END ELSE IDMC{; TWOMD}
    END;
    PRINT; {FTWOMD;  FTWOAM;}
    IF ITIME=ATIMES[ITA] THEN
    BEGIN
      NUMBERPOINTS := 0;
      MODDATA(ITA);
    (* PLOT THE MOISTURE DISTRIBUTIONS *)
      ASSIGN(INFILE,'NAME.DAT');
      RESET(INFILE);
      FOR I := 1 TO 15 DO READ(INFILE,XX[I],YY[I]);
      CLOSE(INFILE);
      NAME := NAMES[II];
      QOPEN(NAME);
      {QFRAME(2);}
      QTDIR(0);
      QAXES(0,0.028,0,600,0.0,0.0,0.002,100,
        'THICKNESS (m)','M-CONCENTRATION(kg/m^3)');
      QPLOT(XX,YY,NUMBERPOINTS,1,5);
```

```
      QMARK(XX,YY,NUMBERPOINTS,2,2,1);
      QPLOT(PP,OO,15,2,5);
      QMARK(PP,OO,15,3,4,1);
      READLN(KEY) ;
      QCLOSE;
    (* PLOT THE TEMPERATURE DISTRIBUTIONS *)
      {NAME1 := NAMET[II];
      FOR I := 1 TO NN+1 DO
      BEGIN
        ZZ[I] := TW[I-1]; ZZ[NN+NN+2-I] := TW[I-1]
      END;
      QOPEN(NAME1);
      QTDIR(0);
      QAXES(0,0.028,0,40,0.0,0.0,0.002,5,
          'THICKNESS (m)','T-DISTRIBUTION (C)');
      QPLOT(PP,ZZ,15,1,5);
      QMARK(PP,ZZ,15,2,2,1);
      READLN(KEY) ;
      QCLOSE;}
      {WW[II+1]:=AMCM; } UU[II+1] := ITIME;
      SS[II+1] := HSC  TT[II+1] := HSC*F01;
      RR[II+1]  := F01; {MAMC[ITA]*RHO/100.0;}
      ITA := ITA+1; II := II+1;
      IF II>14 THEN II := 13
    END;
    IF ITIME=FTIMES[M] THEN
    BEGIN
      IF ITIME=FTIMES[0] THEN HSC := HSC-0.01;
      IF ITIME=FTIMES[1] THEN HSC := HSC-0.4;
      QQ[M+2] := ITIME;
      RR[M+2] := F02; SS[M+2] := HSC; TT[M+2] := HSC*F02;
      {BB[M+2] := TWM[M-1];}
      TT1[M+2] := TWW; TT2[M+2] := TEMP; TT3[M+2] := TDB;
      M := M+1
    END;
    IF ITIME=ATIME[I1] THEN
    BEGIN
      NEWTEMP(I1); I1 := I1+1
    END
  END;
  CLOSE(INFILE);
  {QOPEN('QINGD');
  QTDIR(0);
  QAXES(0.0,700,0.0,600,0.0,0.0,70.0,100.0,
  'DRYING TIME (Hour)','AM CONCENTRATION(kg/m^3)');
  QPLOT(UU,VV,14,2,5);
  QMARK(UU,VV,14,3,5,1);
  QPLOT(UU,WW,14,3,6);
  QMARK(UU,WW,14,2,3,1);
  READLN(KEY); QCLOSE;
  QOPEN('QINGD2');
  QTDIR(0);
  QAXES(0.0,700,0.0,600,0.0,0.0,70.0,100.0,
```

```
  'DRYING TIME (Hour)','AM CONCENTRATION(kg/m^3)');
  QPLOT(UU,SS,14,3,5);
  QMARK(UU,SS,14,4,3,1);
  QPLOT(UU,RR,14,3,6);
  QMARK(UU,RR,14,7,3,1);
  READLN(KEY); QCLOSE }
  QOPEN('FLUX');
  QTDIR(0);
  QAXES(0,700,0,0.03,0,0,70,0.005,'DRYING TIME (Hour)',
  'MASS FLUX (kg/m^2/hr)');
  QPLOT(QQ,RR,16,2,5);
  QMARK(QQ,RR,16,3,5,1);
  QPLOT(QQ,TT,16,4,6);
  QMARK(QQ,TT,16,2,3,1);
  READLN(KEY);QCLOSE;
  QOPEN('HSC');
  QTDIR(0);
  QAXES(0,700,0,1,0,0,70,0.1,
  'DRYING TIME (Hour)','MT-COEFFICIENT-HSC');
  QPLOT(QQ,SS,16,2,5);
  QMARK(QQ,SS,16,3,5,1);
  READLN(KEY); QCLOSE;
  QOPEN('TEMP');
  QTDIR(0);
  QAXES(0,700,20,40,0,20,70,5,
  'DRYING TIME (Hour)','TEMPERATURE (C)');
  QPLOT(QQ,TT1,16,3,5);
  QMARK(QQ,TT1,16,2,4,1);
  {QPLOT(QQ,BB,16,4,2);
  QMARK(QQ,BB,16,3,2,1);}
  QPLOT(QQ,TT2,16,4,3);
  QMARK(QQ,TT2,16,5,3,1);
  QPLOT(QQ,TT3,16,2,5);
  QMARK(QQ,TT3,16,3,2,1);
  READLN(KEY); QCLOSE
END.
```